NRC·CNRC CONSTRUCTION

Detailed Analysis of Sandia Experimental Crude Oil Fire Data

Author: Cecilia Lam
Report No.: A1-016311.1
Report Date: March 1, 2021
Contract No.: A1-016311
Agreement Date: August 22, 2019

Client Document Number: 16933263

National Research Council Canada
Conseil national de recherches Canada

Canada

Paper: Cat. No. NR24-86/2021E
ISBN 978-0-660-37903-6

PDF: Cat. No. NR24-86/2021E-PDF
ISBN 978-0-660-37902-9

Également disponible en français

Detailed Analysis of Sandia Experimental Crude Oil Fire Data

Author

Digitally signed by Lam, Cecilia
Date: 2021.03.15 15:56:13 -04'00'

Cecilia Lam, Research Officer

Approved

Kashef, AH
2021.03.16 19:09:25 -04'00'

Ahmed Kashef, Director
Fire Safety R&D
NRC Construction Research Centre

Report No.: A1-016311.1
Report Date: 1 March 2021
Contract No.: A1-016311
Agreement Date: 22 August 2019
Program: FS R&D

151 pages

(This page is intentionally left blank)

Table of Contents

List of Figures

List of Tables

Executive Summary

This report contains a comprehensive review and analysis of three series of 2 m diameter pool fire tests that were conducted at Sandia National Laboratories under the base project A1-010647. Three fuels were tested: heptane (Series 1), Bakken crude oil (Series 2) and diluted bitumen or dilbit (Series 3). Measurements were made to characterize the external thermal environment around a simulated, 1/10th scale, rail tank car (calorimeter) engulfed in the fire. The analysis in this report focusses on:

A. verifying the time-averaged results (averaged due to their fluctuating nature) of the thermal measurements presented in the Sandia test report;
B. examining changes in the fuel temperature distribution in order to gain insight into the burning behaviour of the tested fuels; and
C. comparing corresponding tests involving the same experimental test conditions to enhance understanding of the test results.

A. Review of Time-Averaged Results in Sandia Test Report

In the Sandia report, the time interval used to average the measured data in each of the Series 1 and 2 tests was different for each of the measurement parameters, making it difficult to draw conclusions about a particular test and to compare between tests. In this work, a single time-averaging period that could be applied to all measurement parameters was therefore identified for each test of Series 1 and 2. For Series 1, the use of the identified time-averaging period resulted in less than 4% difference from Sandia's values for all measurement parameters except the heat flux from the directional flame thermometers (DFTs) as discussed below. For Series 2, the use of the identified time-averaging period generally resulted in less than 7% difference from Sandia's values. The main adjustment made based on reviewing Sandia's data was to recalculate the values of total heat flux to the DFTs in Series 1 and 2 so that the same method was used as in Series 3. This resulted in differences in total heat flux of 30-40% for Series 1 data and 2-40% for Series 2 data. Further, the time intervals used by Sandia to average the heat release rate data were found to require correction due to an invalid assumption about the sampling rate used by the heat release rate measurement system, resulting in up to 5% error in the time-averaged values presented in the Sandia test report.

For Series 3, the Sandia test report used time-averaged values calculated by integrating the data from 0 to 25 minutes and then dividing by 25 minutes. These values thus included the period of fire growth immediately after ignition and were typically associated with larger standard deviations because the fires did not burn steadily. In the present analysis, multiple, shorter time-averaging periods were selected to permit quantification and analysis of the changes in dilbit burning behaviour. In general, Sandia's parameter values compared reasonably well to the range of values determined using the shorter time-averaging periods.

B. Analysis of Burning Behaviour and Fuel Temperature Distribution

As the reference fuel, the heptane tests showed how a pure, single-component fuel burns. Because the pan was pre-filled with fuel prior to ignition, there was an initial temperature stratification in the pool, which gradually diminished until the entire pool was at a uniform temperature near the fuel boiling point. This temperature was then maintained until the fuel completely burned down.

The Bakken crude oil appeared to experience initial preferential burning of the lighter ends (up to C9), as seen through a ~10% increase in heat release rate early during the test in which the fuel was allowed to burn down without replenishment. Partway through this test, a simultaneous increase in heat release rate, decrease in fuel rake temperatures, and increase in temperatures in the upper part of the fire plume were observed, which could potentially be explained by the thermal cracking of heavier ends in the crude oil releasing additional fuel vapours.

In general, the dilbit tests exhibited three distinct stages of burning. The first stage was characterised by moderately high levels of heat release rate and flame height, as well as plume temperature, surface emissive power and heat flux at heights above the calorimeter. It appeared to correspond to fuel temperatures below approximately 150°C and the vapourization of the lighter ends (up to C9). This was followed by a second stage, with noticeably lower levels of the same parameters, that seemed to correspond to fuel temperatures increasing to approximately 300-350°C (with the possible existence of localized hot spots greater than 400°C) and the burning of components in the C10-C24 range. Thermal cracking of the heavier ends (C25+) was likely involved in this stage. Finally, the third stage showed levels of heat release rate, flame height, plume temperature, surface emissive power and heat flux (at heights above the calorimeter) that were similar to or higher than those in the first stage. It appeared to correspond to fuel temperatures greater than 350°C and the burning of the lighter hydrocarbons produced by thermal cracking. The three stages of burning appeared to be consistent with a distillation-type burning process for the dilbit, which is a blended mixture of condensate diluent with light constituents (C4 to C9, with a peak at C5), and bitumen with heavy constituents (C25+).

C. Test Comparisons

Among the tests without the calorimeter, the heptane fire had the highest burning rate and flame height, followed by the Bakken fire and then the dilbit fire. Compared to the heptane fire, the Bakken fire exhibited steeper decreases in plume temperature and narrow-view heat flux with increasing height, consistent with the shorter flame height. Compared to the Bakken fire, the dilbit fire exhibited much lower magnitudes in temperature at each elevation along the plume axis due to the shorter flame height, but only slightly lower levels of surface emissive power across the height of the plume.

Among the tests with the calorimeter at 1 m height, the heptane fire had the highest burning rate and flame height, followed by the Bakken fire and then the dilbit fire. In the heptane fire, similar levels of combustion (i.e. local heat release) appeared to occur both above and below the calorimeter, resulting in uniform levels of total heat flux around the calorimeter surface. In the Bakken fire, because the ends of the calorimeter were less fully engulfed in flame, the total heat flux to the top of the calorimeter was lower than to the bottom in the left and right measurement planes. Insufficient data (due to thermocouple failure) was available to draw conclusions about the centre measurement plane. In the dilbit fire, most of the combustion occurred below the calorimeter, resulting in higher total heat flux to the bottom of the calorimeter than to the top in all measurement planes. Overall, the calorimeter received the lowest levels of total heat flux in the heptane fire because this fire was less optically thick (due to less soot production) than either of the crude oil fires.

Among the tests with the calorimeter at 0.5 m height, the dilbit fire appeared to have a lower burning rate than the Bakken fire, in addition to a lower flame height. Much of the combustion seemed to occur above the calorimeter in the Bakken fire, but below the calorimeter in the dilbit fire. This was consistent with where the highest total heat flux to the calorimeter was measured in each test. In the Bakken fire, the total heat flux was higher to the top of the calorimeter along the centre measurement plane than to the bottom, whereas in the dilbit fire, the total heat flux generally appeared to be higher towards the bottom of the calorimeter.

The tests with the calorimeter at 1 m height were compared to a similar test with the same pool diameter conducted by Sandia using Strategic Petroleum Reserve (SPR) crude oil. The burning rate and heat release rate of the SPR fire were reasonably similar to those of the Bakken fire. Measurements of narrow-view heat flux (surface emissive power) were similar among the SPR, dilbit and Bakken fires, indicating that this parameter was not greatly affected by differences in crude oil composition. The total heat flux to the bottom of the calorimeter was similar among the SPR, dilbit and Bakken fires, but the heat flux profiles in the SPR test were more uniform around the surface of the calorimeter, likely due to the calorimeter in the SPR test being shorter in length and thus more fully engulfed by the fire along its measurement planes.

Additional comparisons were made between the Series 1, 2 and 3 tests and two other sets of pool fire experiments previously conducted at Sandia. One comparison focussed on the effect of changing the scale of

the fire from 2 m to 5 m diameter using the same crude oil (Bakken). Although it was difficult to compare the 2 m and 5 m diameter fire tests because of differences in atmospheric conditions (the 5 m fire test was conducted outdoors), the surface emissive power was found to be similar, indicating that both fires had similar optical thickness and lending credibility to the use of 2 m diameter fires to simulate larger-scale scenarios. The spatially averaged total heat flux to the calorimeter was also similar when the calorimeter was placed in similar relative locations (i.e. similar ratio of calorimeter elevation to pool diameter) inside the fire.

The other comparison focussed on the effect of changing the fuel type from crude oil to other hydrocarbon fuels using the same-sized (2 m diameter) fire. The heptane fire was found to be similar to the Jet Propellant 8 (JP-8) fire in both burning rate and flame height, while the Bakken and dilbit fires had lower burning rates and flame heights. This could be expected because heptane is a pure fuel and JP-8 a highly refined aviation fuel, while Bakken is a crude oil and dilbit a mixture of heavy bitumen and lighter condensate. All four fuels are known to produce sooty flames when burning as a liquid pool fire and thus provided a useful basis for comparison.

1 Introduction

The National Research Council of Canada (NRC) and Transport Canada (TC) conducted three series of pool fire experiments at the Fire Laboratory for Accreditation of Models and Experiments (FLAME) test facility at Sandia National Laboratories [1]. Series 1 (FY2017/18) tested heptane, Series 2 (FY2017/18) tested Bakken crude oil, and Series 3 (FY2018/19) tested diluted bitumen (dilbit). The objective of these experiments was to characterize, at 1/10th scale, the external thermal environment around a rail tank car engulfed in a crude oil pool fire. The experiments used a calorimeter to represent the tank car at reduced scale due to the prohibitive cost of simulating a full-scale scenario. Of particular interest in this work was the effect of volatile compounds in the crude oil on the fires. Of more general interest was the impact of crude oil properties on the severity outcomes of crude oil fires.

The measured experimental data included fuel burning rate, heat release rate, flame height, temperatures and heat flux, as well as fuel properties obtained from fuel samples taken prior to selected fire tests [2, 3]. Residue samples were also collected from the fuel pan after the first and last tests in both Series 2 and 3. A significant amount of data processing and analysis was conducted by Sandia for all three test series and reported to NRC/TC under the base project A1-010647 [1]; however, a follow-on opportunity existed for NRC to independently verify Sandia's results, to analyse the data in greater detail in order to further the understanding and potential impact of the tests, and to support related work being conducted by TC. This opportunity forms the basis of the present report.

2 Summary of Experimental Testing

To facilitate the discussion in the remainder of this report, a summary is provided here of the three test series conducted at Sandia. The test matrix and measurement parameters are presented in Tables 1 and 2 for reference.

Table 1: Test matrix for Series 1, 2 and 3 (adapted from Table 5-1 in [2])

Test	Fuel	Calorimeter elevation[a]	Fuel supply temperature (°C)	Fuel feed method	Fuel depth (mm / inch)
1.1	heptane	1 m, centered	20 ± 5	constant level	38 / 1.5
1.2	heptane	n/a	20 ± 5	constant level	38 / 1.5
1.3	heptane	1 m, centered	60 ± 5	constant level	38 / 1.5
2.1	Bakken	n/a	20 ± 5	constant level	28 / 1.1
2.2	Bakken	0.5 m, centered	20 ± 5	constant level	28 / 1.1
2.3	Bakken	1 m, centered	20 ± 5	constant level	28 / 1.1
2.4	Bakken	1 m, centered	60 ± 5	constant level	28 / 1.1
2.5	Bakken	1 m, centered	20 ± 5	constant level	28 / 1.1
2.6	Bakken	n/a	20 ± 5	non-continuous feed, allowed to burn down	76 / 3.0
3.1	dilbit	1 m, centered	20 ± 5	constant level	30 / 1.2
3.2	dilbit	0.5 m, centered	20 ± 5	constant level	30 / 1.2
3.3	dilbit	n/a	20 ± 5	constant level	30 / 1.2
3.4	dilbit	n/a	20 ± 5	non-continuous feed, allowed to burn down	76 / 3.0
3.5	dilbit	1 m, centered	20 ± 5	constant level	30 / 1.2
3.6	dilbit	1 m, centered	60 ± 5	constant level	30 / 1.2

[a] Measured from center of calorimeter to bottom of fuel pan.

Table 2: Measurement parameters and instrumentation used in Series 1, 2 and 3 (adapted from Table 4-1 in [2])

Measurement parameter	Type of instrumentation
Burning rate	Differential pressure gauge Load cell
Fuel supply temperature	Type K thermocouple in fuel supply line
Liquid fuel temperature	Type K thermocouples near edge of fuel pan, spaced every 2 mm from bottom of pan to height of 60 mm
Heat release rate	IRGAS FTIR/O2 gas analyzer
Flame height	CCD camera Infrared camera
Plume temperature	Type K thermocouples along axis of fuel pan Infrared camera
Surface emissive power	Narrow-view (5.5° view angle) radiometers at ~9 m from fuel pan centre Infrared camera
Heat flux	Wide-view (180° view angle) radiometers at ~9 m from fuel pan centre Directional flame thermometers (DFT) measuring total (incident) heat flux at 2 m and 4 m from fuel pan centre at 1 m height
Heat flux and temperature around simulated tank car	Calorimeter (0.33 m diameter, 1.8 m long) with Type K thermocouples: • on outer surface of inner cylinder, • on inner surface of outer cylinder, and • exterior to outer cylinder at 51 mm (2") from the surface Thermocouples are located on three cross-sectional measurement planes at ¼, ½ and ¾ length of the calorimeter (see Appendix A for further description).

Key differences between the three test series are listed below.

1. Fuel feed and measurement of fuel feed rate
    a. Series 1 used a liquid level control system to automatically maintain a constant fuel level in the pan, which was monitored using a differential pressure gauge. Heptane was pumped directly from the fuel supply tank into the fuel pan. A load cell was used to measure the weight of the tank. The rate of change in the weight of the tank thus gave the fuel feed rate.
    b. Series 2 (with the exception of Test 2.3) relied on manual control of the fuel feed. It was found that the burning rate of the Bakken crude oil was reasonably steady, so the fuel feed rate could be matched to the burning rate without much difficulty, in order to maintain a constant fuel level in the pan. The fuel level was continuously monitored using a differential pressure gauge. Water from a tote was used to transfer the Bakken crude oil from a 4800 gallon tanker into the fuel pan. Load cells were used to measure the weight of the tote and thus the amount of water used to displace an equivalent volume of crude oil out of the tanker. The rate of change in the weight of the tote could thus be used to calculate the feed rate of the crude oil.
        i. Test 2.3 used the same automatic liquid level control system as Series 1, but the fuel control valve was found to be damaged, affecting the system's ability to control the fuel level and causing large fluctuations in the test data [2]. The data from this test is thus considered to be less reliable than the other Series 2 tests.
    c. Series 3 also relied on manual control of the fuel feed, but the burning rate of the dilbit varied throughout the test, so it was more difficult to maintain a constant fuel level in the pan (particularly during Test 3.1, the first test of the series). The differential pressure gauge that was used to monitor the fuel level also failed partway through each test (typically after about 20 minutes). Pressurized nitrogen was used to transfer the dilbit from a 420 lb modified propane tank into the fuel pan. A load cell was used to measure the weight of the tank. The rate of change in the weight of the tank thus gave the fuel feed rate.
        i. In Tests 3.1, 3.2, 3.3 and 3.5, Jet A fuel was introduced into the fuel pan immediately after the crude oil feed was terminated (at around 30 minutes) in order to flush the crude oil out of the transfer lines and minimize the cleanup required between tests. In Test 3.4, which did not involve a continuous fuel feed (Table 1), Jet A fuel was introduced at 54 minutes when the crude oil fire was observed to be nearly extinguished. No Jet A was used in Test 3.6 to allow for collection of a post-test residue sample that was not contaminated with Jet A fuel.
2. Pre-filling of fuel pan
    a. In Series 1, the fuel pan was pre-filled.
    b. In Series 2, the fuel pan was not pre-filled. The Bakken crude oil was ignited immediately upon introduction into the fuel pan in order to capture contributions by any volatile components to the fire behaviour.
    c. In Series 3, the fuel pan was pre-filled in all tests except Test 3.2, in which the dilbit was ignited immediately upon introduction into the fuel pan. Pre-filling was not done in other Series 3 tests because of the length of time (>10 minutes) required to pump the fuel to the desired level.
3. Heat release rate measurements
    a. Heat release rate was measured in Series 1 and 2, but not in Series 3 (with the exception of Test 3.4) due to equipment failure.

3 Selection of Time-Averaging Periods for Analysis

Most of the analysis conducted by Sandia was based on data that was time-averaged over a selected period during each test [2]. In this section, the time-averaging periods that were used by Sandia are reviewed and, in most cases, adjusted. The method used to identify and select the adjusted time-averaging periods is therefore described.

3.1 Series 1 (Heptane) and 2 (Bakken)

For Series 1 and 2 tests, most of the analysis presented in Luketa [2], and subsequently in Ko [1], was based on data averaged over a period of steady burning behaviour during the fire test. Periods selected for averaging the various parameters are listed in Table 3. It can be seen that within each test, the averaging period applied was usually not consistent among the various parameters (e.g. the averaging period used for burning rate was, in all cases except Test 1.3, different from that used for heat release rate, which was also different from that used for flame height). This makes it difficult to draw conclusions about a particular test and to compare between tests.

Table 3: Time-averaging periods for Series 1 and 2 results (all references based on [2])

Test	Test length[a] (min)	Averaging period for fuel temp	Averaging period for burning rate	Averaging period for radiometers	Averaging period for plume temps	Averaging period for heat release rate	Averaging period for flame height	Averaging period for DFTs
1.1	35	10-35 min (Sect 6.1.1.1)	0-32.4 min (Fig 6-3)	20-30 min (Tables 7-7/7-8)	20-35 min (Table 7-13)	20-30 min (Sect 6.1.1.9)	10-20 min[b]	20-35 min (Table 7-19)
1.2	37	10-35 min (Sect 6.1.2.1)	0-36 min (Fig 6-20)	15-35 min (Tables 7-7/7-8)	20-37 min (Table 7-13)	20-30 min (Sect 6.1.2.7)	n/a	20-37 min (Table 7-19)
1.3	44	24-44 min (Sect 6.1.3.1)	24-44 min (Fig 6-30)	24-44 min (Tables 7-7/7-8)	20-44 min (Table 7-13)	24-44 min (Sect 6.1.3.8)	n/a	24-44 min (Table 7-19)
2.1	37	5-35 min (Sect 6.2.1.1)	22-36 min (Fig 6-45)	15-35 min (Tables 7-9/7-10)	15-35 min (Table 7-14)	22-32 min (Sect 6.2.1.8)	10-20 min (Sect 7.8.2)	20-37 min (Table 7-20)
2.2	40	10-40 min (Sect 6.2.2.1)	23-39 min (Fig 6-56)	10-40 min (Tables 7-9/7-10)	10-40 min (Table 7-14)	15-30 min (Sect 6.2.2.9)	10-20 min (Sect 7.8.2)	20-40 min (Table 7-20)
2.3	33	10-30 min (Sect 6.2.3.1)	estimated from water volumes pre-/post-test, divided by 32 min	10-30 min (Tables 7-9/7-10)	10-30 min (Table 7-14)	10-30 min (Sect 6.2.3.9)	10-20 min (Sect 7.8.2)	20-33 min (Table 7-20)
2.4	42	23-42 min (Sect 6.2.4.1)	23-31 min (Fig 6-87)	23-42 min (Tables 7-9/7-10)	23-42 min (Table 7-14)	23-42 min (Sect 6.2.4.9)	10-20 min (Sect 7.8.2)	20-40 min (Table 7-20)
2.5	33	10-35 min (Sect 6.2.5.1)	20-35 min (Fig 6-103)	20-35 min (Tables 7-9/7-10)	20-35 min (Table 7-14)	20-30 min (Sect 6.2.5.9)	10-20 min (Sect 7.8.2)	20-33 min (Table 7-20)
2.6	36	0-4.6 min (while fed into pan)	fuel volume divided by 36 min	20-35 min (Tables 7-9/7-10)	22.5-32.5 min (Table 7-14)	15-30 min (Sect 6.2.6.8)	10-20 min (Sect 7.8.2)	15-36 min (Table 7-20)

[a] The test length is the duration for which a constant fuel level was maintained.
[b] This interval was obtained from the spreadsheets provided by Sandia, but was not reported in [2].

Efforts were thus taken in the present work to systematically identify a single time-averaging period for each test that could be applied to all parameters measured during the test. For Series 1 and 2 tests, appropriate periods for analysis were selected by determining the longest period that met the following criteria:

(1) steady readings from the differential pressure gauge in the fuel pan,
(2) a steady decrease in measurements from the load cells measuring the weight of the tote supplying water to the crude oil tanker, or the load cell measuring the weight of the heptane supply tank,
(3) a constant trend (i.e. neither increasing nor decreasing) in the heat release rate measured using oxygen consumption calorimetry, and
(4) maintenance of the fuel supply temperature (a controlled parameter in Table 1) within the required test conditions of 20 ± 5°C or 60 ± 5°C, as appropriate.

Periods during which the first two criteria were met indicate periods in which the fuel was pumped into the pan at a rate equivalent to the burning rate. This is because the first criterion indicates periods when the fuel level

was constant, while the second criterion indicates that water was being steadily pumped into the crude oil tanker to push an equivalent volume of crude oil into the pan (or that heptane was being steadily pumped out of the supply tank). Meanwhile, the third criterion indicates that the overall fire characteristics were steady, and the fourth criterion provides verification of the desired test conditions.

Figure 1 shows Test 2.4 as an example. The plot in Figure 1a shows measurements from the differential pressure gauge, the load cells, and a flow meter used to measure the flow rate of crude oil into the pan (available in Series 2 tests as a secondary measurement for comparison with the load cells). For the period from 24 to 31.5 minutes (shaded in yellow), the differential pressure gauge readings were constant, the decrease in measurements from the load cells was steady, and the readings from the flow meter were also constant. For the same time period, Figure 1b shows that the heat release rate was relatively constant, and the fuel supply temperature was between 55°C and 60°C. Thus, with all four criteria met, this time period was selected for averaging all other measured data in this test.

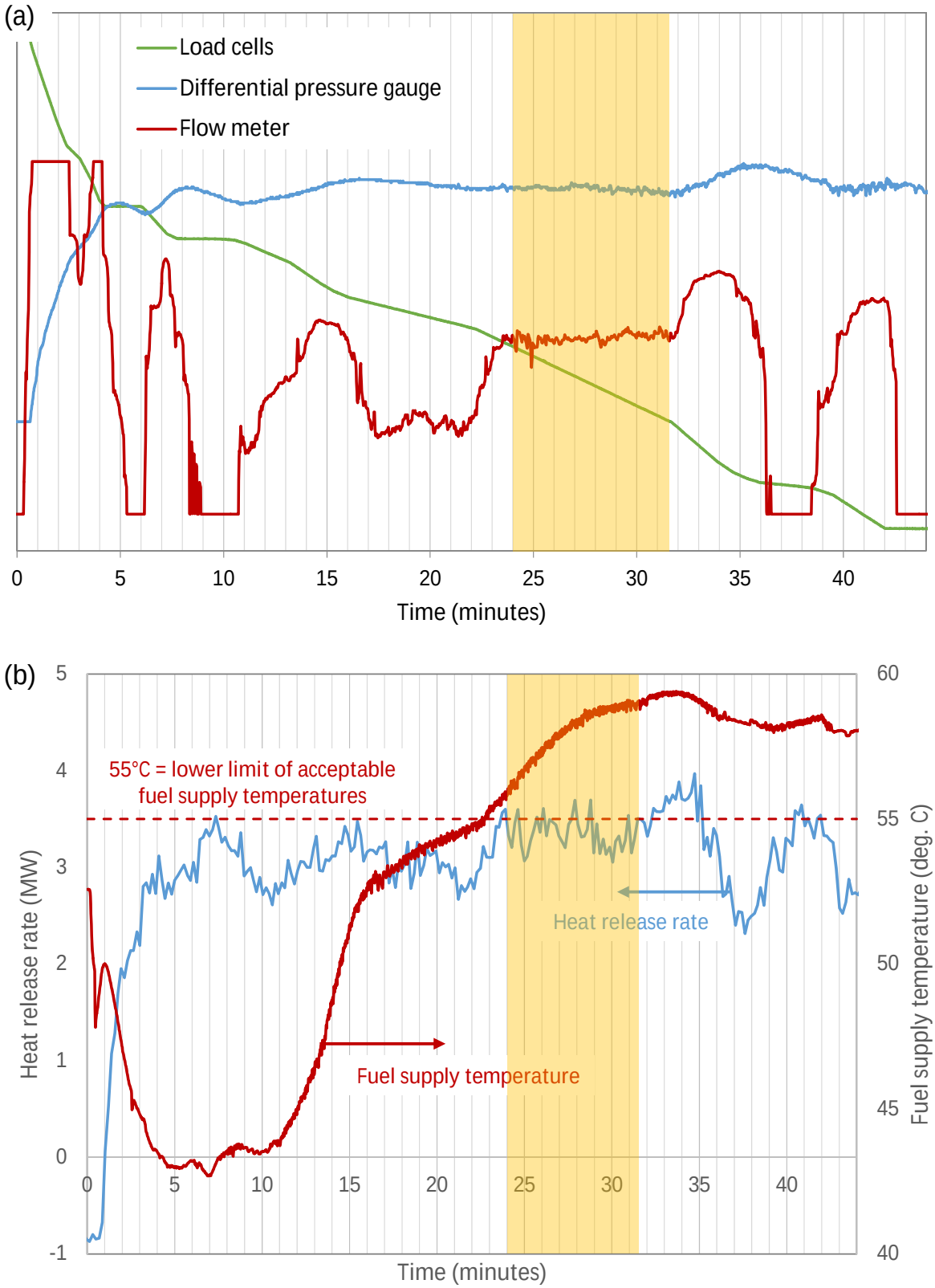

Figure 1: Selection of time-averaging period for Test 2.4 (axes not shown in (a) for simplicity)

Table 4 shows the time periods selected in this manner for all Series 1 and 2 tests.

Table 4: Selected Series 1 and 2 time-averaging periods used in the present analysis

Test	Time-averaging period (minutes)	Duration (minutes)
1.1	10-35	25
1.2	10-35	25
1.3	24-40	16
2.1	22-34	12
2.2	25-40	15
2.3	10-30	20
2.4	24-31.5	7.5
2.5	15-34	19
2.6	12-30	18

Table 5 compares the duration of the time periods in Table 4 to the duration of the time periods used by Luketa [2] in Table 3. For Tests 1.1, 1.2, 2.5 and 2.6, the durations in Table 4 are generally longer than those in Table 3. On the other hand, for Tests 1.3, 2.1, 2.2, 2.3 and 2.4, the opposite is true (with the general exception of flame height).

Table 5: Comparison of durations (in minutes) of selected time periods from Table 4 with those from Table 3

Test	Table 4	Table 3						
		Fuel temp	Burning rate	Radiometers	Plume temps	Heat release rate	Flame height	DFTs
1.1	25	25	32.4	10	15	10	10	15
1.2	25	25	36	20	17	10	n/a	17
1.3	16	20	20	20	24	20	n/a	20
2.1	12	30	14	20	20	10	10	17
2.2	15	30	16	30	30	15	10	20
2.3	20	20	32	20	20	20	10	13
2.4	7.5	19	8	19	19	19	10	20
2.5	19	25	15	15	15	10	10	13
2.6	18	n/a	36	15	10	15	10	21

3.2 Series 3 (Dilbit)

For Series 3 tests, the majority of the analysis in Luketa [2], and subsequently in Ko [1], was based on values calculated by integrating the data from 0 to 25 minutes and then dividing by 25 minutes. This method was selected because none of the fires clearly exhibited steady burning behaviour. Because the fuel burning rate changed throughout the test, it was also difficult to maintain a constant fuel level through manual valve control of the fuel feed (as discussed in Section 2). Thus, due to the variability in the measurements and the likelihood of variation in the fuel level, Luketa [2] selected to compare all data equally from 0 to 25 minutes in each test.

Note that this period includes the period of fire growth immediately after ignition (which typically lasted approximately 2 minutes).

In the present work, attempts were made to identify shorter periods for time-averaging the data from each test, which would not only allow for comparison to the 25-minute integrated values from Luketa [2], but also permit quantification and analysis of the changes in burning behaviour. Overall, the dilbit fires exhibited at least three periods in which the fire parameters (e.g. flame height, plume temperatures, heat flux to the radiometers) were distinctly different. This was potentially due to differences in the composition of the dilbit (a blended mixture of condensate diluent, with light constituents, and bitumen, with heavy constituents) versus the Bakken (a light sweet crude oil), such that initial preferential burning of the diluent and other distillation-type effects may result in more distinct changes in the measured parameters with time. Periods for analysis were selected using the following criteria:

(1) steady readings from the differential pressure gauge in the fuel pan (note that the gauge started to fail typically around 20 minutes into each test, except in Test 3.4 where it lasted approximately 40 minutes, so no data was available past this point),
(2) a steady decrease in measurements from the load cell measuring the weight of the dilbit tank, and
(3) a constant trend (i.e. neither increasing nor decreasing) in temperatures measured by the thermocouples located along the axis of the fire plume.

Periods during which the first two criteria were met indicate periods in which the fuel was pumped into the pan at a rate equivalent to the burning rate (see Section 3.1 for further explanation). After the pressure gauge failed, the second criterion was used with the assumption that the fuel level was constant. The third criterion indicates that the overall fire characteristics were steady; note that heat release rate could not be used as the preferred indicator, as in Series 1 and 2, because of equipment failure in all but one of the Series 3 tests.

Because of the difficulty in maintaining a constant fuel level, only short periods (typically between 2 and 5 minutes; see Table 6) could be identified for analysis. Maintenance of the fuel supply temperature within the required test conditions of 20 ± 5°C or 60 ± 5°C (the fourth criterion discussed in Section 3.1) was not strictly applied to Series 3 tests, due to the inherent difficulty in meeting the other three criteria. For each of the selected time periods, the average fuel temperature did not deviate outside the desired test conditions by more than 1°C (see Section 4.3, Table 31).

Figure 2 shows Test 3.5 as an example. The plot in Figure 2a shows measurements from the differential pressure gauge and load cell, while the plot in Figure 2b shows measurements from the thermocouples located in the fire plume. For the periods 3-10 minutes, 16-19.5 minutes, and 27.5-30.5 minutes (all shaded in yellow), the plume temperatures were relatively constant and the load cell measurements decreased steadily. The pressure gauge readings were also constant during the first two time periods, prior to gauge failure. These three time periods were therefore selected for averaging all other measured data in the test.

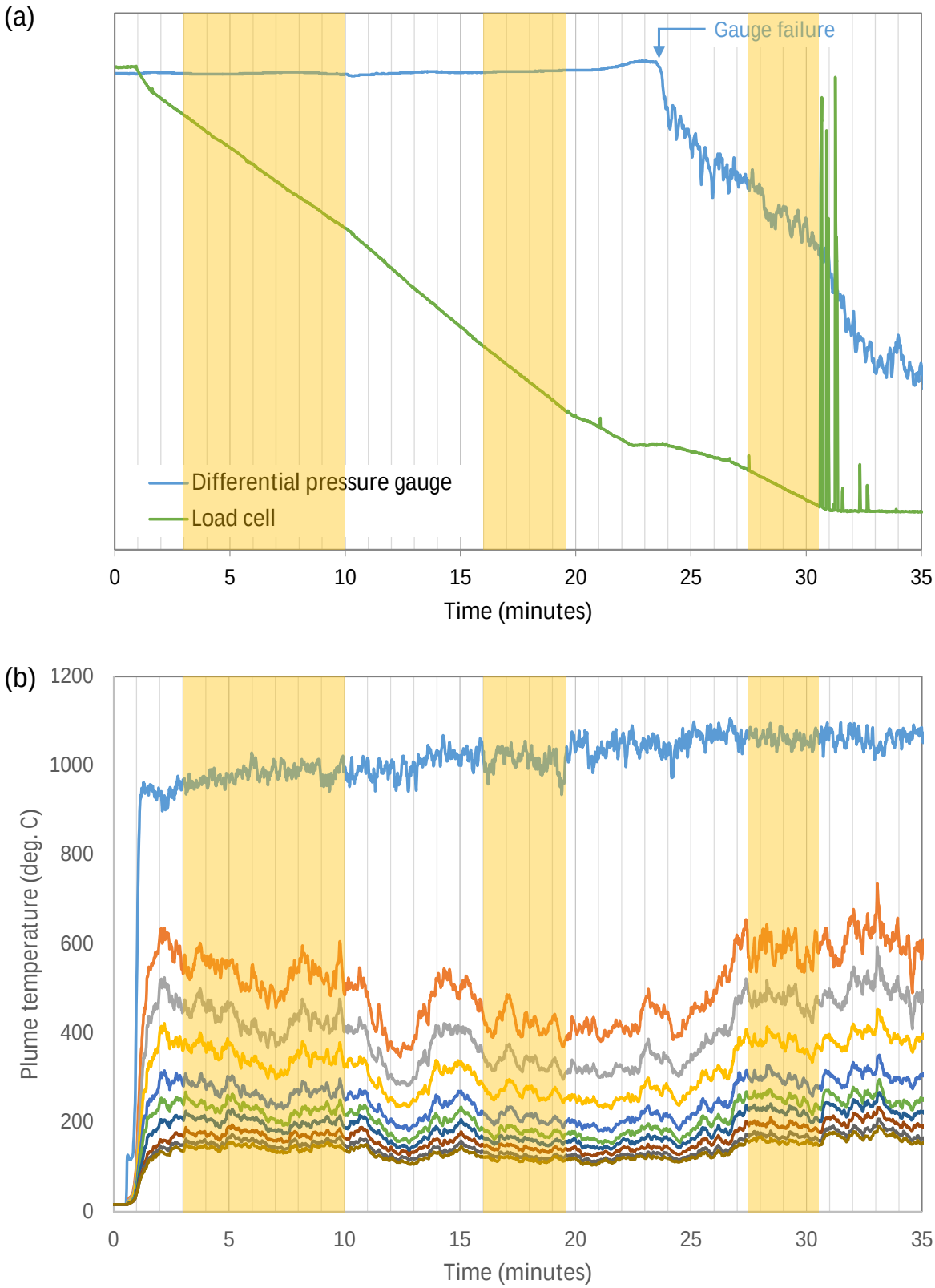

Figure 2: Selection of time-averaging periods for Test 3.5 (axes not shown in (a), legend not shown in (b) for simplicity)

Table 6 shows the time periods identified for the Series 3 tests. All of the selected periods occurred prior to the introduction of Jet A fuel into the pan (Section 2).

Table 6: Selected Series 3 time-averaging periods used in the present analysis

Test	Time-averaging period (minutes)	Duration (minutes)
3.1	3-5	2
	8-11	3
	16.5-18	1.5
3.2	11.9-12.7	0.8
	15-17	2
	18.6-23.5	4.9
3.3	3-5	2
	8-10	2
	12-19	7
	25-28	3
3.4	2-15	13
	18.5-22	3.5
	26-30	4
	30.5-34	3.5
3.5	3-10	7
	16-19.5	3.5
	27.5-30.5	3
3.6	4-6	2
	14.6-20	5.4
	25-29.6	4.6

4 Time-Averaged Results

This section presents the time-averaged results calculated using the time-averaging periods selected in the previous section. General notes relating to the presentation of the results are as follows:

- All average values are reported with a range of one standard deviation.
- For the sake of brevity, polar plots of the temperature and heat flux data from the calorimeter are not presented in this section, but are instead included in Appendix A. Selected polar plots will be used to support the discussion in Section 7.
- Measurement locations on the calorimeter are denoted using a letter followed by a number. The letter denotes the left (L), centre (C) or right (R) measurement plane, while the number denotes the angle in degrees along the plane (with 0 referring to the top of the calorimeter). See Appendix A for further description of the calorimeter.

It should be noted that there was an error in Sandia's processing of the heat release rate data, which was identified only after completion of the Sandia report [2]. In Sandia's analysis, the heat release rate data was assumed to be recorded consistently every 10 seconds. However, examination of the time-stamps associated with each data point revealed that the time interval between consecutive data points varied, usually between 10 and 12 seconds. This therefore affects the accuracy of the time-averaging periods used by Sandia and the associated time-averaged results (up to 5% difference). In this section, time-averaged heat release rates are compared between the present analysis and Sandia's analysis. The averages from Sandia's analysis were taken directly from Luketa [2] (with incorrect time intervals and time-averaging periods), whereas the averages from the present analysis were based on the corrected time intervals. The corrected time intervals were verified by ensuring that the initial increase, final decay and other significant changes in the heat release rate occurred at the same time as in the plume temperature time traces.

4.1 Series 1 (Heptane)

The following tables show, for Series 1 tests calculated using the periods identified in Table 4, time-averaged values for the fuel supply temperature (Table 7), burning rate (Table 8), heat release rate (Table 9), flame height (Table 10), plume axis temperatures (Table 11), and heat flux to the narrow-view (Table 12) and wide-view (Table 13) radiometers. The differences between these values and those presented in Luketa [2] are also provided. Overall, for these parameters, none of the differences was greater than 3%, indicating that for Tests 1.1 and 1.2, the effect of using a longer time-averaging period (Table 5) was minimal. For Test 1.3, there was only a 4-minute difference between the time-averaging periods (24-40 min instead of 24-44 min), so only small differences would be expected between the different analyses.

Table 7: Time-averaged values for fuel supply temperature, Series 1

Test	Present analysis		Sandia analysis [2]		Percent difference
	Time period (min)	°C	Time period (min)	°C	
1.1	10-35	22.3 ± 0.2	10-35	22.3 ± 0.2	equivalent
1.2	10-35	24.2 ± 0.3	10-35	24.2 ± 0.3	equivalent
1.3	24-40	57.6 ± 0.4	24-44	57.7 ± 0.4	-0.1%

Table 8: Time-averaged values for burning rate, Series 1

Test	Present analysis			Sandia analysis [2]			Percent difference[a]
	Time period (min)	mm/min	kg/m^{2}s	Time period (min)	mm/min	kg/m^{2}s	
1.1	10-35	3.24 ± 0.04	0.037 ± 0.000	0-32.4	3.21 ± 0.04	0.037 ± 0.000	0.8%
1.2	10-35	3.57 ± 0.04	0.041 ± 0.000	0-36	3.51 ± 0.04	0.040 ± 0.000	1.6%
1.3	24-40	3.53 ± 0.04	0.040 ± 0.000	24-44	3.49 ± 0.04	0.040 ± 0.000	1.1%

[a] Equivalent for both mm/min and kg/m^{2}s values.

Table 9: Time-averaged values for heat release rate (by oxygen consumption calorimetry), Series 1

Test	Present analysis		Sandia analysis [2]		Percent difference
	Time period (min)	MW	Time period (min)	MW	
1.1	10-35	4.4 ± 0.2	20-30	4.4 ± 0.2	-0.4%
1.2	10-35	5.2 ± 0.2	20-30	5.2 ± 0.2	-0.8%
1.3	24-40	5.2 ± 0.2	24-44	5.4 ± 0.3	-2.4%

Table 10: Time-averaged values for flame height, Series 1

Test	Present analysis		Sandia analysis [2]		Percent difference
	Time period (min)	m	Time period (min)	m	
1.1	10-35	5.8 ± 0.9	10-20	5.7 ± 0.9	1.8%
1.2 and 1.3	Comparison was not made because these two tests used a different method to estimate flame height than all other tests. In Tests 1.2 and 1.3, a single time-averaged video image was compared to a stadia board to estimate the flame height, whereas in all other tests, a time history of flame height was obtained for the entire fire duration by analysing each instantaneous image taken by the infrared camera, with the values subsequently averaged over a selected time period [2].				

Table 11: Time-averaged values for temperatures from thermocouple rake in fire plume, Series 1

Test	Height (m)	Present analysis		Sandia analysis [2]		Percent difference
		Time period (min)	°C	Time period (min)	°C	
1.1	0.5	10-35	719.8 ± 41.4	20-35	719.1 ± 50.1	0.1%
	1.5		876.4 ± 20.4		878.3 ± 20.7	-0.2%
	2		793.1 ± 31.2		798.6 ± 30.3	-0.7%
	2.5		732.3 ± 33.6		739.2 ± 32.8	-0.9%
	3		645.2 ± 32.1		652.1 ± 31.4	-1.1%
	3.5		583.7 ± 31.6		590.8 ± 29.2	-1.2%
	4		548.6 ± 30.7		557.5 ± 26.7	-1.6%
	4.5		483.9 ± 27.9		492.8 ± 23.7	-1.8%
	5		420.2 ± 24.1		428.4 ± 20.2	-1.9%
	5.5		396.0 ± 26.4		403.6 ± 23.2	-1.9%
1.2	1.5	10-35	849.2 ± 12.2	20-37	848.2 ± 12.5	0.1%
	2		885.6 ± 15.4		885.7 ± 14.8[a]	0.0%
	2.5		895.4 ± 18.3		897.4 ± 15.5	-0.2%
	3		877.2 ± 25.0		881.3 ± 21.0	-0.5%
	3.5		846.5 ± 33.4		854.5 ± 27.8	-0.9%
	4		812.7 ± 39.9		824.9 ± 32.2	-1.5%
	4.5		741.6 ± 41.7		756.7 ± 34.0	-2.0%
	5		661.6 ± 41.1		679.3 ± 31.7	-2.6%
	5.5		602.7 ± 45.1		620.3 ± 37.1	-2.8%
1.3	0.5	24-40	661.2 ± 19.8	20-44	660.0 ± 19.9	0.2%
	1.5		877.0 ± 18.4		877.4 ± 18.1	0.0%
	2		832.8 ± 27.8		835.4 ± 27.7	-0.3%
	2.5		768.7 ± 32.0		771.5 ± 31.4	-0.4%
	3		695.0 ± 29.5		698.0 ± 29.9	-0.4%
	3.5		623.1 ± 34.3		625.6 ± 33.8	-0.4%
	4		589.3 ± 33.4		591.1 ± 33.2	-0.3%
	4.5		530.1 ± 29.8		530.7 ± 29.0	-0.1%
	5		460.3 ± 24.3		460.0 ± 24.2	0.1%
	5.5		429.6 ± 28.0		428.7 ± 28.0	0.2%

[a] Value in Table 7-13 of Luketa [2] for standard deviation is incorrect.

Table 12: Time-averaged values for heat flux to narrow-view radiometers, Series 1

Test	Height (m)	Present analysis		Sandia analysis [2]		Percent difference
		Time period (min)	kW/m^2	Time period (min)	kW/m^2	
1.1	0.5	10-35	89.0 ± 6.0	20-30	89.1 ± 5.8	-0.2%
	1		93.0 ± 8.0		93.1 ± 7.7	-0.1%
	1.5		91.5 ± 14.1		91.3 ± 13.6	0.2%
	2		77.2 ± 17.1		77.4 ± 16.5	-0.2%
	3		46.8 ± 17.8		47.6 ± 17.3	-1.8%
	4		32.7 ± 18.5		33.8 ± 17.9	-3.0%
1.2	0.5	10-35	94.7 ± 12.5	15-35	94.7 ± 12.4	0.0%
	1		84.8 ± 15.6		84.8 ± 15.3	0.0%
	1.5		84.7 ± 17.5		84.4 ± 17.0	0.4%
	2		81.3 ± 18.2		80.9 ± 17.5	0.5%
	3		70.7 ± 21.1		70.4 ± 20.9	0.4%
	4		61.4 ± 27.1		61.6 ± 26.5	-0.4%
1.3	0.5	24-40	88.9 ± 6.6	24-44	88.9 ± 6.5	0.0%
	1		92.2 ± 7.9		92.1 ± 7.8	0.1%
	1.5		96.6 ± 13.4		96.4 ± 13.3	0.2%
	2		85.2 ± 17.9		85.1 ± 17.7	0.2%
	3		53.8 ± 19.2		53.9 ± 19.0	-0.1%
	4		38.5 ± 20.3		38.8 ± 20.3	-0.8%

Table 13: Time-averaged values for heat flux to wide-view radiometers, Series 1

Test	Height (m)	Present analysis		Sandia analysis [2]		Percent difference
		Time period (min)	kW/m^2	Time period (min)	kW/m^2	
1.1	1	10-35	2.3 ± 0.2	20-30	2.3 ± 0.2	-0.9%
	1.5		2.9 ± 0.2		2.9 ± 0.2	-1.0%
	2		2.5 ± 0.2		2.5 ± 0.2	-1.1%
	3		2.5 ± 0.2		2.5 ± 0.2	-1.0%
	4		2.2 ± 0.2		2.3 ± 0.2	-1.3%
1.2	1	10-35	2.5 ± 0.3	15-35	2.5 ± 0.3	0.2%
	1.5		3.1 ± 0.2		3.1 ± 0.2	-0.2%
	2		2.7 ± 0.3		2.7 ± 0.3	-0.1%
	3		2.7 ± 0.3		2.7 ± 0.3	0.0%
	4		2.6 ± 0.3		2.6 ± 0.3	-0.3%
1.3	1	24-40	2.4 ± 0.2	24-44	2.4 ± 0.2	-0.4%
	1.5		2.9 ± 0.2		3.0 ± 0.2	-0.3%
	2		2.6 ± 0.2		2.6 ± 0.2	-0.3%
	3		2.6 ± 0.2		2.6 ± 0.2	-0.4%
	4		2.3 ± 0.2		2.4 ± 0.3	-0.7%

During review of Sandia's results, it was noticed that the method used to calculate total heat flux to the DFTs (which measure temperature data) was different among Series 1, 2 and 3 tests. Reasons for the different calculation methods were unclear, and, upon discussion with Sandia, were unable to be verified given the length of time which had passed since Series 1 and 2 tests were conducted. As a result, in the present analysis, it was selected to reprocess the Series 1 and 2 DFT data using the same method as in Series 3, thereby providing a consistent basis for comparison between all test series. Note that the absorbed heat flux values were unaffected.

In comparing Series 1 and 3, the main difference in the DFT heat flux calculation method was the use of different values for the convection coefficient, *h* [4]. A higher convection coefficient implies greater convection to the DFT, which would occur with higher velocity gases flowing past the DFT surface. Because velocities were not measured in the region near the DFTs, a value for the convection coefficient must be assumed. Table 14 shows that, without changing the time averaging period, the total heat flux values were approximately 30% to 40% lower when calculated using a convection coefficient of 10 W/m^{2}K (as per Series 3), instead of 30 W/m^{2}K (as originally used for Series 1).

Table 14: Time-averaged values for total heat flux to DFTs, Series 1

Test	Distance from pool centre (m)	Sandia analysis [2] (h=30 W/m^{2}K)		Using same method as Series 3 (h=10 W/m^{2}K)			Present analysis, using same method as Series 3 (h=10 W/m^{2}K)		
		Time period (min)	kW/m^2	Time period (min)	kW/m^2	Percent difference from [2]	Time period (min)	kW/m^2	Percent difference from [2]
1.1	2	20-35	39.4 ± 1.2	20-35	27.5 ± 1.2	-30%	10-35	27.7 ± 1.3	-30%
	4		18.2 ± 0.5		11.0 ± 0.5	-40%		11.1 ± 0.5	-39%
1.2	2	20-37	35.6[a] ± 1.0	20-37	24.4 ± 1.0	-32%	10-35	24.4 ± 1.1	-31%
	4		15.1 ± 0.4		8.8 ± 0.4	-42%		8.8 ± 0.4	-41%
1.3	2	24-44	44.2 ± 1.1	24-44	31.5 ± 1.1	-29%	24-40	31.5 ± 1.1	-29%
	4		17.8 ± 0.5		10.7 ± 0.5	-40%		10.7 ± 0.5	-40%

[a] An average value of 35.5 kW/m^2 was reported in Table 7-19 of Luketa [2], which differs slightly from the value of 35.6 kW/m^2 averaged directly from the data. This difference is minimal and assumed to be due to rounding error.

The rightmost three columns of Table 14 show that use of the time averaging periods identified in Table 4 had minimal additional effect on the DFT total heat flux values, since the percent differences were approximately -30% to -40%, similar to the percent differences calculated previously. This is therefore consistent with Tables 8-13 for the measurement parameters discussed earlier, which showed only small differences resulting from the use of the time periods in Table 4.

Tables 15-17 show the time-averaged values, based on Table 4 time intervals, for total heat flux to the calorimeter, temperatures exterior to the calorimeter, and temperatures on the outer cylinder of the calorimeter. Comparison to the corresponding values in Luketa [2] indicated differences of less than 4%, consistent with the other parameters discussed above.

Table 15: Time-averaged values for total heat flux to calorimeter, Series 1

Test	Location	Present analysis		Sandia analysis [2]		Percent difference
		Time period (min)	kW/m²	Time period (min)	kW/m²	
1.1	L0[a]	10-35	12.9 ± 2.0	20-35	12.7 ± 1.8	1.7%
	L45		82.4 ± 1.7		82.8 ± 1.6	-0.4%
	L90		52.8 ± 2.0		52.9 ± 2.0	-0.1%
	L135		54.4 ± 3.3		53.6 ± 3.0	1.4%
	L180		63.3 ± 6.7		62.7 ± 6.3	1.0%
	L225		69.6 ± 4.2		70.9 ± 4.1	-1.9%
	L270[a]		10.2 ± 1.7		10.3 ± 1.6	-1.7%
	L315[b]		n/a		n/a	n/a
	C0		64.9 ± 3.8		62.5 ± 2.1	3.8%
	C45		68.7 ± 2.6		67.5 ± 2.3	1.8%
	C90		57.3 ± 1.4		56.7 ± 1.0	1.2%
	C135		57.7 ± 2.0		56.8 ± 1.2	1.6%
	C180		63.5 ± 3.4		62.2 ± 3.0	2.1%
	C225		63.6 ± 2.2		63.0 ± 2.1	0.9%
	C270		56.3 ± 1.5		55.7 ± 1.0	1.2%
	C315		58.8 ± 3.2		56.9 ± 1.7	3.4%
	R0		64.1 ± 4.7		64.3 ± 4.7	-0.2%
	R45		69.1 ± 2.6		68.8 ± 2.6	0.5%
	R90		58.5 ± 2.2		58.4 ± 1.9	0.0%
	R135		64.4 ± 2.1		63.9 ± 1.8	0.7%
	R180[b]		n/a		n/a	n/a
	R225		69.2 ± 4.2		68.6 ± 4.7	0.8%
	R270		57.2 ± 3.7		58.2 ± 3.0	-1.7%
	R315		55.7 ± 4.5		56.2 ± 4.2	-1.0%

Table 15: Time-averaged values for total heat flux to calorimeter, Series 1

Test	Location	Present analysis		Sandia analysis [2]		Percent difference
		Time period (min)	kW/m²	Time period (min)	kW/m²	
1.3	L0	24-40	67.5 ± 5.5	24-44	67.7 ± 5.7	-0.3%
	L45		79.2 ± 2.9		79.5 ± 3.0	-0.3%
	L90		54.0 ± 2.0		54.2 ± 2.0	-0.2%
	L135		57.1 ± 4.6		57.0 ± 4.7	0.1%
	L180		69.8 ± 8.8		69.7 ± 8.8	0.1%
	L225		72.3 ± 4.2		72.5 ± 4.1	-0.3%
	L270[a]		13.6 ± 1.8		13.6 ± 2.0	0.5%
	L315[b]		n/a		n/a	n/a
	C0		76.1 ± 2.8		75.9 ± 2.9	0.3%
	C45		76.5 ± 4.8		76.4 ± 4.8	0.2%
	C90		58.0 ± 1.9		57.9 ± 1.8	0.1%
	C135		53.8 ± 1.8		53.6 ± 1.7	0.3%
	C180		55.5 ± 4.0		55.1 ± 3.9	0.7%
	C225[c]	25-40	62.2 ± 5.2	25-44	62.0 ± 4.9	0.4%
	C270	24-40	56.7 ± 1.8	24-44	56.5 ± 1.7	0.4%
	C315[a]		14.5 ± 1.7		14.3 ± 1.6	1.1%
	R0		68.8 ± 5.5		68.5 ± 5.4	0.4%
	R45		72.8 ± 2.0		72.5 ± 2.1	0.4%
	R90		54.9 ± 2.4		54.5 ± 2.5	0.7%
	R135		61.6 ± 2.8		61.2 ± 2.8	0.7%
	R180[b]		n/a		n/a	n/a
	R225		63.2 ± 6.5		62.9 ± 6.4	0.5%
	R270		55.8 ± 4.7		55.5 ± 4.6	0.6%
	R315		54.9 ± 5.7		54.5 ± 5.6	0.7%

[a] Although this location was included in the spatially averaged total heat flux reported in Table 7-22 of Luketa [2], it is not considered to show a realistic value and is thus neglected in the present analysis.

[b] No reliable data was available at this location due to faulty thermocouple readings.

[c] The averaging time period for this location was selected to start at 25 min due to excessive noise in the thermocouple readings between 24 and 25 min.

Table 16: Time-averaged temperature values from thermocouples exterior to calorimeter, Series 1

Test	Location	Present analysis		Sandia analysis [2][a]		Percent difference
		Time period (min)	°C	Time period (min)	°C	
1.1	L0	10-35	893.2 ± 17.9	20-35	898.8 ± 14.8	-0.6%
	L45		946.4 ± 5.7		948.0 ± 5.0	-0.2%
	L90		834.4 ± 15.3		831.7 ± 14.7	0.3%
	L135		805.8 ± 16.6		800.5 ± 14.4	0.7%
	L180		867.5 ± 14.1		864.7 ± 13.4	0.3%
	L225		891.5 ± 12.1		896.9 ± 10.4	-0.6%
	L270		867.0 ± 16.5		874.4 ± 13.7	-0.8%
	L315		819.2 ± 19.5		828.3 ± 14.6	-1.1%
	C0[b]		n/a		n/a	n/a
	C45		880.4 ± 13.8		873.7 ± 9.8	0.8%
	C90		821.8 ± 9.8		817.8 ± 8.4	0.5%
	C135		806.1 ± 13.3		800.3 ± 10.4	0.7%
	C180		817.2 ± 17.9		809.6 ± 13.8	0.9%
	C225		843.8 ± 16.1		837.6 ± 13.3	0.7%
	C270		872.1 ± 16.3		868.5 ± 15.7	0.4%
	C315		912.8 ± 14.4		909.8 ± 14.2	0.3%
	R0		876.0 ± 20.8		879.8 ± 19.8	-0.4%
	R45[b]		n/a		n/a	n/a
	R90		899.1 ± 16.2		900.5 ± 16.1	-0.2%
	R135		873.3 ± 16.8		872.1 ± 16.3	0.1%
	R180[b]		n/a		n/a	n/a
	R225		898.6 ± 9.5		900.7 ± 8.8	-0.2%
	R270[b]		n/a		n/a	n/a
	R315		856.5 ± 19.2		860.6 ± 18.0	-0.5%

Table 16: Time-averaged temperature values from thermocouples exterior to calorimeter, Series 1

Test	Location	Present analysis		Sandia analysis [2][a]		Percent difference
		Time period (min)	°C	Time period (min)	°C	
1.3	L0	24-40	845.1 ± 24.8	24-44	846.5 ± 25.4	-0.2%
	L45		917.2 ± 9.8		918.2 ± 10.4	-0.1%
	L90		839.5 ± 15.7		840.1 ± 16.1	-0.1%
	L135		815.6 ± 17.6		816.5 ± 19.0	-0.1%
	L180		878.5 ± 17.7		878.3 ± 17.3	0.0%
	L225		906.8 ± 9.6		907.7 ± 9.7	-0.1%
	L270		868.4 ± 14.2		870.1 ± 15.1	-0.2%
	L315		824.0 ± 22.8		826.3 ± 23.7	-0.3%
	C0[b]		n/a		n/a	n/a
	C45		880.9 ± 9.6		879.8 ± 10.0	0.1%
	C90		808.5 ± 5.4		807.6 ± 5.7	0.1%
	C135		796.3 ± 10.1		795.2 ± 10.0	0.1%
	C180		819.1 ± 15.9		817.9 ± 15.2	0.1%
	C225		846.5 ± 13.8		846.0 ± 13.0	0.1%
	C270		883.3 ± 16.6		883.4 ± 16.2	0.0%
	C315		921.2 ± 14.1		921.2 ± 13.8	0.0%
	R0		870.8 ± 27.3		870.1 ± 26.9	0.1%
	R45[b]		n/a		n/a	n/a
	R90		860.9 ± 19.0		858.6 ± 20.0	0.3%
	R135		834.2 ± 23.8		831.0 ± 24.8	0.4%
	R180[c]		21.3 ± 0.2		21.3 ± 0.1	0.0%
	R225		859.1 ± 12.8		857.8 ± 12.8	0.2%
	R270[b]		n/a		n/a	n/a
	R315		838.9 ± 24.2		837.7 ± 24.1	0.1%

[a] The thermocouple locations used to produce Figure 8-28 of Luketa [2] contain errors in all tests and are shown corrected in this table.

[b] No reliable data was available at this location due to faulty thermocouple readings.

[c] Although this location was included in the spatially averaged exterior cylinder temperature reported in Table 7-22 of Luketa [2], it is not considered to show a realistic value and is thus neglected in the present analysis.

Table 17: Time-averaged temperature values from thermocouples on outer cylinder of calorimeter, Series 1

Test	Location	Present analysis		Sandia analysis [2][a]		Percent difference
		Time period (min)	°C	Time period (min)	°C	
1.1	L0[b]	10-35	n/a	20-35	n/a	n/a
	L45		875.2 ± 5.7		878.4 ± 1.8	-0.4%
	L90		751.7 ± 3.4		752.8 ± 2.4	-0.2%
	L135		762.8 ± 7.4		758.1 ± 2.8	0.6%
	L180		802.3 ± 8.6		797.5 ± 4.7	0.6%
	L225		824.5 ± 12.2		832.0 ± 5.3	-0.9%
	L270[b]		n/a		n/a	n/a
	L315		784.2 ± 12.7		792.0 ± 4.9	-1.0%
	C0		812.6 ± 15.1		802.1 ± 6.5	1.3%
	C45		826.3 ± 6.8		821.7 ± 4.1	0.6%
	C90		776.5 ± 3.0		774.5 ± 2.0	0.3%
	C135		779.9 ± 8.2		774.8 ± 1.7	0.7%
	C180		805.7 ± 9.5		800.3 ± 5.7	0.7%
	C225		804.1 ± 3.5		803.6 ± 4.1	0.1%
	C270		771.4 ± 3.0		769.7 ± 2.0	0.2%
	C315		784.9 ± 12.0		776.5 ± 5.7	1.1%
	R0		803.8 ± 7.1		806.0 ± 5.5	-0.3%
	R45		826.3 ± 3.1		825.9 ± 2.8	0.0%
	R90		779.9 ± 5.1		782.0 ± 2.5	-0.3%
	R135		807.3 ± 2.7		806.0 ± 2.5	0.2%
	R180[b]		n/a		n/a	n/a
	R225		825.5 ± 7.4		826.4 ± 7.3	-0.1%
	R270		770.7 ± 16.3		780.5 ± 2.8	-1.3%
	R315		764.8 ± 10.3		769.9 ± 4.5	-0.7%

Table 17: Time-averaged temperature values from thermocouples on outer cylinder of calorimeter, Series 1

Test	Location	Present analysis		Sandia analysis [2][a]		Percent difference
		Time period (min)	°C	Time period (min)	°C	
1.3	L0	24-40	821.2 ± 4.5	24-44	821.8 ± 4.6	-0.1%
	L45		865.9 ± 2.5		866.5 ± 2.8	-0.1%
	L90		760.1 ± 2.5		760.7 ± 2.7	-0.1%
	L135		774.6 ± 4.2		774.4 ± 4.0	0.0%
	L180		827.9 ± 7.6		828.3 ± 7.2	0.0%
	L225		838.5 ± 4.8		839.9 ± 5.2	-0.2%
	L270[c]		458.4 ± 1.6		458.6 ± 1.6	0.0%
	L315		774.8 ± 4.7		775.4 ± 4.6	-0.1%
	C0		855.8 ± 1.7		855.0 ± 2.4	0.1%
	C45		857.2 ± 3.3		856.5 ± 3.7	0.1%
	C90		779.9 ± 1.4		779.9 ± 1.4	0.0%
	C135		760.4 ± 2.2		759.9 ± 2.3	0.1%
	C180		768.7 ± 5.1		767.4 ± 5.3	0.2%
	C225[d]	25-40	799.0 ± 5.4		792.9 ± 39.5	0.8%
	C270	24-40	773.4 ± 2.2		772.6 ± 2.5	0.1%
	C315[c]		472.9 ± 2.1		472.4 ± 2.2	0.1%
	R0		825.3 ± 5.3		825.1 ± 4.9	0.0%
	R45		842.0 ± 1.7		841.4 ± 2.1	0.1%
	R90		767.0 ± 4.7		765.4 ± 5.3	0.2%
	R135		797.1 ± 4.1		795.4 ± 5.1	0.2%
	R180[b]		n/a		n/a	n/a
	R225		803.7 ± 6.1		802.0 ± 6.6	0.2%
	R270		769.4 ± 4.4		768.2 ± 4.8	0.2%
	R315		764.5 ± 6.1		763.5 ± 5.9	0.1%

[a] The thermocouple locations used to produce Figure 8-25 of Luketa [2] contain errors in all tests and are shown corrected in this table.

[b] No reliable data was available at this location due to faulty thermocouple readings.

[c] Although this location was included in the spatially averaged outer cylinder temperature reported in Table 7-22 of Luketa [2], it is not considered to show a realistic value and is thus neglected in the present analysis.

[d] In the present analysis, the averaging time period for this location was selected to start at 25 min due to excessive noise in the thermocouple readings between 24 and 25 min. However, in Luketa [2], the averaging time period started at 24 min, resulting in a much larger standard deviation.

Luketa [2] reported overall values of heat flux, temperature exterior to the calorimeter, and outer cylinder temperature that were averaged across all measurement locations on the calorimeter. For comparison, spatially averaged values were also calculated in the present analysis, using the adjusted time periods in Table 4 and neglecting the locations that were not considered to show realistic values (as per the footnotes in Tables 15-17). As shown in Table 18, there were differences of 8-9% in total heat flux and up to 5% in the exterior and outer cylinder temperatures. This is considered reasonable given that the number of neglected locations was not the same between the two analyses.

Table 18: Comparison of spatially averaged temperature and heat flux values among all calorimeter thermocouple locations, Series 1

Test	Parameter	Present analysis	Neglected locations in present analysis	Sandia analysis [2], Table 7-22	Neglected locations in Sandia analysis	Percent difference
1.1	Outer cylinder temperature (°C)	797.2 ± 7.8	L0, L270, R180	796.7 ± 3.9	L0, L270, R180	0.1%
	Exterior cylinder temperature (°C)	864.1 ± 15.1	C0, R45, R180, R270	863.7 ± 13.3	C0, R45, R180, R270	0.0%
	Total heat flux (kW/m^2)	62.6 ± 3.1	L0, L270, L315, R180	57.5 ± 2.6	L315, R180	8.8%
1.3	Outer cylinder temperature (°C)	801.3 ± 4.0	L270, C315, R180	771.4 ± 5.5	R180	3.9%
	Exterior cylinder temperature (°C)	855.7 ± 16.2	C0, R45, R180, R270	815.8 ± 15.7	C0, R45, R270	4.9%
	Total heat flux (kW/m^2)	63.5 ± 4.0	L270, L315, C315, R180	58.9 ± 3.8	L315, R180	7.9%

4.2 Series 2 (Bakken)

The following tables show, for Series 2 tests calculated using the periods identified in Table 4, time-averaged values for the fuel supply temperature (Table 19), burning rate (Table 20), heat release rate (Table 21), flame height (Table 22), plume axis temperatures (Table 23), and heat flux to the narrow-view (Table 24) and wide-view (Table 25) radiometers. The differences between these values and those presented in Luketa [2] are also provided.

Overall, the differences were reasonably small, within 3% for the fuel supply temperature, 0.2% for the burning rate, 5% for the heat release rate, 6% for the flame height, 7% for the plume temperatures, and 5% for the wide-view radiometers. The differences for the narrow-view radiometers (Table 24) were more variable, up to 15% in Test 2.4 and 19% in Test 2.6 (as opposed to within 4% in the other four tests). These larger differences reflected the presence of significant fluctuations in the fire behaviour between 31.5 and 42 minutes in Test 2.4 (due to changes in the fuel feed rate; see Figure 1a), and the beginning of decay of the fire after 30 minutes in Test 2.6.

Table 19: Time-averaged values for fuel supply temperature, Series 2

Test	Present analysis		Sandia analysis [2]		Percent difference
	Time period (min)	°C	Time period (min)	°C	
2.1	22-34	21.6 ± 0.2	5-35	21.0 ± 0.9	2.9%
2.2	25-40	21.3 ± 0.2	10-40	21.7 ± 0.5	-1.7%
2.3	10-30	equivalent to [2]	10-30	22.2 ± 0.5	n/a
2.4	24-31.5	58.0 ± 0.9	23-42	58.2 ± 1.0	-0.5%
2.5	15-34	21.4 ± 0.6	10-35	21.3 ± 0.6	0.6%
2.6	pan pre-filled	equivalent to [2]	0-4.63	20.0 ± 1.7	n/a

Table 20: Time-averaged values for burning rate, Series 2

Test	Present analysis			Sandia analysis [2]			Percent difference[a]
	Time period (min)	mm/min	kg/m^{2}s	Time period (min)	mm/min	kg/m^{2}s	
2.1	22-34	2.23 ± 0.03	0.030 ± 0.000	22-36	2.23 ± 0.03[b]	0.030 ± 0.000	-0.2%
2.2	25-40	1.89 ± 0.03	0.026 ± 0.000	23-39	1.89 ± 0.03	0.026 ± 0.000	0.1%
2.3	n/a			estimated from water volumes pre/post test, divided by 32 min	2.01 ± 0.10	0.027 ± 0.001	n/a
2.4	24-31.5	2.12 ± 0.03	0.029 ± 0.000	23-31	2.12 ± 0.03	0.029 ± 0.000	0.0%
2.5	15-34	1.90 ± 0.03	0.026 ± 0.000	20-35	1.90 ± 0.03	0.026 ± 0.000	0.2%
2.6	n/a			fuel volume divided by 36 min	2.21 +0.10/-0.09	0.030 ± 0.001	n/a

[a] Equivalent for both mm/min and kg/m^{2}s values.

[b] An asymmetrical standard deviation of +0.03/-0.02 mm/min was reported in Table 7-4 of Luketa [2], which was caused by rounding. It is reported here more precisely as ±0.03 mm/min.

Table 21: Time-averaged values for heat release rate (by oxygen consumption calorimetry), Series 2

Test	Present analysis		Sandia analysis [2]		Percent difference
	Time period (min)	MW	Time period (min)	MW	
2.1	22-34	4.8 ± 0.9	22-32	4.8 ± 0.9	-0.3%
2.2	25-40	3.5 ± 0.6	15-30	3.5 ± 0.7	0.3%
2.3	10-30	3.7 ± 0.9	9-29[a]	3.8 ± 0.9	-0.9%
2.4	24-31.5	3.3 ± 0.6	23-42	3.2 ± 0.8	4.4%
2.5	15-34	3.6 ± 0.7	20-30	3.6 ± 0.8	-0.3%
2.6	12-30	3.5 ± 0.7	15-30	3.5 ± 0.7	-0.1%

[a] The averaging time period was reported incorrectly as 10-30 min in Section 6.2.3.9 of Luketa [2], which gives an average of 3.7 ± 0.9 MW. However, this difference is insignificant and does not affect the analysis in this report.

Table 22: Time-averaged values for flame height, Series 2

Test	Present analysis		Sandia analysis [2]		Percent difference
	Time period (min)	m	Time period (min)	m	
2.1	22-34	4.6 ± 1.0	10-20	4.4 ± 1.1	5.8%
2.2	25-40	4.5 ± 1.0	10-20	4.3 ± 1.0	4.8%
2.3	10-30	4.4 ± 1.2	10-20	4.3 ± 1.1	2.2%
2.4	24-31.5	4.6 ± 1.0	10-20	4.5 ± 1.0	1.4%
2.5	15-34	4.6 ± 0.9	10-20	4.5 ± 0.9	3.6%
2.6	12-30	4.5 ± 1.0	10-20	4.5 ± 1.0	0.6%

Table 23: Time-averaged values for temperatures from thermocouple rake in fire plume, Series 2

Test	Height (m)	Present analysis		Sandia analysis [2]		Percent difference
		Time period (min)	°C	Time period (min)	°C	
2.1	1.5	22-34	943.8 ± 27.1	15-35	938.4 ± 30.2	0.6%
	2		895.4 ± 27.8		890.3 ± 34.3	0.6%
	2.5		803.2 ± 32.7		799.9 ± 43.2	0.4%
	3		689.8 ± 31.4		688.3 ± 43.5	0.2%
	3.5		575.2 ± 30.8		573.8 ± 48.0	0.2%
	4		483.7 ± 26.3		485.3 ± 41.6	-0.3%
	4.5		393.3 ± 19.2		391.8 ± 30.1	0.4%
	5		319.2 ± 14.9		318.1 ± 22.9	0.3%
	5.5		268.1 ± 13.4		269.0 ± 20.2	-0.3%
2.2	0.18	25-40	666.5 ± 17.3	10-40	672.7 ± 40.4	-0.9%
	1.5		947.1 ± 25.8		935.9 ± 33.0	1.2%
	2		916.3 ± 21.9		904.3 ± 33.2	1.3%
	2.5		827.3 ± 26.0		814.5 ± 41.1	1.6%
	3		730.1 ± 23.2		714.3 ± 43.7	2.2%
	3.5		627.3 ± 23.1		610.6 ± 47.9	2.7%
	4		545.9 ± 20.2		529.3 ± 48.4	3.1%
	4.5		454.0 ± 15.4		439.0 ± 40.9	3.4%
	5		368.8 ± 11.6		355.8 ± 32.9	3.7%
	5.5		311.7 ± 9.8		301.3 ± 27.6	3.4%
2.3	0.5	10-30	equivalent to [2]	10-30	967.8 ± 79.3	n/a
	1.5				847.8 ± 56.5	
	2				757.5 ± 68.2	
	2.5				621.3 ± 83.4	
	3				521.7 ± 85.6	
	3.5				420.2 ± 95.0	
	4				360.8 ± 87.5	
	4.5				302.7 ± 74.8	
	5				250.1 ± 60.6	
	5.5				220.2 ± 58.1	

Table 23: Time-averaged values for temperatures from thermocouple rake in fire plume, Series 2

Test	Height (m)	Present analysis		Sandia analysis [2]		Percent difference
		Time period (min)	°C	Time period (min)	°C	
2.4	0.5	24-31.5	980.2 ± 17.3	23-42	971.5 ± 51.5	0.9%
	1.5		922.9 ± 30.3		925.7 ± 45.2	-0.3%
	2		843.6 ± 29.2		854.3 ± 60.2	-1.3%
	2.5		710.6 ± 31.6		727.4 ± 74.9	-2.3%
	3		599.4 ± 24.7		616.2 ± 78.0	-2.7%
	3.5		484.5 ± 21.0		504.7 ± 81.1	-4.0%
	4		407.0 ± 13.4		431.3 ± 74.1	-5.6%
	4.5		328.5 ± 8.6		349.4 ± 59.0	-6.0%
	5		264.4 ± 7.2		282.4 ± 43.9	-6.4%
	5.5		229.8 ± 8.0		243.6 ± 37.2	-5.7%
2.5	0.5	15-34	967.9 ± 20.2	20-35	973.5 ± 19.6[a]	-0.6%
	1.5		923.7 ± 37.6		932.8 ± 33.3	-1.0%
	2		849.0 ± 37.8		858.1 ± 35.6	-1.1%
	2.5		717.7 ± 39.2		726.0 ± 38.1	-1.1%
	3		609.7 ± 28.5		615.5 ± 28.2	-0.9%
	3.5		502.5 ± 23.4		507.4 ± 23.2	-1.0%
	4		420.9 ± 17.3		423.8 ± 17.2	-0.7%
	4.5		340.5 ± 12.6		343.0 ± 12.0	-0.7%
	5		272.7 ± 11.3		275.9 ± 9.6	-1.2%
	5.5		236.0 ± 10.6		238.0 ± 10.0	-0.8%
2.6	1.5	12-30	924.6 ± 52.5	22.5-32.5	949.9 ± 46.8	-2.7%
	2		864.1 ± 57.5		882.6 ± 52.2	-2.1%
	2.5		761.8 ± 64.7		770.3 ± 63.4	-1.1%
	3		651.5 ± 62.0		660.1 ± 59.6	-1.3%
	3.5		534.6 ± 62.8		537.4 ± 63.1	-0.5%
	4		443.9 ± 56.4		447.5 ± 57.3	-0.8%
	4.5		357.4 ± 41.5		366.9 ± 38.6	-2.6%
	5		290.9 ± 30.0		302.7 ± 24.2[a]	-3.9%
	5.5		244.8 ± 24.0		253.8 ± 21.6	-3.5%

[a] Value in Table 7-14 of Luketa [2] for standard deviation is incorrect.

Table 24: Time-averaged values for heat flux to narrow-view radiometers, Series 2

Test	Height (m)	Present analysis		Sandia analysis [2]		Percent difference
		Time period (min)	kW/m^2	Time period (min)	kW/m^2	
2.1	0.5	22-34	121.3 ± 10.0	15-35	120.2 ± 10.3	0.9%
	1		103.3 ± 14.2		102.5 ± 14.4	0.8%
	1.5		89.1 ± 20.1		88.7 ± 20.2	0.5%
	2		73.7 ± 24.1		73.9 ± 24.1	-0.4%
	3		38.3 ± 23.2		39.6 ± 23.9	-3.1%
	4		21.2 ± 17.5		22.0 ± 18.2	-4.0%
2.2	0.5	25-40	99.9 ± 6.6	10-40	99.6 ± 6.8	0.4%
	1		105.8 ± 12.9		105.6 ± 13.6	0.2%
	1.5		86.4 ± 18.6		86.5 ± 20.3	-0.1%
	2		66.6 ± 21.6		66.7 ± 23.5	0.0%
	3		31.3 ± 18.4		31.0 ± 19.0	0.9%
	4		17.0 ± 13.9		16.9 ± 14.4	0.6%
2.3	0.5	10-30	equivalent to [2]	10-30	58.4 ± 4.3	n/a
	1				74.2 ± 14.3	
	1.5				77.0 ± 24.7	
	2				57.6 ± 25.4	
	3				24.6 ± 17.7	
	4				13.3 ± 14.3	
2.4	0.5	24-31.5	64.9 ± 3.9	23-42	65.1 ± 4.2	-0.3%
	1		84.0 ± 11.6		84.1 ± 13.4	-0.1%
	1.5		88.7 ± 20.9		89.1 ± 23.0	-0.5%
	2		66.6 ± 22.3		68.2 ± 24.3	-2.4%
	3		28.3 ± 14.9		31.3 ± 18.0	-9.5%
	4		14.0 ± 10.4		16.4 ± 13.2	-14.7%
2.5	0.5	15-34	65.1 ± 4.0	20-35	65.4 ± 4.0	-0.6%
	1		85.0 ± 11.8		85.1 ± 11.8	-0.2%
	1.5		89.8 ± 20.5		89.9 ± 20.6	0.0%
	2		68.0 ± 22.1		68.1 ± 22.0	-0.1%
	3		29.8 ± 16.2		29.5 ± 15.9	1.1%
	4		15.2 ± 11.2		14.8 ± 10.7	2.9%
2.6	0.5	12-30	117.0 ± 10.0	20-35	116.3 ± 11.2	0.5%
	1		98.4 ± 14.1		93.6 ± 16.6	5.1%
	1.5		83.5 ± 20.5		75.0 ± 22.5	11.4%
	2		69.5 ± 24.3		60.7 ± 25.1	14.6%
	3		35.7 ± 21.5		30.1 ± 20.8	18.5%
	4		18.1 ± 15.6		15.5 ± 14.8	16.7%

Table 25: Time-averaged values for heat flux to wide-view radiometers, Series 2

Test	Height (m)	Present analysis		Sandia analysis [2]		Percent difference
		Time period (min)	kW/m^2	Time period (min)	kW/m^2	
2.1	1	22-34	2.3 ± 0.3	15-35	2.3 ± 0.3	0.2%
	1.5		2.8 ± 0.2		2.8 ± 0.2	-0.2%
	2		2.5 ± 0.3		2.5 ± 0.3	-0.2%
	3		2.5 ± 0.3		2.5 ± 0.3	-0.1%
	4		2.2 ± 0.3		2.2 ± 0.3	0.1%
2.2	1	25-40	2.0 ± 0.2	10-40	2.0 ± 0.2	0.6%
	1.5		2.4 ± 0.2		2.4 ± 0.2	0.6%
	2		2.1 ± 0.2		2.1 ± 0.2	0.6%
	3		2.1 ± 0.2		2.1 ± 0.2	0.7%
	4		1.8 ± 0.2		1.8 ± 0.2	1.1%
2.3	1	10-30	equivalent to [2]	10-30	1.8 ± 0.4	n/a
	1.5				2.2 ± 0.4	
	2				1.9 ± 0.4	
	3				1.9 ± 0.4	
	4				1.7 ± 0.4	
2.4	1	24-31.5	1.9 ± 0.2	23-42	1.9 ± 0.3	-0.7%
	1.5		2.4 ± 0.2		2.4 ± 0.3	-0.3%
	2		2.1 ± 0.2		2.1 ± 0.3	-0.6%
	3		2.1 ± 0.2		2.1 ± 0.3	-1.0%
	4		1.8 ± 0.2		1.9 ± 0.3	-1.3%
2.5	1	15-34	1.9 ± 0.2	20-35	1.9 ± 0.2	0.3%
	1.5		2.4 ± 0.2		2.4 ± 0.2	0.3%
	2		2.1 ± 0.2		2.1 ± 0.2	0.2%
	3		2.1 ± 0.2		2.1 ± 0.2	0.3%
	4		1.9 ± 0.2		1.9 ± 0.2	0.2%
2.6	1	12-30	2.2 ± 0.3	20-35	2.1 ± 0.3	3.9%
	1.5		2.6 ± 0.2		2.5 ± 0.3	4.4%
	2		2.3 ± 0.3		2.2 ± 0.3	4.1%
	3		2.3 ± 0.3		2.2 ± 0.3	4.1%
	4		2.0 ± 0.2		2.0 ± 0.3	3.8%

Similar to Series 1, the temperature data measured by the DFTs in Series 2 had to be reprocessed to calculate the total heat flux using the same method as in Series 3. Table 26 shows that, for Tests 2.1, 2.3, 2.4 and 2.5 without changing the time averaging period, the total heat flux values were approximately 26% to 40% lower when calculated using a convection coefficient of 10 W/m^{2}K (as per Series 3), instead of 30 W/m^{2}K (as originally used in Luketa [2]). For reasons unclear, the method used in Luketa [2] to calculate heat flux to the DFTs was different for Tests 2.2 and 2.6, in that a convection coefficient of 5 W/m^{2}K was used, along with a multiplication factor of 1.105. This resulted in a 2% to 13% difference when the heat flux values were recalculated using the Series 3 method without changing the time averaging period.

Table 26: Time-averaged values for total heat flux to DFTs, Series 2

Test	Distance from pool centre (m)	Sandia analysis [2]			Using same method as Series 3 (h=10 W/m^{2}K and without factor of 1.105[b])			Present analysis, using same method as Series 3		
		Time period (min)[a]	h (W/m^2/K)	kW/m^2	Time period (min)	kW/m^2	Percent difference from [2]	Time period (min)	kW/m^2	Percent difference from [2]
2.1	2	20-36.7	30	49.8 ± 1.6	20-36.7	36.4 ± 1.6	-27%	22-34	36.1 ± 1.6	-28%
	4	20-40		17.0 ± 0.7	20-40	10.2 ± 0.7	-40%		10.2 ± 0.5	-40%
2.2	2	20-40	5	33.6 ± 1.2	20-40	34.2 ± 1.2	2%	25-40	34.4 ± 1.2	2%
	4			9.1[c] ± 0.4		10.2 ± 0.4	12%		10.2 ± 0.4	12%
2.3	2	20-33	30	52.5 ± 2.0	20-33	38.6 ± 2.0	-26%	10-30	38.7 ± 1.7	-26%
	4	20-30		18.3 ± 1.7	20-30	11.2 ± 1.7	-39%		11.2 ± 1.5	-39%
2.4	2	20-40	30	53.8 ± 1.9	20-40	39.8 ± 1.9	-26%	24-31.5	40.0 ± 1.4	-26%
	4			18.8 ± 1.1		11.4 ± 1.1	-39%		11.4 ± 0.6	-39%
2.5	2	20-33	30	52.9[d] ± 1.4	20-33	39.1 ± 1.4	-26%	15-34	39.1 ± 1.4	-26%
	4	20-35		18.7[d] ± 0.4	20-35	11.4 ± 0.4	-39%		11.5 ± 0.5	-39%
2.6	2	15-36	5	32.4 ± 1.4	15-36	33.1 ± 1.4	2%	12-30	33.5 ± 1.4	3%
	4			8.3 ± 0.3		9.3 ± 0.3	13%		9.7 ± 0.4	17%

[a] In Tests 2.1, 2.3 and 2.5, the averaging time period was not consistent between the DFTs at 2 m and 4 m. Although the effect is minimal (less than 1% difference), the exact time periods are listed here for accuracy.
[b] Factor of 1.105 was applied to data from Tests 2.2 and 2.6 only.
[c] Value in Table 7-20 of Luketa [2] is incorrect; see Figure 6-62 of [2].
[d] Value in Luketa [2] (Table 7-20 and Figure 6-109) is incorrect because convection effects were unintentionally neglected while processing the DFT data from this test. Note that the absorbed heat flux values are unaffected.

The time-averaged values calculated using the Series 3 method for the time periods identified in Table 4 were subsequently compared to those presented in Luketa [2] (Table 26). It can be seen that use of the different time periods had minimal effect, since the percent differences shown in the rightmost column of Table 26 are similar to those calculated previously. It may be noted that for Test 2.6, the 15-36 min time period used in Luketa [2] included the beginning of decay of the fire after 30 minutes, resulting in a slightly higher percent difference for the 4 m DFT (17% instead of 13%). Overall, though, the comparison in Table 26 is consistent with the measurement parameters discussed previously, which showed small differences resulting from the use of the time periods in Table 4.

Tables 27-29 show the time-averaged values, based on Table 4 time intervals, for total heat flux to the calorimeter, temperatures exterior to the calorimeter, and temperatures on the outer cylinder of the calorimeter. Comparison to the corresponding values in Luketa [2] indicated differences generally less than 4%, consistent with the other parameters discussed above. It may be noted that for Test 2.3, there were issues with the automatic liquid level control system, which likely contributed to the slightly higher differences (up to ~10%) in total heat flux (Table 27) for this test.

Table 27: Time-averaged values for total heat flux to calorimeter, Series 2

Test	Location	Present analysis		Sandia analysis [2]		Percent difference
		Time period (min)	kW/m²	Time period (min)	kW/m²	
2.2	L0[a]	n/a	n/a	20-40	n/a	n/a
	L45[b]	30-40	101.3 ± 3.9		n/a	n/a
	L90[c]	25-40	75.5 ± 2.7		n/a	n/a
	L135		60.1 ± 1.5		60.0 ± 2.0	0.1%
	L180		57.2 ± 1.5		56.9 ± 1.8	0.6%
	L225		71.3 ± 1.3		70.8 ± 1.9	0.8%
	L270		74.0 ± 6.5		73.8 ± 6.4	0.3%
	L315[a]		n/a		n/a	n/a
	C0		123.6 ± 4.3		122.5 ± 4.7	0.9%
	C45		117.7 ± 4.4		116.3 ± 5.7	1.3%
	C90		73.0 ± 4.0		72.7 ± 4.7	0.4%
	C135		54.2 ± 2.2		53.9 ± 3.3	0.6%
	C180		47.3 ± 2.3		46.5 ± 3.1	1.7%
	C225		64.6 ± 3.0		63.4 ± 4.3	2.0%
	C270		103.6 ± 6.1		101.5 ± 7.8	2.1%
	C315		109.6 ± 5.6		108.3 ± 6.1	1.2%
	R0		71.6 ± 9.5		71.5 ± 9.2	0.1%
	R45		80.9 ± 4.3		80.4 ± 4.5	0.7%
	R90		78.5 ± 2.4		78.3 ± 2.7	0.2%
	R135[d]		72.3 ± 1.8		n/a	n/a
	R180		62.6 ± 1.5		62.4 ± 2.2	0.3%
	R225		76.7 ± 1.5		76.3 ± 2.1	0.5%
	R270		78.8 ± 8.2		78.4 ± 8.1	0.5%
	R315		68.9 ± 11.4		69.1 ± 11.1	-0.2%

Table 27: Time-averaged values for total heat flux to calorimeter, Series 2

Test	Location	Present analysis		Sandia analysis [2]		Percent difference
		Time period (min)	kW/m²	Time period (min)	kW/m²	
2.3	L0	10-30	66.4 ± 16.5	20-33	74.0 ± 16.0	-10.3%
	L45		98.8 ± 12.5		108.0 ± 9.4	-8.5%
	L90		117.0 ± 14.6		125.0 ± 13.4	-6.4%
	L135		121.3 ± 13.3		128.8 ± 10.3	-5.8%
	L180[e]		92.7 ± 10.0		n/a	n/a
	L225		77.3 ± 3.0		77.5 ± 3.0	-0.2%
	L270		54.6 ± 12.1		58.4 ± 12.1	-6.6%
	L315		54.0 ± 17.1		57.9 ± 18.2	-6.7%
	C0		89.2 ± 8.8		83.8 ± 9.2	6.4%
	C45		96.8 ± 10.2		104.7 ± 6.7	-7.5%
	C90[f]		124.5 ± 28.0		n/a	n/a
	C135[f]		125.0 ± 19.0		n/a	n/a
	C180		115.1 ± 16.2		123.1 ± 14.6	-6.5%
	C225		77.5 ± 9.4		79.7 ± 9.0	-2.8%
	C270		85.3 ± 7.4		81.8 ± 7.6	4.2%
	C315		83.7 ± 9.7		78.3 ± 9.7	6.8%
	R0		99.1 ± 10.1		102.0 ± 9.9	-2.8%
	R45[a]		n/a		n/a	n/a
	R90		112.7 ± 10.3		115.9 ± 10.0	-2.7%
	R135		133.1 ± 13.5		137.2 ± 13.3	-3.0%
	R180		104.0 ± 9.3		109.1 ± 7.4	-4.7%
	R225[a]		n/a		n/a	n/a
	R270		69.9 ± 11.4		69.8 ± 12.3	0.3%
	R315		73.7 ± 14.2		73.2 ± 16.2	0.7%

Table 27: Time-averaged values for total heat flux to calorimeter, Series 2

Test	Location	Present analysis		Sandia analysis [2]		Percent difference
		Time period (min)	kW/m^2	Time period (min)	kW/m^2	
2.4	L0	24-31.5	64.4 ± 6.9	20-33	64.4 ± 8.8	0.0%
	L45		76.2 ± 6.1		75.8 ± 8.0	0.4%
	L90		112.7 ± 4.3		112.1 ± 4.9	0.5%
	L135		127.9 ± 4.3		130.3 ± 5.3	-1.9%
	L180		138.4 ± 3.8		138.4 ± 5.3	0.0%
	L225		110.4 ± 4.9		110.9 ± 5.1	-0.5%
	L270		81.2 ± 6.4		81.2 ± 6.8	0.0%
	L315		67.6 ± 8.2		67.8 ± 9.0	-0.4%
	C0		130.1 ± 4.6		130.3 ± 5.3	-0.1%
	C45		140.2 ± 3.8		139.9 ± 6.2	0.2%
	C90		134.0 ± 3.0		135.1 ± 3.9	-0.8%
	C135[a]		n/a		n/a	n/a
	C180[a]		n/a		n/a	n/a
	C225		116.6 ± 2.0		117.7 ± 4.1	-0.9%
	C270		97.0 ± 1.3		98.4 ± 1.7	-1.5%
	C315		111.3 ± 3.8		112.3 ± 4.1	-0.9%
	R0[a]		n/a		n/a	n/a
	R45		109.4 ± 5.7		112.4 ± 6.3	-2.7%
	R90[g]		102.5 ± 1.6		n/a	n/a
	R135		115.3 ± 3.0		117.8 ± 4.6	-2.1%
	R180		136.7 ± 4.1		137.7 ± 6.0	-0.8%
	R225		119.3 ± 3.6		120.6 ± 4.0	-1.0%
	R270		95.7 ± 5.9		96.9 ± 6.7	-1.2%
	R315		88.4 ± 9.7		90.3 ± 10.6	-2.1%

Table 27: Time-averaged values for total heat flux to calorimeter, Series 2

Test	Location	Present analysis		Sandia analysis [2]		Percent difference
		Time period (min)	kW/m²	Time period (min)	kW/m²	
2.5	L0	15-34	63.6 ± 8.1	20-33	65.4 ± 8.6	-2.8%
	L45		73.4 ± 7.0		75.6 ± 6.9	-2.9%
	L90		106.7 ± 5.4		108.8 ± 4.2	-1.8%
	L135[h]		126.3 ± 4.9		n/a	n/a
	L180		136.0 ± 4.1		137.9 ± 3.2	-1.4%
	L225		108.9 ± 6.2		111.6 ± 4.8	-2.5%
	L270		80.3 ± 7.6		82.8 ± 6.9	-3.1%
	L315		67.4 ± 9.2		69.6 ± 9.5	-3.0%
	C0		126.4 ± 5.8		128.8 ± 5.0	-1.9%
	C45		133.1 ± 6.1		135.7 ± 4.6	-1.9%
	C90[a]		n/a		n/a	n/a
	C135[a]		n/a		n/a	n/a
	C180[a]		n/a		n/a	n/a
	C225[a]		n/a		n/a	n/a
	C270[i]	20-34	127.9 ± 7.7		n/a	n/a
	C315	15-34	106.9 ± 2.9		108.5 ± 2.6	-1.4%
	R0[a]		n/a		n/a	n/a
	R45		104.0 ± 6.4		105.5 ± 6.6	-1.4%
	R90		96.6 ± 1.8		97.6 ± 1.8	-1.0%
	R135		108.6 ± 3.1		109.8 ± 3.2	-1.1%
	R180		132.6 ± 4.3		134.1 ± 3.7	-1.1%
	R225		115.9 ± 4.8		117.8 ± 4.3	-1.6%
	R270[j]		92.4 ± 6.8		n/a	n/a
	R315		86.9 ± 9.6		89.0 ± 9.7	-2.4%

[a] No reliable data was available at this location due to faulty thermocouple readings.
[b] The averaging time period for this location was selected to start at 30 min due to faulty thermocouple readings prior to 30 min. Due to the faulty readings, this location was not included in the spatially averaged heat flux reported in Table 7-23 of Luketa [2].
[c] This location was not included in the spatially averaged heat flux reported in Table 7-23 of Luketa [2], due to faulty thermocouple readings prior to 11 min.
[d] This location was not included in the spatially averaged heat flux reported in Table 7-23 of Luketa [2], due to faulty thermocouple readings prior to 7 min.
[e] This location was not included in the spatially averaged heat flux reported in Table 7-23 of Luketa [2], due to faulty thermocouple readings after 70 min.
[f] This location was not included in the spatially averaged heat flux reported in Table 7-23 of Luketa [2], due to faulty thermocouple readings after 31 min.
[g] It is unclear why this location was not included in the spatially averaged heat flux reported in Table 7-23 of Luketa [2] (there were no faulty thermocouple readings).
[h] This location was not included in the spatially averaged heat flux reported in Table 7-23 of Luketa [2], due to faulty readings by the thermocouple on the inner cylinder of the calorimeter throughout the entire test. However, this has minimal influence on the heat flux calculations, which depend predominantly on

the thermocouple readings from the outer cylinder of the calorimeter. A sensitivity analysis showed that if the heat flux was calculated using the non-faulty thermocouple data from the adjacent interior thermocouples (L90 or L180), the difference in the time-averaged total heat flux to the L135 location would be less than 1%.

[i] The averaging time period for this location was selected to start at 20 min due to faulty thermocouple readings prior to 20 min. Due to the faulty readings, this location was not included in the spatially averaged heat flux reported in Table 7-23 of Luketa [2].

[j] This location was not included in the spatially averaged heat flux reported in Table 7-23 of Luketa [2], due to faulty thermocouple readings after 41 min.

Table 28: Time-averaged temperature values from thermocouples exterior to calorimeter, Series 2

Test	Location	Present analysis		Sandia analysis [2][a]		Percent difference
		Time period (min)	°C	Time period (min)	°C	
2.2	L0	25-40	771.2 ± 24.5	20-40	772.0 ± 25.1	-0.1%
	L45		966.0 ± 14.1		961.4 ± 16.0	0.5%
	L90		886.5 ± 9.8		886.0 ± 13.1	0.1%
	L135		824.0 ± 6.8		822.9 ± 9.6	0.1%
	L180		856.1 ± 14.0		852.2 ± 16.4	0.5%
	L225		903.9 ± 8.0		899.9 ± 11.0	0.4%
	L270		861.0 ± 15.8		861.1 ± 15.7	0.0%
	L315		766.3 ± 23.8		767.8 ± 23.2	-0.2%
	C0		998.6 ± 13.3		996.3 ± 13.5	0.2%
	C45		1005.7 ± 7.8		1001.7 ± 12.0	0.4%
	C90[b]		n/a		n/a	n/a
	C135		796.6 ± 8.9		794.0 ± 14.6	0.3%
	C180		783.4 ± 11.8		777.6 ± 17.8	0.7%
	C225		864.7 ± 12.5		856.6 ± 20.2	0.9%
	C270		950.9 ± 12.7		944.9 ± 17.9	0.6%
	C315		982.4 ± 14.2		978.3 ± 16.0	0.4%
	R0[b]		n/a		n/a	n/a
	R45		914.7 ± 20.3		911.2 ± 21.1	0.4%
	R90		906.9 ± 11.3		905.8 ± 12.2	0.1%
	R135		858.2 ± 9.7		857.2 ± 12.3	0.1%
	R180		874.9 ± 13.4		871.6 ± 18.6	0.4%
	R225		917.7 ± 8.5		915.2 ± 10.2	0.3%
	R270		897.3 ± 20.2		895.7 ± 20.0	0.2%
	R315		852.0 ± 32.3		851.6 ± 31.2	0.1%

Table 28: Time-averaged temperature values from thermocouples exterior to calorimeter, Series 2

Test	Location	Present analysis		Sandia analysis [2][a]		Percent difference
		Time period (min)	°C	Time period (min)	°C	
2.3	L0	10-30	781.4 ± 82.3	20-33	833.8 ± 70.1	-6.3%
	L45[b]		n/a		n/a	n/a
	L90		799.2 ± 43.8		812.3 ± 44.9	-1.6%
	L135		869.2 ± 32.6		884.0 ± 28.1	-1.7%
	L180		943.1 ± 25.7		959.3 ± 17.2	-1.7%
	L225		998.7 ± 34.6		1020.8 ± 22.5	-2.2%
	L270		991.3 ± 34.0		1014.9 ± 22.9	-2.3%
	L315		971.1 ± 33.3		996.5 ± 19.7	-2.5%
	C0		976.4 ± 28.5		980.4 ± 31.1	-0.4%
	C45[b]		n/a		n/a	n/a
	C90		1014.9 ± 34.2		1029.6 ± 28.3	-1.4%
	C135		1036.8 ± 56.7		1049.5 ± 61.3	-1.2%
	C180		1045.7 ± 72.8		1063.4 ± 84.7	-1.7%
	C225		1035.8 ± 59.3		1051.1 ± 65.6	-1.5%
	C270		1019.0 ± 43.5		1034.1 ± 43.9	-1.5%
	C315		982.1 ± 30.7		993.8 ± 26.3	-1.2%
	R0		845.0 ± 35.5		838.2 ± 43.2	0.8%
	R45		990.3 ± 26.0		991.7 ± 28.9	-0.1%
	R90		922.6 ± 39.9		926.0 ± 47.1	-0.4%
	R135		1011.1 ± 27.1		1012.0 ± 31.1	-0.1%
	R180		1032.3 ± 30.4		1035.9 ± 33.8	-0.3%
	R225		1029.8 ± 28.8		1040.4 ± 27.9	-1.0%
	R270		969.3 ± 23.5		978.4 ± 19.5	-0.9%
	R315		907.6 ± 26.4		911.6 ± 27.0	-0.4%

Table 28: Time-averaged temperature values from thermocouples exterior to calorimeter, Series 2

Test	Location	Present analysis		Sandia analysis [2][a]		Percent difference
		Time period (min)	°C	Time period (min)	°C	
2.4	L0	24-31.5	795.7 ± 19.9	20-33	790.5 ± 29.0	0.7%
	L45		852.8 ± 23.4		851.2 ± 27.2	0.2%
	L90		918.6 ± 16.7		917.9 ± 18.6	0.1%
	L135		993.0 ± 13.8		994.0 ± 14.7	-0.1%
	L180		1065.9 ± 12.9		1063.5 ± 15.0	0.2%
	L225		1054.5 ± 13.1		1051.0 ± 13.5	0.3%
	L270		1034.5 ± 14.5		1030.9 ± 14.7	0.4%
	L315		839.1 ± 17.5		833.2 ± 27.4	0.7%
	C0		1054.3 ± 9.4		1050.8 ± 12.4	0.3%
	C45		1075.6 ± 8.3		1071.1 ± 14.9	0.4%
	C90		1023.0 ± 6.4		1025.3 ± 16.3	-0.2%
	C135		1035.5 ± 9.9		1036.8 ± 25.8	-0.1%
	C180		1050.7 ± 15.2		1049.1 ± 29.9	0.2%
	C225		1035.7 ± 10.1		1037.4 ± 23.2	-0.2%
	C270		1007.4 ± 9.1		1008.1 ± 16.5	-0.1%
	C315		1040.6 ± 11.1		1036.4 ± 13.6	0.4%
	R0		934.2 ± 24.4		937.0 ± 29.5	-0.3%
	R45		976.1 ± 17.4		981.1 ± 21.2	-0.5%
	R90		1037.3 ± 10.2		1037.0 ± 17.9	0.0%
	R135		1058.3 ± 10.0		1058.9 ± 16.6	-0.1%
	R180		1070.1 ± 9.7		1070.3 ± 12.4	0.0%
	R225		1027.2 ± 13.2		1027.2 ± 14.0	0.0%
	R270		965.1 ± 12.9		965.4 ± 16.0	0.0%
	R315		912.8 ± 28.1		915.9 ± 32.2	-0.3%

Table 28: Time-averaged temperature values from thermocouples exterior to calorimeter, Series 2

Test	Location	Present analysis		Sandia analysis [2][a]		Percent difference
		Time period (min)	°C	Time period (min)	°C	
2.5	L0	15-34	789.6 ± 29.0	20-33	798.2 ± 27.5	-1.1%
	L45		853.1 ± 28.9		862.5 ± 27.0	-1.1%
	L90		918.7 ± 20.7		926.2 ± 17.8	-0.8%
	L135		1005.3 ± 21.1		1013.9 ± 17.6	-0.8%
	L180		1070.2 ± 16.2		1076.2 ± 12.9	-0.6%
	L225		1054.6 ± 14.2		1059.0 ± 11.6	-0.4%
	L270		1032.8 ± 16.4		1038.5 ± 12.9	-0.6%
	L315		832.1 ± 24.7		840.9 ± 20.7	-1.0%
	C0		1042.5 ± 13.5		1047.8 ± 9.4	-0.5%
	C45		1058.6 ± 16.6		1065.7 ± 10.9	-0.7%
	C90		1005.8 ± 9.9		1008.5 ± 6.2	-0.3%
	C135		1018.0 ± 10.9		1019.4 ± 8.7	-0.1%
	C180		1031.7 ± 15.2		1033.5 ± 14.2	-0.2%
	C225		1025.9 ± 10.9		1025.3 ± 10.4	0.1%
	C270		998.6 ± 10.1		996.9 ± 10.0	0.2%
	C315		1030.7 ± 11.0		1033.6 ± 9.0	-0.3%
	R0		924.1 ± 24.4		926.3 ± 26.0	-0.2%
	R45		964.2 ± 20.1		966.4 ± 21.4	-0.2%
	R90		1022.8 ± 10.6		1024.1 ± 10.6	-0.1%
	R135		1047.8 ± 11.4		1049.5 ± 11.2	-0.2%
	R180		1060.8 ± 10.2		1062.2 ± 9.5	-0.1%
	R225		1021.2 ± 17.3		1025.0 ± 17.0	-0.4%
	R270		965.2 ± 16.7		967.9 ± 17.3	-0.3%
	R315		907.6 ± 29.3		910.7 ± 31.0	-0.3%

[a] The thermocouple locations used to produce Figure 8-29 of Luketa [2] contain errors in all tests and are shown corrected in this table.

[b] No reliable data was available at this location due to faulty thermocouple readings.

Table 29: Time-averaged temperature values from thermocouples on outer cylinder of calorimeter, Series 2

Test	Location	Present analysis		Sandia analysis [2][a]		Percent difference
		Time period (min)	°C	Time period (min)	°C	
2.2	L0[b]	n/a	n/a	20-40	n/a	n/a
	L45[c]	30-40	938.8 ± 4.3		n/a	n/a
	L90	25-40	850.4 ± 2.4		848.8 ± 4.3	0.2%
	L135		789.4 ± 1.9		788.8 ± 2.9	0.1%
	L180		775.7 ± 2.6		774.5 ± 3.3	0.2%
	L225		835.7 ± 1.9		833.3 ± 4.6	0.3%
	L270		845.5 ± 6.9		844.3 ± 6.6	0.1%
	L315		781.4 ± 9.3		782.5 ± 8.7	-0.1%
	C0		1001.7 ± 4.2		998.5 ± 6.8	0.3%
	C45		985.5 ± 5.0		981.1 ± 9.4	0.5%
	C90		843.0 ± 3.2		841.1 ± 5.7	0.2%
	C135		761.1 ± 2.7		758.8 ± 5.7	0.3%
	C180		724.5 ± 5.2		720.5 ± 8.5	0.6%
	C225		807.3 ± 6.7		801.8 ± 11.3	0.7%
	C270		944.4 ± 8.9		937.3 ± 15.2	0.8%
	C315		963.1 ± 5.8		958.8 ± 9.2	0.4%
	R0		837.2 ± 10.9		838.0 ± 10.6	-0.1%
	R45		871.9 ± 4.1		870.2 ± 5.2	0.2%
	R90		863.5 ± 2.0		861.8 ± 4.1	0.2%
	R135		837.9 ± 1.8		836.1 ± 4.1	0.2%
	R180		800.5 ± 2.0		799.2 ± 3.9	0.2%
	R225		856.6 ± 1.7		854.6 ± 4.3	0.2%
	R270		863.5 ± 7.8		862.1 ± 7.7	0.2%
	R315		826.4 ± 12.4		827.7 ± 11.7	-0.2%

Table 29: Time-averaged temperature values from thermocouples on outer cylinder of calorimeter, Series 2

Test	Location	Present analysis		Sandia analysis [2][a]		Percent difference
		Time period (min)	°C	Time period (min)	°C	
2.3	L0	10-30	794.8 ± 55.9	20-33	842.8 ± 24.5	-5.7%
	L45		921.3 ± 36.0		951.8 ± 11.3	-3.2%
	L90		979.2 ± 24.6		998.3 ± 13.1	-1.9%
	L135		991.7 ± 22.5		1008.9 ± 10.4	-1.7%
	L180		903.7 ± 33.1		932.0 ± 10.3	-3.0%
	L225		859.3 ± 5.5		859.7 ± 6.0	0.0%
	L270		751.4 ± 32.4		777.9 ± 17.6	-3.4%
	L315		745.8 ± 40.0		777.6 ± 27.2	-4.1%
	C0		903.8 ± 18.6		887.0 ± 20.6	1.9%
	C45		919.9 ± 26.8		943.2 ± 10.2	-2.5%
	C90[d]		999.9 ± 32.8		n/a	n/a
	C135[d]		1002.1 ± 25.4		n/a	n/a
	C180		972.9 ± 32.1		994.3 ± 18.3	-2.2%
	C225		855.5 ± 19.2		867.1 ± 11.5	-1.3%
	C270		888.9 ± 12.7		879.8 ± 18.6	1.0%
	C315		886.3 ± 20.7		868.2 ± 21.2	2.1%
	R0		927.3 ± 21.9		940.0 ± 13.2	-1.3%
	R45		942.0 ± 29.3		960.0 ± 13.5	-1.9%
	R90		968.8 ± 18.8		978.1 ± 12.5	-1.0%
	R135		1023.3 ± 18.2		1031.5 ± 15.7	-0.8%
	R180		942.1 ± 22.8		958.7 ± 8.2	-1.7%
	R225		864.6 ± 41.6		858.3 ± 51.9	0.7%
	R270		828.6 ± 14.7		831.6 ± 16.4	-0.4%
	R315		842.5 ± 19.7		846.5 ± 23.0	-0.5%

Table 29: Time-averaged temperature values from thermocouples on outer cylinder of calorimeter, Series 2

Test	Location	Present analysis		Sandia analysis [2][a]		Percent difference
		Time period (min)	°C	Time period (min)	°C	
2.4	L0	24-31.5	802.4 ± 7.0	20-33	796.2 ± 16.5	0.8%
	L45		848.7 ± 9.2		843.6 ± 14.8	0.6%
	L90		970.5 ± 4.2		968.3 ± 6.0	0.2%
	L135		1018.8 ± 2.8		1016.9 ± 5.0	0.2%
	L180		1038.2 ± 2.8		1037.2 ± 4.0	0.1%
	L225		965.4 ± 3.0		963.6 ± 6.1	0.2%
	L270		870.4 ± 4.9		867.2 ± 9.9	0.4%
	L315		817.3 ± 7.0		813.5 ± 12.7	0.5%
	C0		1019.9 ± 3.5		1017.8 ± 4.6	0.2%
	C45		1043.1 ± 2.8		1041.4 ± 5.0	0.2%
	C90		1028.1 ± 3.7		1027.1 ± 7.5	0.1%
	C135[b]		n/a		n/a	n/a
	C180[b]		n/a		n/a	n/a
	C225		983.9 ± 2.3		985.5 ± 5.0	-0.2%
	C270		927.7 ± 0.9		929.0 ± 2.4	-0.1%
	C315		970.5 ± 2.8		970.7 ± 3.7	0.0%
	R0		914.1 ± 10.5		913.7 ± 13.4	0.0%
	R45		967.1 ± 6.3		969.5 ± 7.2	-0.2%
	R90		945.6 ± 1.8		947.2 ± 5.4	-0.2%
	R135		983.0 ± 3.2		986.4 ± 7.8	-0.3%
	R180		1035.5 ± 3.0		1037.7 ± 7.4	-0.2%
	R225		992.3 ± 1.7		992.4 ± 2.3	0.0%
	R270		925.1 ± 4.4		922.8 ± 7.0	0.2%
	R315		902.6 ± 7.7		900.9 ± 11.1	0.2%

Table 29: Time-averaged temperature values from thermocouples on outer cylinder of calorimeter, Series 2

Test	Location	Present analysis		Sandia analysis [2][a]		Percent difference
		Time period (min)	°C	Time period (min)	°C	
2.5	L0	15-34	796.7 ± 24.6	20-33	808.2 ± 14.3	-1.4%
	L45		836.7 ± 25.0		848.7 ± 12.0	-1.4%
	L90		952.3 ± 14.7		959.2 ± 5.3	-0.7%
	L135		1008.1 ± 10.5		1013.1 ± 3.8	-0.5%
	L180		1030.5 ± 10.5		1035.7 ± 3.6	-0.5%
	L225		957.5 ± 19.2		966.9 ± 9.1	-1.0%
	L270		863.1 ± 25.6		875.6 ± 13.2	-1.4%
	L315		812.8 ± 26.7		825.5 ± 14.9	-1.5%
	C0		1007.1 ± 13.8		1013.3 ± 8.1	-0.6%
	C45		1023.5 ± 15.7		1030.5 ± 8.0	-0.7%
	C90[b]		n/a		n/a	n/a
	C135[b]		n/a		n/a	n/a
	C180[b]		n/a		n/a	n/a
	C225[b]		n/a		n/a	n/a
	C270		996.9 ± 28.3		1010.4 ± 13.9	-1.3%
	C315		955.5 ± 6.6		958.5 ± 3.8	-0.3%
	R0		904.2 ± 9.0		906.5 ± 9.1	-0.3%
	R45		947.7 ± 6.4		949.0 ± 6.8	-0.1%
	R90		924.6 ± 3.5		925.9 ± 2.4	-0.1%
	R135		961.3 ± 3.3		962.0 ± 3.5	-0.1%
	R180		1024.5 ± 6.2		1026.6 ± 4.1	-0.2%
	R225		979.8 ± 9.2		983.9 ± 5.7	-0.4%
	R270		910.3 ± 9.0		914.2 ± 7.5	-0.4%
	R315		893.4 ± 9.0		896.5 ± 8.6	-0.3%

[a] The thermocouple locations used to produce Figure 8-26 of Luketa [2] contain errors in all tests except Test 2.2 and are shown corrected in this table.

[b] No reliable data was available at this location due to faulty thermocouple readings.

[c] The averaging time period for this location was selected to start at 30 min due to faulty thermocouple readings prior to 30 min. Due to the faulty readings, this location was not included in the spatially averaged outer cylinder temperature reported in Table 7-23 of Luketa [2].

[d] This location was not included in the spatially averaged outer cylinder temperature reported in Table 7-23 of Luketa [2], due to faulty thermocouple readings after 31 min.

Luketa [2] reported overall values of heat flux, temperature exterior to the calorimeter, and outer cylinder temperature that were averaged across all measurement locations on the calorimeter. For comparison, spatially averaged values were also calculated in the present analysis, using the adjusted time periods in Table 4 and neglecting the locations that were not considered to show realistic values (as per the footnotes in Tables 27-29). As shown in Table 30, the results from the present analysis are very similar to those in Luketa [2], within 2%.

Table 30: Comparison of spatially averaged temperature and heat flux values among all calorimeter thermocouple locations, Series 2

Test	Parameter	Present analysis	Neglected locations in present analysis	Sandia analysis [2], Table 7-23	Neglected locations in Sandia analysis	Percent difference
2.2	Outer cylinder temperature (°C)	852.4 ± 4.9	L0	846.4 ± 7.0	L0, L45	0.7%
	Exterior cylinder temperature (°C)	883.6 ± 14.3	C90, R0	880.9 ± 16.7	C90, R0	0.3%
	Total heat flux (kW/m2)	78.3 ± 4.1	L0, L315	77.0 ± 4.8	L0, L45, L90, L315, R135	1.7%
2.3	Outer cylinder temperature (°C)	904.8 ± 26.1	none	908.8 ± 17.1	C90, C135	-0.4%
	Exterior cylinder temperature (°C)	962.4 ± 38.6	L45, C45	975.4 ± 37.5	L45, C45	-1.3%
	Total heat flux (kW/m2)	94.2 ± 12.6	R45, R225	94.1 ± 11.0	L180, C90, C135, R45, R225	0.1%
2.4	Outer cylinder temperature (°C)	953.2 ± 4.3	C135, C180	952.2 ± 7.5	C135, C180	0.1%
	Exterior cylinder temperature (°C)	994.1 ± 14.0	none	993.3 ± 19.7	none	0.1%
	Total heat flux (kW/m2)	108.3 ± 4.6	C135, C180, R0	109.5 ± 5.8	C135, C180, R0, R90	-1.1%
2.5	Outer cylinder temperature (°C)	939.3 ± 13.8	C90, C135, C180, C225	945.5 ± 7.9	C90, C135, C180, C225	-0.7%
	Exterior cylinder temperature (°C)	986.7 ± 17.1	none	990.8 ± 15.5	none	-0.4%
	Total heat flux (kW/m2)	104.9 ± 5.9	C90, C135, C180, C225, R0	104.9 ± 5.3	L135, C90, C135, C180, C225, C270, R0, R270	0.0%

4.3 Series 3 (Dilbit)

The following tables and figures show, for Series 3 tests calculated using the periods identified in Table 6, time-averaged values for the fuel supply temperature (Table 31), burning rate (Table 32), heat release rate (Table 33), flame height (Table 34), plume axis temperatures (Figure 3), heat flux to the narrow-view (Figure 4) and wide-view (Figure 5) radiometers, and heat flux to the DFTs (Figure 6). For comparison, the values presented in Luketa [2] are also provided. Recall that in Sandia's analysis, the plume temperature data and heat flux data from all radiometers and DFTs were averaged by integrating from 0 to 25 minutes and then dividing by 25 minutes. In general, the values from the Sandia analysis fall within the range of values from the present analysis, with the values from the present analysis exhibiting smaller standard deviations due to the shorter time-averaging periods.

Table 31: Time-averaged values for fuel supply temperature, Series 3

Test	Present analysis		Sandia analysis [2]		Maximum absolute percent difference
	Time period (min)	°C	Time period (min)	°C	
3.1	3-5	21.1 ± 0.2	5-25	21.7 ± 0.5	3%
	8-11	21.5 ± 0.4			
	16.5-18	22.0 ± 0.2			
3.2	11.9-12.7	20.9 ± 0.1	0-30	22.1 ± 1.2	5%
	15-17	21.9 ± 0.5			
	18.6-23.5	23.0 ± 0.3			
3.3	3-5	17.5 ± 0.0	0-30	17.6 ± 0.1	1%
	8-10	17.6 ± 0.0			
	12-19	17.7 ± 0.0			
	25-28	17.5 ± 0.0			
3.4	not compared because test did not involve continuous fuel feed		during fill time prior to ignition	22.1 ± 1.5	n/a
3.5	3-10	24.1 ± 0.3	5-30	24.9 ± 0.4	3%
	16-19.5	24.9 ± 0.1			
	27.5-30.5	25.6 ± 0.1			
3.6	4-6	55.6 ± 0.6	0-30	57.3 ± 2.1	3%
	14.6-20	58.3 ± 0.2			
	25-29.6	58.5 ± 0.1			

Table 32: Time-averaged values for burning rate, Series 3

Test	Present analysis			Sandia analysis [2]			Percent difference (absolute)[a]
	Time period (min)	mm/min	kg/m²s	Time period (min)	mm/min	kg/m²s	
3.1	3-5	4.11 ± 0.03	0.063 ± 0.000				
	8-11	3.79 ± 0.03	0.058 ± 0.000	9.8-10.6	3.21 ± 0.03	0.049 ± 0.000	18%
	16.5-18	2.26 ± 0.03	0.035 ± 0.000	16.6-17.4	2.18 ± 0.03	0.034 ± 0.000	4%
3.2	11.9-12.7	3.94 ± 0.03	0.061 ± 0.000	11.9-12.6	3.89 ± 0.03	0.060 ± 0.000	1%
	15-17	1.00 ± 0.03	0.015 ± 0.000	17.3-18.3	1.47 ± 0.03	0.023 ± 0.000	32%
	18.6-23.5	1.86 ± 0.03	0.029 ± 0.000				26%
3.3	3-5	2.16 ± 0.03	0.033 ± 0.000				
	8-10	1.12 ± 0.03	0.017 ± 0.000	8.5-10	1.11 ± 0.03	0.017 ± 0.000	1%
	12-19	1.03 ± 0.03	0.016 ± 0.000	16.8-18.5	0.94 ± 0.03	0.014 ± 0.000	10%
	25-28	0.81 ± 0.03	0.012 ± 0.000				
3.4	not compared			estimated burned fuel mass divided by 54 min	1.16 ± 0.03	0.018 ± 0.000	n/a
3.5	3-10	1.04 ± 0.03	0.016 ± 0.000	2-20	1.00 to 1.27 (+0.04/-0.03)	0.015 to 0.019	4% to 18%
	16-19.5	1.15 ± 0.03	0.018 ± 0.000				9% to 15%
	27.5-30.5	0.76 ± 0.03	0.012 ± 0.000				
3.6	4-6	1.25 ± 0.03	0.019 ± 0.000	6.2-9.6	1.20 ± 0.03	0.018 ± 0.000	4%
	14.6-20	0.62 ± 0.03	0.009 ± 0.000	12.3-19.3	0.32 to 0.62 (+0.03/-0.04)	0.005 to 0.010	0% to 93%
	25-29.6	0.57 ± 0.03	0.009 ± 0.000				

[a] In producing this table, the time periods used in [2] were matched (to the closest extent possible) to the time periods used in the present analysis. The percent differences therefore reflect this alignment.

Table 33: Time-averaged values for heat release rate (by oxygen consumption calorimetry), Series 3

Test[a]	Present analysis		Sandia analysis [2]		Maximum absolute percent difference
	Time period (min)	MW	Time period (min)	MW	
3.4	2-15	4.6 ± 0.7	0-50[b]	3.7 ± 1.2	37%
	18.5-22	3.6 ± 0.6			
	26-30	4.6 ± 0.7			
	30.5-34	5.1 ± 0.6			

[a] Test 3.4 was the only test with heat release rate measurements available [2].

[b] Note that this time period includes both the initial rise in heat release rate as the fire was established and the decay at the end of the burning period as the fire died down.

Table 34: Time-averaged values for flame height, Series 3

Test	Present analysis		Sandia analysis [2]		Maximum absolute percent difference
	Time period (min)	m	Time period (min)	m	
3.1	3-5	3.7 ± 0.8	5-25	3.5[a] ± 0.9	13%
	8-11	3.8 ± 0.8			
	16.5-18	3.0 ± 0.6			
3.2	11.9-12.7	3.9 ± 0.8	3-30	3.6 ± 0.8	10%
	15-17	3.3 ± 0.7			
	18.6-23.5	3.6 ± 0.7			
3.3	3-5	3.9 ± 0.9	3-30	3.4 ± 0.8	14%
	8-10	3.4 ± 0.8			
	12-19	3.2 ± 0.6			
	25-28	3.8 ± 0.8			
3.4	2-15	3.9 ± 0.8	3-25	3.5 ± 0.8	15%
	18.5-22	3.1 ± 0.6			
	26-30	3.7 ± 0.8			
	30.5-34	4.1 ± 1.0			
3.5	3-10	3.5 ± 0.8	3-30	3.6 ± 0.8	10%
	16-19.5	3.4 ± 0.7			
	27.5-30.5	4.0 ± 0.9			
3.6	4-6	3.8 ± 0.8	3-30	3.5 ± 0.8	10%
	14.6-20	3.3 ± 0.7			
	25-29.6	3.9 ± 0.9			

[a] In Luketa [2], the flame height for Test 3.1 was reported as 3.5 m in Section 6.3.1.10 and 3.4 m in Table 7-33. The latter value is considered to be incorrect because it unintentionally includes zeros in the time average.

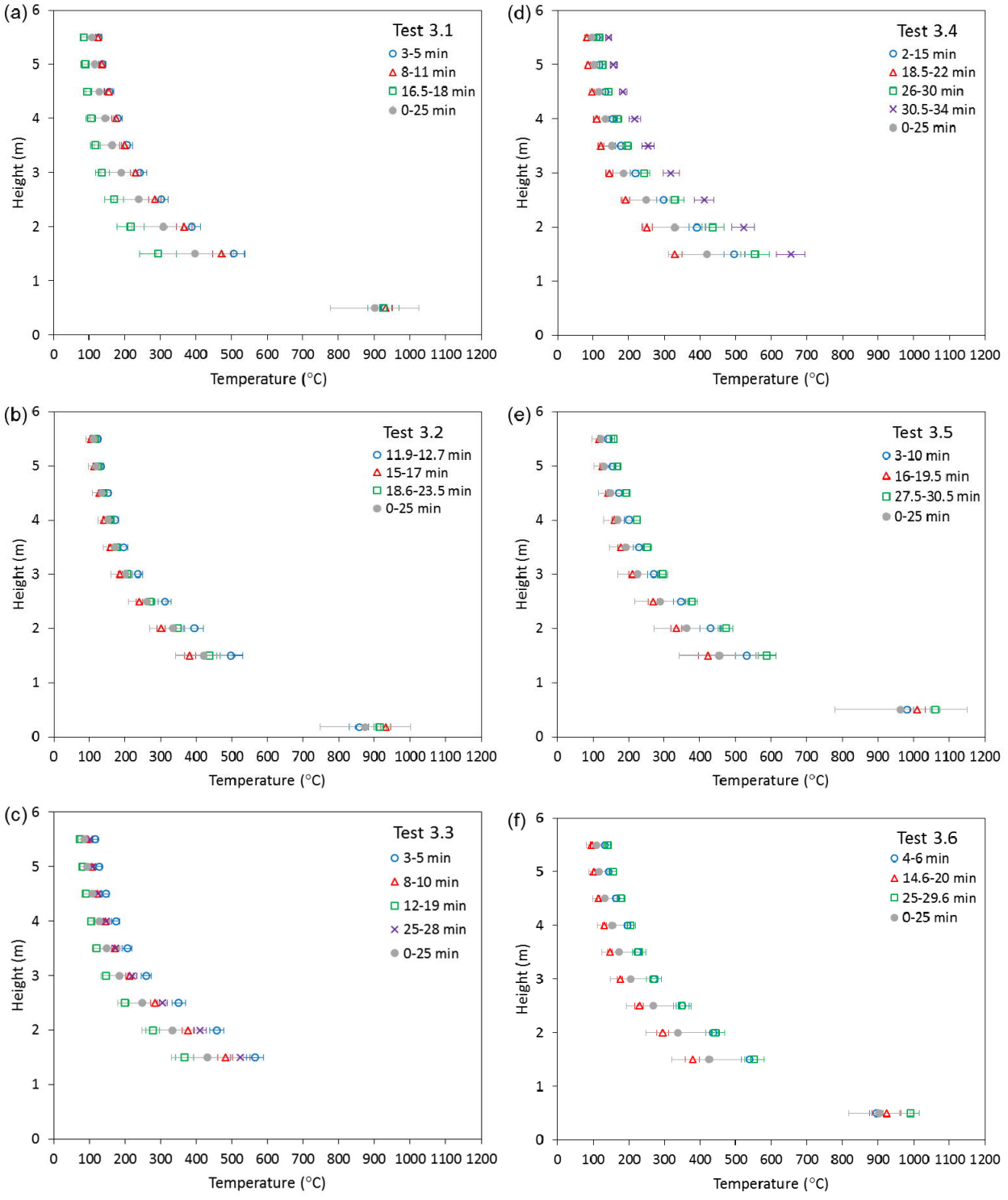

Figure 3: Time-averaged values for temperatures from thermocouple rake in fire plume, Series 3 (all 0-25 min data from [2])

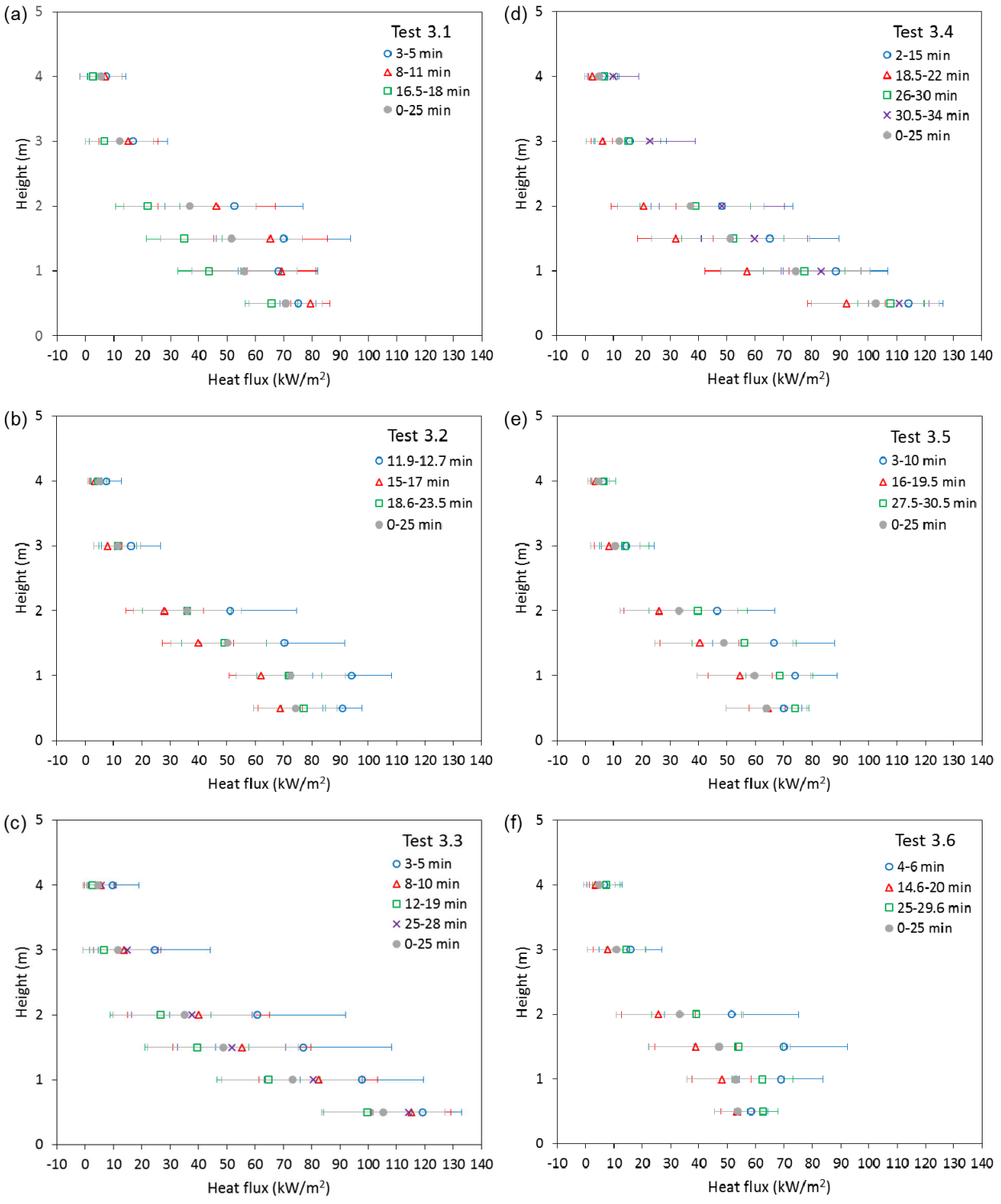

Figure 4: Time-averaged values for heat flux to narrow-view radiometers, Series 3 (all 0-25 min data from [2])

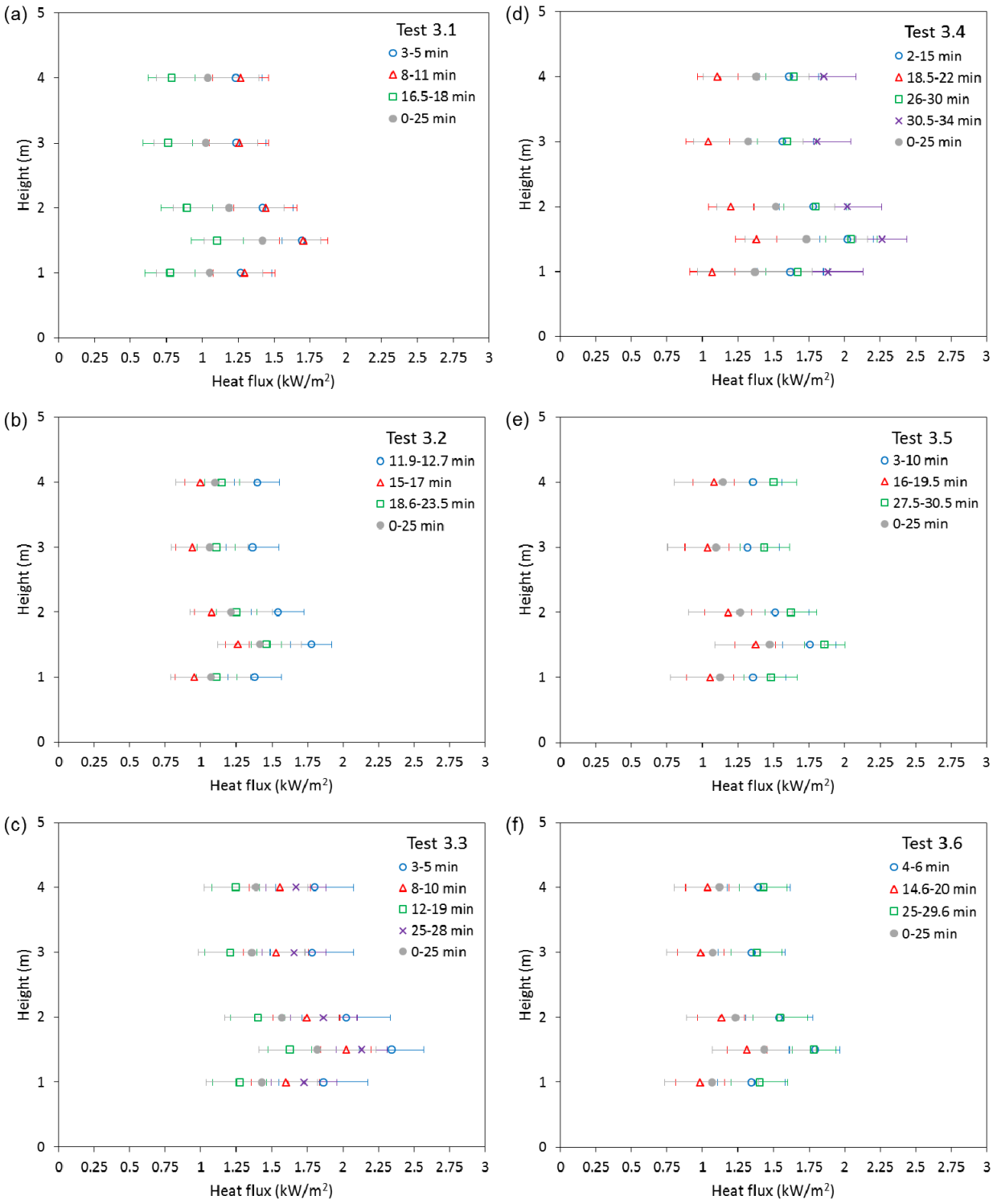

Figure 5: Time-averaged values for heat flux to wide-view radiometers, Series 3 (all 0-25 min data from [2])

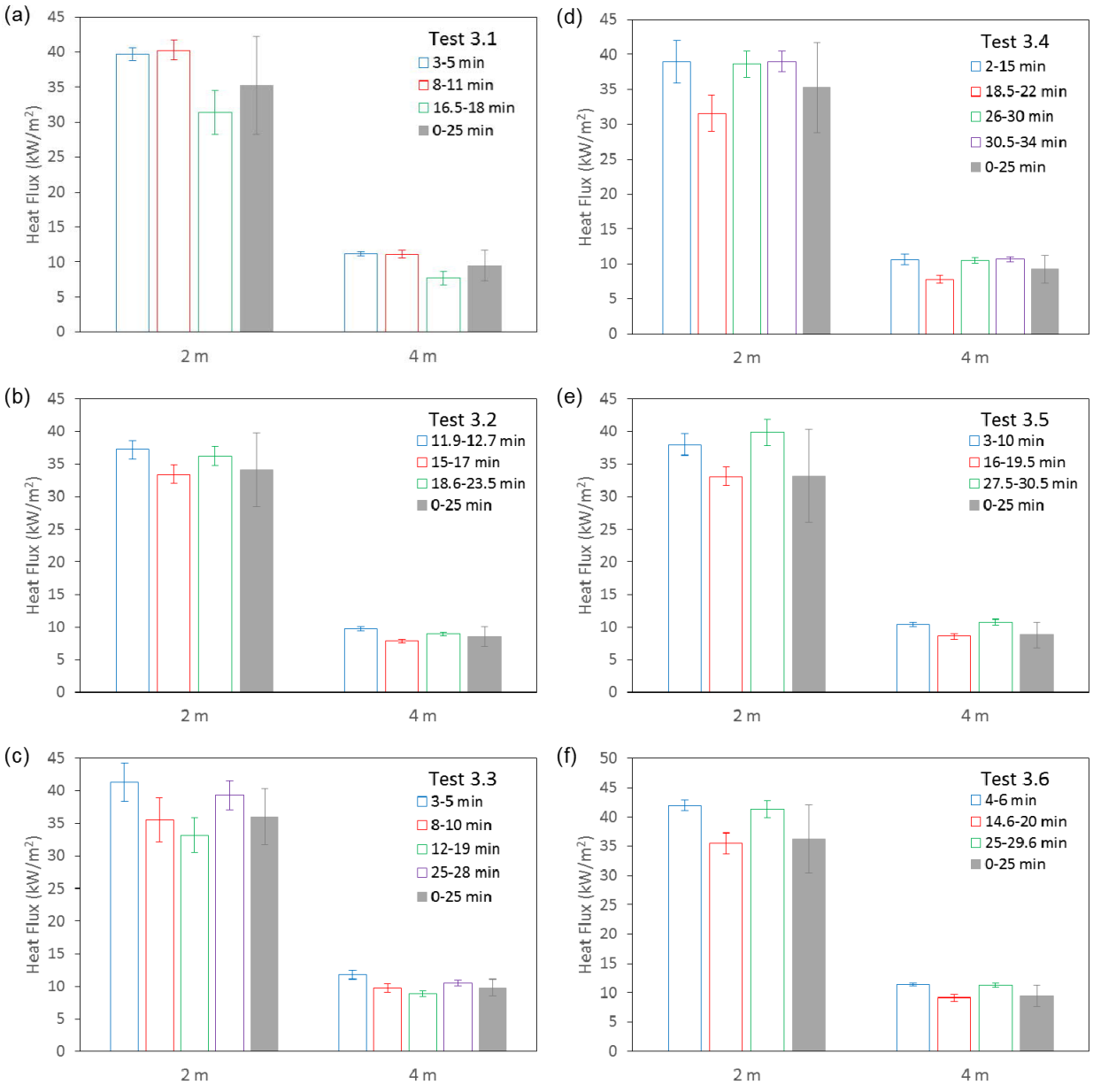

Figure 6: Time-averaged values for total heat flux to DFTs, Series 3 (all 0-25 min data from [2])

Table 32 shows that in general, the burning rates reported in Luketa [2] compare reasonably well to those from the present analysis, despite differences in how the time-averaging periods were selected.[1] However, there are some inconsistencies. For Tests 3.1 to 3.3, given the available data (which was limited by the difficulty in maintaining a constant fuel level in the pan), Sandia's values suggest a decrease in burning rate with increasing time, whereas the present analysis indicates a consistent decrease in burning rate only for Tests 3.1 and 3.3, compared to a decrease and then increase in burning rate in Test 3.2. For Tests 3.5 and 3.6, Luketa [2] selected to report ranges in burning rate over a particular time period. For Test 3.5, Luketa [2] found that the burning rate tended to fluctuate across an average value of approximately 1.12 mm/min between 2 and 20 minutes (see Figure 6-184 in [2]), whereas in the present analysis, the burning rate appeared to increase from 1.04 to 1.15 mm/min between 3 and 19.5 minutes. For Test 3.6, Luketa [2] showed that the burning rate gradually increased from 0.32 to 0.62 mm/min between 12.3 and 19.3 minutes (see Figure 6-200 in [2]), whereas in the present analysis, a burning rate of 0.62 mm/min was evaluated between 14.6 and 20 minutes, matching the upper end of this range. Overall, these differences indicate that the burning rate values were highly influenced by the selection of the time-averaging period, and are consistent with the observation that the dilbit fires did not burn steadily.

The results shown in Tables 33-34 and Figures 3-6 all seem to suggest that there were three stages of burning in the dilbit fires. The first stage appeared to be characterised by moderately high levels of heat release rate (Table 33), flame height (Table 34), plume temperatures (Figure 3), and heat flux (Figures 4-6). This was followed by a second stage, with noticeably lower levels of the same parameters, and a final stage, with levels similar to or higher than in the first stage. No consistent trend could be immediately identified in terms of what time during the test the fire would transition between stages. Note, however, that this may have been partially affected by differences in the experimental test conditions: for example, in Test 3.2, the fuel was ignited immediately upon entry into the fuel pan instead of after the pan was pre-filled, while in Test 3.4, the pan was pre-filled to a depth of 76 mm (3") (instead of 30 mm, or 1.2") and allowed to burn down without maintaining a constant fuel level (Section 2). Further discussion of the three stages of burning can be found in Section 5.3.

For the sake of brevity, the time-averaged heat flux and temperature data from each measurement location on the calorimeter are not presented here, but are instead included in Appendix A (Section A.3). Also not included is a direct comparison of the polar plots in Section A.3 to Figures 8-27 (outer cylinder temperatures), 8-30 (exterior temperatures), and 8-33 (total heat flux) in Luketa [2]. Instead, Tables 35-37 provide comparisons of the spatially averaged values of outer cylinder temperature, temperature exterior to the calorimeter, and total heat flux, taken across all measurement locations on the calorimeter. In general, the average values from the Sandia analysis are lower and have larger standard deviations, compared to those from the present analysis, due to the fact that they were based on a time integration from 0 to 25 minutes and thus included the early portion of the test while the fire was still being established.

[1] To select appropriate time-averaging periods for the burning rate, Luketa [2] used only the first two criteria discussed in Section 3.2 (steady readings from the differential pressure gauge and a steady decrease in the load cell measurements). On the other hand, the present analysis used an additional criterion of steady fire plume temperatures.

Table 35: Comparison of spatially averaged outer cylinder temperatures across all calorimeter thermocouple locations, Series 3

Test	Time period (min)	Present analysis (°C)	Neglected locations in present analysis	Sandia analysis [2], Table 7-26 (°C, based on 0-25 min integration)	Neglected locations in Sandia analysis
3.1	3-5	624.3 ± 57.9	L135[a], C180, C270, R270, R315	640.7 ± 176.2	none
	8-11	800.8 ± 6.5	L135, C180, C270, R270, R315		
	16.5-18	730.1 ± 7.0	L135[a], C180, C270, R270, R315		
3.2	11.9-12.7	844.2 ± 3.2	L135, L270, L315, C180, C225, C270, R270, R315	615.4 ± 182.6	none
	15-17	855.7 ± 7.3	L135, L270, L315, C180, C225, C270, R270, R315		
	18.6-23.5	883.1 ± 3.9	L135, L270, L315, C180, C225, C270, R270, R315		
3.5	3-10	787.3 ± 104.3	L135, L270, C90, C270, R270	707.6[b] ± 241.8	none
	16-19.5	899.5 ± 6.7	L135, L270, C90[a], C270, R270		
	27.5-30.5	1001.8 ± 11.9	L135, L270, C90, C270, R270		
3.6	4-6	739.6 ± 25.9	L135, L270, C45, C90, C270	696.3[c] ± 219.8	none
	14.6-20	803.5 ± 8.8	L135, L270, C45, C90, C270		
	25-29.6	901.0 ± 16.5	L135, L270, C45, C90, C270		

[a] Although data was available at this location, it was neglected in order to allow consistent comparison with other time periods in the test. The difference between including the available data and neglecting it was less than 2%.
[b] This spatial average includes a value of 0°C at L135. Without it, the average would be 738.3 ± 241.8°C.
[c] This spatial average includes a value of 0°C at L135, and was erroneously based on a time integration from -1 to 24 minutes. Without the L135 value, the average would be 726.5 ± 219.8°C if integrated from -1 to 24 minutes and 752.4 ± 184.8°C if corrected to 0-25 minutes.

Table 36: Comparison of spatially averaged exterior temperatures across all calorimeter thermocouple locations, Series 3

Test	Time period (min)	Present analysis (°C)	Neglected locations in present analysis	Sandia analysis [2], Table 7-26 (°C, based on 0-25 min integration)	Neglected locations in Sandia analysis
3.1	3-5	812.7 ± 17.7	none	774.6 ± 133.4	none
	8-11	833.2 ± 16.3			
	16.5-18	746.0 ± 45.7			
3.2	11.9-12.7	868.9 ± 24.5	none	824.8 ± 147.2	none
	15-17	869.4 ± 27.4			
	18.6-23.5	892.6 ± 27.2			
3.5	3-10	910.8 ± 32.1	none	869.9 ± 175.6	none
	16-19.5	915.1 ± 35.7			
	27.5-30.5	1008.4 ± 32.8			
3.6	4-6	833.7 ± 21.6	none	773.3 ± 181.8	none
	14.6-20	817.5 ± 30.1			
	25-29.6	917.9 ± 26.5			

Table 37: Comparison of spatially averaged total heat flux values across all calorimeter thermocouple locations, Series 3

Test	Time period (min)	Present analysis (kW/m^2)	Neglected locations in present analysis	Sandia analysis [2], Table 7-26 (kW/m^2, based on 0-25 min integration)	Neglected locations in Sandia analysis
3.1	3-5	74.8 ± 5.5	L135[a], C180, C270, R270, R315	63.9 ± 15.7	L135, L270, L315, C45, C90, C180, C270, R315
	8-11	68.6 ± 5.6	L135, C180, C270, R270, R315		
	16.5-18	55.2 ± 9.8	L135, C180, C270, R270, R315		
3.2	11.9-12.7	77.8 ± 4.7	L135, L270, L315, C180, C225, C270, R270, R315	67.1 ± 13.9	L135, L270, L315, C45, C90, C180, C270, R315
	15-17	81.3 ± 4.3	L135, L270, L315, C180, C225, C270, R270, R315		
	18.6-23.5	87.5 ± 4.2	L135, L270, L315, C180, C225, C270, R270, R315		
3.5	3-10	86.3 ± 8.2	L135, L270, C45, C90, C270, R270	83.1 ± 21.3	L135, L270, L315, C45, C90, C180, C270, R315
	16-19.5	91.5 ± 10.0	L135, L270, C45[a], C90[a], C270, R270		
	27.5-30.5	128.5 ± 10.2	L135, L270, C45[a], C90, C270, R270		
3.6	4-6	71.3 ± 4.9	L135, L270, C45, C90, C270	75.5 ± 21.5	L135, L270, L315, C45, C90, C180, C270, R315
	14.6-20	73.3 ± 7.7	L135, L270, C45, C90, C270		
	25-29.6	102.6 ± 7.3	L135, L270, C45, C90, C270		

[a] Although data was available at this location, it was neglected in order to allow consistent comparison with other time periods in the test. The difference between including the available data and neglecting it was less than 3%.

Table 35 indicates that with the exception of Test 3.1 (which is considered less reliable due to initial difficulties in controlling the fuel level [2]), the spatially averaged outer cylinder temperature increased with time. This could be expected because the calorimeter contained significant thermal mass and would therefore continue to heat up over the course of each 30 minute test. The large thermal mass would also result in a thermal lag when compared to changes in the surrounding plume temperatures (e.g. during transitions between the three stages of burning).

No consistent trend in time could be identified in Table 36 for the spatially averaged temperature exterior to the calorimeter. This may be explained by comparing trends in time at the top versus bottom of the calorimeter, shown for the centre measurement plane in Figure 7. Test 3.1 was the only one in which the exterior temperatures at the top and bottom both followed the same trend, i.e. increased between the first and second time-averaging periods, then decreased between the second and third time-averaging periods. In all other tests, the top and bottom temperatures followed different trends from the first to third time-averaging periods: for example, in Test 3.2, the top temperature decreased and then increased (Figure 7a), while the bottom temperature increased and then decreased (Figure 7b). As a result, the spatially averaged temperatures for

Test 3.2 in Table 36 were similar among all time-averaging periods. It may be noted that the trends in time shown in Figure 7 are consistent with those shown by the plume axis temperatures immediately adjacent to the calorimeter in Figure 3. For instance, referring again to Test 3.2 (Figure 3b), the plume axis temperature at 1.5 m decreased and then increased between the first, second and third time-averaging periods, consistent with Figure 7a, while the temperature at 0.18 m increased and then decreased slightly, consistent with Figure 7b.

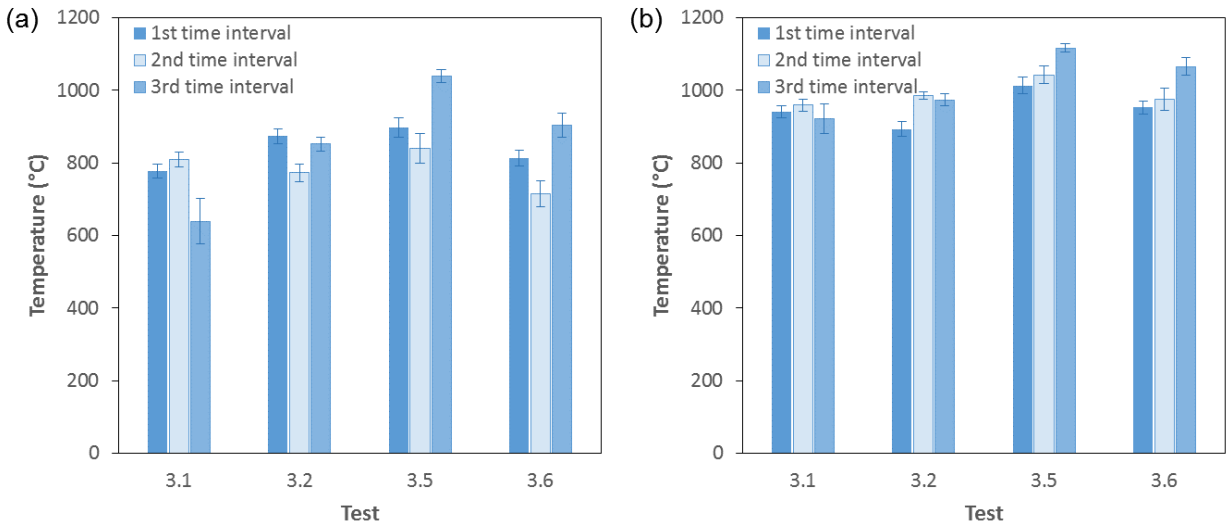

Figure 7: Time-averaged temperatures exterior to calorimeter, (a) top centre plane, C0, (b) bottom centre plane, C180

Overall, the above observations indicate that the characteristics of the three stages of burning, described previously as high levels of temperature and heat flux in the first stage, followed by lower levels in the second stage and finally high levels in the third stage, are valid only at heights above the calorimeter. The three stages of burning are characterised differently below the calorimeter because the calorimeter is a thermally massive object that interacts with and influences the surrounding flames. This influence is seen most prominently in Tests 3.5 and 3.6, in which the exterior temperatures at the bottom of the calorimeter in the centre plane (Figure 7b) increased continually from the first to third time-averaging periods, consistent with the outer cylinder temperatures in Table 35 and the plume temperatures at 0.5 m height in Figures 3e and f. Because the calorimeter was heating up during the test, radiation from its outer surface would be expected to be a driving factor in determining the temperatures measured below the calorimeter.

In Table 37, the spatially averaged total heat flux to the calorimeter decreased with time in Test 3.1, but increased with time in Tests 3.2, 3.5 and 3.6. Again, there are differences between the top and bottom of the calorimeter, as shown in Figure 8. In this figure, the bottom of the calorimeter is represented using the left and right planes (L180 and R180) because no data was available for the centre plane (C180) in Tests 3.1 and 3.2.

In Test 3.1, the total heat flux to both the top and bottom of the calorimeter decreased with time, most likely due to the fact that a constant fuel level was not being maintained throughout this test. In the remaining tests, the heat flux to the top of the calorimeter (Figure 8a) decreased from the first to second time-averaging periods, then increased from the second to third time-averaging periods, consistent with the three-stage burning characteristics seen among other parameters at heights above the calorimeter. Underneath the calorimeter,

however (Figures 8b and c), the heat flux consistently increased from the first to second, then from the second to third, time-averaging periods. This is in agreement with the continually increasing temperatures measured below the calorimeter (Figure 7b) and suggests that there was very little heat loss in the region underneath the calorimeter, so that the total heat flux from the fire would continually increase throughout the test.

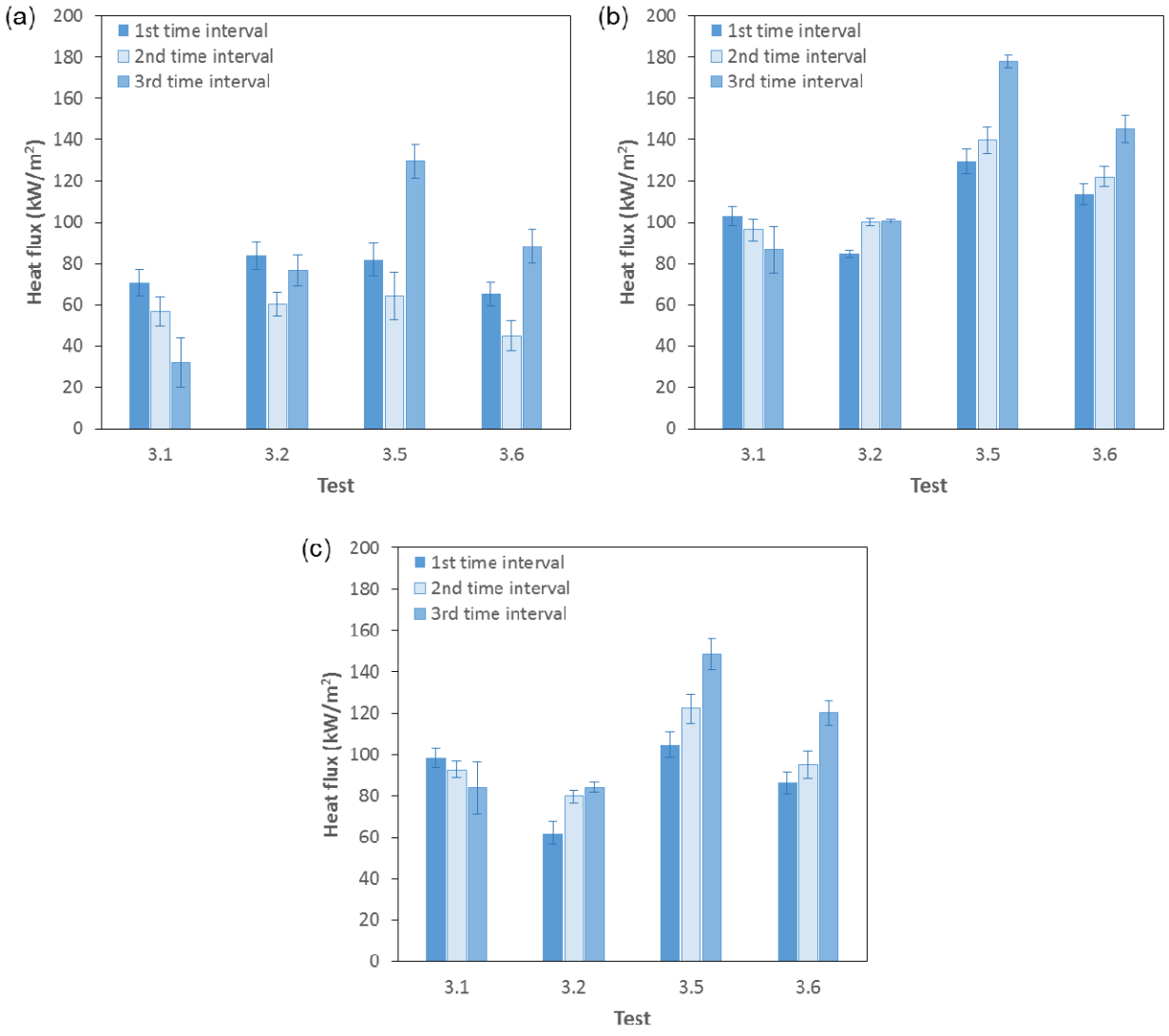

Figure 8: Time-averaged total heat flux to calorimeter, (a) top centre plane, C0, (b) bottom left plane, L180, (c) bottom right plane, R180

5 Liquid Fuel Temperature Results

Luketa [2] described the use of a thermocouple rake in the fuel pan to monitor the temperature distribution within the fuel layer. The rake was composed of 30 Type K Inconel thermocouples, each 1 mm in diameter and mounted 2 mm apart on a steel plate that was placed at the edge of the pan.

Although time traces of the fuel rake temperatures were presented in Luketa [2] for each test, limited analysis was conducted on the data. Therefore, in this section, the fuel rake temperatures are examined in more detail in an attempt to gain insights into the burning behaviour of each fuel.

5.1 Series 1 (Heptane)

Figure 9 shows a typical example of fuel rake temperatures from a Series 1 test. In Series 1, the fuel level was maintained constant using an automatic control system based on differential pressure gauge measurements of the fuel height in the pan. As seen in the figure, a constant fuel level was maintained until approximately 44 minutes in this test, after which the fuel was allowed to burn down until the fire self-extinguished. All thermocouples reached a temperature near the boiling point of heptane (98.4°C) after approximately 30 minutes, indicating that the fuel temperature distribution was no longer stratified. With TC 12 (the orange line in Figure 9) being the thermocouple closest to the fuel surface during the period of constant fuel level, its temperatures remained steady near the boiling point until 44 minutes, as would be expected.

After 44 minutes, there was a noticeable increase in heat release rate as the fuel began to burn down. This may be due to the increasing lip height of the pan above the fuel surface (as a result of the decreasing fuel height), which affects both heat feedback to the fuel surface and entrainment dynamics in the fire.

Overall, this example shows how the vertical temperature distribution in the fuel pool can evolve for a pure, single-component fuel. Because the pan was pre-filled with fuel prior to ignition, the initial temperature stratification gradually decreased until the entire pool was at a uniform temperature near the boiling point. This temperature was then maintained until the fuel completely burned down.

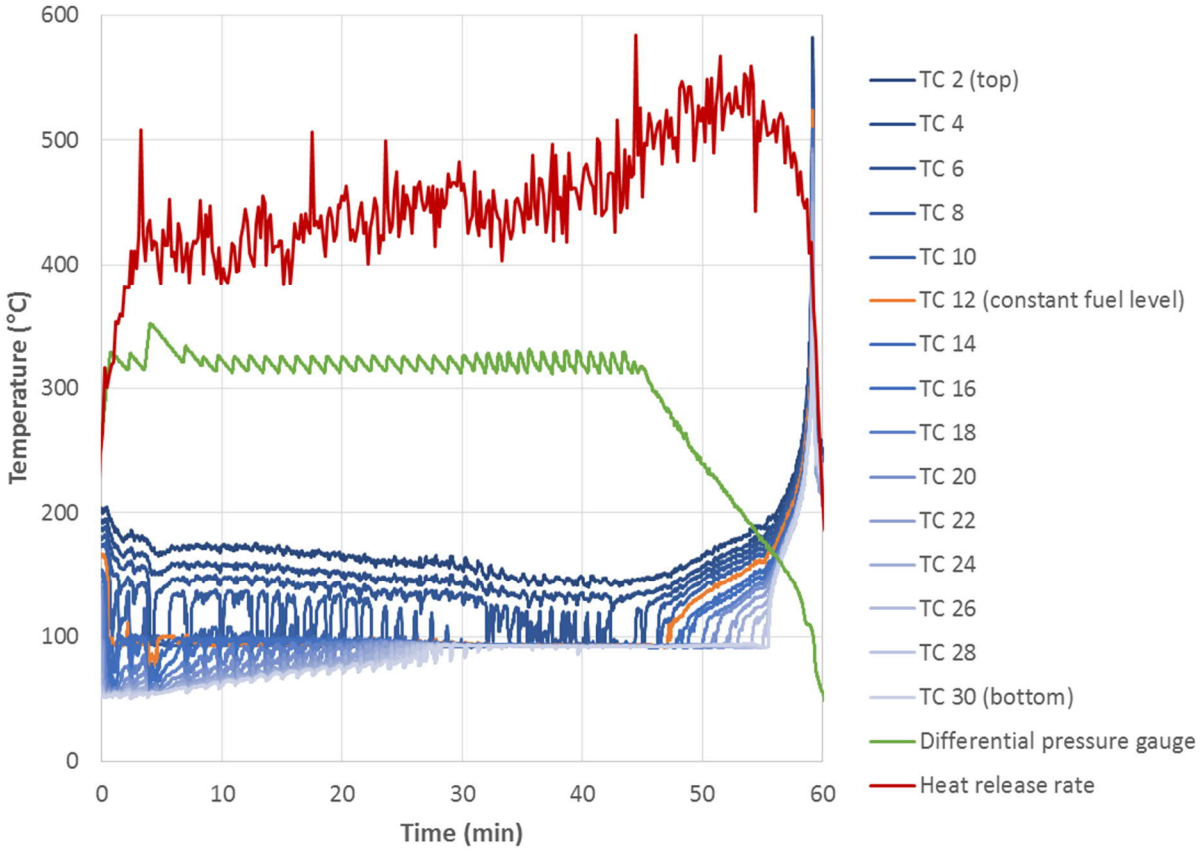

Figure 9: Fuel rake temperatures for Test 1.3 (for simplicity, axes are not shown for differential pressure gauge or heat release rate measurements)

5.2 Series 2 (Bakken)

Figure 10 shows the fuel rake temperatures for Test 2.6, which involved no calorimeter and a non-continuous fuel feed, i.e. the “burn-down” test (Table 1). Unlike Test 1.3 above, the tests in Series 2 depended on manual control of the fuel feed, which resulted in irregular changes in the fuel rake temperatures as the fuel supply was manually started and stopped. Since Test 2.6 provides experimental conditions with the least external influence on the fuel rake temperatures, it was selected as the primary test for examining changes in the fuel temperature distribution.

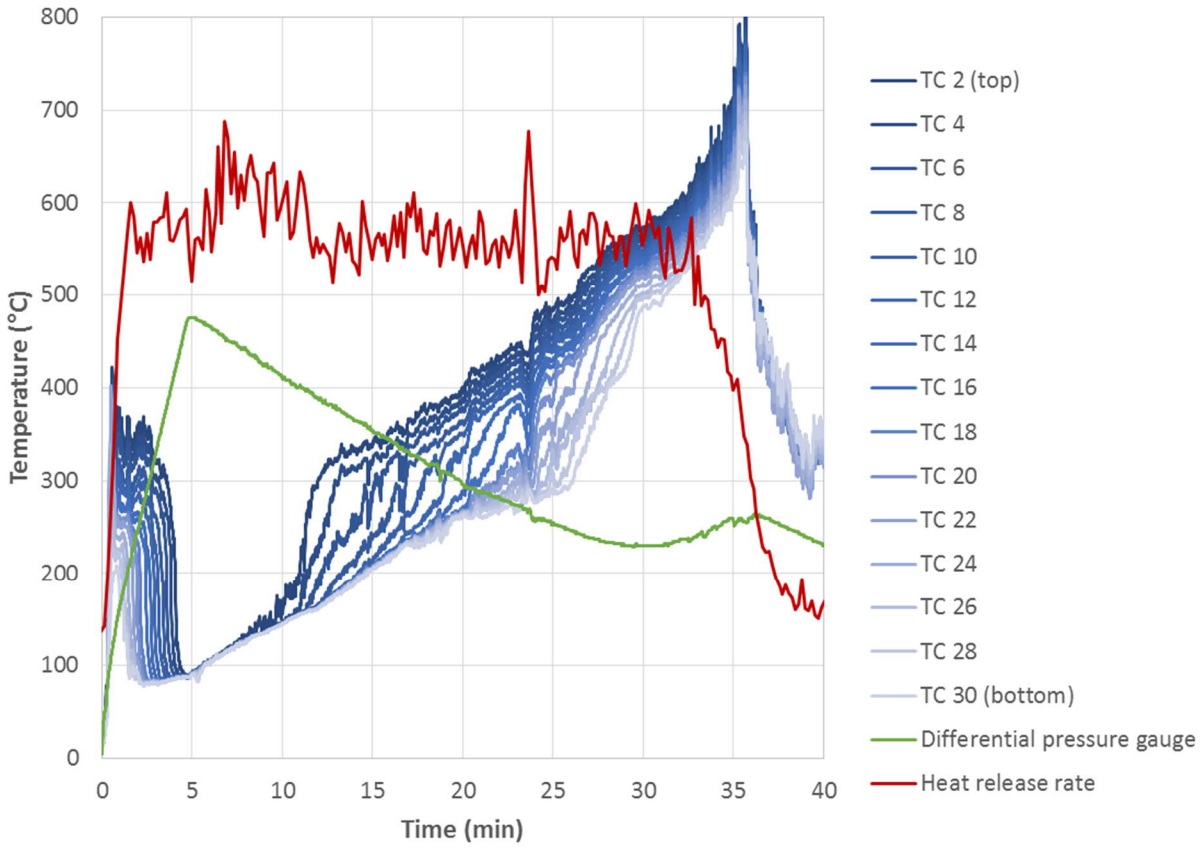

Figure 10: Fuel rake temperatures for Test 2.6 (for simplicity, axes are not shown for differential pressure gauge or heat release rate measurements)

In this test, ignition occurred at 0 minutes, as soon as fuel started entering the pan. This was done in order to ensure that any effects of volatiles in the crude oil were captured. During the first 4.6 minutes, fuel continued to be added to the pan until it reached a height of approximately 76 mm (3"). Note that TC 2 in Figure 10 was located at a height of approximately 58 mm (2.3"). Therefore, the entire thermocouple rake was submerged in the fuel by 5 minutes, with all temperatures around 100°C.

From 5 to approximately 11 minutes, the fuel rake temperatures gradually increased to about 155°C. This coincided with a slight increase (~10%) in the average heat release rate, compared to the remainder of the test. The higher heat release rate suggests potential preferential burning of lighter ends in the crude oil. Considering the boiling point distribution of the tested Bakken crude oil as evaluated by Lord [3] (Figure 11), it appears that crude oil components with a carbon number up to C9 could be burning off during this time period.[2] The compositional analysis conducted by Lord [3] shows that the tested Bakken samples indeed had a peak in composition at C7 and C8 (Figure 12).

[2] Note that in the generation of Figure 11, the fuel was assumed to be burning down and not replenished (as per Test 2.6). Crude oil composition was represented by assigning a boiling point to each component and simulating distillation of the material with increasing temperature [3].

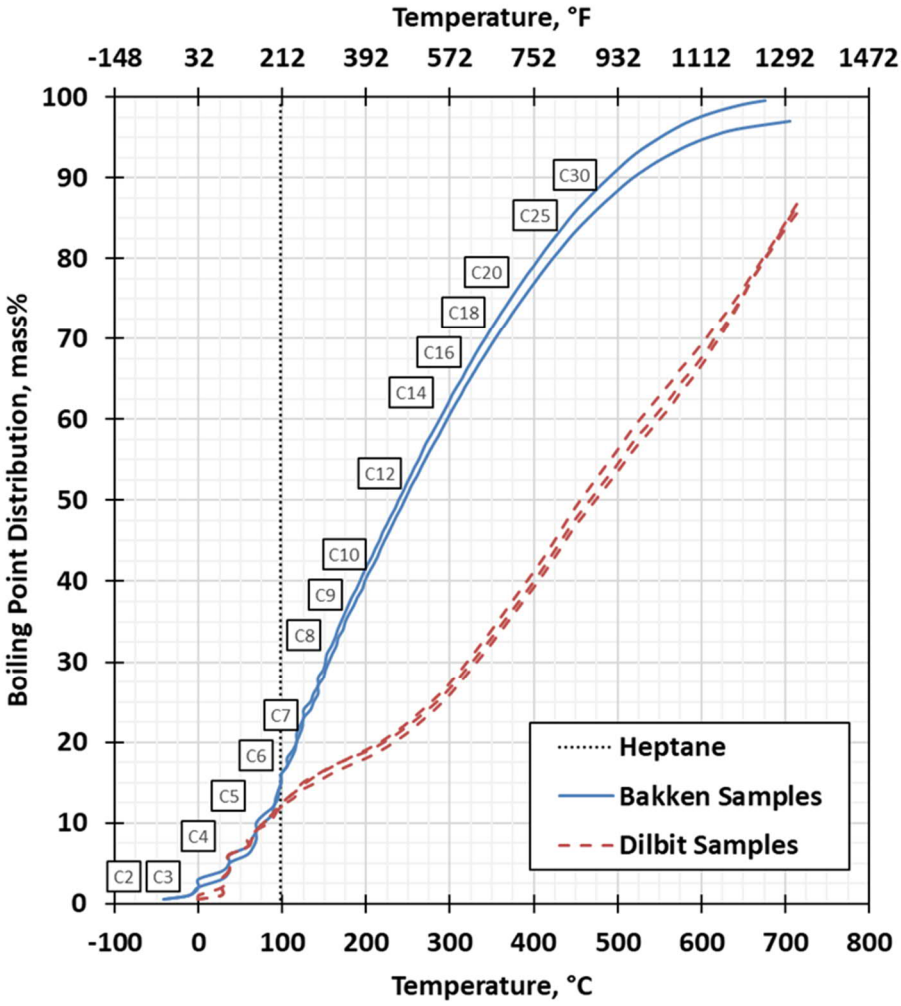

Figure 11: Temperature vs. boiling point distribution for the fuels tested in Series 1, 2 and 3 (reproduced from [3])

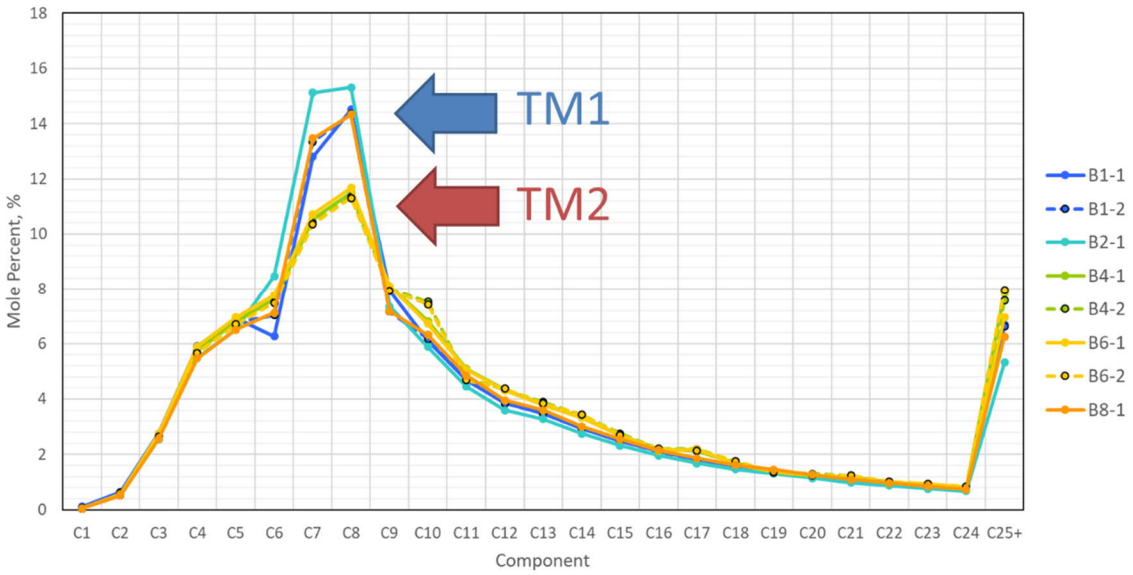

Figure 12: Whole oil composition of the tested Bakken samples (reproduced from [3]; TM1 refers to GPA 2103-M merge method and TM2 refers to ASTM D8003 merge method)

After 11 minutes, the temperatures from each thermocouple were observed to increase in turn, starting with TC 2 (the top thermocouple), as the fuel gradually burned down and each thermocouple passed from being submerged in the liquid fuel to being exposed to the hotter vapour region immediately above the fuel surface.

At approximately 21 minutes, the rate of decrease (i.e. negative slope) of the differential pressure curve (which represents the fuel height) in Figure 10 started to decline until it reached zero at 30 minutes (resulting in a local minimum), indicating a gradual decrease in the burning rate. The curve then increased between 30 and 36 minutes, before subsequently decreasing again. The increase in differential pressure could potentially indicate formation of solids in the pan, although further research would be needed to confirm this.

Between 23 and 24 minutes, there was a simultaneous sudden increase in the heat release rate and decrease in the fuel rake temperatures (Figure 10). These changes coincided with a sudden increase in temperatures measured along the plume axis at heights of 2.5 m and higher, immediately followed by a decrease in temperatures at all heights in the plume (Figure 13). Although more research is warranted to determine exactly what may have been occurring here, it is surmised that a sudden increase in available fuel vapours caused the region immediately above the fuel surface to become fuel-rich, creating the decrease in fuel rake temperatures. Then, burning of these fuel vapours would have corresponded to the increase in temperatures observed at higher elevations in the fire plume, as well as the increase in heat release rate.

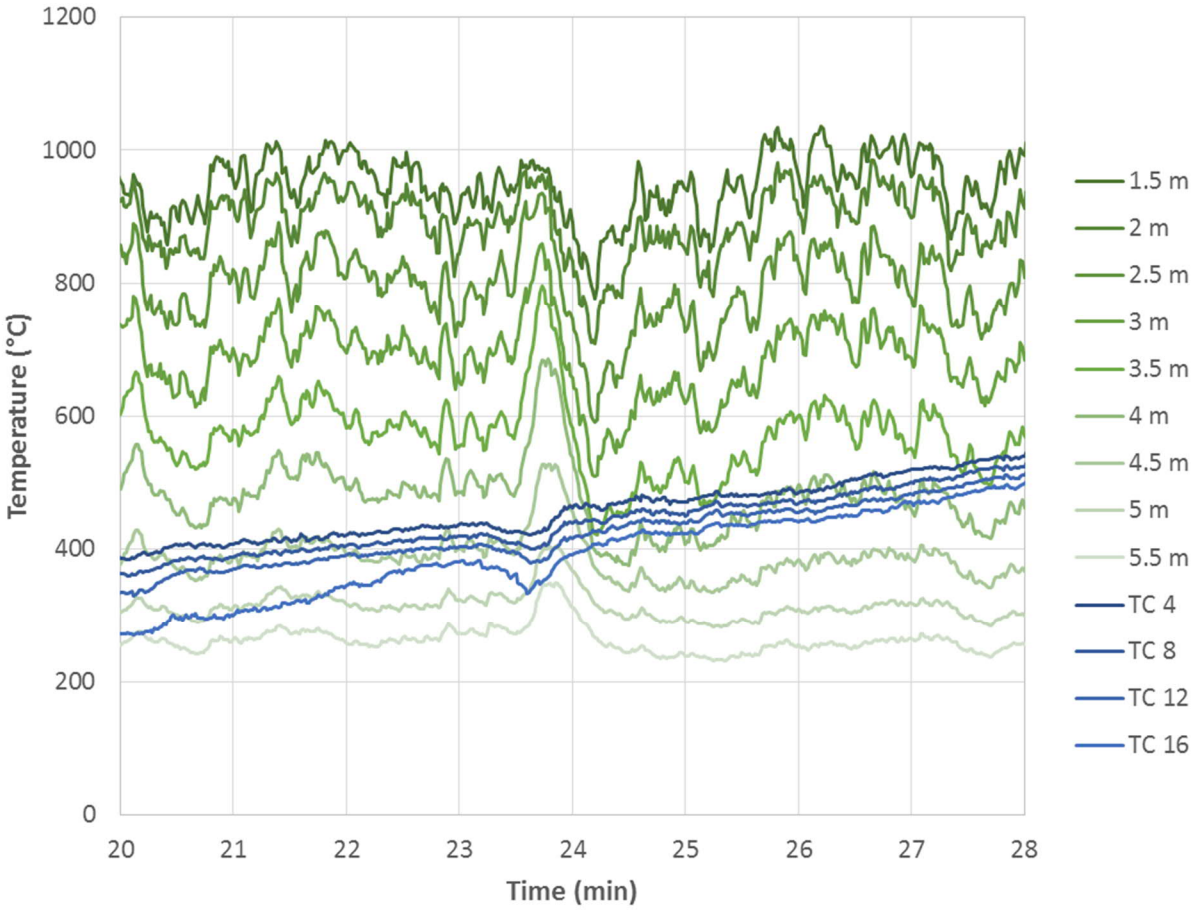

Figure 13: Temperatures from thermocouple rake along axis of fire plume (green lines) and from thermocouple rake in liquid fuel (blue lines), Test 2.6

From Figure 10, it may be noted that the liquid fuel temperature at 21 minutes (when the burning rate started to decrease) was approximately 260°C, which, according to Figure 11, would correspond to the vapourization of crude oil components with a carbon number up to C14. The fuel temperature at 23-24 minutes (when the fuel rake temperatures suddenly decreased, and the plume temperatures and heat release rate suddenly increased) was approximately 270-290°C, which would correspond to the vapourization of crude oil components with a carbon number up to C16 or even C18. It should be noted that heavier hydrocarbons likely do not vapourize directly (as may be initially interpreted by looking at Figure 11) but instead go through a series of chemical reactions to break down into lighter hydrocarbons that are then capable of vapourizing and burning (referred to as thermal cracking or pyrolysis). Mild thermal cracking of crude oil can occur starting at around 300°C, but this occurs at very slow rates [5]. Because the fuel rake thermocouples likely indicate an average liquid temperature, it is possible that localized regions with higher temperatures could exist in the liquid fuel, which would permit more severe cracking and greater generation of lighter hydrocarbons [5]. If thermal cracking were indeed occurring starting at around 23 minutes due to localized high temperature regions, this could explain the sudden increase in available fuel vapours at 23-24 minutes that was surmised above.

It is acknowledged that the synchrony of the events observed at 23-24 minutes is affected by potential time lag differences in the various measurements. Time lag in thermocouple measurements is affected by the size and

thermal mass of the thermocouple; however, *differences* in time lag between the fuel rake and plume temperature measurements could be minimized by using the same type of thermocouple in both thermocouple rakes, as was done in these experiments [2]. More importantly, it should be noted that not only were the heat release rate measurements taken using a different data acquisition system than the thermocouple measurements, but there is a large inherent time lag when measuring heat release rate because the combustion products must be collected in the duct system and sampled at a location where the gases are sufficiently well mixed (which is far from the actual fire) before being further sent to the combustion gas analyser. Thus, it is assumed here that synchrony of the thermocouple measurements in Figure 13 is reasonably accurate, whereas synchrony of the heat release rate measurements to the thermocouple measurements is associated with greater uncertainty (as per the discussion at the beginning of Section 4).

5.3 Series 3 (Dilbit)

In this test series, the fuel rake temperature data was noisier and more thermocouples experienced failure, compared to Series 1 and 2. Test 3.6 was selected as a primary test for examining changes in the fuel temperature distribution because it used a newly rebuilt thermocouple rake and had a reasonably well-controlled fuel feed to maintain a constant fuel level. However, because there was a limited number of thermocouples available to rebuild the rake, only three thermocouples were submerged in the fuel [2]. Figure 14 shows the fuel rake temperatures for Test 3.6, in which the calorimeter was at 1 m height and a constant fuel level was maintained for approximately 30 minutes. Note that the pan was pre-filled to the desired fuel height of approximately 30 mm (1.2") prior to ignition. Also shown in the figure are measurements from the differential pressure gauge (which started to fail shortly before 20 minutes) and measurements from the load cell placed underneath the fuel supply tank, which indicate when fuel was being supplied to the pan.

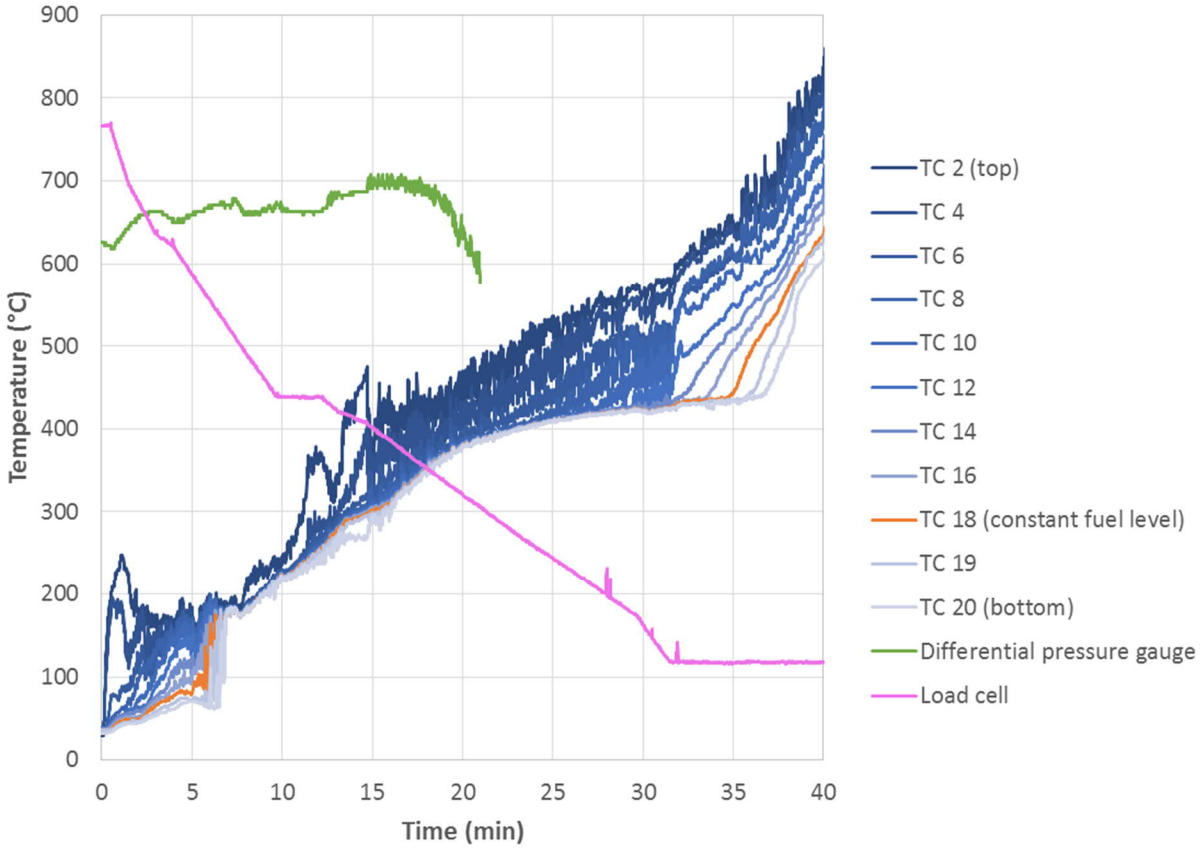

Figure 14: Fuel rake temperatures for Test 3.6 (for simplicity, axes are not shown for differential pressure gauge or fuel scale measurements)

As ignition occurred after the pan was pre-filled with fuel, the fuel temperature distribution was initially stratified over approximately the first 6 minutes of the test. After about 7 minutes, all three thermocouples in the fuel (TCs 18, 19 and 20) were at approximately the same temperature (180°C), and remained at temperatures similar to each other for the remainder of the test.

Figure 15 shows that after about 7 minutes, the thermocouples along the plume axis at heights of 1.5 m and above measured a sudden temperature increase, immediately followed by a sharp decrease, after which the temperatures remained at relatively low levels before gradually increasing towards the end of the test. This suggests potential preferential burning of lighter ends in the crude oil once the entire pool reached a uniform temperature of about 180°C. It is consistent with Figure 11, which indicates that crude oil components with a carbon number up to C10 could be burning off at temperatures of 180°C, as well as Figure 16, which shows a peak in composition at C5 for the tested dilbit.

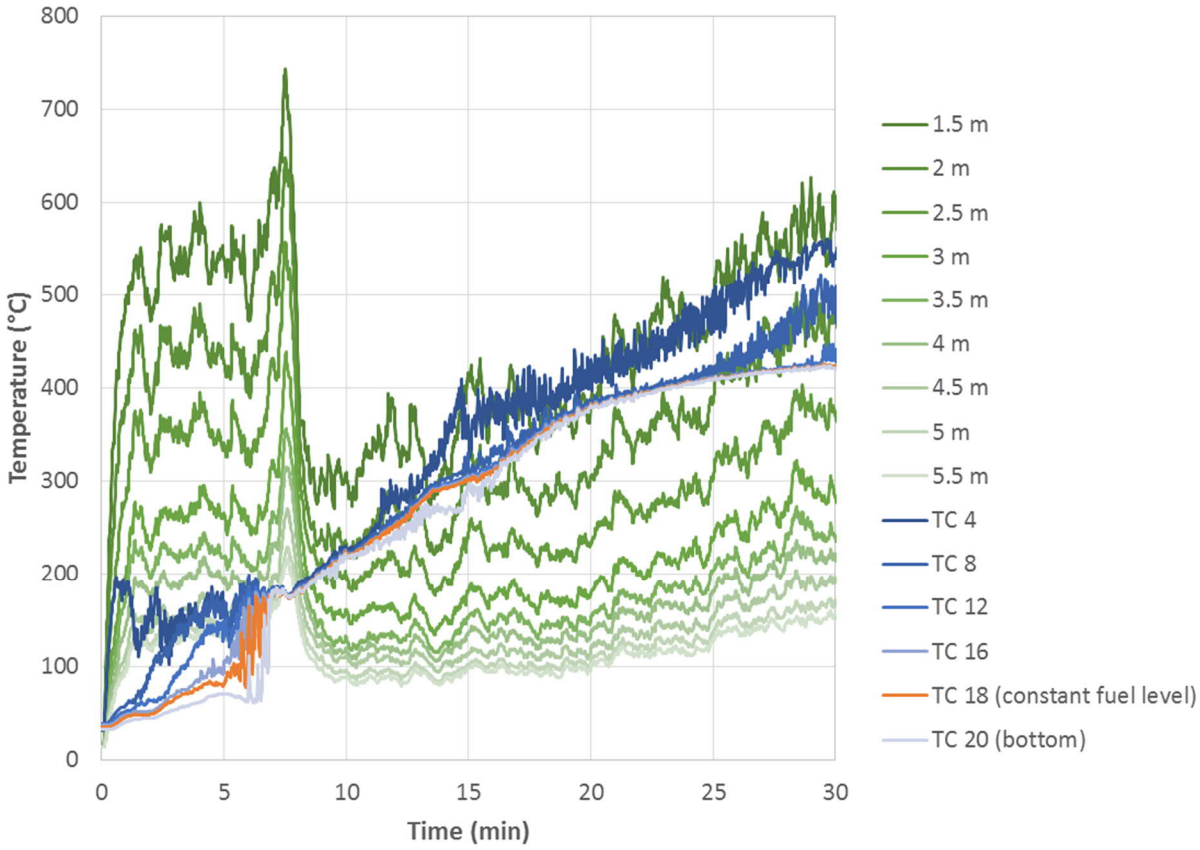

Figure 15: Temperatures from thermocouple rake along axis of fire plume (green lines) and from thermocouple rake in liquid fuel (blue and orange lines), Test 3.6

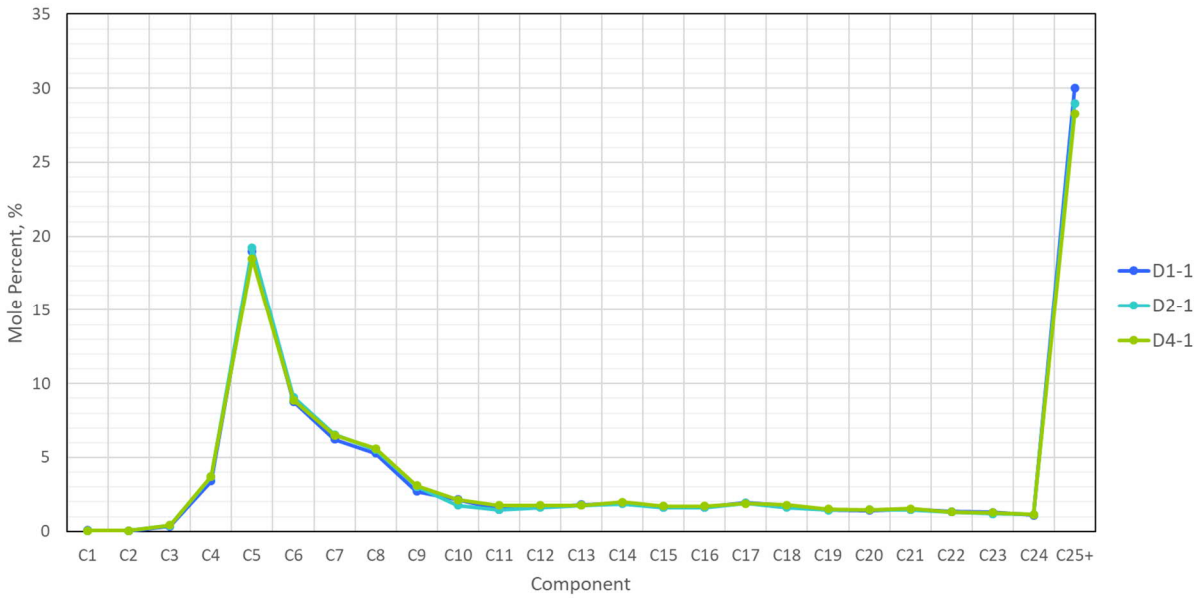

Figure 16: Whole oil composition of the tested dilbit samples (reproduced from [3])

In an attempt to gain further insight into what may have been happening in the dilbit as it burned, Figure 17 shows a plot of flame height[3] versus fuel temperature as indicated by the lowest thermocouple on the fuel temperature rake. Each data point is based on values averaged over the time intervals in Table 6. Increasing fuel temperature represents increasing time throughout each test. It may be observed that the data points for Test 3.3 at 136°C and Test 3.4 at 58°C were associated with large horizontal error bars (which denote the maximum/minimum fuel temperatures measured during the time interval). This occurred because during that time interval, the fuel changed from a stratified to uniform temperature distribution (due to convective mixing), causing a sharp increase in the temperature measured by the thermocouple at the bottom of the rake. It should be noted that for data points less than 100°C, the fuel temperature distribution was stratified, whereas for data points around 300°C or greater, the fuel temperature distribution was no longer stratified. Test 3.2 was not included in the plot because in that test, the fuel was ignited immediately upon entry into the fuel pan, affecting comparability of the average fuel temperature measurements to the other tests. Test 3.5 was also not included because most of the thermocouples on the fuel temperature rake failed early in that test.

It may be seen from Figure 17 that as the fuel temperature increased up to approximately 300°C, the flame height decreased. Then, as the fuel temperature continued to increase above 300°C, the flame height increased. This same trend was observed in other parameters, such as the narrow-view and wide-view radiometers at 1 m height (Figures 18 and 19), and corresponds to the three-stage nature of burning that was identified in Section 4.3. Thus it appears that the first stage, with high levels of flame height, plume temperature and heat flux, would correspond to fuel temperatures below approximately 100°C, when the fuel temperature distribution was still stratified. The second stage, with the lowest levels of flame height, plume temperature and heat flux, would correspond to fuel temperatures between approximately 300°C and 350°C, while the third stage, again with high levels of flame height, plume temperature and heat flux, would correspond to fuel temperatures greater than 350°C.

[3] Flame height is representative of the overall fire behaviour and is dependent on heat release rate; recall that heat release rate measurements were not successful in Series 3.

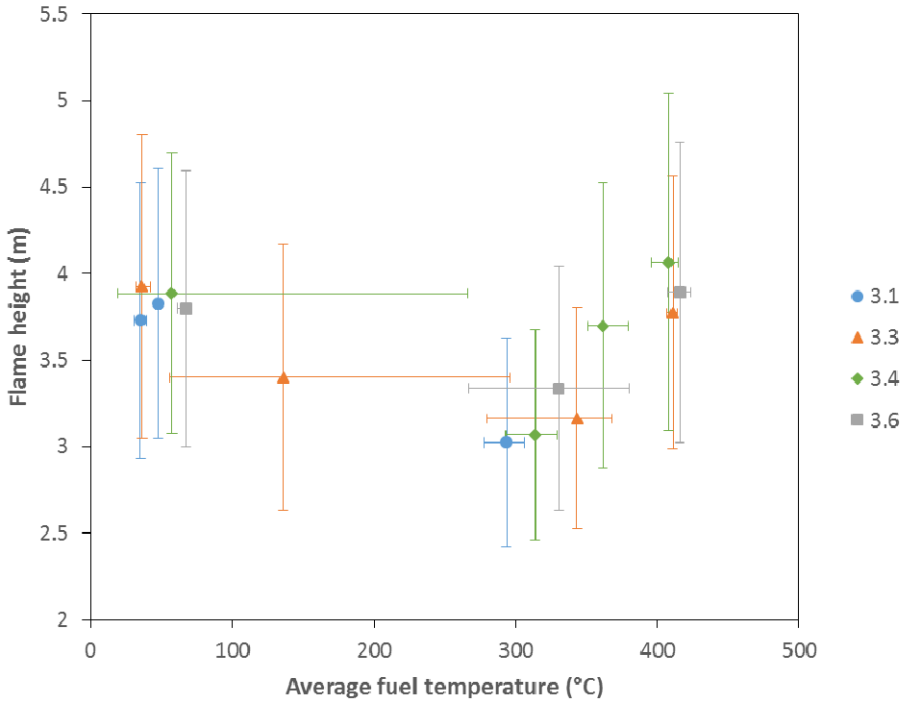

Figure 17: Flame height versus fuel temperature as indicated by lowest thermocouple on fuel temperature rake (vertical error bars denote flame height standard deviation; horizontal error bars denote minimum/maximum fuel temperatures during the time-averaging period)

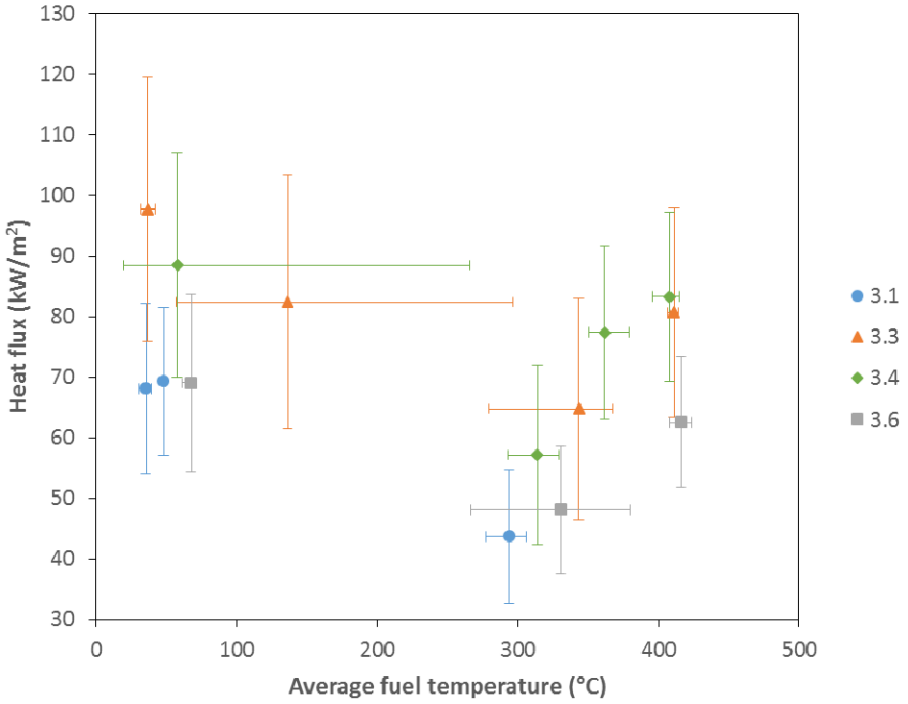

Figure 18: Heat flux measured by narrow-view radiometer at 1 m height, versus fuel temperature as indicated by lowest thermocouple on fuel temperature rake (vertical error bars denote heat flux standard deviation; horizontal error bars denote minimum/maximum fuel temperatures during the time-averaging period)

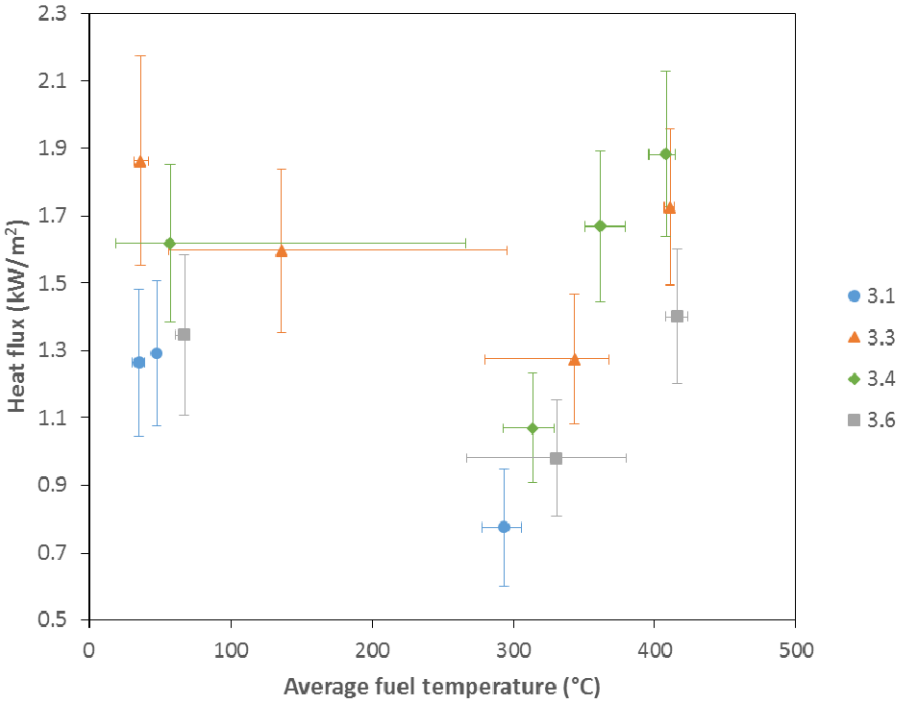

Figure 19: Heat flux measured by wide-view radiometer at 1 m height, versus fuel temperature as indicated by lowest thermocouple on fuel temperature rake (vertical error bars denote heat flux standard deviation; horizontal error bars denote minimum/maximum fuel temperatures during the time-averaging period)

Now considering the dilbit compositional analysis previously conducted by Lord [3], Figure 16 shows that the dilbit had higher composition between C4 and C9, with a peak at C5, and low composition between C10 and C24. According to Figure 11, the C4-C9 range corresponds to boiling points up to approximately 150°C, while the C10-C24 range corresponds to boiling points between approximately 175°C and slightly less than 400°C. Therefore, with increasing fuel temperature up to 150°C, the lighter ends would be expected to boil off, resulting in high levels of flame height, plume temperature and heat flux (the first stage). With a further increase through the range of 175°C-400°C, one would expect to see a decrease in these parameters (the second stage), since there are lower concentrations of C10-C24 components in the dilbit (and only a small amount of C1-C9 components entering the fuel pan in tests involving a continuous fuel feed). Once the fuel temperature passes above 400°C, the same parameters would then increase (the third stage), since there is a high composition of C25+ components. Note that this description does not take into account effects of thermal cracking, which was discussed earlier (Section 5.2) and may contribute to an increase in the fire parameters at average fuel temperatures less than 400°C, if localized regions of high temperature existed within the fuel.

In an attempt to gain insight into the occurrence of thermal cracking, Test 3.4 (the “burn-down” test with no calorimeter) was examined in light of the three stages of burning. This test corresponds more closely to the conditions assumed in the generation of Figure 11 (i.e. no fuel replenishment); however, it also includes effects of increasing lip height that could affect comparison to other Series 3 tests.

Figure 20 shows measurements from the thermocouple rake along the plume axis and from the differential pressure gauge measuring fuel level in the pan. From about 2 to 15 minutes (the first stage of burning), the fuel level decreased steadily, with plume temperatures averaging around 500°C at a height of 1.5 m. From about 18 to 24 minutes (the second stage), the plume temperatures at all heights were noticeably lower, and this roughly

coincided with a period of steady differential pressure measurements (between about 21 and 26 minutes[4]), indicating that the fuel level remained constant. At approximately 24 minutes (beginning of the third stage), the plume temperatures sharply increased, eventually reaching 750°C at about 31 minutes at the 1.5 m height. The fuel level also began decreasing again after the plume temperatures increased.

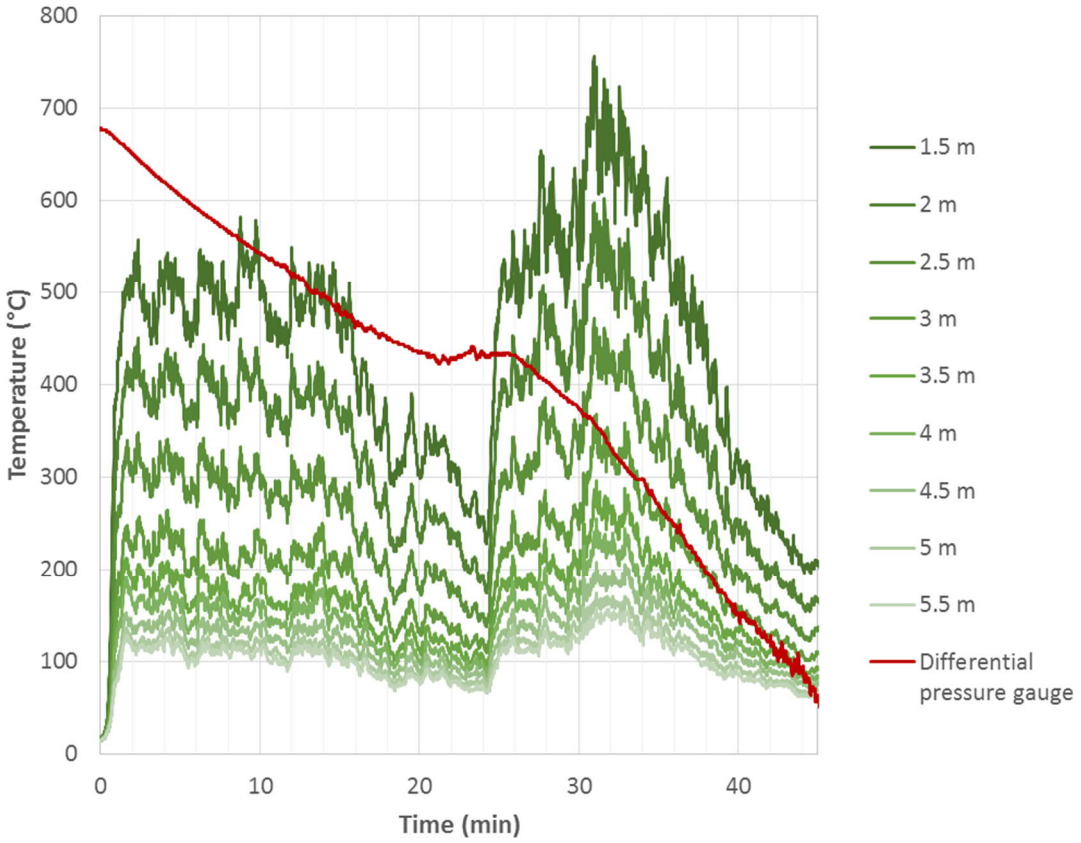

Figure 20: Temperatures from thermocouple rake along axis of fire plume, Test 3.4 (for simplicity, axes are not shown for differential pressure gauge measurements)

Meanwhile, Figure 21 shows temperatures from the fuel temperature rake. It should be noted that the data in Figure 21 is somewhat suspect because the temperature gradient that would be expected to occur along the height of the thermocouple rake was inconsistent (i.e. some of the lower thermocouples exhibited higher temperatures than the upper thermocouples), indicating that many of the thermocouples were on the verge of failure. Nonetheless, this figure is assumed to provide a reasonable general indication of the temperature within the fuel. Based on the available data, it appears that the fuel temperature was below 100°C for the first 14 minutes. This corresponds to the initial period of high plume temperature in Figure 20 (the first stage of burning), which suggests that lighter ends (up to C7 according to Figure 11) were mainly burning off.

[4] A time lag is to be expected in the differential pressure measurements, compared to the thermocouple measurements.

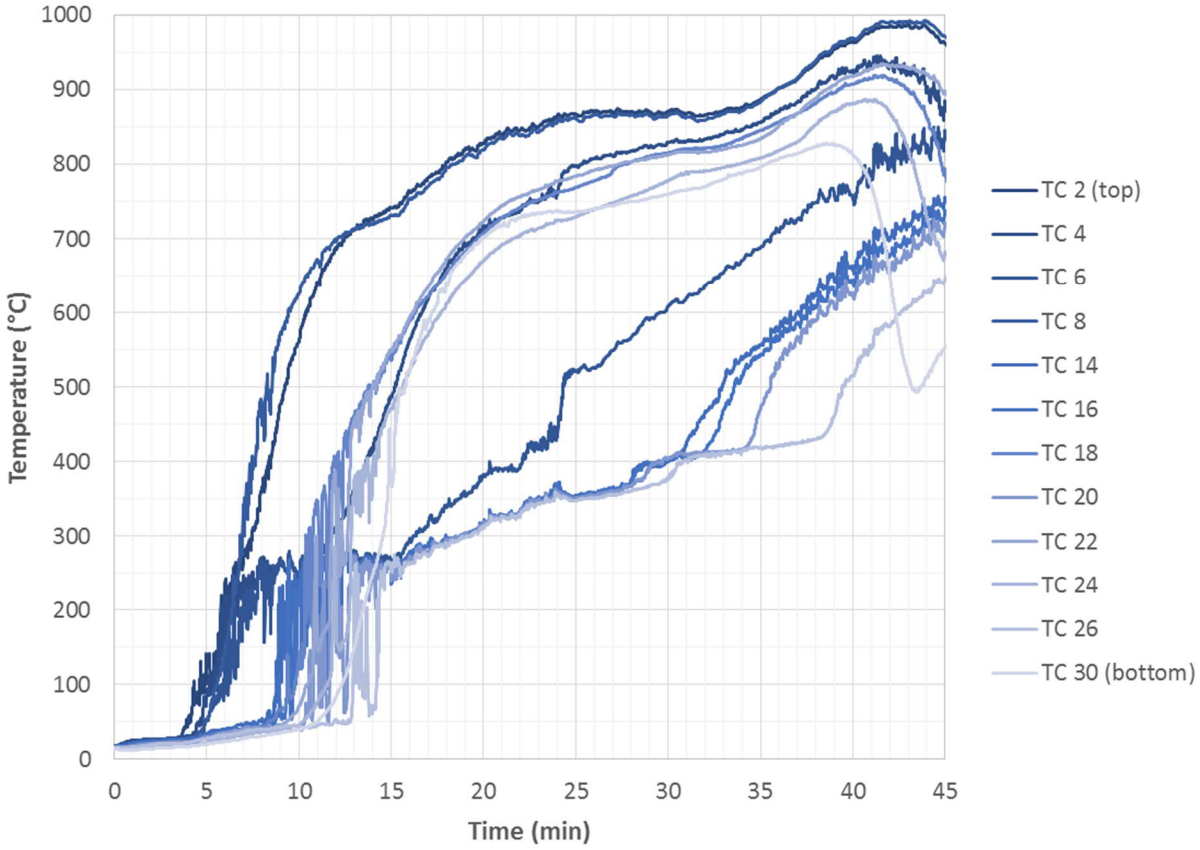

Figure 21: Fuel rake temperatures for Test 3.4

At 14 minutes, the fuel temperature sharply increased to roughly 275°C (suggesting that the fuel changed from a stratified to uniform temperature distribution), then passed 300°C at approximately 18 minutes and 350°C at about 23-24 minutes. This coincided with the period in Figure 20 in which the plume temperatures decreased to much lower levels and the fuel level became constant (the second stage of burning). Based on Figure 11, C16-C20 components (which were at low concentrations in the dilbit) would have been involved during this time. Thermal cracking of the heavier components may have been occurring, because at 24 minutes, the plume temperatures suddenly increased to approximately the same levels as at the beginning of the test (the third stage) and the fuel level started decreasing again, indicating that components in the crude oil were now vapourizing and burning. At approximately 30-31 minutes, the fuel temperature passed 400°C, and this coincided with a further increase in plume temperature (to approximately 750°C at the 1.5 m height), suggesting the occurrence of more severe thermal cracking.

The above observations thus indicate that thermal cracking likely occurred when temperatures of 300-350°C were measured by the fuel temperature rake, in line with the discussion in Section 5.2, where it was proposed that there could be localized, high temperature regions in the fuel with moderately high rates of cracking even though the readings from the fuel temperature rake were relatively low.

6 Residue Analysis

In Series 2 and 3, residue samples were collected from the fuel pan (at the pan centre, half-radius and outer edge) after the first and last fire tests. At the time of writing of this report, analysis of the samples is planned in order to determine residue characteristics and composition. Tests being considered include:

- Total Oil Chemistry: n-Alkanes C9-C40+, Aromatics/PAC/APAC, “biomarker” hopanes and steranes
- Physical residue analysis (density, viscosity, etc.)
- Total elemental sulphur
- Pyrogenic index

The results, which would be documented separately, may be compared to the findings in this report and used to support or question hypotheses in the present discussion, e.g. the preferential burning of light ends and thermal cracking of heavy ends. If the hypotheses in the present discussion are supported, then the residue analysis will lend further evidence towards a distillation-type burning process for the crude oils examined in this study (a question that was under consideration at the start of the entire experimental testing program [6]).

7 Comparison of Series 1 to 3 Test Data

In this section, the time-averaged results from Section 4 are compared between corresponding tests in Series 1, 2 and 3 that involve the same experimental test conditions (Table 1). Although some comparisons were previously made in both Luketa [2] and Ko [1], they tended to be general comparisons between all tests in all three test series, rather than systematic comparisons between tests involving the same experimental test condition. Further, the Series 3 results used in the comparisons of Luketa [2] and Ko [1] were based on data integrated from 0 to 25 minutes, whereas those used in this section involve the multiple time-averaging periods identified in Table 6. Recall, also, that in Section 4, and therefore this section, results for the DFTs and heat release rate have been corrected, whereas the corrections were not applied in Luketa [2] and Ko [1].

General notes relating to presentation of the comparisons in this section are as follows:

- When discussing the calorimeter, representative plots (particularly from the Series 3 tests, which involve multiple time-averaging periods) have been selected to support the discussion. All calorimeter plots are available in Appendix A.
- Although not included in Section 4, time-averaged vertical profiles of surface emissive power, measured by the infrared camera and adapted from Luketa [2] (via the offset described below), have been used to support the comparisons. Each profile was time-averaged over the main burning period of the fire (exact periods were not documented in [2]). This means that although the profiles did not include the initial establishment and final decay of the fire, they did include any unsteady behaviour that occurred in between (for example, the three stages of burning in the dilbit tests). Since no infrared camera was used in Tests 1.2 and 1.3, surface emissive power profiles are not available for those tests. In the present comparisons, the height of each profile has been offset such that 0 m is located at the bottom of the fuel pan. This was done because the view of the infrared camera was not consistent from test to test. Thus, when comparing profiles between tests, there is some uncertainty in their vertical alignment, but this uncertainty is not expected to be large enough to affect general trends and observations. In addition, although most profiles were approximately aligned with the axis of the fuel pan, they would not be aligned with the axis of the fire plume if the plume was not exactly vertical. The profiles also do not represent any measurements along the axis of the fire plume because they are based on photon emissions from near the flame surface and not from the interior of the fire.
- Because heat release rate data was not available for Series 3 (with the exception of Test 3.4), little focus was placed on this parameter in the present comparisons. However, the available data are included for reference.

7.1 DFT Total Heat Flux

Because the total heat flux to the DFTs was recalculated for Series 1 and 2 (Tables 14 and 26), the comparison of DFT results between Series 1, 2 and 3 (Figures 8-16 and 8-17 in Luketa [2]) must be revisited. Recall that the absorbed heat flux values were not affected. Figures 22 and 23 show the time-averaged total heat flux from the DFTs placed at 2 m and 4 m, respectively, from the centre of the fuel pan for all tests. In general, at the 2 m location (Figure 22), the heptane tests (Series 1) involved the lowest total heat flux, while the Bakken and dilbit tests (Series 2 and 3) involved higher, similar levels of heat flux. Since the 2 m DFT was only 1 m away from the pan edge, these measurements would be expected to be largely influenced by the surface emissive power of the fire in the region near the 1 m height of the DFT. Meanwhile, at the 4 m location (Figure 23), all three test series generally showed similar levels of total heat flux. Being further from the fire, this DFT would be expected to have a better view of the entire fire and be influenced not only by differences in surface emissive power but also by differences in flame height (e.g. the greater flame height of the heptane fire counteracts the lower surface emissive power of that fire). Further discussion and comparison of these results and the other measured variables may be found in Sections 7.2 to 7.6.

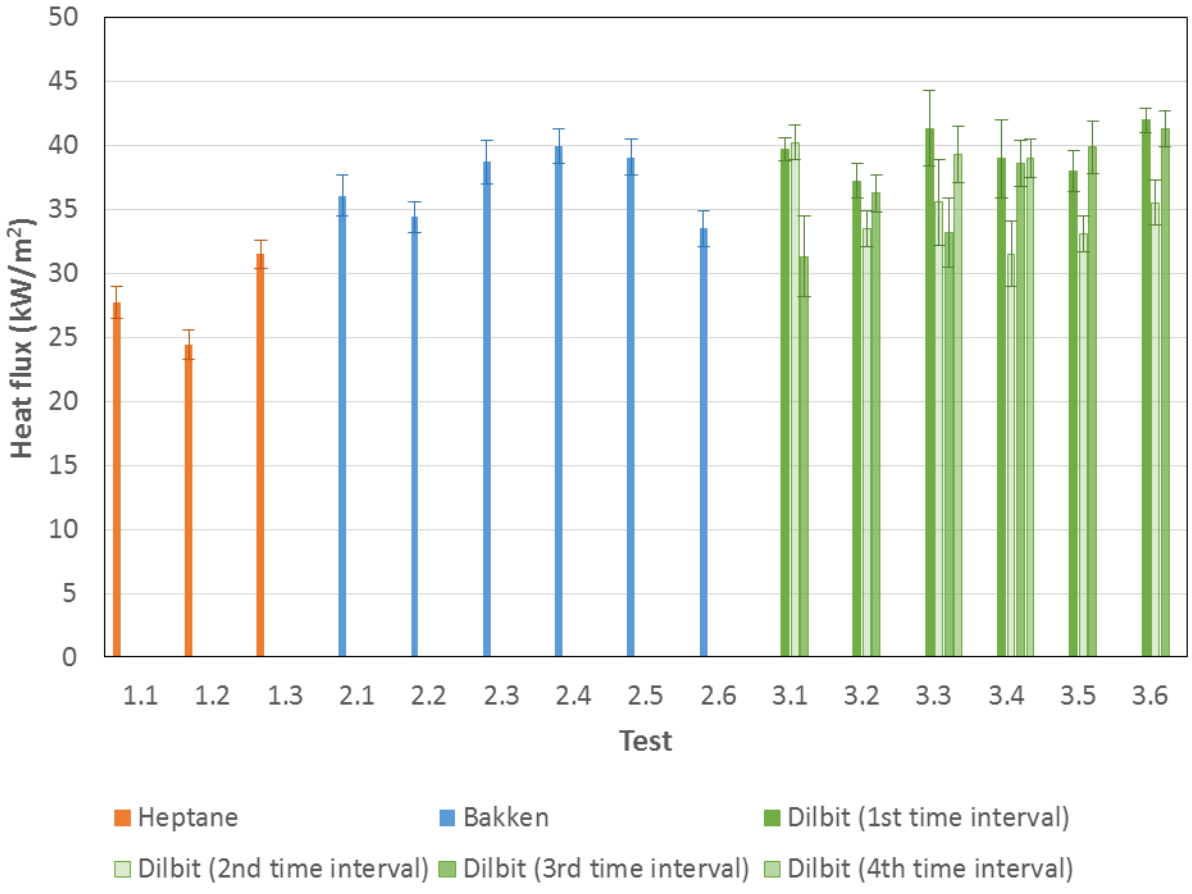

Figure 22: Comparison of time-averaged total heat flux values from 2 m DFT for all tests

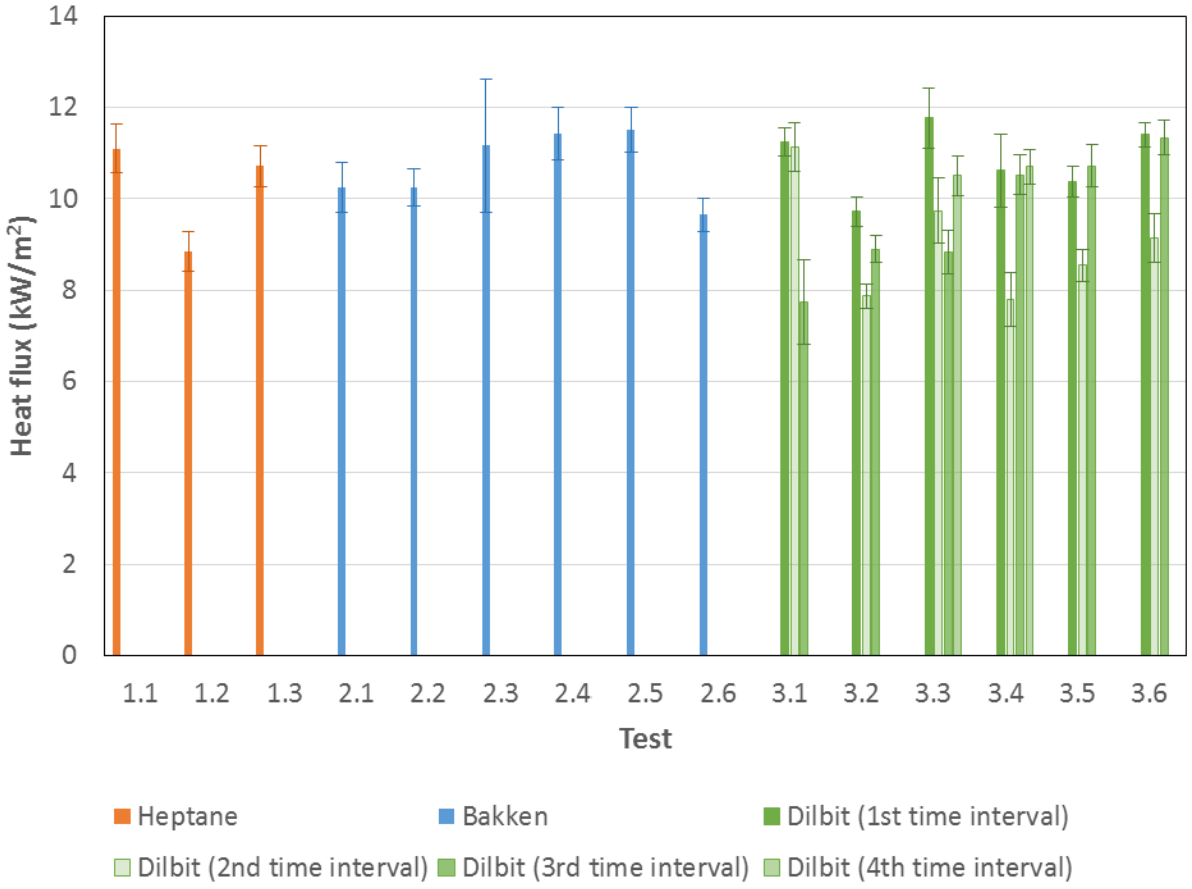

Figure 23: Comparison of time-averaged total heat flux values from 4 m DFT for all tests

7.2 Tests with No Calorimeter and 20°C Constant Level Fuel Supply

The tests involved in this comparison are Tests 1.2, 2.1 and 3.3. Table 38 provides a comparison of the burning rates and flame heights in these tests. The heptane fire had the highest burning rate and flame height, followed by the Bakken fire and then the dilbit fire. This trend is reflected in Figures 24 and 25, which show the plume axis temperatures and narrow-view radiometer measurements from the three tests. With the highest flame height, the heptane fire would be expected to show a profile with the highest temperatures and highest levels of narrow-view heat flux, particularly at the higher elevations (2 m and above). However, the Bakken fire had a higher plume axis temperature at the 1.5 m height and higher levels of narrow-view heat flux at heights of 1.5 m and below. This indicates that much of the combustion and radiative emission occurred at lower elevations than in the heptane fire, which exhibited flatter temperature and heat flux profiles. The dilbit fire had significantly lower plume axis temperatures than the Bakken fire (Figure 24), as expected given that it had the lowest flame height, but only slightly lower levels of surface emissive power (Figures 25 and 26). This suggests that even though the combustion gases were substantially cooler inside the dilbit fire at heights of 1.5 m and greater, soot levels and thus radiative emission near the flame surface were relatively similar to the Bakken fire at all heights.

Table 38: Burning rates and flame heights for tests with no calorimeter and 20°C constant level fuel supply

Test	Time period (min)	Burning rate (mm/min)	Flame height (m)	Heat release rate (MW)
1.2	10-35	3.57 ± 0.04	6.8[a] ± 0.9	5.2 ± 0.2
2.1	22-34	2.23 ± 0.03	4.6 ± 1.0	4.8 ± 0.9
3.3	3-5	2.16 ± 0.03	3.9 ± 0.9	n/a
	8-10	1.12 ± 0.03	3.4 ± 0.8	
	12-19	1.03 ± 0.03	3.2 ± 0.6	
	25-28	0.81 ± 0.03	3.8 ± 0.8	

[a] A different method (visible camera instead of infrared camera) was used to evaluate flame height.

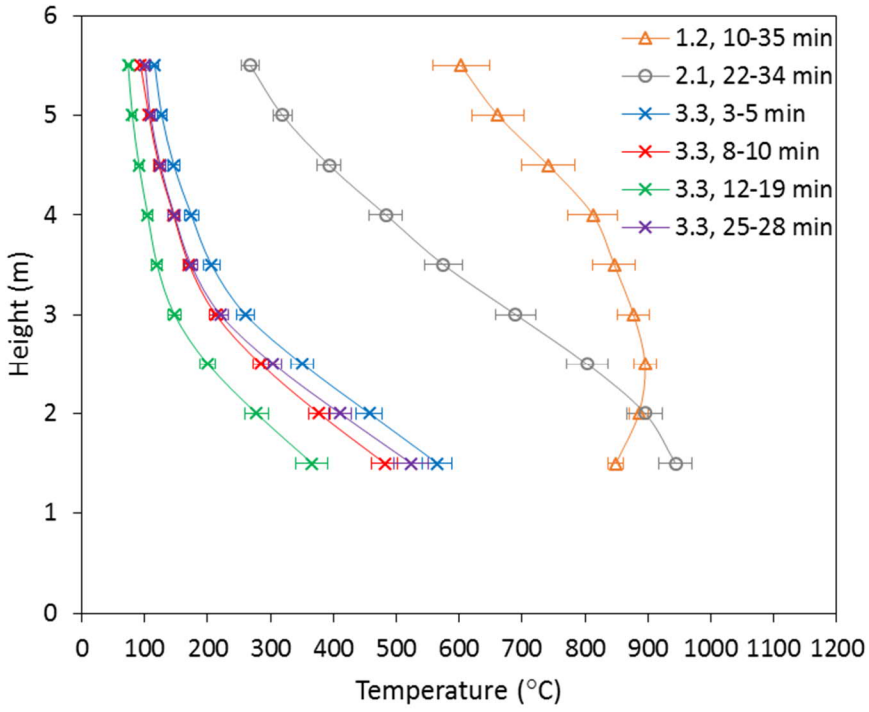

Figure 24: Plume axis temperatures for tests with no calorimeter and 20°C constant level fuel supply

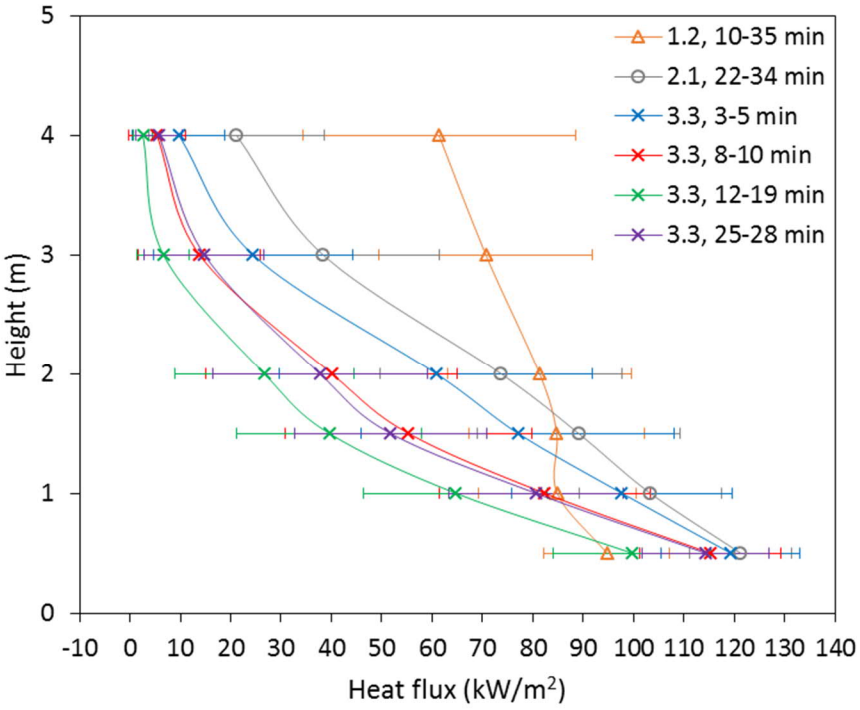

Figure 25: Narrow-view radiometer measurements for tests with no calorimeter and 20°C constant level fuel supply

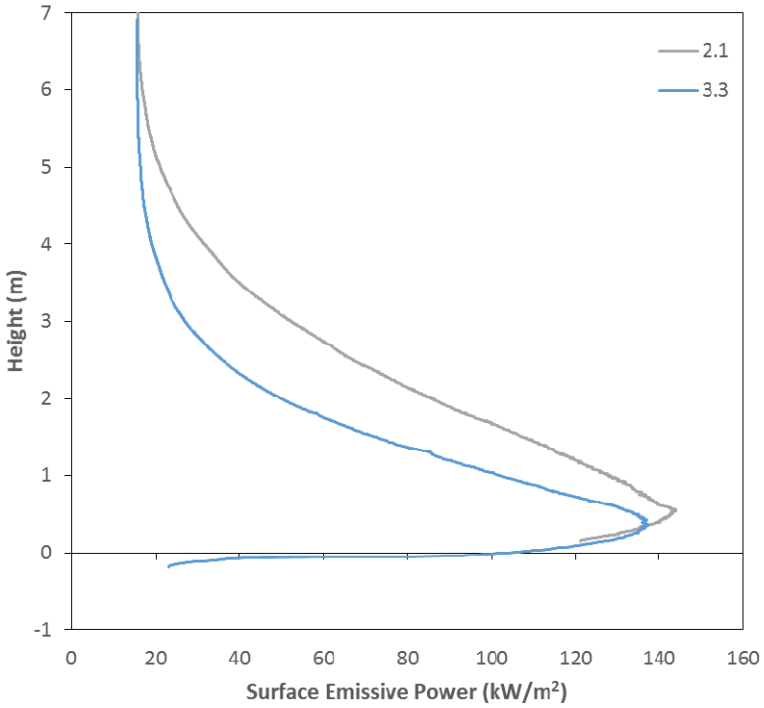

Figure 26: Infrared camera surface emissive power centreline profiles for tests with no calorimeter and 20°C constant level fuel supply (no data available for Test 1.2)

Considering the wide-view radiometer measurements (Figure 27), the heptane fire had the highest heat flux levels, followed by the Bakken fire and then the dilbit fire. This may have been influenced by the higher heptane flame height, since the wide-view radiometers would have been able to see the entire flame. However, the DFT measurements (Figure 28) showed conflicting trends, with the heptane fire exhibiting the lowest levels of DFT heat flux, followed by the Bakken and dilbit fires (the dilbit values from 3-5 minutes were higher than the Bakken values, but the ones during the other time intervals were either similar to or lower than the Bakken values). This is most likely because the DFTs were close to the fire at an elevation of 1 m, so the trend could be expected to be similar to that of the 1 m narrow-view radiometer data in Figure 25. They would not be expected to be the same, however, because the DFT measures both radiative and convective heat flux and has a view angle of 180°, whereas the narrow-view radiometers measure only radiation and were placed such that they viewed a spot diameter on the fire of approximately 0.8 m [2].

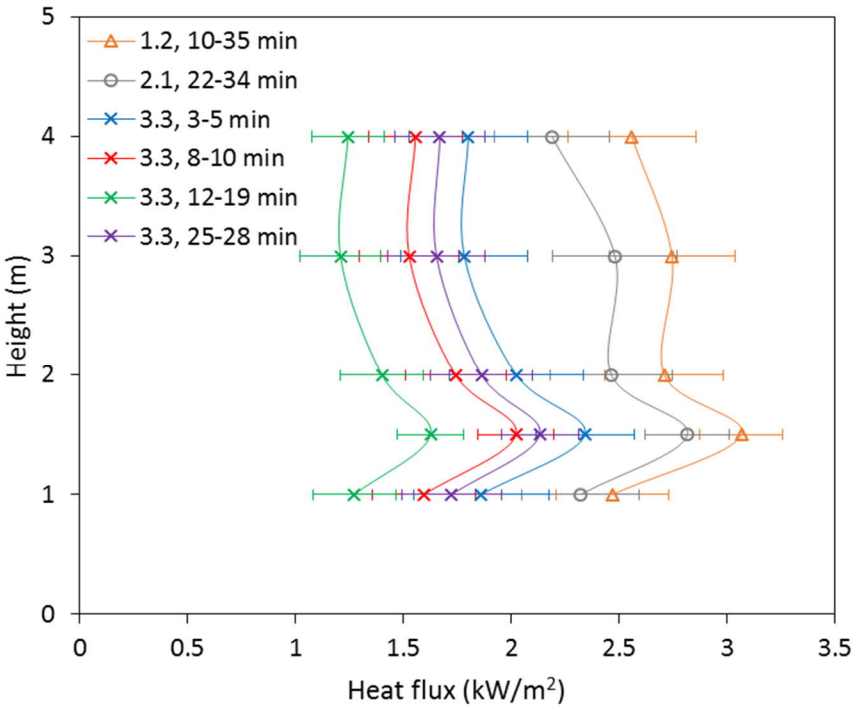

Figure 27: Wide-view radiometer measurements for tests with no calorimeter and 20°C constant level fuel supply

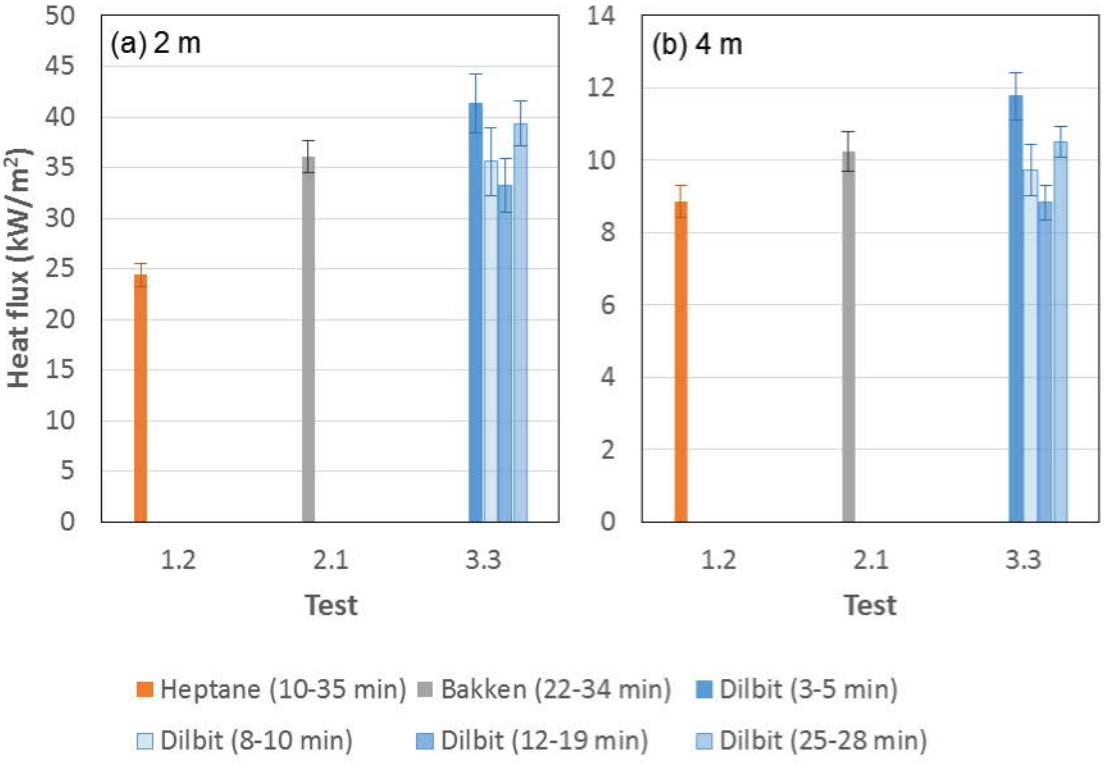

Figure 28: DFT measurements for tests with no calorimeter and 20°C constant level fuel supply

7.3 "Burn-Down" Tests with No Calorimeter

The tests involved in this comparison are Tests 2.6 and 3.4. The data from these tests (Table 39 and Figures 29-33) are similar to those in Section 7.2, indicating that the fuel feed method did not have much of an effect on the time-averaged values. The Bakken test generally indicated higher values than the dilbit test for all measurement parameters, except for the DFT heat flux (Figure 33). The apparent discrepancy between the trend shown by the DFT data and those shown by the narrow- and wide-view radiometer data may be due to differences between the various measurement devices. The DFTs measured total heat flux from the lower regions of the fire to a location close to, but not inside, the fire, whereas the narrow-view radiometers measured localized radiative heat flux at the flame surface (surface emissive power) and the wide-view radiometers measured radiative heat flux from the entire flame to a location much further from the fire than the DFTs.

Table 39: Burning rates and flame heights for burn-down tests with no calorimeter

Test	Burning rate[a] (mm/min)	Time period (min)	Flame height (m)	Heat release rate (MW)[b]
2.6	2.21 +0.10/-0.09	12-30	4.5 ± 1.0	3.5 ± 0.7
3.4	1.16 ± 0.03	2-15	3.9 ± 0.8	4.6 ± 0.7
		18.5-22	3.1 ± 0.6	3.6 ± 0.6
		26-30	3.7 ± 0.8	4.6 ± 0.7
		30.5-34	4.1 ± 1.0	5.1 ± 0.6

[a] Because the burning rate was calculated using the estimated mass/volume of fuel burned over the entire test duration, the time periods in the third column do not apply to the burning rate values.
[b] The heat release rates for Test 3.4 appear to be too high and are not considered to be reliable for comparison.

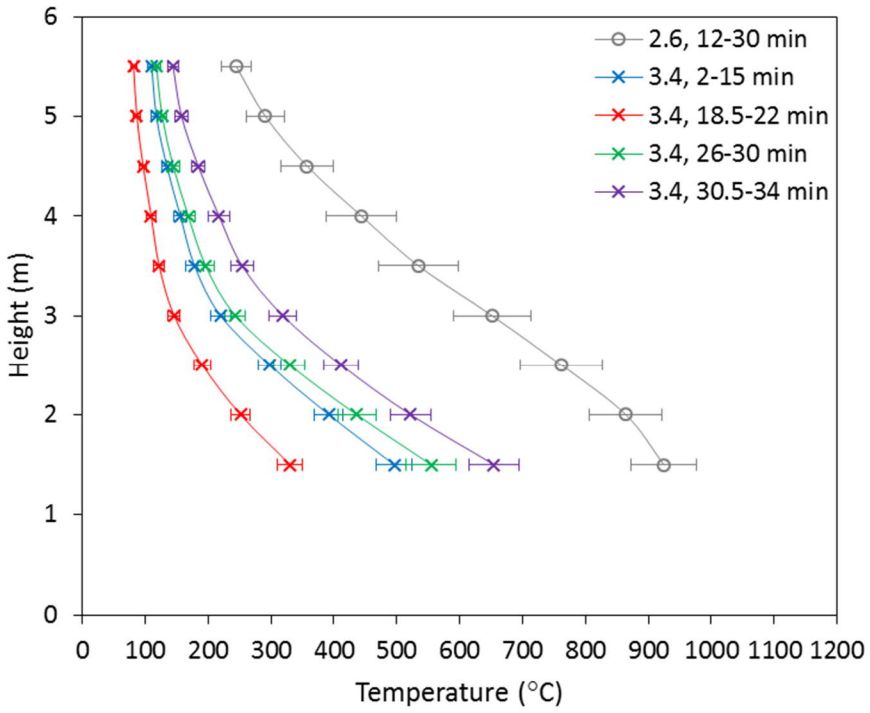

Figure 29: Plume axis temperatures for burn-down tests with no calorimeter

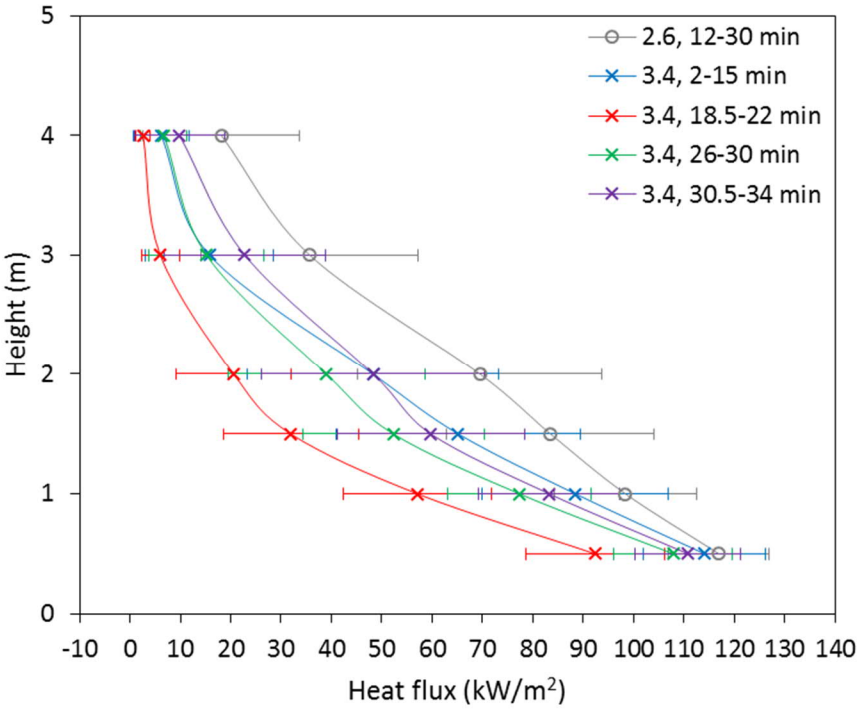

Figure 30: Narrow-view radiometer measurements for burn-down tests with no calorimeter

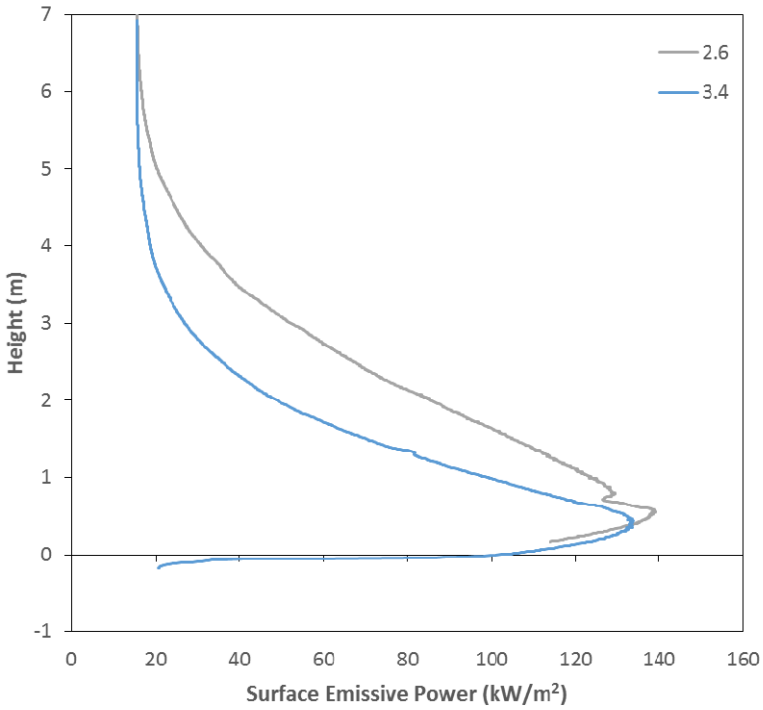

Figure 31: Infrared camera surface emissive power centreline profiles for burn-down tests with no calorimeter

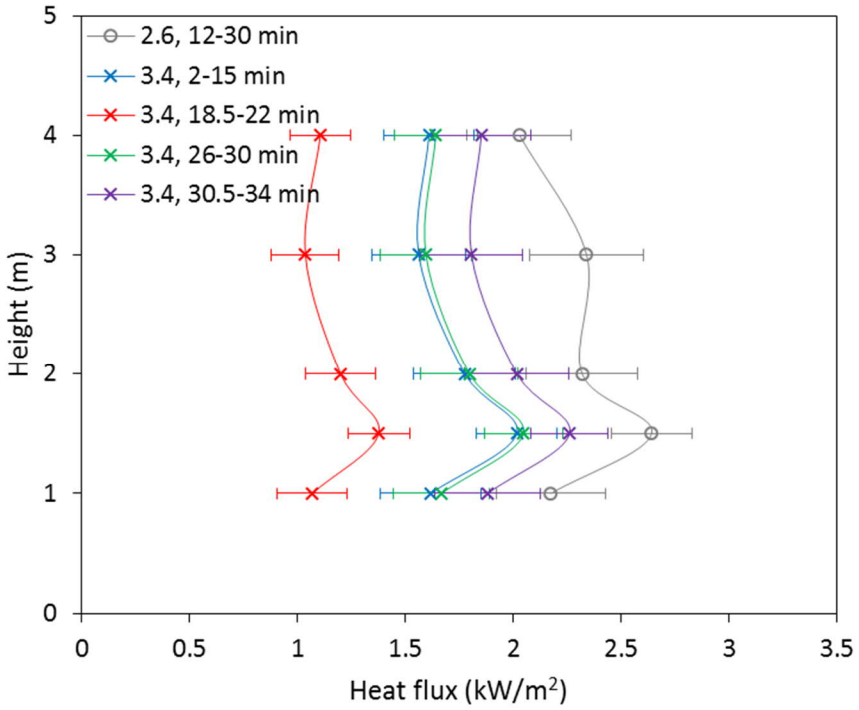

Figure 32: Wide-view radiometer measurements for burn-down tests with no calorimeter

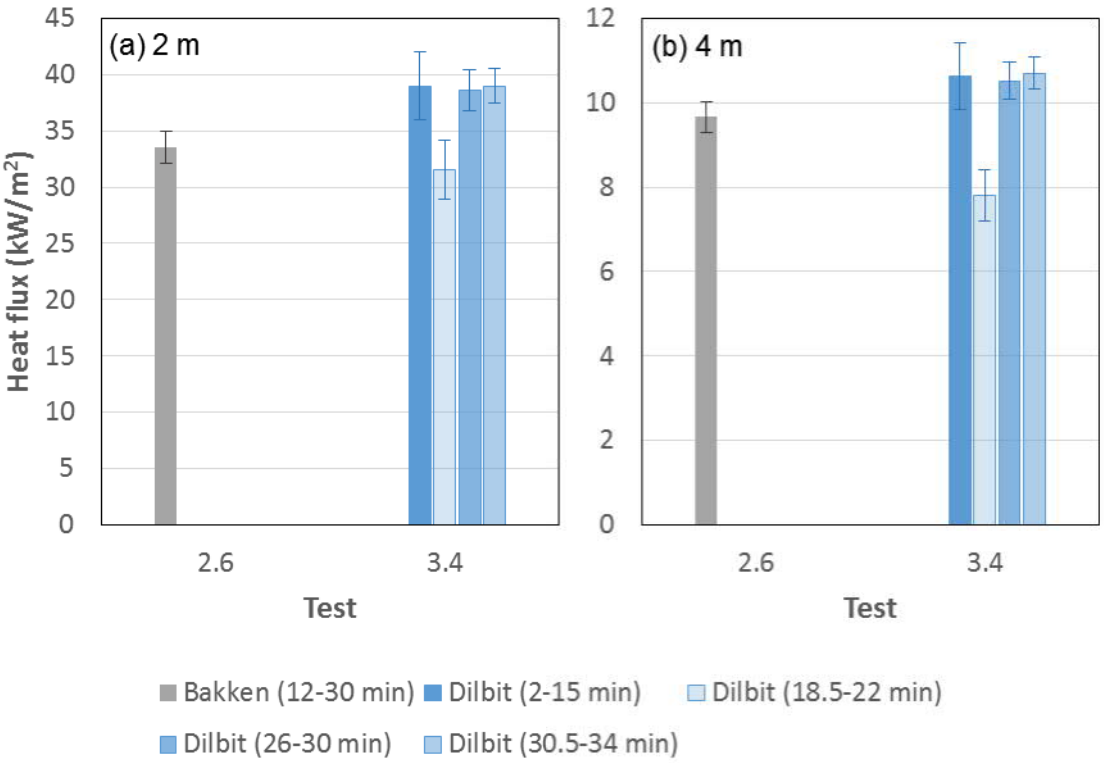

Figure 33: DFT measurements for burn-down tests with no calorimeter

7.4 Tests with Calorimeter at 1 m Height and 20°C Constant Level Fuel Supply

This comparison focusses on Tests 1.1, 2.5 and 3.5. Although Tests 2.3 and 3.1 also involved the calorimeter at a 1 m height and a 20°C constant level fuel supply, they are not included here because Test 2.3 had a damaged fuel control valve, resulting in large fluctuations in the data, while Test 3.1 provided less reliable results than Test 3.5 due to difficulties experienced in maintaining a constant fuel level during this first test of the dilbit series [2].

Table 40 compares the burning rates and flame heights from the three selected tests. The heptane fire had the highest burning rate and flame height, followed by the Bakken fire and then the dilbit fire. This trend is supported by the plume axis temperature profiles in Figure 34, which show the heptane and Bakken fires exhibiting higher temperatures than the dilbit fire at the upper elevations. At the 0.5 m height, though, the heptane profile showed a significantly lower temperature than the Bakken and dilbit fires. This suggests that the heptane fire may have had a larger fuel-rich, non-combusting vapour zone immediately above the fuel surface (which is characteristic of all buoyancy-dominated pool fires because very little air is transported to the interior of the fire, particularly near the base [7]). The higher burning rate of the heptane fire would have meant that the fuel vapours left the fuel surface with greater velocity and combusted at relatively higher elevations. Investigation of how the presence of the calorimeter may have affected the development and size of such a fuel-rich vapour zone is recommended.

Table 40: Burning rates and flame heights for tests with calorimeter at 1 m height and 20°C constant level fuel supply

Test	Time period (min)	Burning rate (mm/min)	Flame height (m)	Heat release rate (MW)
1.1	10-35	3.24 ± 0.04	5.8 ± 0.9	4.4 ± 0.2
2.5	15-34	1.90 ± 0.03	4.6 ± 0.9	3.6 ± 0.7
3.5	3-10	1.04 ± 0.03	3.5 ± 0.8	n/a
	16-19.5	1.15 ± 0.03	3.4 ± 0.7	
	27.5-30.5	0.76 ± 0.03	4.0 ± 0.9	

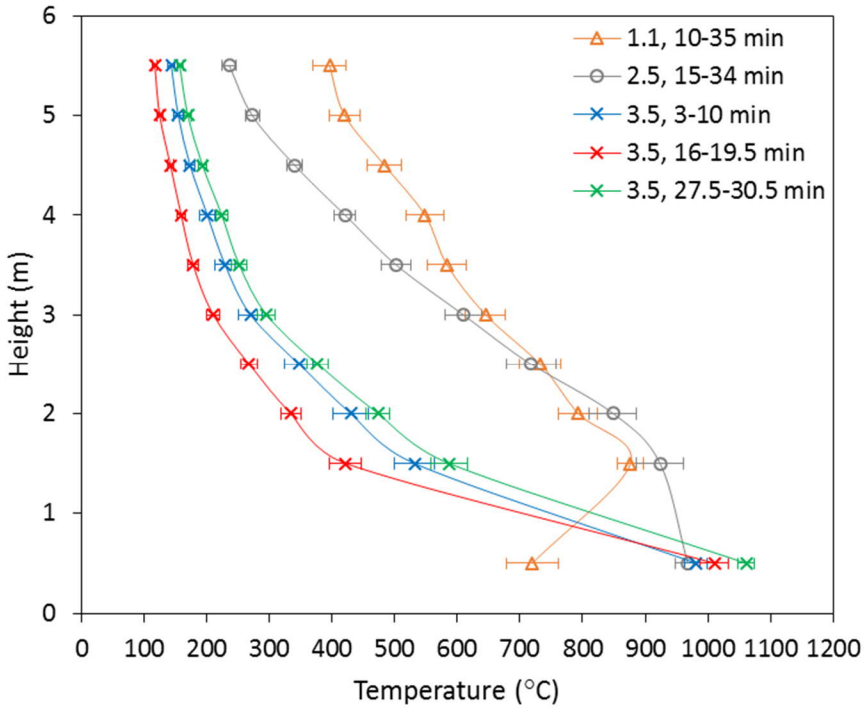

Figure 34: Plume axis temperatures for tests with calorimeter at 1 m height and 20°C constant level fuel supply

Figure 34 thus suggests that much of the combustion occurred above the calorimeter in the heptane fire, whereas it clearly occurred below the calorimeter in the dilbit fire. However, this is only somewhat supported by the measurements of total heat flux to the calorimeter, shown in Figure 35. In the heptane fire (Figure 35a), the calorimeter experienced reasonably uniform heat flux around its circumference, suggesting that sufficient combustion did occur below the calorimeter, although this did not appear to be captured by the single temperature measurement along the plume axis at 0.5 m height in Figure 34. In the dilbit fire (Figures 35c and d), the bottom of the calorimeter received greater heat flux than the top, consistent with the corresponding temperature profiles in Figure 34. For the Bakken fire, Figure 34 suggests that similar levels of combustion occurred both above and below the calorimeter, but this cannot be confirmed by the centre plane measurements of Figure 35b due to insufficient data (although the exterior temperature measurements along the centre plane, shown in Figure A-14, do support such speculation). Certainly in the left and right planes, Figure 35b shows that the heat flux to the bottom was greater than to the top, which could be expected given that the top of the calorimeter in these planes would have been closer to the edges of the fire plume and thus would not have been as fully engulfed in flame.

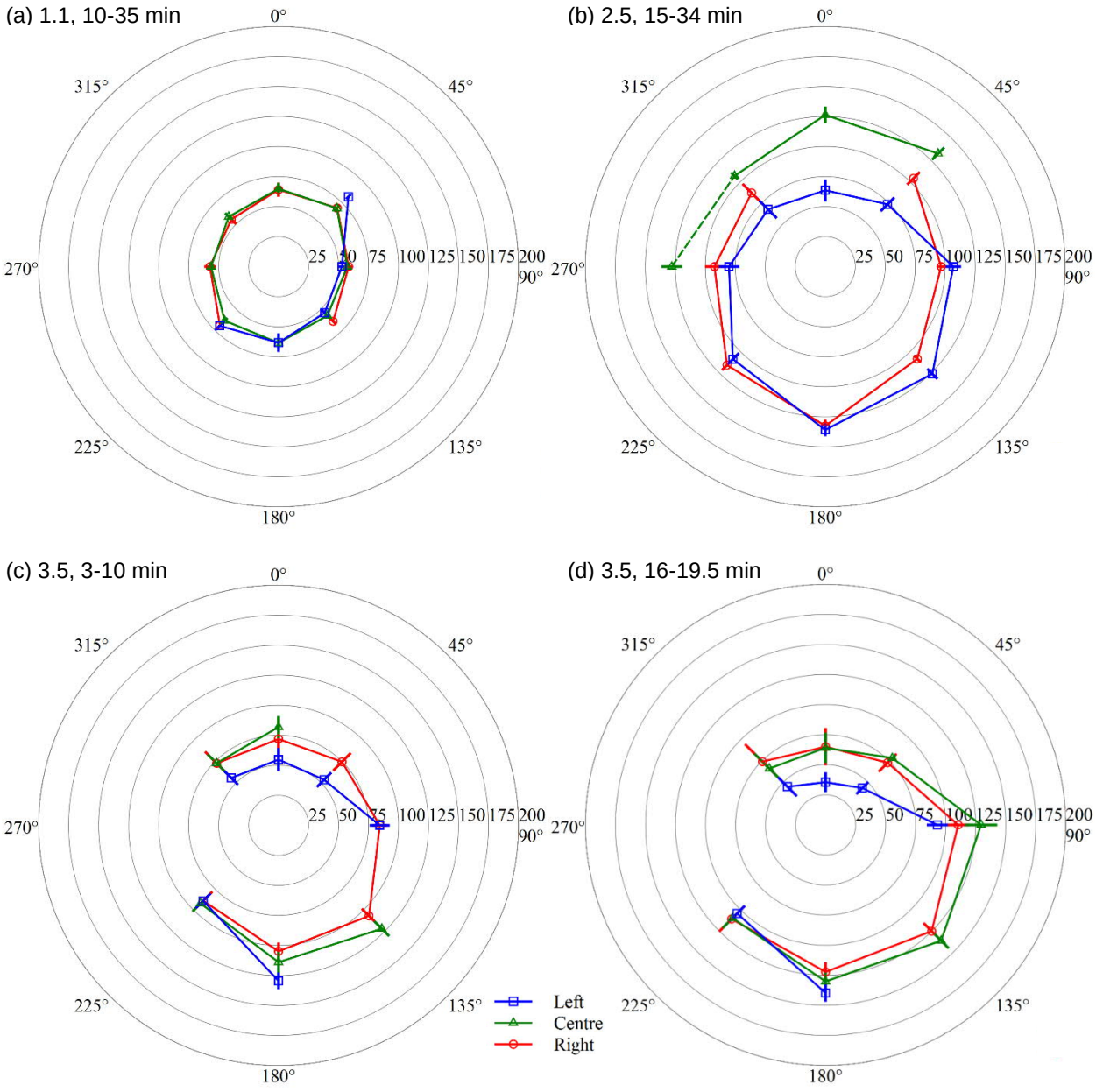

Figure 35: Selected plots of total heat flux (kW/m^2) to calorimeter, for tests with calorimeter at 1 m height and 20°C constant level fuel supply

Figure 36, which compares the narrow-view radiometer profiles from the three tests, shows that generally, the heptane fire had the highest surface emissive power, followed by the Bakken fire and then the dilbit fire. This is only consistent with the surface emissive power profiles from the infrared camera (Figure 37) at heights greater than approximately 2 m. In Figure 37, below the calorimeter, the Bakken fire had the highest surface emissive power, followed by the dilbit fire and then the heptane fire. It should be noted that the two methods for measuring surface emissive power are different, affecting their comparability: the narrow-view radiometer measurements were averaged over a spot diameter on the fire of approximately 0.8 m, while the infrared camera profiles were based on time-averaged photon counts from pixels which correspond to much smaller areas on the fire.

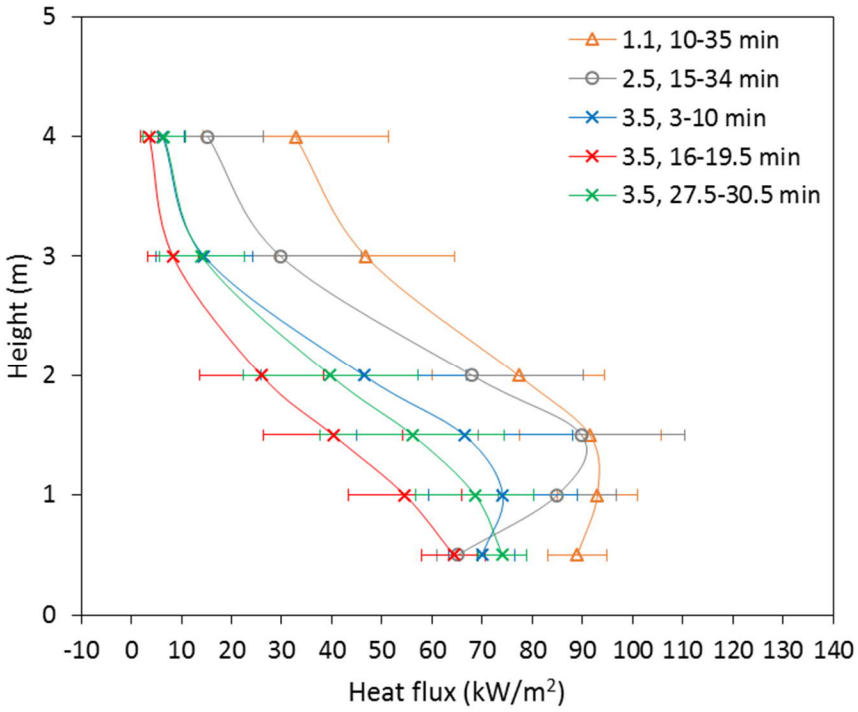

Figure 36: Narrow-view radiometer measurements for tests with calorimeter at 1 m height and 20°C constant level fuel supply

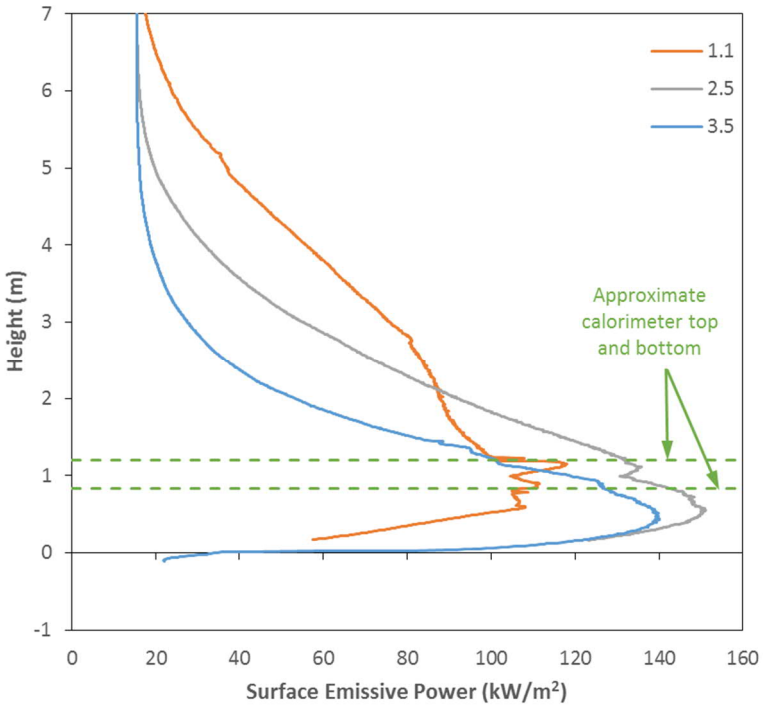

Figure 37: Infrared camera surface emissive power centreline profiles for tests with calorimeter at 1 m height and 20°C constant level fuel supply

Figure 37 appears to be consistent with the heat flux profiles of Figure 35. Although Figure 37 shows the emissive power at the flame surface, while Figure 35 shows heat flux measurements inside the fire, both figures suggest that the heat flux to the calorimeter along the centre plane would be lowest in the heptane fire and highest in the Bakken fire. For the dilbit fire, the heat flux to the top of the calorimeter appeared to be similar to that in the heptane fire, while the heat flux to the bottom was clearly higher than in the heptane fire. Overall, the heptane fire is expected to be less optically thick (less sooty and luminous, and thus considered more “transparent”) than either of the crude oil fires, so heat flux to the calorimeter would be expected to be the lowest (since radiation would not be trapped within the flame envelope), as would the surface emissive power in the lower regions of the fire (where differences in flame height would not affect the measurements).

The DFT measurements at 2 m (Figure 38a) showed the lowest values for the heptane fire and similar, higher values for the Bakken and dilbit fires. This is consistent with the surface emissive power profiles near the 1 m height in Figure 37, which could be expected given that this DFT was only 1 m outside the fuel pan. Meanwhile, the DFT measurements at 4 m (Figure 38b) were generally similar for all three fires. This DFT would be expected to see more of the entire fire and thus would be more greatly affected by differences in flame height (the greater flame height of the heptane fire would increase the heat flux to the DFT, counteracting the lower surface emissive power of the fire).

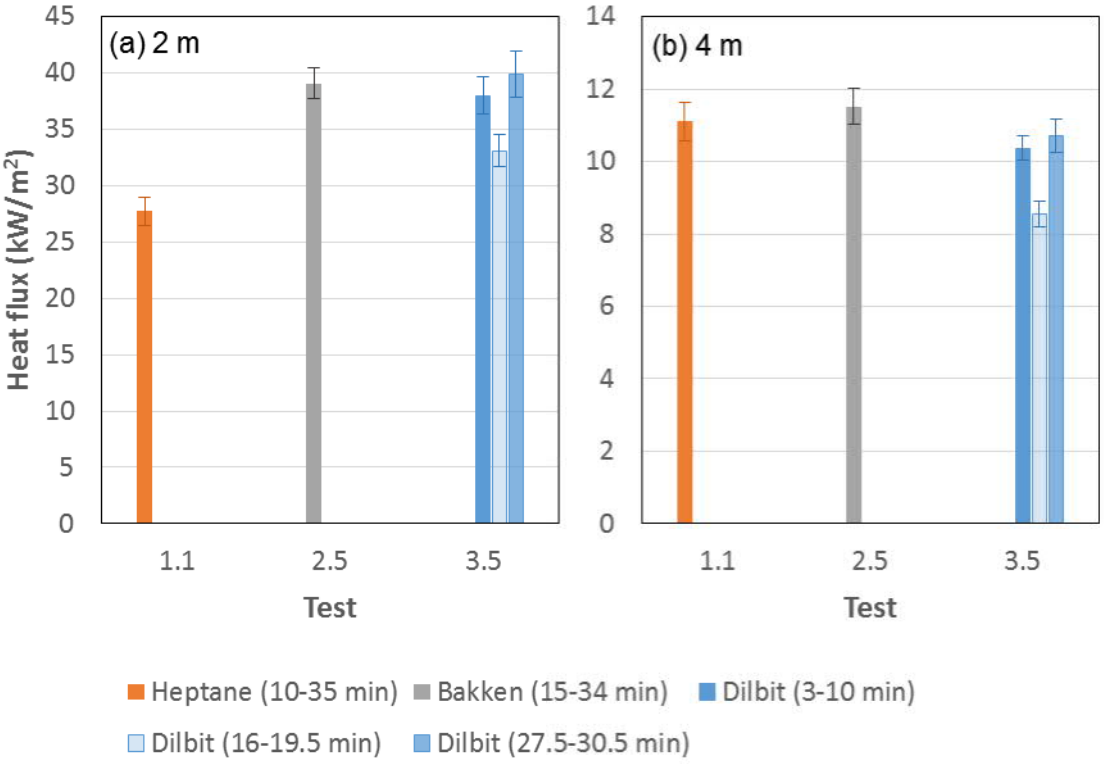

Figure 38: DFT measurements for tests with calorimeter at 1 m height and 20°C constant level fuel supply

The wide-view radiometer measurements in Figure 39 were highest for the heptane fire, then the Bakken fire and lowest for the dilbit fire. Similar to the 4 m DFT measurements, these profiles are expected to reflect differences in flame height, since the wide-view radiometers would have seen the entire fire.

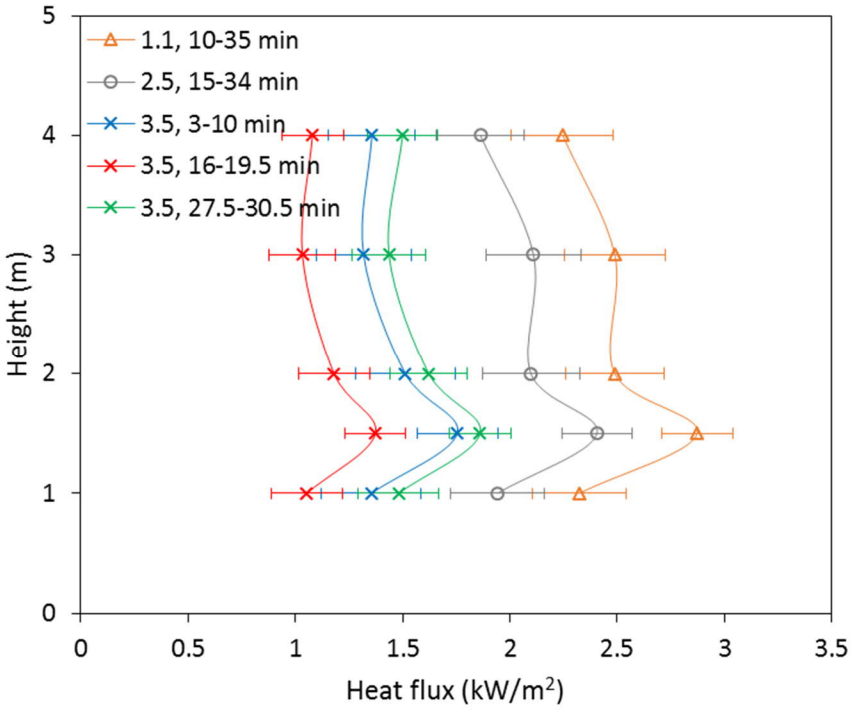

Figure 39: Wide-view radiometer measurements for tests with calorimeter at 1 m height and 20°C constant level fuel supply

In Figure 40a, the data in Figure 38 are plotted together with the data at 1 m in Figure 39 to show how the heat flux at a height of 1 m decreased with increasing distance from the fire. Because the DFT values for Series 1 and 2 were recalculated using the same method as for Series 3 (Tables 14 and 26), the comparison between fuel types differs from the one presented previously in Ko [1] (replotted in Figure 40b). Based on the recalculated values, the difference between fuel types was much less significant than originally suggested. At 2 m from the fuel pan centre, the heat flux was lowest for the heptane fire (mainly due to the lower optical thickness of this fire); then the next lowest was the dilbit fire during the time interval from 16 to 19.5 minutes (the second stage of burning). The heat flux from the dilbit fire during the other time intervals (first and third stages) was similar to the heat flux from the Bakken fire. At 4 m from the pan centre, the heat flux was lowest for the dilbit fire during the 16-19.5 minute time interval, while the remaining values were similar (10-12 kW/m^2). At 9 m from the pan centre, the heat flux ranged from 1 to 2.5 kW/m^2 for all three fires.

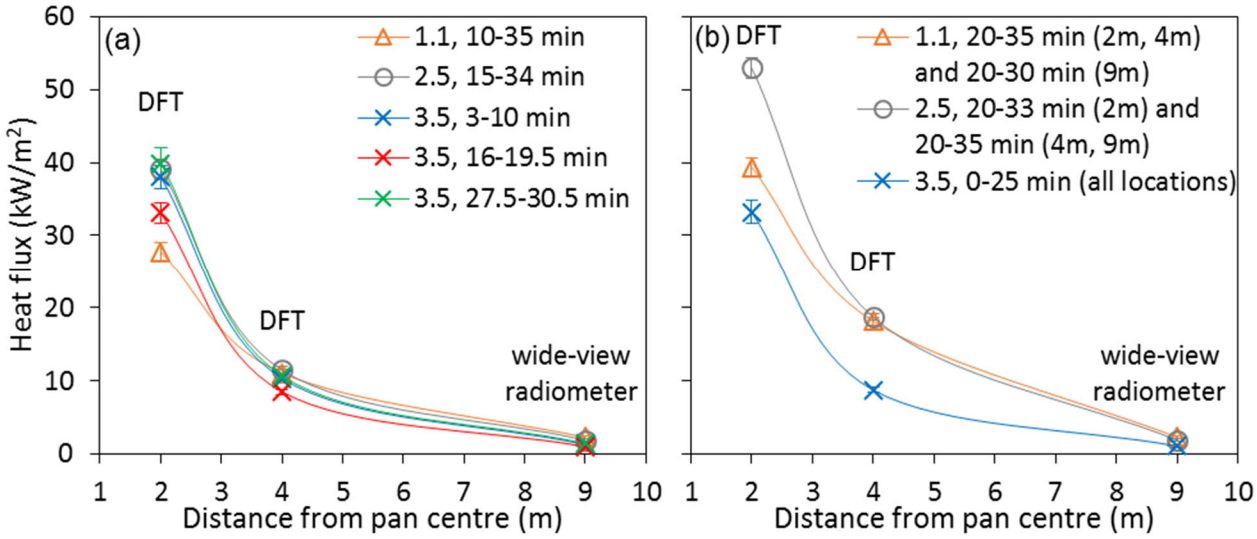

Figure 40: Variation in heat flux at 1 m height with distance from pan centre, for tests with calorimeter at 1 m height and 20°C constant level fuel supply, (a) using recalculated DFT values, (b) using DFT values from [2]

7.5 Tests with Calorimeter at 1 m Height and 60°C Constant Level Fuel Supply

The tests included in this comparison are Tests 1.3, 2.4 and 3.6. Also included is a related test conducted by Sandia using crude oil from the US Strategic Petroleum Reserve (referred to as the 2 m SPR 'hot' test in [8]). Similar to the other tests, the SPR test involved a 60°C constant level fuel supply and a calorimeter centered at 1 m height above the pan. Key differences between all four tests are provided in Table 41.

Table 41: Differences between tests with calorimeter at 1 m height and 60°C constant level fuel supply

Test	Test 1.3	Test 2.4	Test 3.6	SPR test [8]
Fuel	Heptane	Bakken crude	Dilbit	SPR crude
Height of constant fuel level	38 mm (1.5")	28 mm (1.1")	30 mm (1.2")	76 mm (3")
Height of pan lip above fuel surface	267 mm (10.5")	277 mm (10.9")	274 mm (10.8")	229 mm (9")
Ignition time	After pan pre-filled	Immediately upon fuel entry	After pan pre-filled	After pan pre-filled
Calorimeter dimensions	0.33 m (13.125") diameter by 1.8 m (72") long	0.33 m (13.125") diameter by 1.8 m (72") long	0.33 m (13.125") diameter by 1.8 m (72") long	0.27 m (10.75") diameter by 1.0 m (39.25") long

Overall, the measurements in this section for the heptane, Bakken and dilbit fires are similar to those presented in Section 7.4, indicating little effect from the higher fuel supply temperature. This section will thus focus on comparison with the SPR test. Because no data was available from the SPR test for temperatures along the plume axis or for surface emissive power from the infrared camera, Figures 41 and 42 are included mainly for reference.

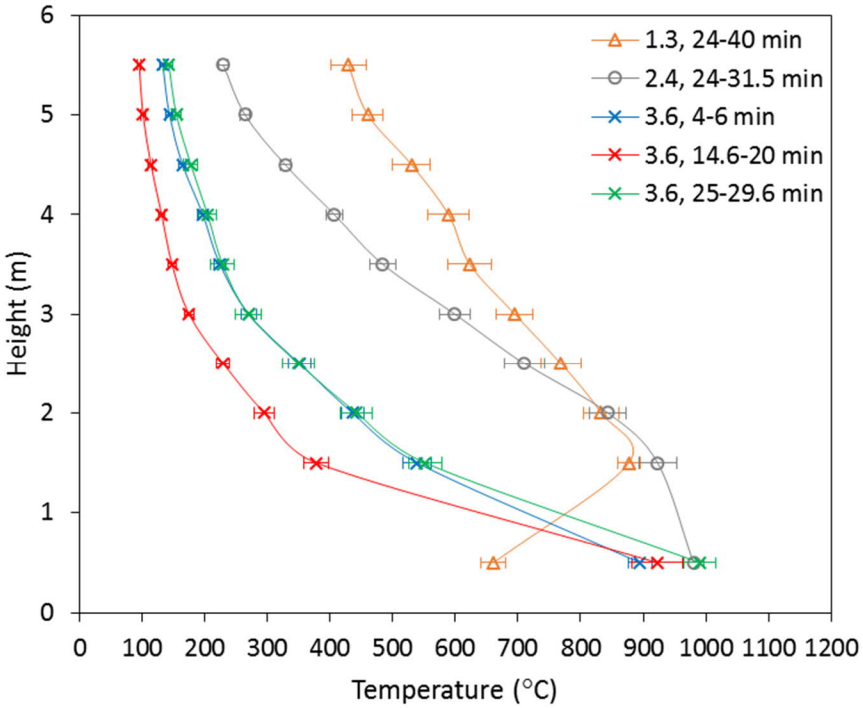

Figure 41: Plume axis temperatures for tests with calorimeter at 1 m height and 60°C constant level fuel supply (no data available for SPR test)

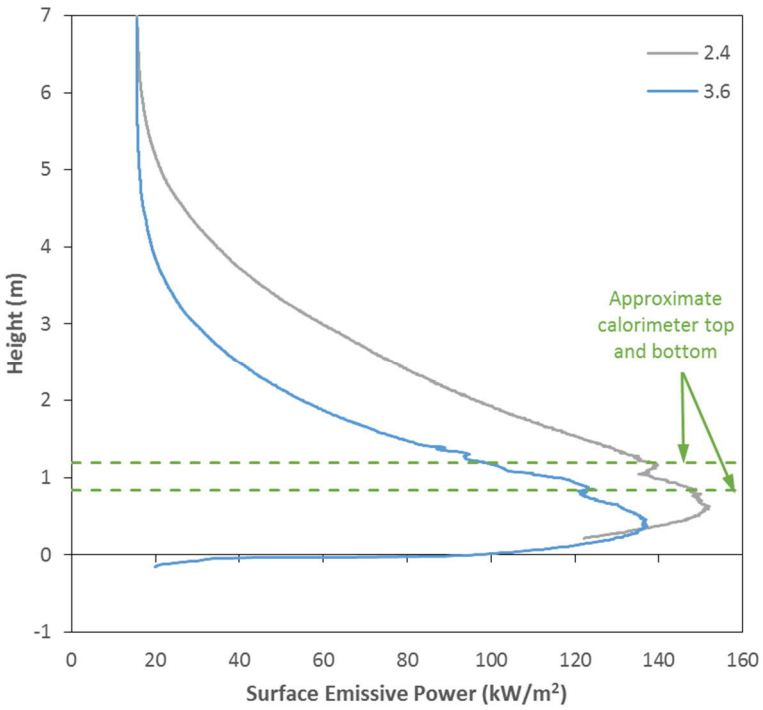

Figure 42: Infrared camera surface emissive power centreline profiles for tests with calorimeter at 1 m height and 60°C constant level fuel supply (no data available for Test 1.3 or SPR test)

Table 42 shows that the SPR fire had a burning rate similar to the Bakken fire and higher than the dilbit fire, but a flame height lower than both the Bakken and dilbit fires. Given that the heat release rate of the SPR fire was relatively similar to that of the Bakken fire (the standard deviation ranges of both values overlap), it is likely that the low value of flame height for the SPR fire was affected by the different method used to measure flame height in this test.

Table 42: Burning rates and flame heights for tests with calorimeter at 1 m height and 60°C constant level fuel supply

Test	Time period (min)	Burning rate (mm/min)	Flame height (m)	Heat release rate (MW)
1.3	24-40	3.53 ± 0.04	5.8[a] ± 0.8	5.2 ± 0.2
2.4	24-31.5	2.12 ± 0.03	4.6 ± 1.0	3.3 ± 0.6
3.6	4-6	1.25 ± 0.03	3.8 ± 0.8	n/a
	14.6-20	0.62 ± 0.03	3.3 ± 0.7	
	25-29.6	0.57 ± 0.03	3.9 ± 0.9	
SPR [8]	assumed to be averaged over test duration	1.95 ± 0.02	2.9[a] ± 0.8[b]	3.7 ± 0.6

[a] A different method (visible camera instead of infrared camera) was used to evaluate flame height.

[b] This has been adjusted from the two standard deviation value of 1.6 m reported in [8] to one standard deviation in order to permit comparison.

In Figure 43, the narrow-view heat flux measurements from the SPR fire are reasonably similar to those from the dilbit and Bakken fires, indicating that the surface emissive power was not greatly affected by differences in the composition of the various crude oils. Unlike the other profiles, though, the SPR profile exhibited a lower value at the 1.5 m height than at the 2 m height. This apparent anomaly is not considered significant, however, because the difference between the 1.5 m and 2 m average values (4 kW/m^2) is much lower than the standard deviation ranges of both values (±17 to 20 kW/m^2).

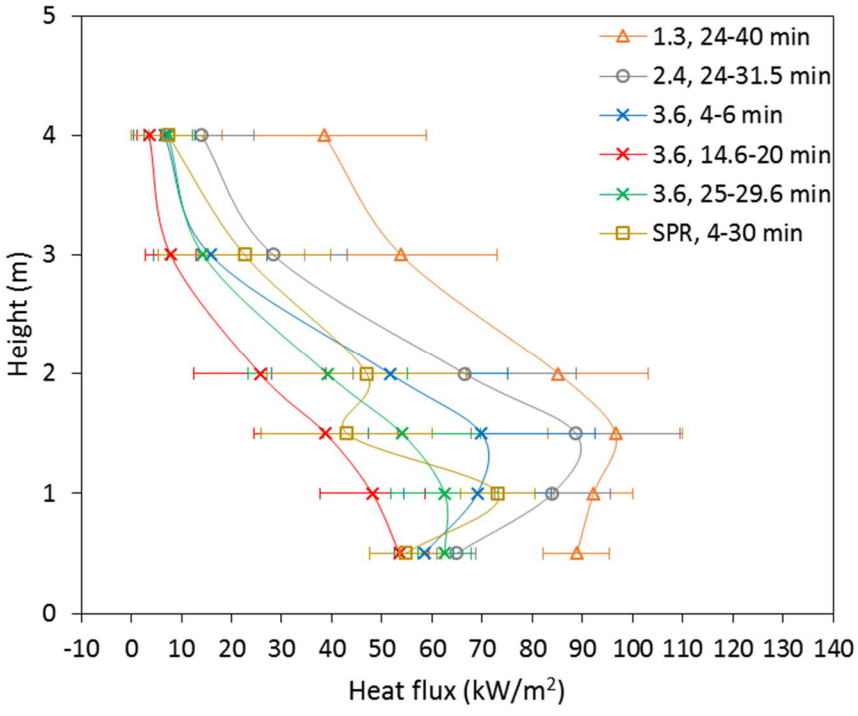

Figure 43: Narrow-view radiometer measurements for tests with calorimeter at 1 m height and 60°C constant level fuel supply (SPR data from [8])

The DFT measurements for the SPR fire were somewhat lower than those for the dilbit and Bakken fires at the 2 m location (Figure 44a), but noticeably higher than those for the other fires at the 4 m location (Figure 44b). The latter is consistent with the wide-view radiometer measurements in Figure 45. A possible cause of the higher heat flux levels measured from the SPR fire by the wide-view radiometers and the 4 m DFT is the smaller lip height used in the SPR test (Table 41). Differences in lip height affect air entrainment into the fire and plume dynamics, and such effects may have been more apparent in heat flux measurements taken at locations further away from the fire (using the 4 m DFT and wide-view radiometers), as opposed to close to the flame surface (using the 2 m DFT and narrow-view radiometers). Additional testing is recommended to evaluate this supposition.

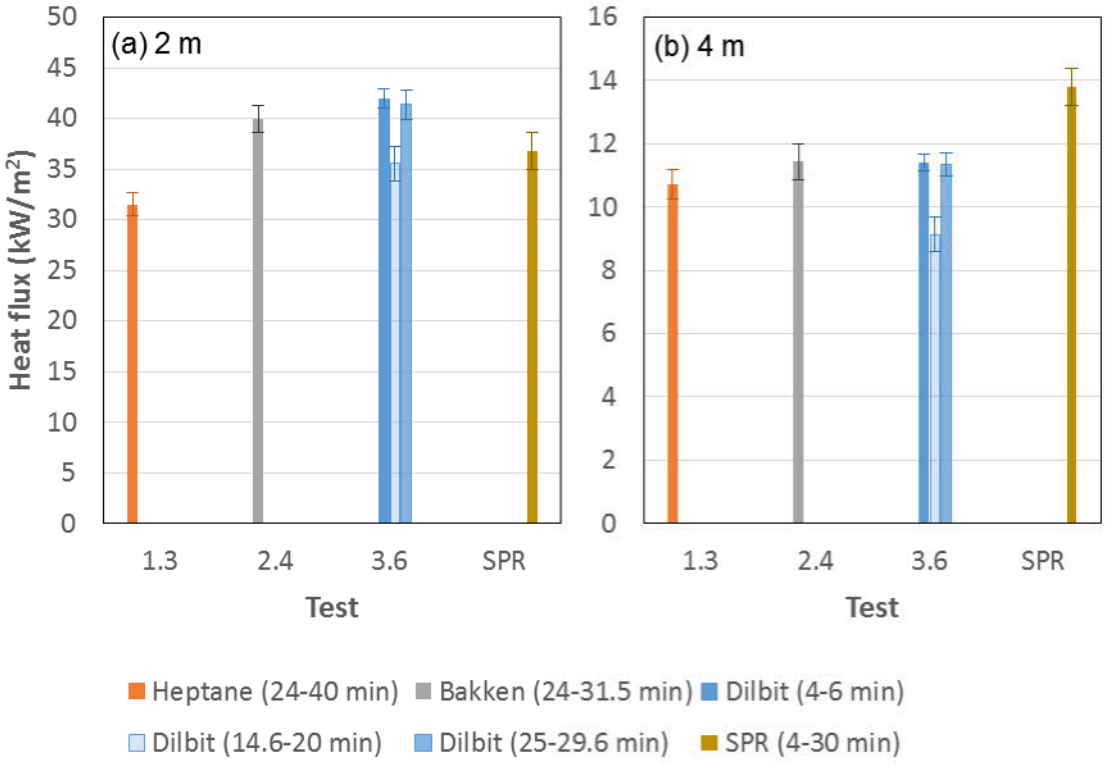

Figure 44: DFT measurements for tests with calorimeter at 1 m height and 60°C constant level fuel supply (SPR data from [8])

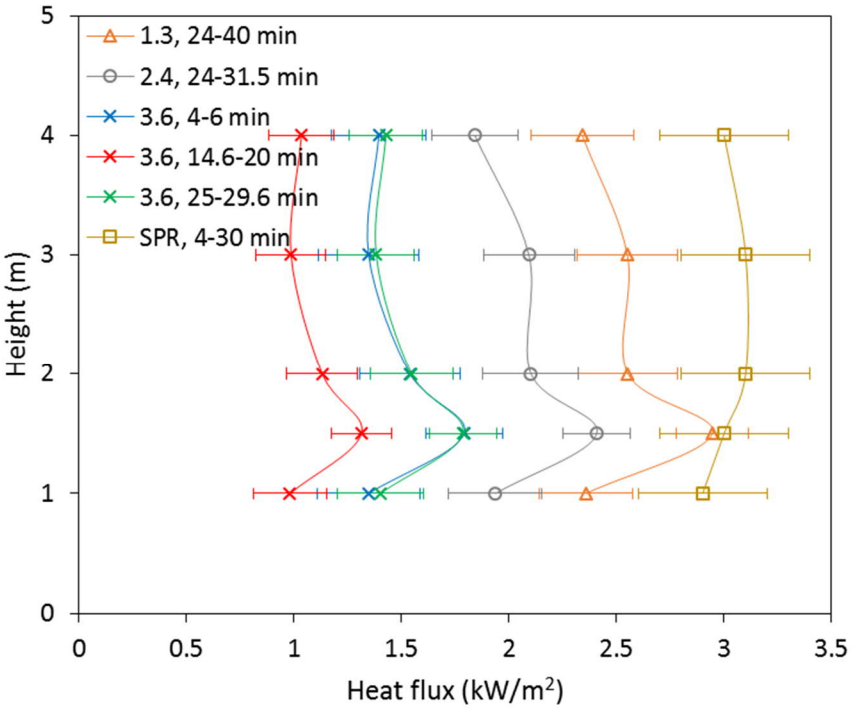

Figure 45: Wide-view radiometer measurements for tests with calorimeter at 1 m height and 60°C constant level fuel supply (SPR data from [8])

In the SPR test, the calorimeter was seen to receive reasonably uniform levels of total heat flux along its surface (Figure 46d). This was similar to the calorimeter in the heptane fire (Figure 46a), although the heat flux levels were higher in the SPR test (~100 kW/m^2 as opposed to 75 kW/m^2 or less). The heat flux profiles for the SPR test were quite different from those for the Bakken and dilbit tests (Figures 46b and c, respectively), as the latter indicated higher heat flux levels to the bottom of the calorimeter than the top. Particularly along the centre measurement plane, this trend was clearly observed for the dilbit fire, but insufficient data was available to verify that the same occurred in the Bakken fire. It should be noted that due to the shorter length of the calorimeter used in the SPR test (Table 41), the left and right measurement planes (at ¼, ½ and ¾ length of the calorimeter in all cases) were closer to the axis of the fire in Figure 46d than in Figures 46a-c. This may partially explain the uniformity of the heat flux profiles in Figure 46d, as all three measurement planes would have been more likely to be fully engulfed by flame, being closer to the plume axis. The different lip height used in the SPR test may also have been a factor influencing heat flux uniformity, since the calorimeter would have been situated effectively lower in the fire, which could be expected to result in higher heat flux to the top of the calorimeter. Nonetheless, it may be noted that the heat flux to the bottom of the calorimeter in the SPR fire was similar in magnitude to that in both the dilbit and Bakken fires (given the data available).

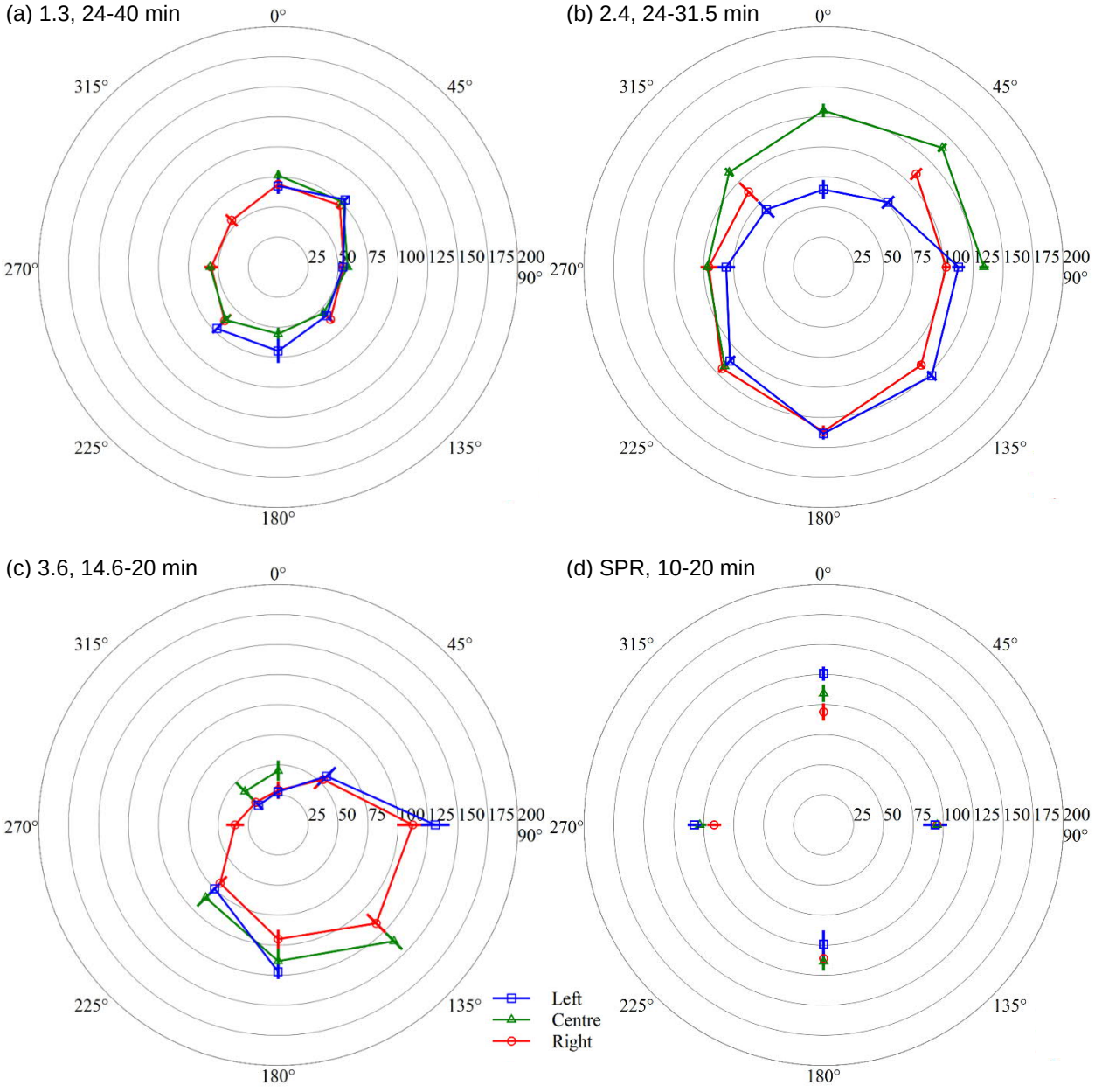

Figure 46: Selected plots of total heat flux (kW/m^2) to calorimeter, for tests with calorimeter at 1 m height and 60°C constant level fuel supply (SPR data from [8])

7.6 Tests with Calorimeter at 0.5 m Height and 20°C Constant Level Fuel Supply

The tests involved in this comparison are Tests 2.2 and 3.2. Table 43 compares the burning rates and flame heights from these tests. Recall that in Test 3.2, the dilbit was ignited as soon as it entered the fuel pan; then the pan was filled to the desired fuel level over approximately the first 13.5 minutes of the test. Thus the period between 11.9 and 12.7 minutes occurred near the end of this initial fuelling, whereas during the other time periods, fuel was being added to the pan at approximately the same rate as the burning rate (Section 3.2). The much higher burning rate of 3.94 mm/min measured from 11.9 to 12.7 minutes may have been affected by a still-changing lip height or other as-yet unidentified factors associated with the initial fuelling process. If this measurement were neglected, the dilbit fire would appear to have a generally lower burning rate than the Bakken fire, as well as a lower flame height.

Table 43: Burning rates and flame heights for tests with calorimeter at 0.5 m height and 20°C constant level fuel supply

Test	Time period (min)	Burning rate (mm/min)	Flame height (m)	Heat release rate (MW)
2.2	25-40	1.89 ± 0.03	4.5 ± 1.0	3.5 ± 0.6
3.2	11.9-12.7	3.94 ± 0.03	3.9 ± 0.8	n/a
	15-17	1.00 ± 0.03	3.3 ± 0.7	
	18.6-23.5	1.86 ± 0.03	3.6 ± 0.7	

The lower flame height of the dilbit fire is apparent when looking at the plume axis temperature plots in Figure 47. At heights of 1.5 m and above, the Bakken fire exhibited significantly higher temperatures, whereas at the 0.18 m height (below the calorimeter), the dilbit fire was hotter. This is consistent with Figure 48, which shows the exterior temperatures around the calorimeter. The exterior temperature at the top of the calorimeter in the centre plane was higher in the Bakken fire than in the dilbit fire, while the one at the bottom in the centre plane was higher in the dilbit fire. Figures 47 and 48 therefore suggest that much of the combustion occurred above the calorimeter in the Bakken fire, but below the calorimeter in the dilbit fire. There may have been a larger fuel-rich, non-combusting vapour zone below the calorimeter in the Bakken fire than in the dilbit fire, although further testing would be needed to confirm how the presence of the calorimeter affects the development of this zone. The surface emissive power measurements in Figure 49 are consistent with the above description of the Bakken fire (the data available from [2] for the dilbit fire was not suitable for comparison).

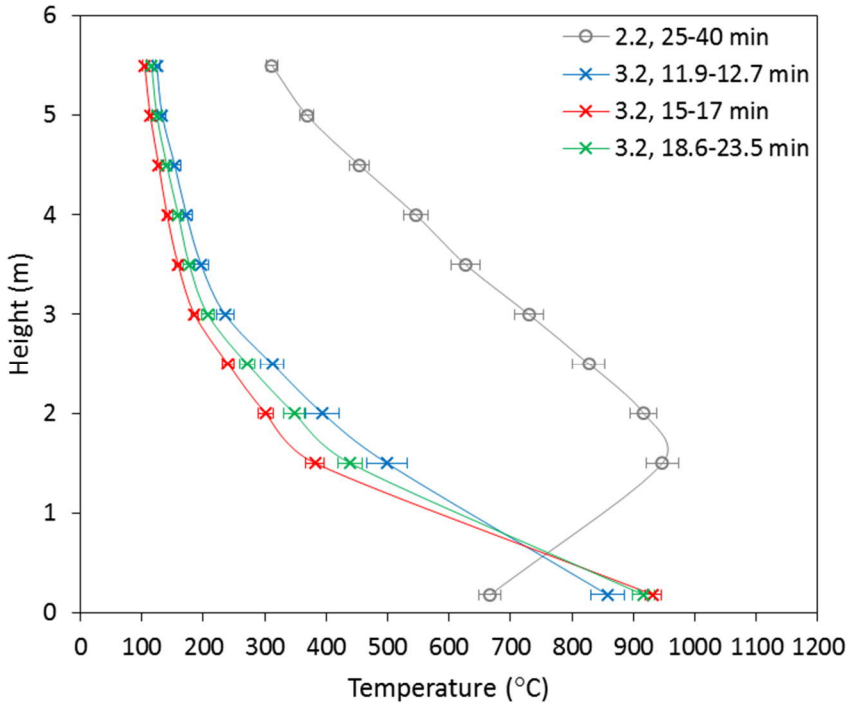

Figure 47: Plume axis temperatures for tests with calorimeter at 0.5 m height and 20°C constant level fuel supply

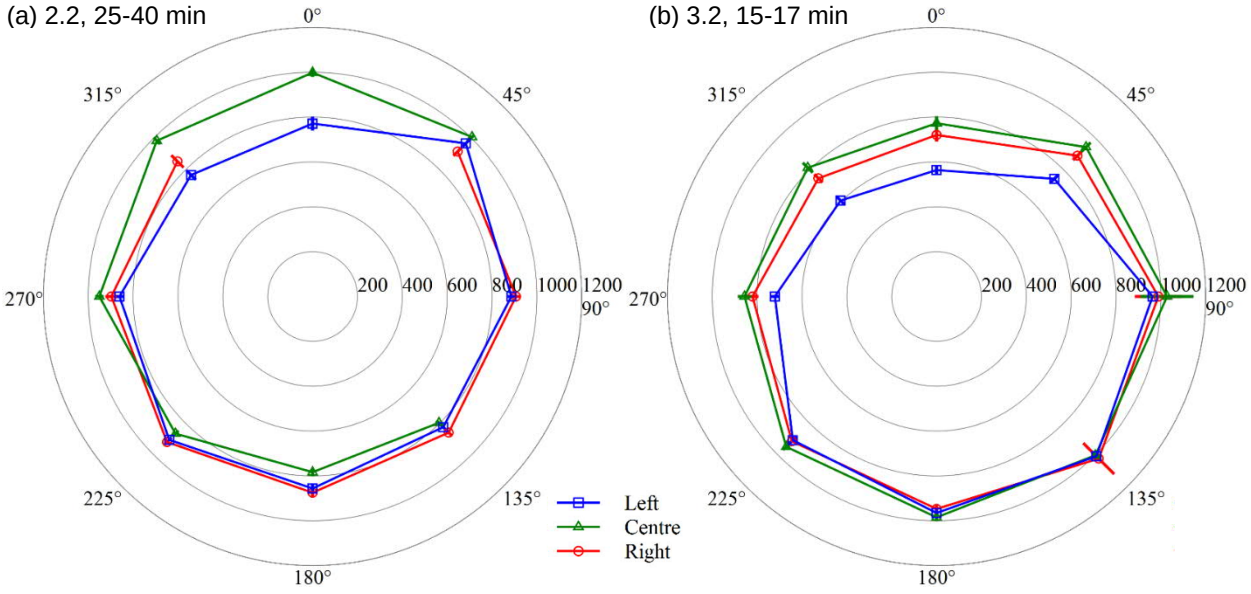

Figure 48: Selected plots of temperatures (°C) exterior to calorimeter, for tests with calorimeter at 0.5 m height and 20°C constant level fuel supply

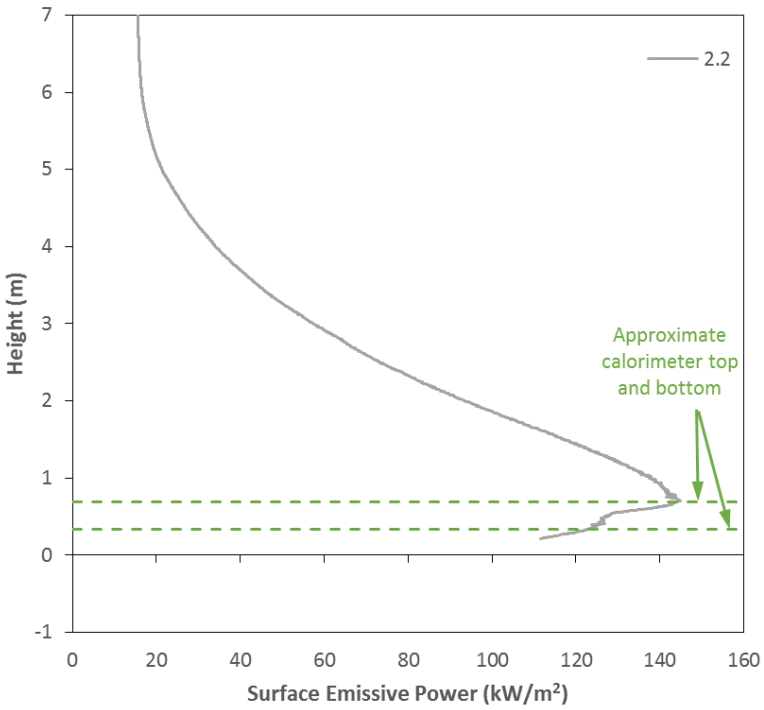

Figure 49: Infrared camera surface emissive power centreline profiles for tests with calorimeter at 0.5 m height and 20°C constant level fuel supply (available data for Test 3.2 not valid for comparison)

Figure 50 provides further evidence supporting the above differences between the Bakken and dilbit fires. In Figure 50a for the Bakken fire, the heat flux along the centre measurement plane was clearly higher to the top of the calorimeter than to the bottom, while the difference was less substantial in the left and right measurement planes due to those being closer to the edges of the fire. Although limited data was available for the dilbit fire in Figure 50b, the heat flux generally appeared to be higher towards the bottom of the calorimeter. The dilbit fire also appeared to be skewed towards the 90° side of the calorimeter, consistent with Figure 48b.

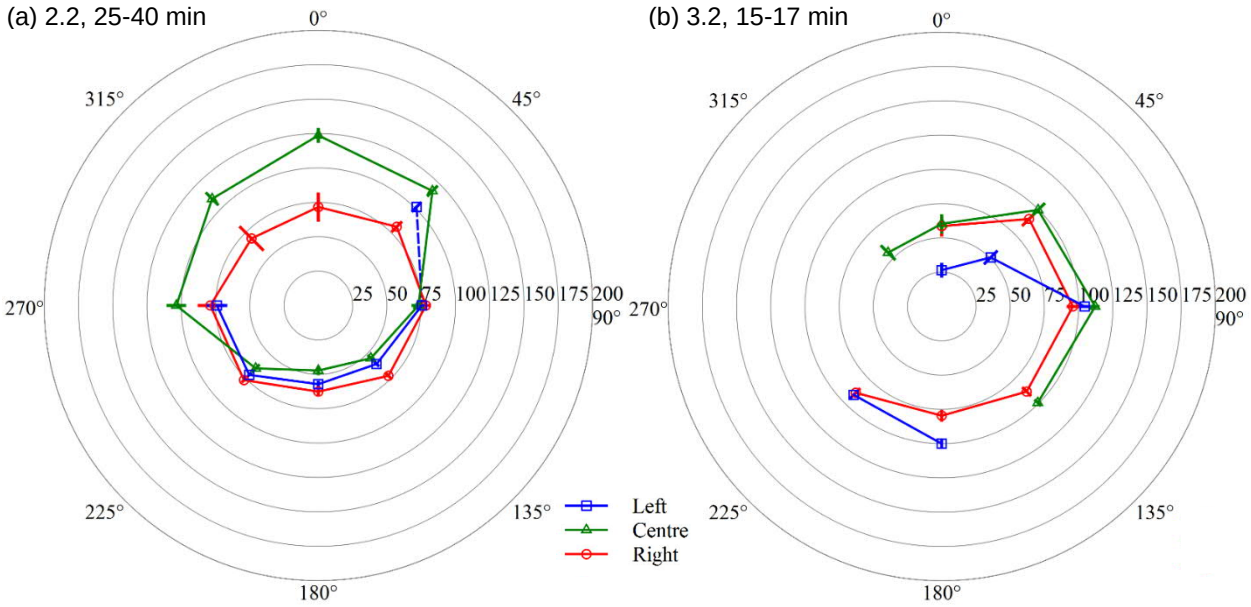

Figure 50: Selected plots of total heat flux (kW/m^2) to calorimeter, for tests with calorimeter at 0.5 m height and 20°C constant level fuel supply

Figure 51 indicates that slightly higher levels of narrow-view heat flux were measured in the Bakken fire than in the dilbit fire, although Figure 52a shows similar heat flux measurements in both fires by the 2 m DFT. This apparent inconsistency may be due to differences in what the two devices measure, as discussed previously in Sections 7.2 and 7.3. Meanwhile, both Figure 52b and Figure 53 show higher heat flux levels from the Bakken fire to the 4 m DFT and the wide-view radiometers, compared to the dilbit fire. This trend is most likely due to the larger flame height of the Bakken fire (Table 43).

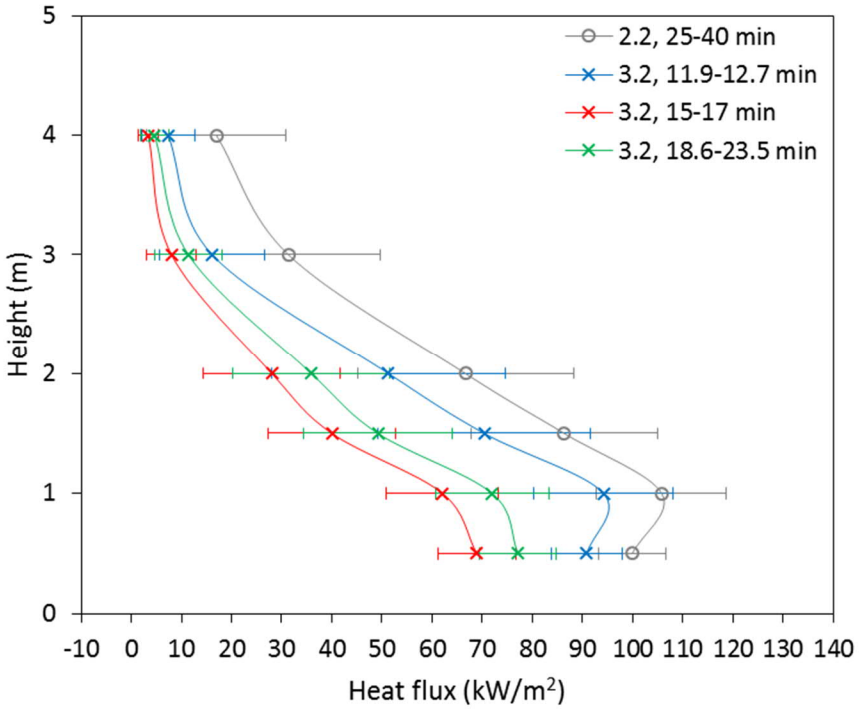

Figure 51: Narrow-view radiometer measurements for tests with calorimeter at 0.5 m height and 20°C constant level fuel supply

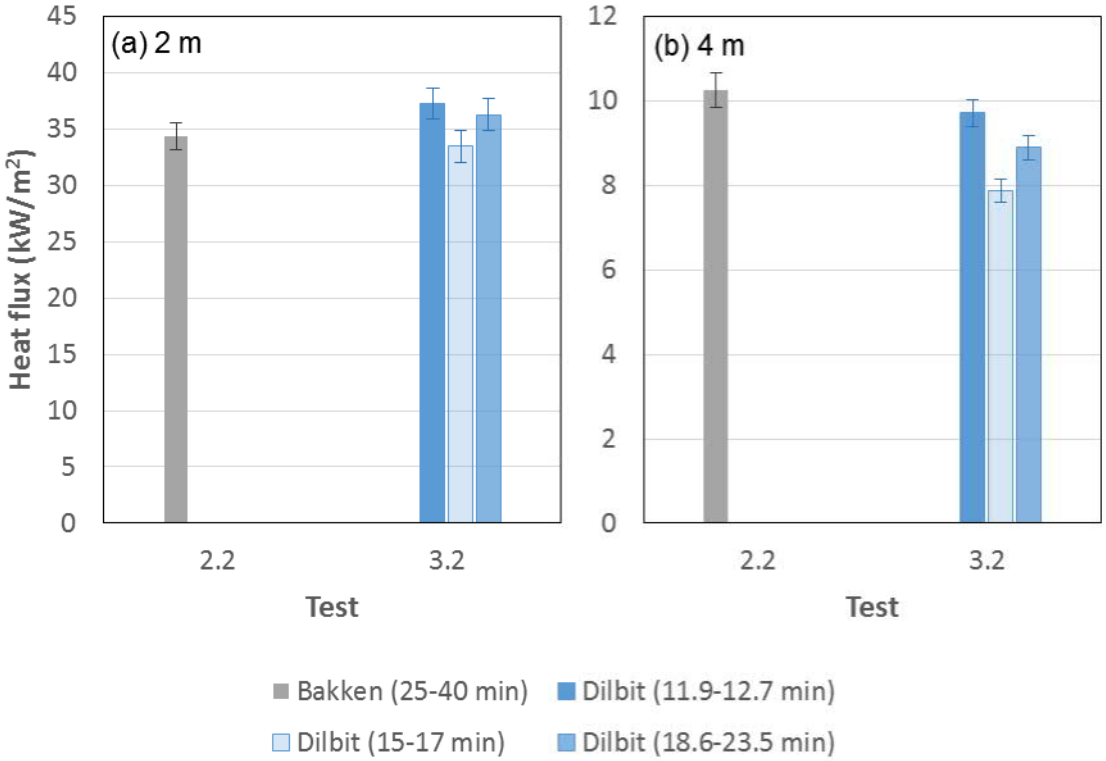

Figure 52: DFT measurements for tests with calorimeter at 0.5 m height and 20°C constant level fuel supply

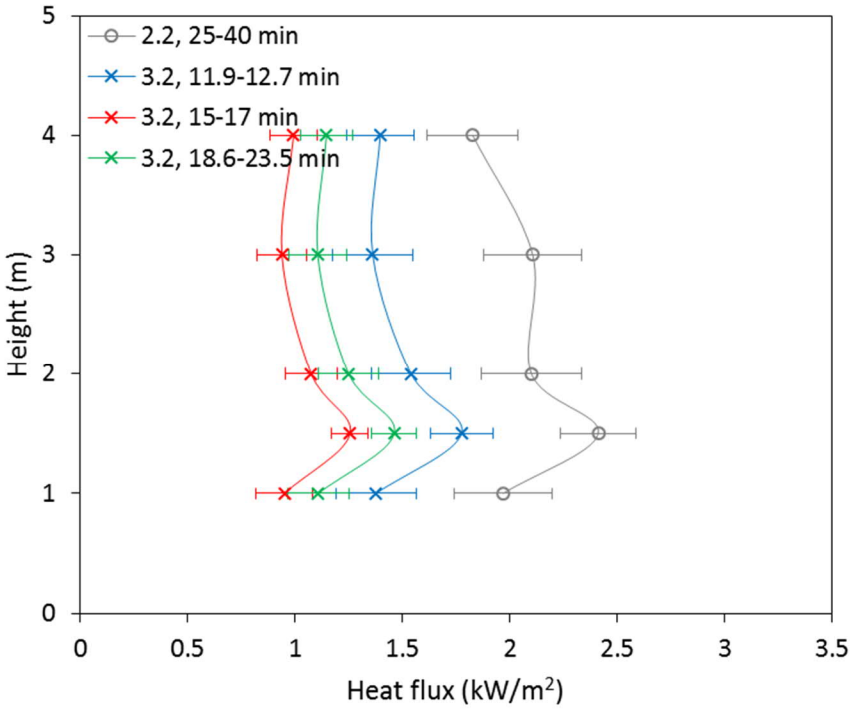

Figure 53: Wide-view radiometer measurements for tests with calorimeter at 0.5 m height and 20°C constant level fuel supply

8 Comparison to Other Sandia Test Series

Appendix B contains an analysis, conducted by Sandia National Laboratories, that compares data from three separate sets of pool fire experiments all performed at Sandia:

(1) the NRC/TC experiments [2], which considered 2 m diameter heptane and crude oil fires,
(2) the DOE/DOT/TC experiments [8], which considered 2 m and 5 m diameter crude oil fires, and
(3) the 2010 experiments described in [9], which considered 2 m diameter fires of various hydrocarbon fuels.

Comparisons were made between different-sized pool fires using the same crude oil (Bakken), and between same-sized (2 m diameter) pool fires using different fuels. Due to differences between the experimental setups used in the different studies, comparison of the NRC/TC experiments to the DOE/DOT/TC experiments was done separately from comparison of the NRC/TC experiments to the 2010 experiments.

During this author's review of Appendix B, numerous errors were found in the tables, particularly in the comparison of the 2 m diameter fires from the NRC/TC experiments (using heptane, Bakken and dilbit) and the DOE/DOT/TC experiments (using SPR). As a result, a more comprehensive and systematic comparison of the tests, using corrected data, has been conducted in Section 7.5.

Based on the other comparisons made in Appendix B (comparison of 2 m to 5 m diameter fires for the same crude oil, and comparison of crude oil fires to other hydrocarbon fuel fires at 2 m diameter), general conclusions that can be drawn from the discussion are as follows:

- Although it was difficult to compare the 2 m diameter Bakken fire (conducted indoors) to the 5 m diameter Bakken fire (conducted outdoors) because of differences in atmospheric conditions, the surface emissive power was found to be similar, indicating that both fires had similar optical thickness and lending credibility to the use of 2 m diameter fires to simulate larger-scale scenarios. Further, the spatially averaged total heat flux to the calorimeter was similar when the calorimeter was placed in similar relative locations (i.e. similar ratio of calorimeter elevation to pool diameter) inside the fire. This could be expected because in both cases (the 2 m fire with the calorimeter at 0.5 m height and the 5 m diameter fire with the calorimeter at 1 m height), the calorimeter was fully engulfed in the fire. Note that this comparison only considers changes in the scale of the fire and not changes in the scale of the calorimeter (which was at approximately $1/10^{th}$ scale in both cases).
- In comparing the 2 m diameter heptane, Bakken and dilbit fires of the NRC/TC experiments to the 2 m diameter fires of the 2010 experiments using other hydrocarbon fuels, it was found that the heptane fire was similar to the JP-8 fire in both burning rate and flame height. On the other hand, the Bakken and dilbit fires had lower burning rates and flame heights. This could be expected because heptane is a pure fuel and JP-8 is a highly refined aviation fuel, while Bakken is a crude oil and dilbit is a mixture of heavy bitumen and lighter condensate. Comparison of these four fuels is deemed the most useful, since they all produce relatively sooty fires, whereas methanol and ethanol (also included in the comparison) produce very little soot and thus have very different fire characteristics.

9 Conclusions

This report contains a comprehensive review and analysis of three series of 2 m diameter pool fire tests that were conducted at Sandia National Laboratories under the base project A1-010647 [1, 2]. The analysis was focussed on reviewing and verifying the time-averaged results presented in the Sandia test report [2]; examining changes in the fuel temperature distribution in order to gain insight into the burning behaviour of the tested crude oils; and comparing corresponding tests involving the same experimental test conditions to enhance understanding of the test results. Below are the conclusions from each of these activities.

Review of Time-Averaged Results in Sandia Test Report [2]

- In the Sandia report, the total heat flux to the DFTs in Series 1 and 2 was calculated using methods different from Series 3. Therefore, for consistency, the total heat flux values for Series 1 and 2 were recalculated in the present analysis using the method of Series 3. This resulted in differences of 30-40% for Series 1 data and 2-40% for Series 2 data.
- In all test series, the time intervals used to average the heat release rate data were found to require correction, due to an invalid assumption that the sampling rate was consistent during each test. This resulted in up to 5% error in the time-averaged values presented in the Sandia report.
- In the Sandia report, the time interval used to average the measured data in each of the Series 1 and 2 tests was not the same for all measurement parameters, making it difficult to draw conclusions about a particular test and to compare between tests. A single time-averaging period that could be applied to all measured parameters was therefore identified for each Series 1 and 2 test. For Series 1, the use of the adjusted time periods resulted in less than 4% difference from Sandia's values. For Series 2, the use of the adjusted time periods generally resulted in less than 7% difference from Sandia's values, although there were a few instances with larger differences (up to 19%) due to Sandia's time-averaging interval including a period of significant change in the fuel feed rate or the beginning of fire decay.
- For Series 3, Luketa [2] used time-averaged values calculated by integrating the data from 0 to 25 minutes and then dividing by 25 minutes. This method was selected because of large variations in the measurements due to unsteady burning of the dilbit and a high probability of variation in the manually controlled fuel level. The time-averaged values thus included the period of fire growth immediately after ignition and were typically associated with larger standard deviations. In the present analysis, multiple, shorter time-averaging periods were selected to permit quantification and analysis of the changes in burning behaviour. In general, Sandia's values compared reasonably well to the range of values provided using the shorter time-averaging periods, although burning rate values appeared to be highly influenced by the selected time period and the spatially averaged calorimeter values from Sandia's analysis tended to be lower than those from the present analysis.

Analysis of Burning Behaviour and Fuel Temperature Distribution

- For the Bakken crude oil, analysis of Test 2.6 (the "burn-down" test with no calorimeter) indicated the possibility of preferential burning of the lighter ends (up to C9) through a ~10% increase in heat release rate near the beginning of the test. Approximately two-thirds of the way through the test, there was a simultaneous sudden increase in heat release rate, decrease in the fuel rake temperatures, and increase in temperatures in the upper part of the fire plume. This may have been due to a sudden increase in available fuel vapours released as a result of thermal cracking of heavier ends in the crude oil.
- In the dilbit tests, all of the fire characteristics except burning rate indicated three stages of burning. The first stage appeared to be characterised by moderately high levels of heat release rate and flame height, as well as plume temperature, surface emissive power and heat flux at heights above the calorimeter. This was followed by a second stage, with noticeably lower levels of the same

parameters, and a final stage, with levels similar to or higher than in the first stage. Characteristics of these three stages of burning were different below the calorimeter because the calorimeter is a thermally massive object that interacts with and influences the surrounding flames through reradiation. Since the calorimeter continually heated up throughout the test, temperatures and heat flux measured below the calorimeter also continually increased.

- Analysis of the dilbit fuel temperatures suggested that the first stage of burning corresponded to fuel temperatures below approximately 150°C (with the fuel typically exhibiting a stratified temperature distribution) and the vapourization of lighter ends (up to C9, of which the dilbit had high composition). The preferential burning of the lighter ends was supported by the observation of a sudden increase in temperature in the upper part of the fire plume during the early part of Test 3.6, which coincided with the fuel pool suddenly reaching a uniform temperature of about 180°C as it rapidly changed from a stratified to uniform temperature distribution. The second stage of burning appeared to correspond to fuel temperatures increasing to approximately 300-350°C (with the possible existence of localized hot spots greater than 400°C) and the burning of components in the C10-C24 range (of which the dilbit had low composition). Thermal cracking of the heavier ends (C25+) would likely be involved, as indicated by the burning rate suddenly decreasing to zero (i.e. the fuel level becoming constant) during this stage in Test 3.4. Finally, the third stage corresponded to fuel temperatures greater than 350°C and the burning of the lighter hydrocarbons produced by thermal cracking.

Comparison of Tests Involving the Same Experimental Conditions

- Among the tests without the calorimeter, the heptane fire had the highest burning rate and flame height, followed by the Bakken fire and then the dilbit fire. Compared to the heptane fire, the Bakken fire exhibited steeper decreases in plume temperature and narrow-view heat flux with increasing height, consistent with the shorter flame height. Compared to the Bakken fire, the dilbit fire exhibited much lower temperatures along the plume axis due to the lower flame height, but only slightly lower levels of surface emissive power (narrow-view heat flux) across the height of the plume.
- Among the tests with the calorimeter at 1 m height, the heptane fire had the highest burning rate and flame height, followed by the Bakken fire and then the dilbit fire. In the heptane fire, similar levels of combustion appeared to occur both above and below the calorimeter, resulting in uniform levels of total heat flux around the calorimeter surface. In the Bakken fire, there may have been similar levels of combustion both above and below the calorimeter near the centre measurement plane (more data is needed to confirm this), but because the ends of the calorimeter were less fully engulfed in flame, the total heat flux to the top of the calorimeter was lower than to the bottom in the left and right measurement planes. In the dilbit fire, most of the combustion occurred below the calorimeter, resulting in higher total heat flux to the bottom of the calorimeter than to the top in all measurement planes. Overall, the calorimeter received the lowest levels of total heat flux in the heptane fire because this fire was less optically thick than either of the crude oil fires.
- The tests with the calorimeter at 1 m height were compared to a similar test conducted by Sandia using SPR oil [8]. The burning rate and heat release rate of the SPR fire were reasonably similar to those of the Bakken fire. Measurements of narrow-view heat flux (surface emissive power) were similar among the SPR, dilbit and Bakken fires, indicating that this parameter was not greatly affected by differences in crude oil composition. The total heat flux to the bottom of the calorimeter was similar among the SPR, dilbit and Bakken fires, but the heat flux profiles in the SPR test were more uniform around the surface of the calorimeter, likely due to the SPR calorimeter being shorter in length and thus more fully engulfed by the fire along its measurement planes.
- Among the tests with the calorimeter at 0.5 m height, the dilbit fire appeared to have a lower burning rate than the Bakken fire, in addition to a lower flame height. Much of the combustion seemed to occur above the calorimeter in the Bakken fire (due to the likely presence of a fuel-rich, non-combusting vapour zone above the fuel surface), but below the calorimeter in the dilbit fire. In the Bakken fire, the

total heat flux was higher to the top of the calorimeter along the centre measurement plane than to the bottom, whereas in the dilbit fire, the total heat flux generally appeared to be higher towards the bottom of the calorimeter.

- During comparison of the test data, it was found that trends in heat flux and surface emissive power seemed to depend on which measurement device was under consideration. This sometimes led to inconsistencies when comparing heat flux and surface emissive power measurements among the different fires. The inconsistencies stemmed from the fact that each device measured slightly different things, affecting the comparability of their data. The narrow-view radiometers (whose line of sight passed through the fuel pan axis at the height of each gauge) measured surface emissive power over a 0.8 m diameter region on the fire. The infrared camera also measured surface emissive power, but provided values for pixel-sized areas corresponding to much smaller regions on the fire. The 2 m DFT was placed 1 m outside the fuel pan edge, so its measurements of total heat flux would have been influenced mainly by the surface emissive power near the 1 m height of the DFT, plus any potential convective contributions. As the 4 m DFT was further away (3 m outside the fuel pan edge), its measurements would have been additionally influenced by differences in flame height. The wide-view radiometers were placed ~9 m from the fire, so their measurements would have been influenced mostly by differences in flame height.

10 Recommendations

Key recommendations based on the present study are as follows:

- Verification is needed on the potential for thermal cracking to occur when the lowest thermocouple on the fuel temperature rake measures 300-350°C. Additional measurements are recommended to verify the existence of localized hot spots in the fuel that would promote higher rates of cracking. This could potentially be accomplished through small-scale experimentation.
- Analysis of the residue samples (Section 6) would be beneficial as it may allow confirmation of the preferential burning of light ends and thermal cracking of heavy ends that were discussed in this report.
- Effects on the development of a fuel-rich, non-combusting vapour zone immediately above the fuel surface, caused by the presence of the calorimeter (a thermally massive object), should be investigated experimentally at the tested 1/10th scale and/or numerically using a validated model. Additional effects caused by varying the calorimeter elevation (e.g. from 1 m to 0.5 m height) should also be studied.
- Effects of a changing lip height on fire characteristics, including heat flux from the fire, should be studied experimentally at the tested 1/10th scale and/or numerically using a validated model. This may help verify the cause of the higher heat flux levels from the SPR fire measured by the wide-view radiometers and the 4 m DFT, compared to the Bakken and dilbit fires (Section 7.5).
- Levels of soot production should be investigated through small-scale experimentation and/or numerical modelling for the tested crude oils (as well as additional crude oils representing a range of composition). This may help provide insight into why the dilbit fire exhibited only slightly lower levels of surface emissive power (narrow-view heat flux) than the Bakken fire across the height of the fire plume, even though the interior plume temperatures were significantly lower.
- Further experimental testing is recommended for simulating a typical fire scenario involving the railcar sitting upright on the ground inside the fire. This testing would be conducted at 1/10th scale to allow comparison with the present results, meaning that the calorimeter height (from the pan bottom to the calorimeter centre) would be approximately 0.3 m.
- Before applying the results from the present work to a realistic fire scenario, one would need to understand effects of scaling on the fire characteristics, including burning rate, optical thickness, and size of the fuel-rich, non-combusting vapour zone. Although simulation of a realistic fire scenario could

be done with a numerical model, such a model would first need to be sufficiently validated by experiments, including at scales larger than 1/10. Results involving any modelling of the fuel pyrolysis should be compared to the temporal trends in fire behaviour that were identified in this report.

Acknowledgments

The author would like to acknowledge Robert Berzins for assisting in data verification; Mark Weinfurter and Nour Elsagan for assisting in producing plots for the report; and Yoon Ko for providing technical review of the report. The author would also like to acknowledge Anay Luketa from Sandia National Laboratories for responding to the wide range of questions that came up during the course of this study.

References

[1] Y. Ko, C. Lam, E. Gibbs, P.S. Lafrance and M. Weinfurter, Rail Tank Cars Exposed to Fires: Experimental Analyses of Thermal Conditions Imposed to a Railcar Engulfed in Crude Oil Fires (Series 1-3 Tests), NRC Report A1-010647-01, National Research Council Canada, Ottawa, ON, 2020.

[2] A. Luketa, A. Cruz-Cabrera, W. Gill, S. Adee and J. Hogge, Experimental Results of 2-m Heptane, Bakken Crude Oil, and Dilbit Crude Oil Pool Fire Tests Performed for the National Research Council of Canada, SAND2021-3206, Sandia National Laboratories, Albuquerque, NM, 2021.

[3] D. Lord, J. Hogge and R. Allen, Fuels Characterization for National Research Council Canada 2-m Pool Fire Test Series, SAND2021-3389, Sandia National Laboratories, Albuquerque, NM, 2021.

[4] ASTM International, E3057-19 Standard Test Method for Measuring Heat Flux Using Directional Flame Thermometers with Advanced Data Analysis Techniques. West Conshohocken, PA, ASTM International, 2019. DOI: https://doi.org/10.1520/E3057-19.

[5] R. Symonds, personal communication, CanmetENERGY, Natural Resources Canada, Ottawa, ON, September 2020.

[6] C. Lam, D. Edwards and G. Lougheed, Rail tank cars exposed to fire: literature review of crude oil, condensate and ethanol behaviour, NRC Report A1-005795-01.1, National Research Council Canada, Ottawa, ON, 2015, http://doi.org/10.4224/23001492.

[7] L.A. Gritzo, W. Gill and V.F. Nicolette, Estimates of the extent and character of the oxygen-starved interior in large pool fires. Very Large-Scale Fires, N.R. Keltner, N.J. Alvares and S.J. Grayson (editors). American Society for Testing and Materials, Special Technical Publication 1336, pp. 84-98, 1998.

[8] A. Luketa, T. Blanchat, D. Lord, J. Hogge, A. Cruz-Cabrera and R. Allen, Pool Fire and Fireball Experiments in Support of the US DOE/DOT/TC Crude Oil Characterization Research Study, SAND2019-9189, Sandia National Laboratories, Albuquerque, NM, 2019.

[9] T. Blanchat and J. Suo-Anttila, Hydrocarbon Characterization Experiments in Fully Turbulent Fires – Results and Data Analysis, SAND2010-6377, Sandia National Laboratories, Albuquerque, NM, 2011.

Appendix A - Calorimeter Plots

The calorimeter was constructed from two concentric stainless steel cylinders and instrumented along three cross-sectional measurement planes spaced equally along its length (i.e. at ¼, ½ and ¾ length). In each measurement plane, there were eight measurement directions spaced 45° apart, along each of which three thermocouples were placed in the following locations:

1) outside the calorimeter, offset from the outer surface by 51 mm (2");
2) inside the calorimeter, attached to the inner surface of the larger cylinder; and
3) inside the calorimeter, attached to the outer surface of the smaller cylinder.

In this report, the three measurement planes are denoted left (L), centre (C) and right (R), while the measurement directions refer to the top of the calorimeter as 0°. Measurement locations may be represented using a letter (L, C or R) to identify the measurement plane, immediately followed by a number (0, 45, 90, 135, 180, 225, 270 or 315) to identify the measurement direction.

This appendix presents polar plots of time-averaged data from the calorimeter for all three test series. Three sets of plots are presented for each test: total heat flux to the calorimeter, temperatures measured exterior to the calorimeter, and temperatures measured on the outer, larger cylinder. The temperatures measured on the inner cylinder are not shown because they increased continually throughout every test, so the time-averaged values are not considered to provide valuable information. (The inner cylinder temperatures were mainly used to provide a boundary condition for estimation of total heat flux to the calorimeter.)

In the plots, error bars representing one standard deviation are included. Many are difficult to see because they are smaller than the size of the marker representing the data point. In a few plots (Figures A-7, A-10 and A-15), dotted lines are used to indicate data points that were averaged over a time period different from the rest of the data. Different time-averaging periods were selected for these data points because of faulty thermocouple readings, as indicated in the footnotes of Tables 27 and 29.

A.1 Series 1 (Heptane)

A.1.1 Total Heat Flux

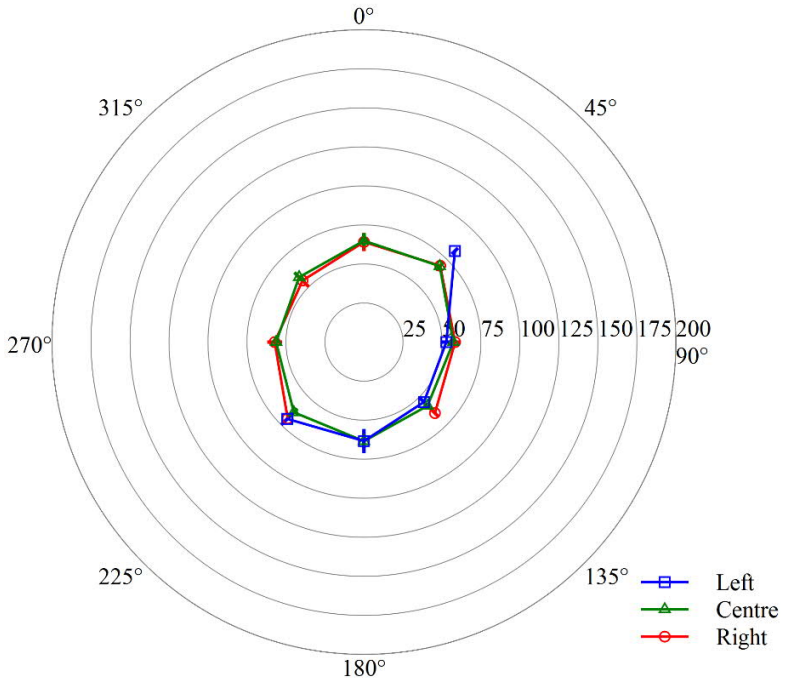

Figure A-1: Time-averaged total heat flux (kW/m^2) to calorimeter, Test 1.1 (10-35 min)

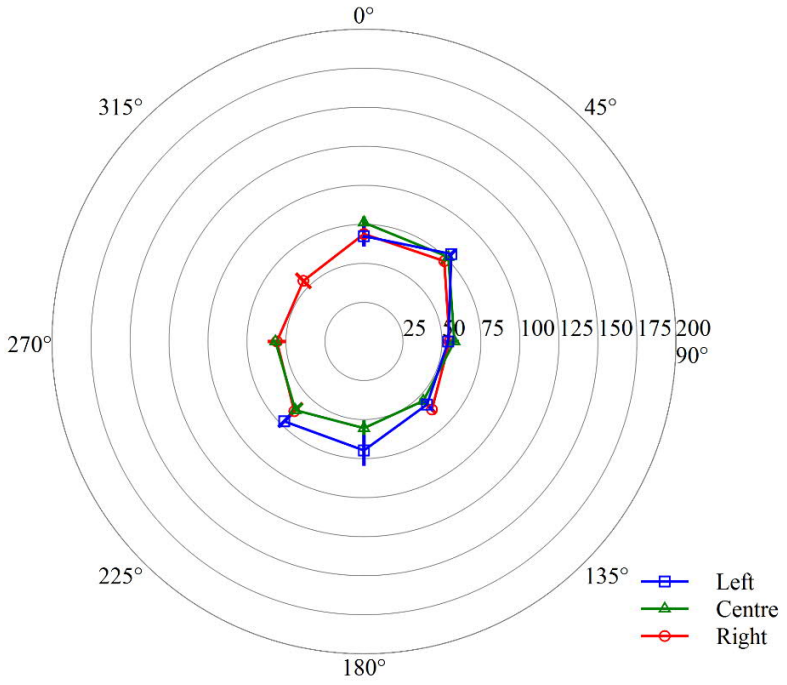

Figure A-2: Time-averaged total heat flux (kW/m^2) to calorimeter, Test 1.3 (24-40 min)

A.1.2 Exterior Temperatures

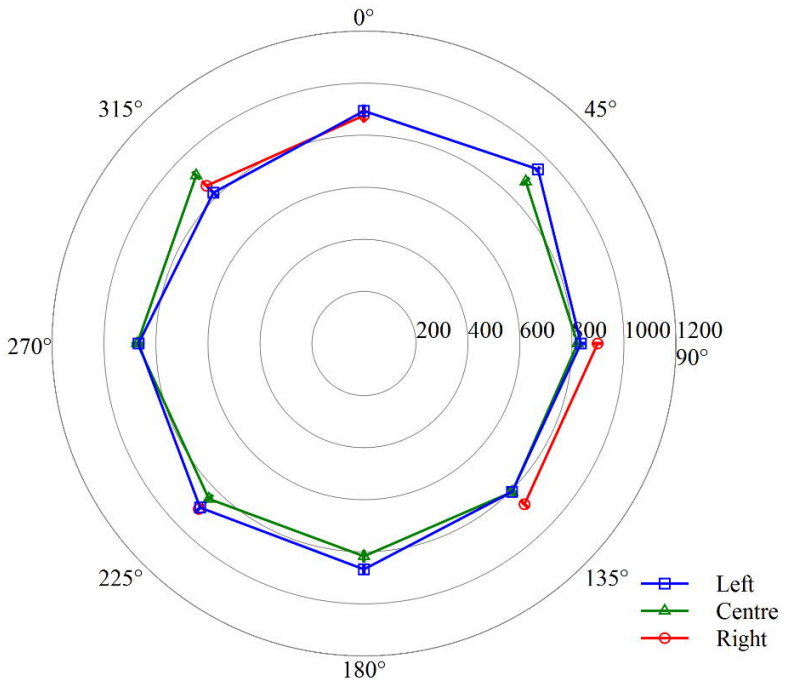

Figure A-3: Time-averaged temperatures (°C) exterior to calorimeter, Test 1.1 (10-35 min)

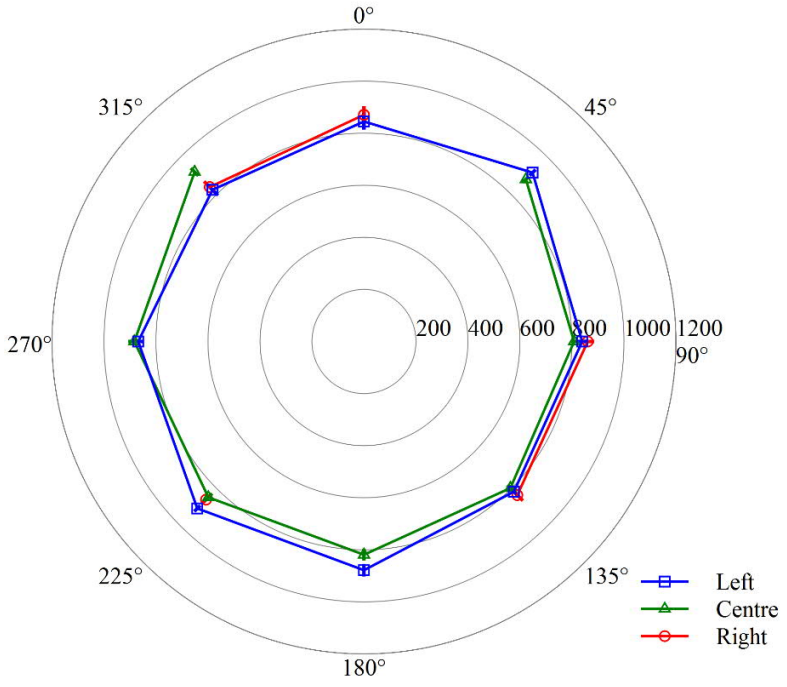

Figure A-4: Time-averaged temperatures (°C) exterior to calorimeter, Test 1.3 (24-40 min)

A.1.3 Outer Cylinder Temperatures

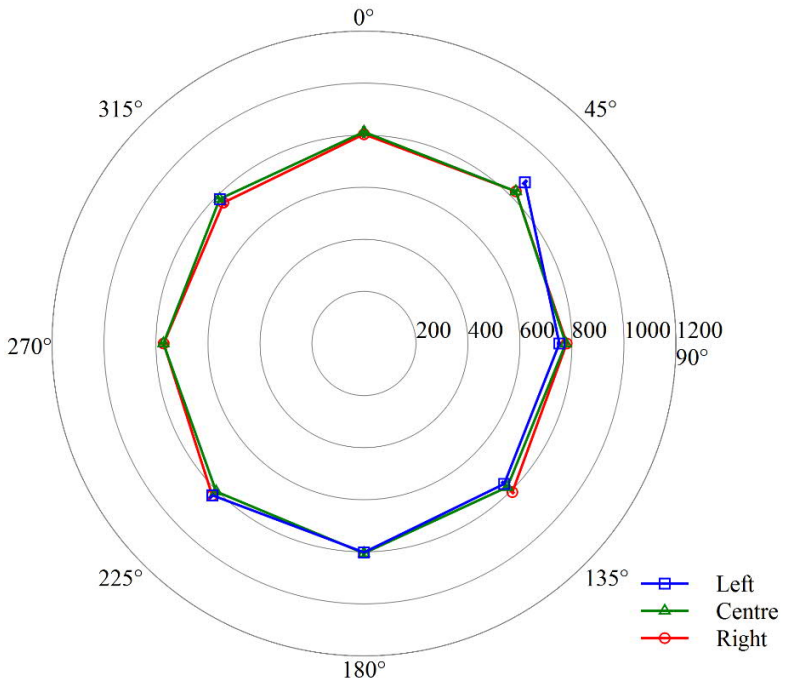

Figure A-5: Time-averaged temperatures (°C) on outer cylinder of calorimeter, Test 1.1 (10-35 min)

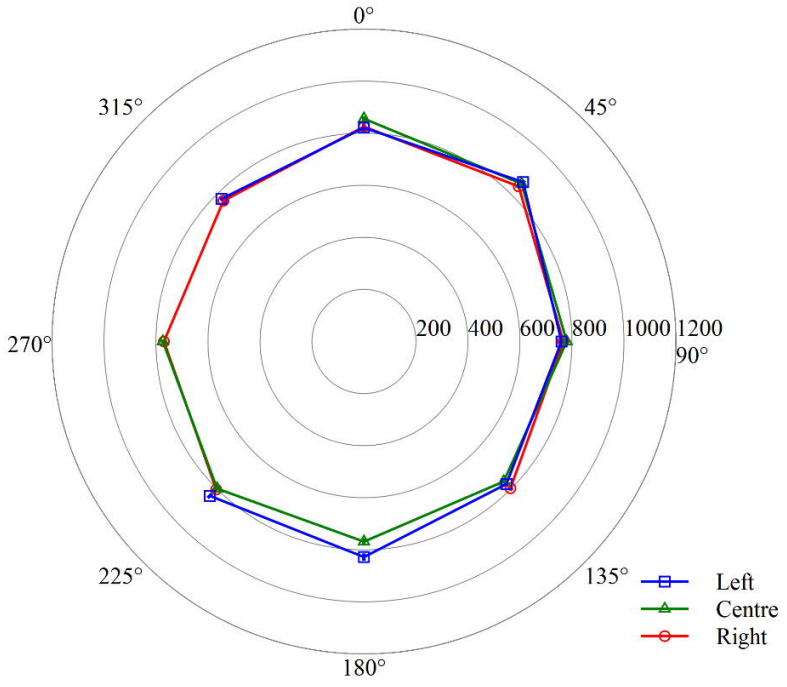

Figure A-6: Time-averaged temperatures (°C) on outer cylinder of calorimeter, Test 1.3 (24-40 min)

A.2 Series 2 (Bakken)

A.2.1 Total Heat Flux

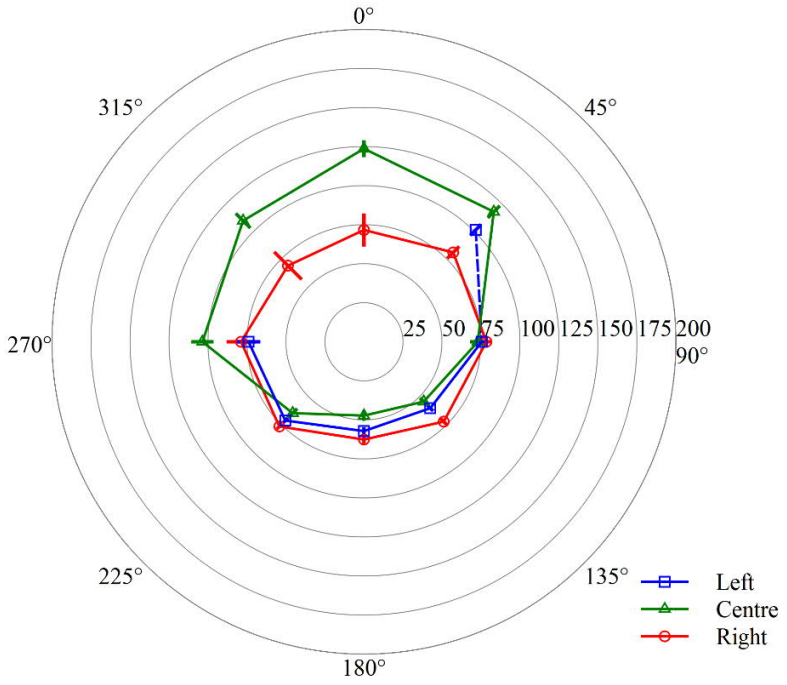

Figure A-7: Time-averaged total heat flux (kW/m^2) to calorimeter, Test 2.2 (25-40 min except L45 which is averaged over 30-40 min; see Table 27)

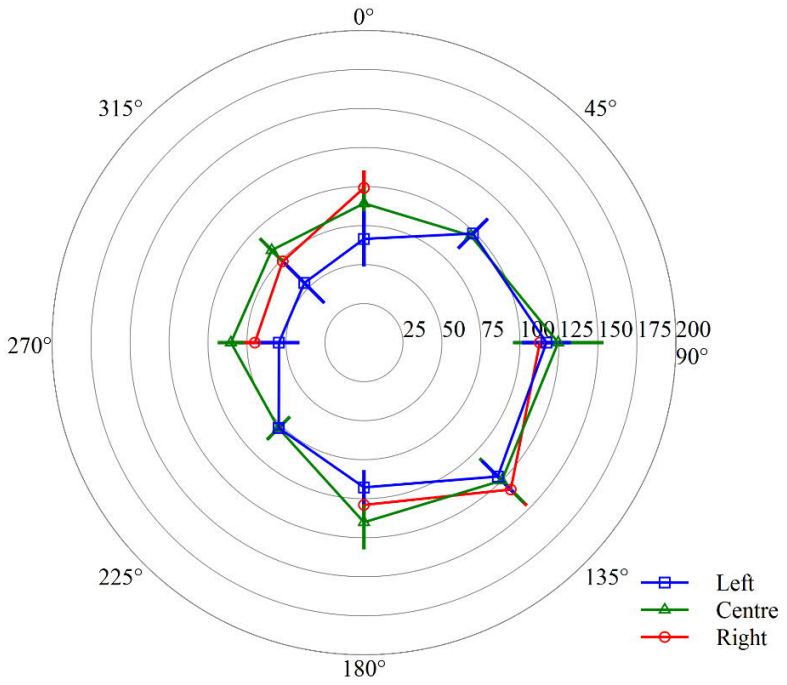

Figure A-8: Time-averaged total heat flux (kW/m^2) to calorimeter, Test 2.3 (10-30 min)

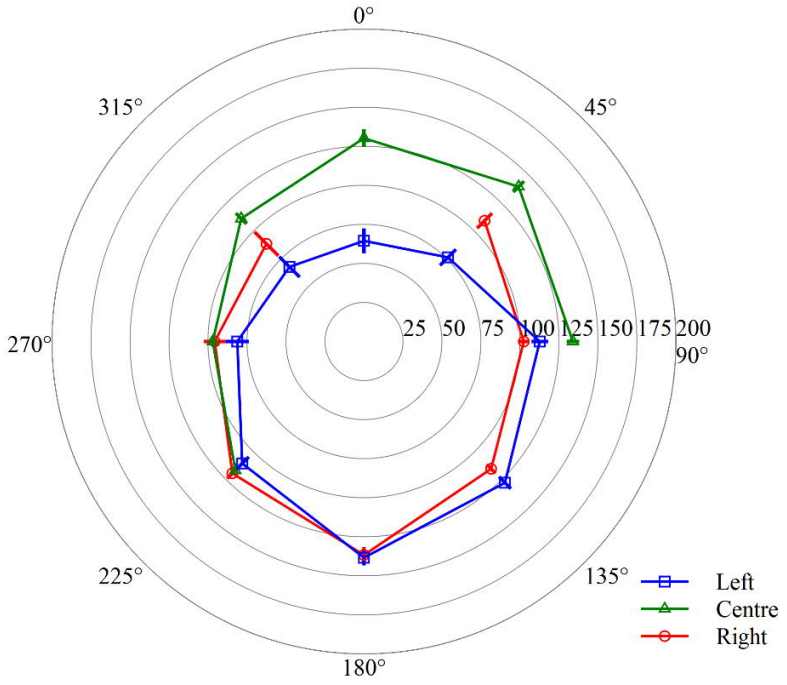

Figure A-9: Time-averaged total heat flux (kW/m^2) to calorimeter, Test 2.4 (24-31.5 min)

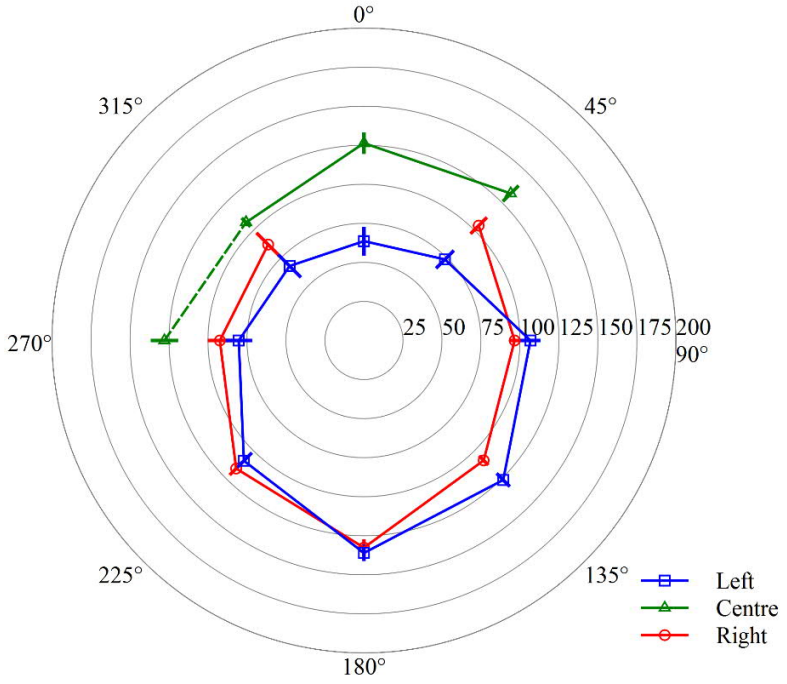

Figure A-10: Time-averaged total heat flux (kW/m^2) to calorimeter, Test 2.5 (15-34 min except C270 which is averaged over 20-34 min; see Table 27)

A.2.2 Exterior Temperatures

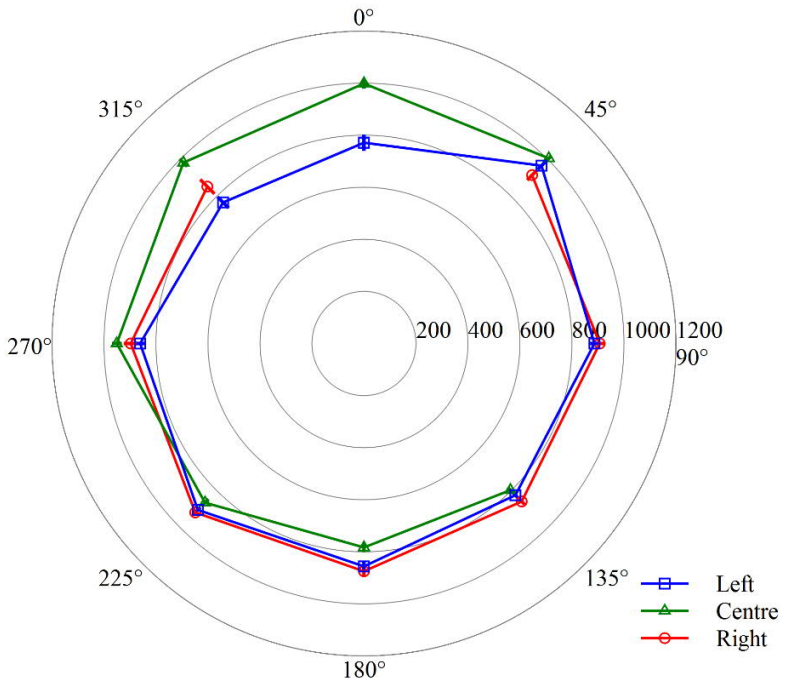

Figure A-11: Time-averaged temperatures (°C) exterior to calorimeter, Test 2.2 (25-40 min)

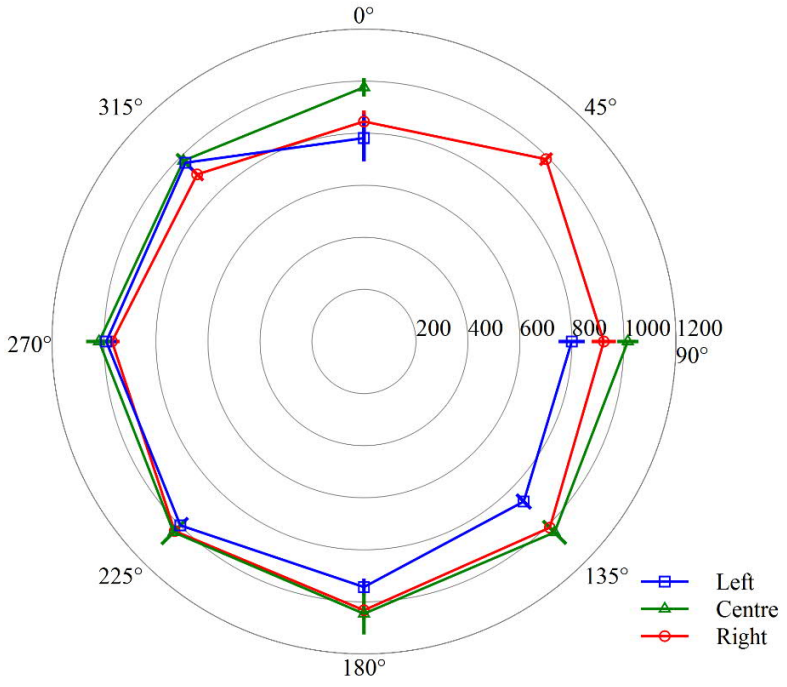

Figure A-12: Time-averaged temperatures (°C) exterior to calorimeter, Test 2.3 (10-30 min)

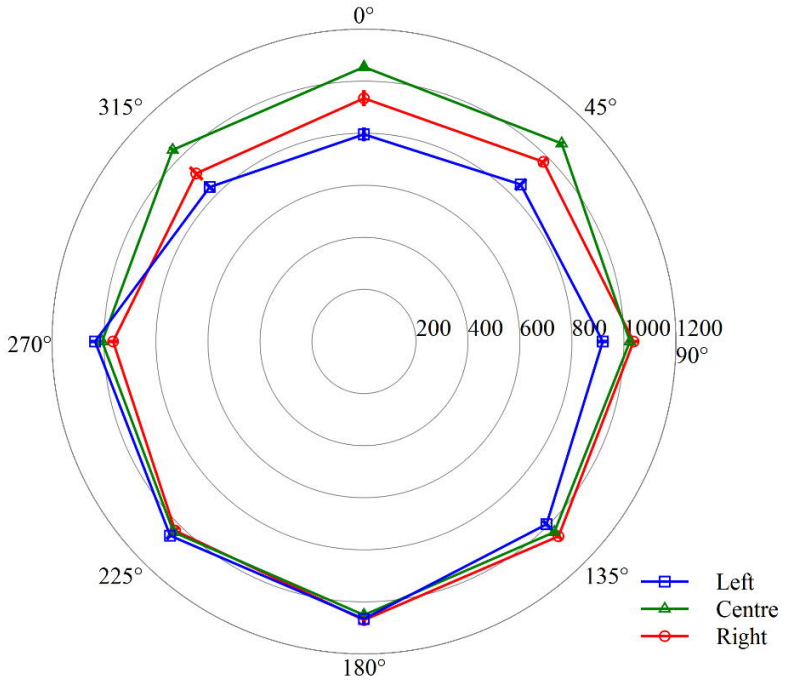

Figure A-13: Time-averaged temperatures (°C) exterior to calorimeter, Test 2.4 (24-31.5 min)

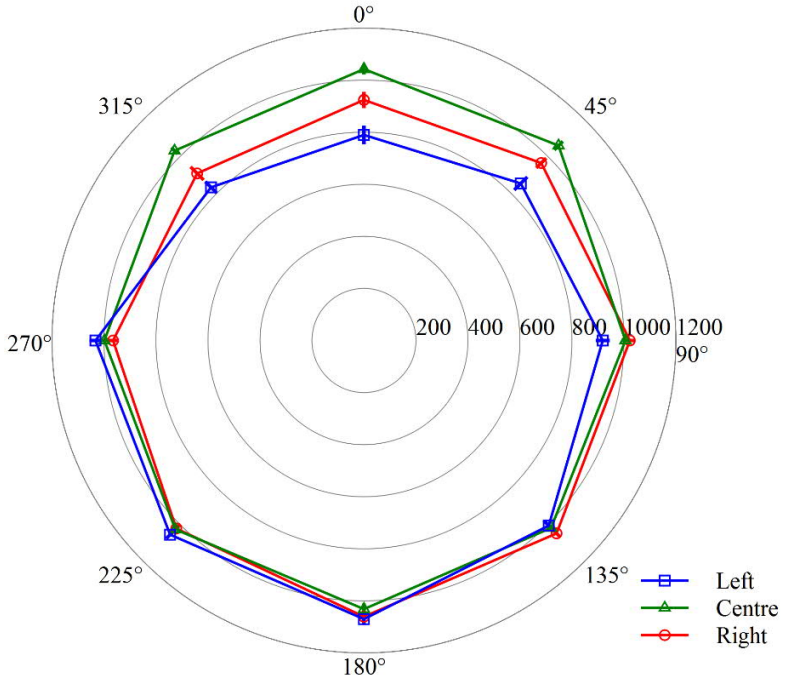

Figure A-14: Time-averaged temperatures (°C) exterior to calorimeter, Test 2.5 (15-34 min)

A.2.3 Outer Cylinder Temperatures

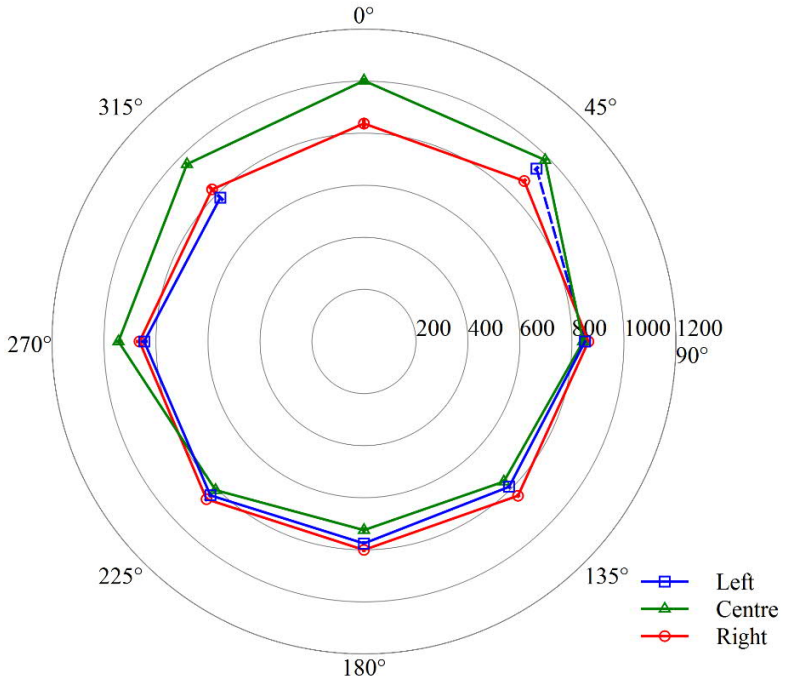

Figure A-15: Time-averaged temperatures (°C) on outer cylinder of calorimeter, Test 2.2 (25-40 min except L45 which is averaged over 30-40 min; see Table 29)

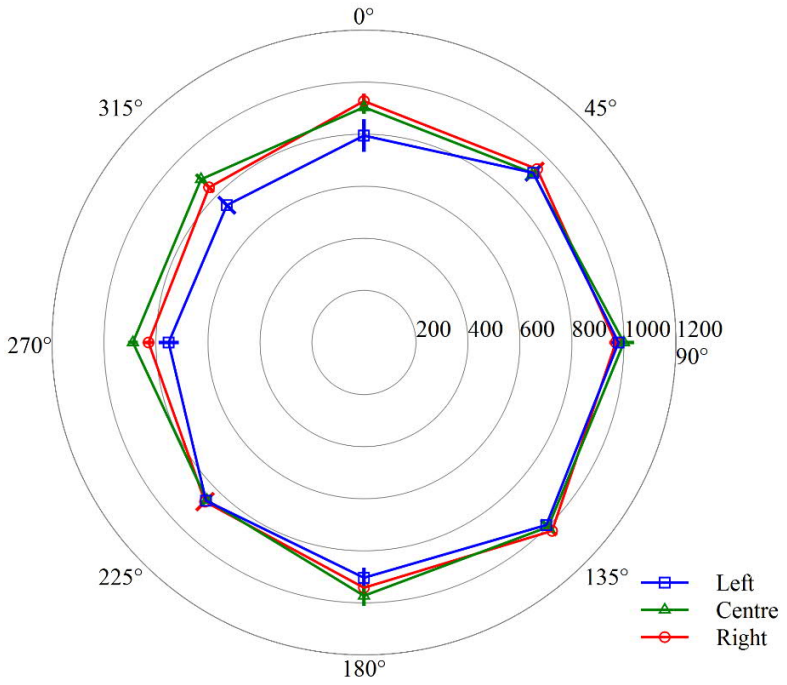

Figure A-16: Time-averaged temperatures (°C) on outer cylinder of calorimeter, Test 2.3 (10-30 min)

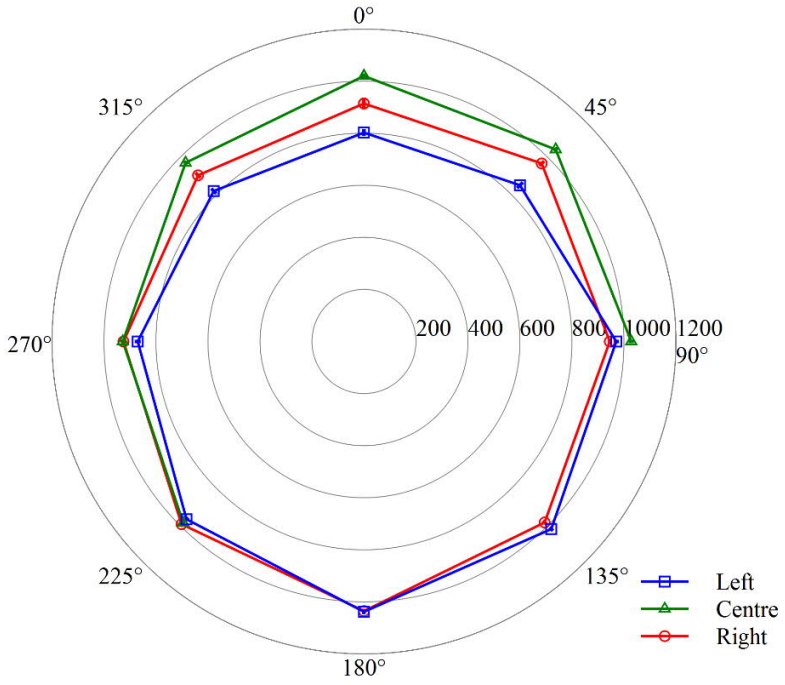

Figure A-17: Time-averaged temperatures (°C) on outer cylinder of calorimeter, Test 2.4 (24-31.5 min)

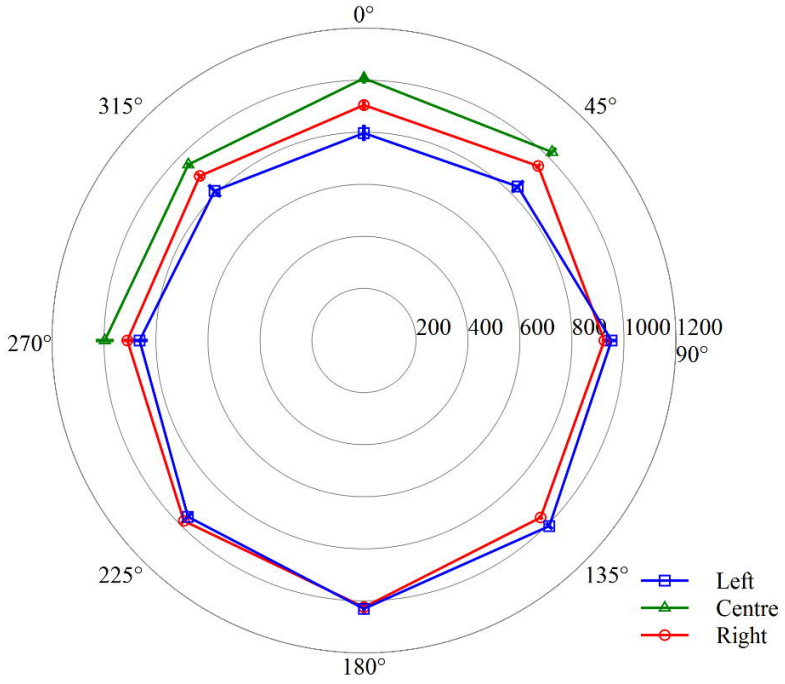

Figure A-18: Time-averaged temperatures (°C) on outer cylinder of calorimeter, Test 2.5 (15-34 min)

A.3 Series 3 (Dilbit)

A.3.1 Total Heat Flux

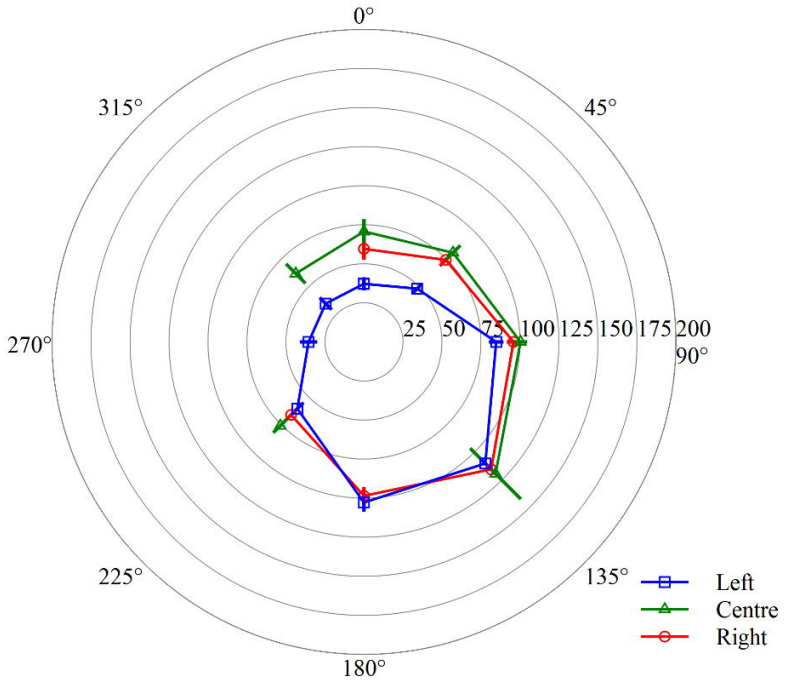

Figure A-19: Time-averaged total heat flux (kW/m^2) to calorimeter, Test 3.1 (3-5 min)

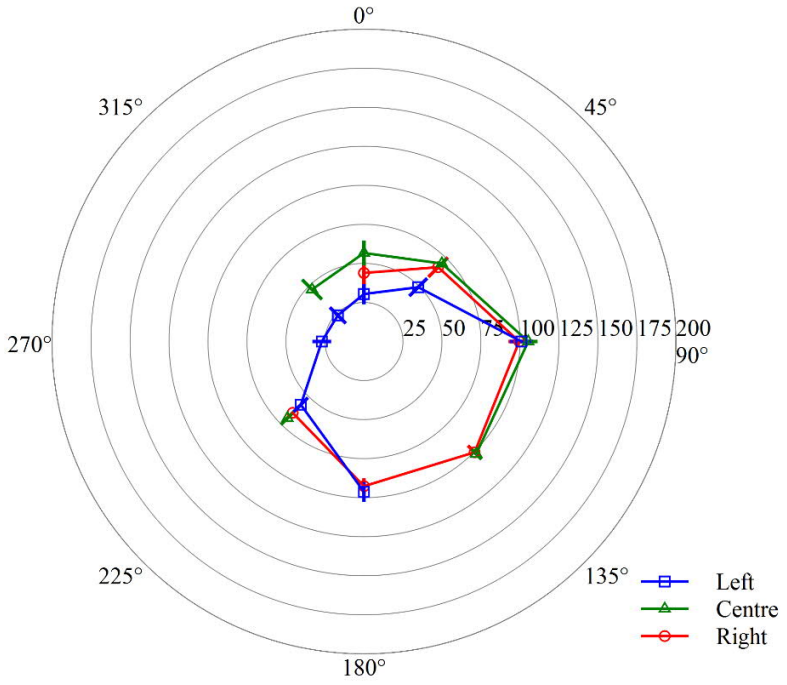

Figure A-20: Time-averaged total heat flux (kW/m^2) to calorimeter, Test 3.1 (8-11 min)

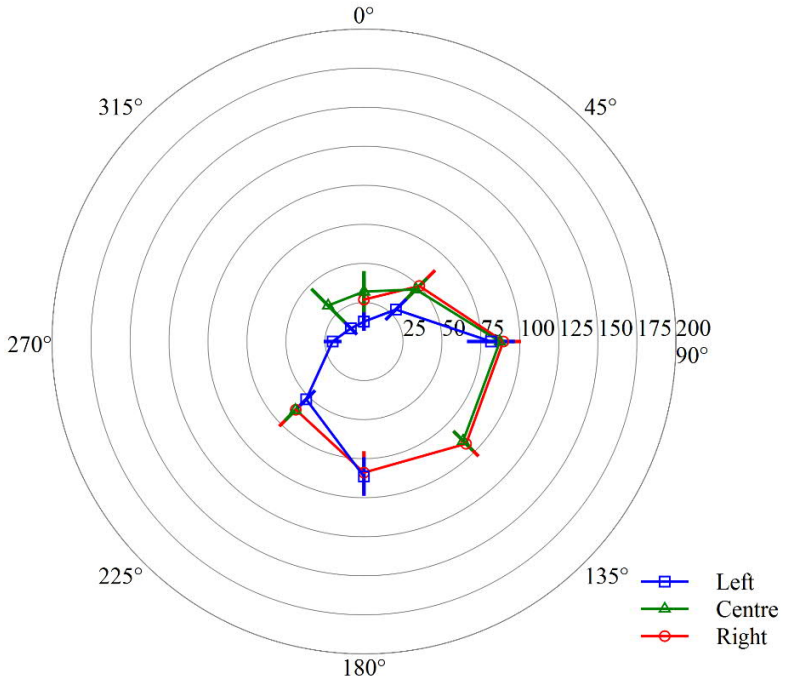

Figure A-21: Time-averaged total heat flux (kW/m^2) to calorimeter, Test 3.1 (16.5-18 min)

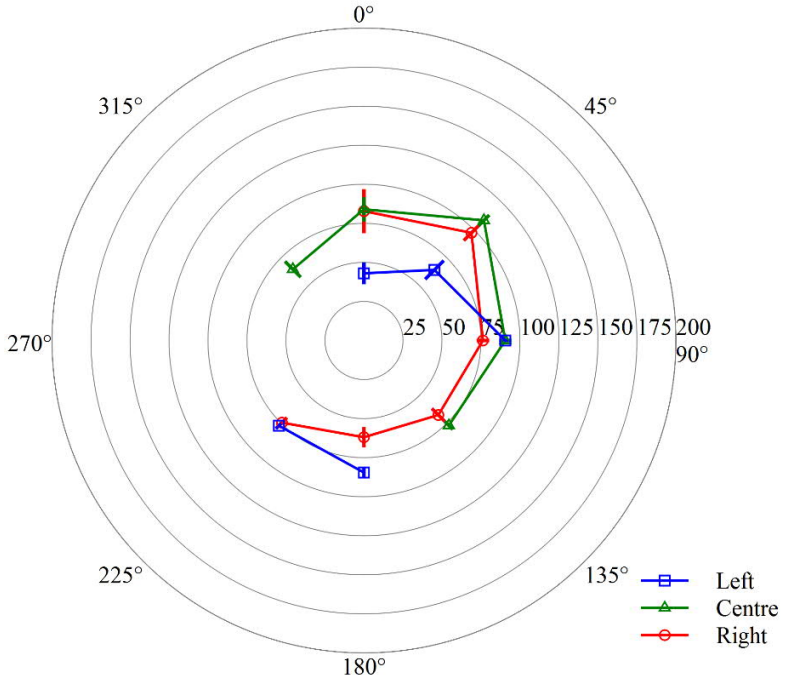

Figure A-22: Time-averaged total heat flux (kW/m^2) to calorimeter, Test 3.2 (11.9-12.7 min)

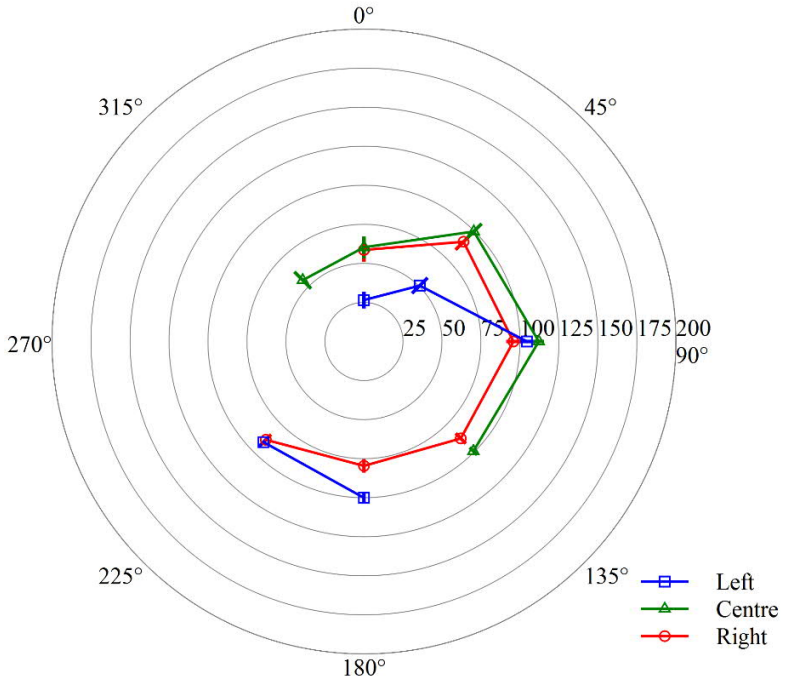

Figure A-23: Time-averaged total heat flux (kW/m^2) to calorimeter, Test 3.2 (15-17 min)

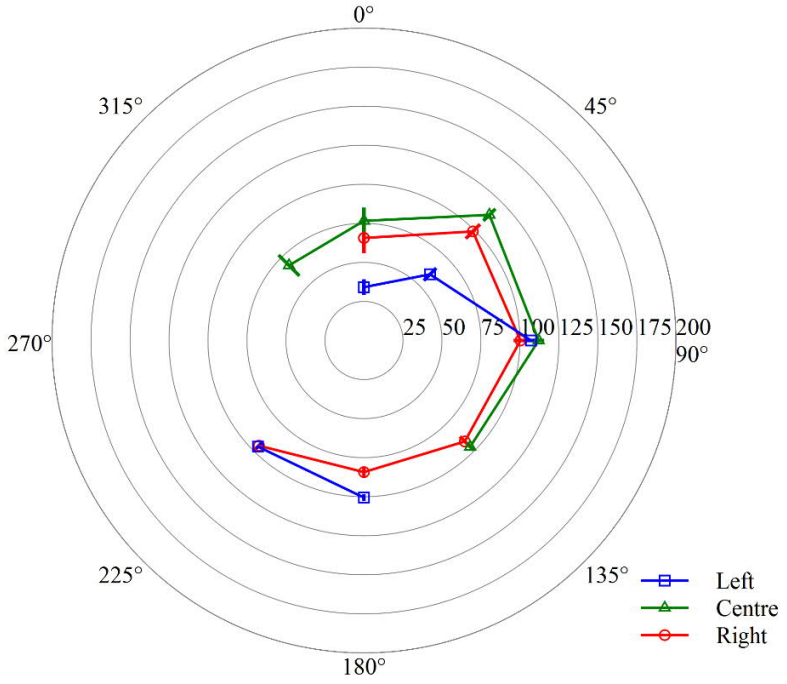

Figure A-24: Time-averaged total heat flux (kW/m^2) to calorimeter, Test 3.2 (18.6-23.5 min)

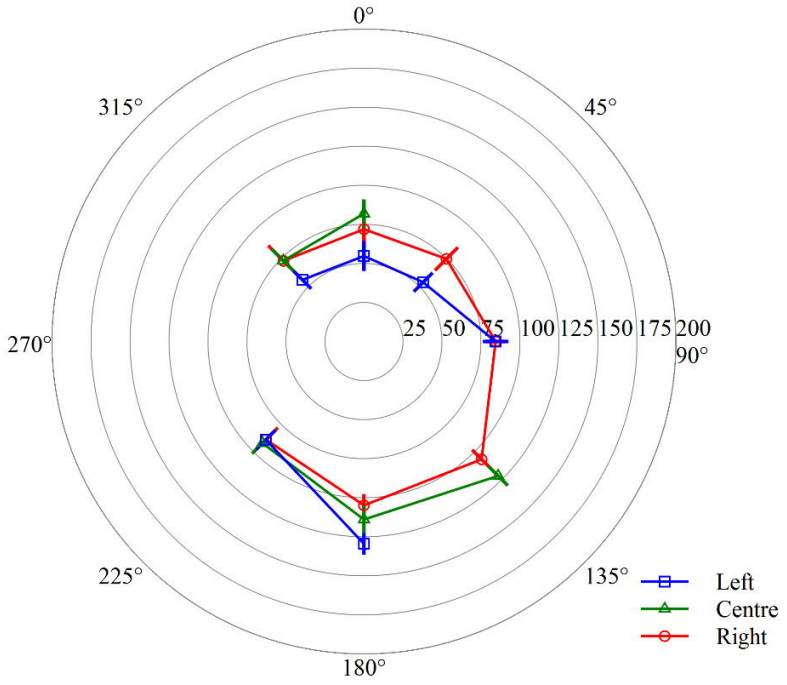

Figure A-25: Time-averaged total heat flux (kW/m^2) to calorimeter, Test 3.5 (3-10 min)

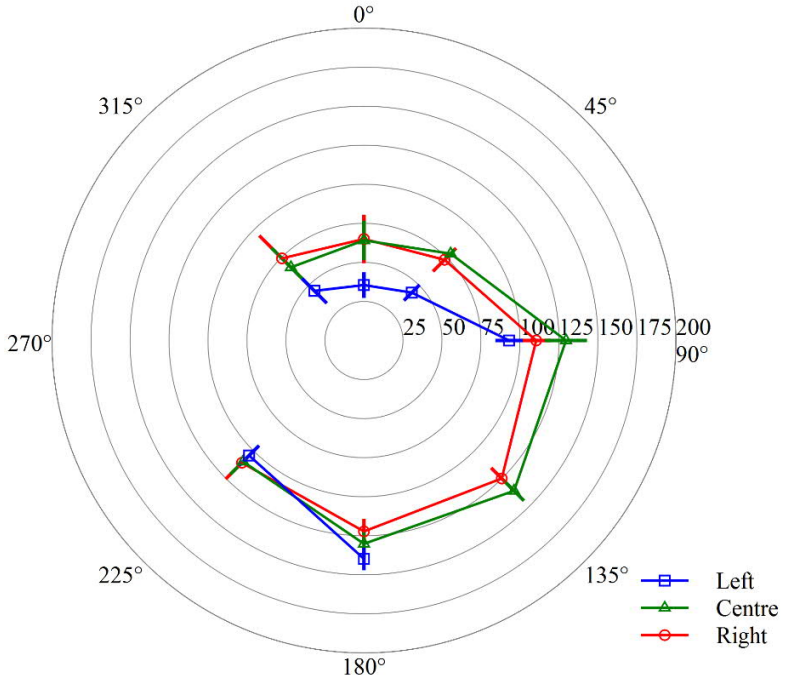

Figure A-26: Time-averaged total heat flux (kW/m^2) to calorimeter, Test 3.5 (16-19.5 min)

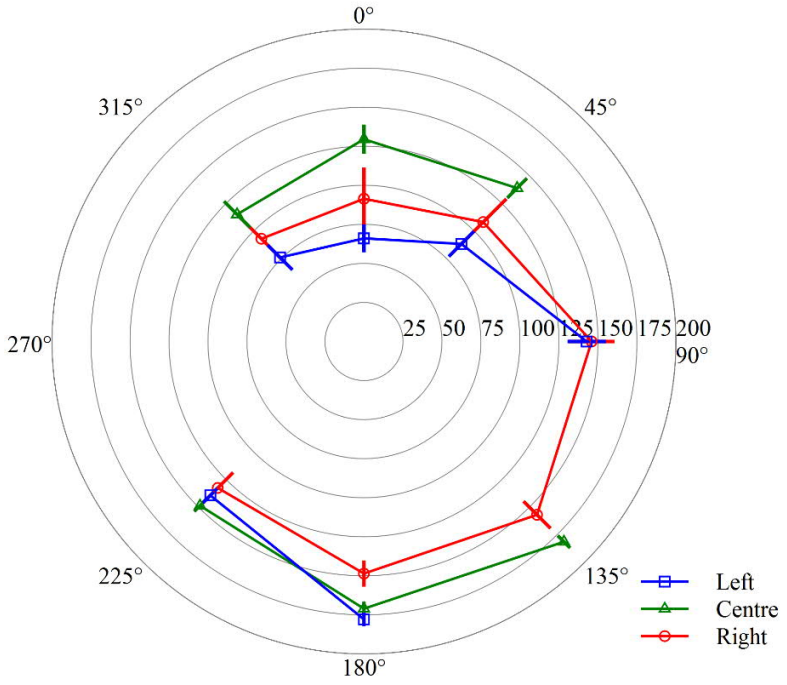

Figure A-27: Time-averaged total heat flux (kW/m^2) to calorimeter, Test 3.5 (27.5-30.5 min)

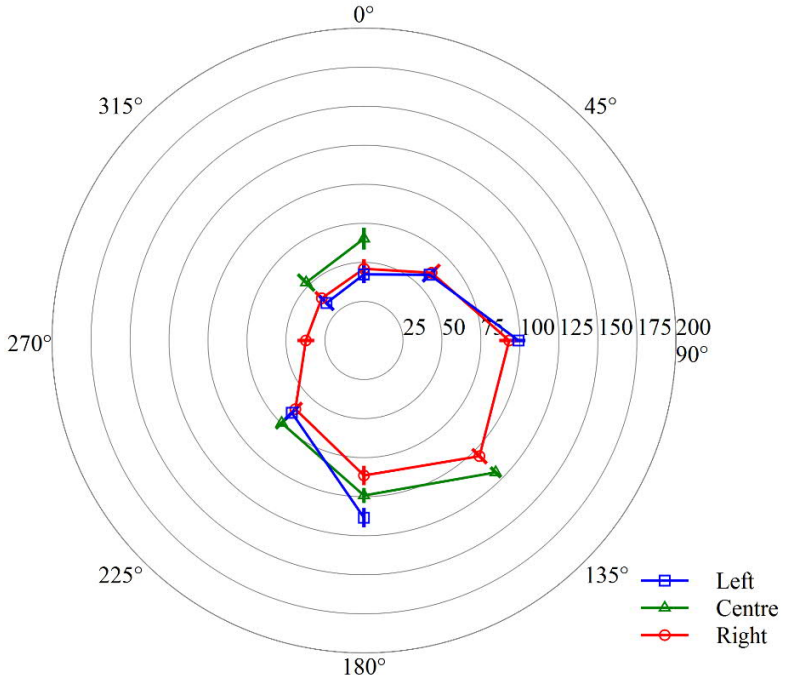

Figure A-28: Time-averaged total heat flux (kW/m^2) to calorimeter, Test 3.6 (4-6 min)

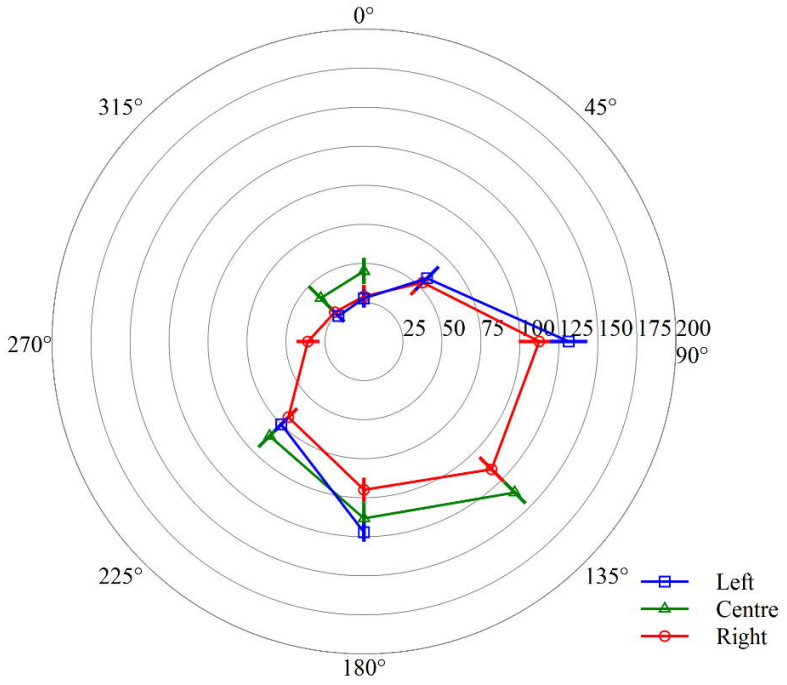

Figure A-29: Time-averaged total heat flux (kW/m^2) to calorimeter, Test 3.6 (14.6-20 min)

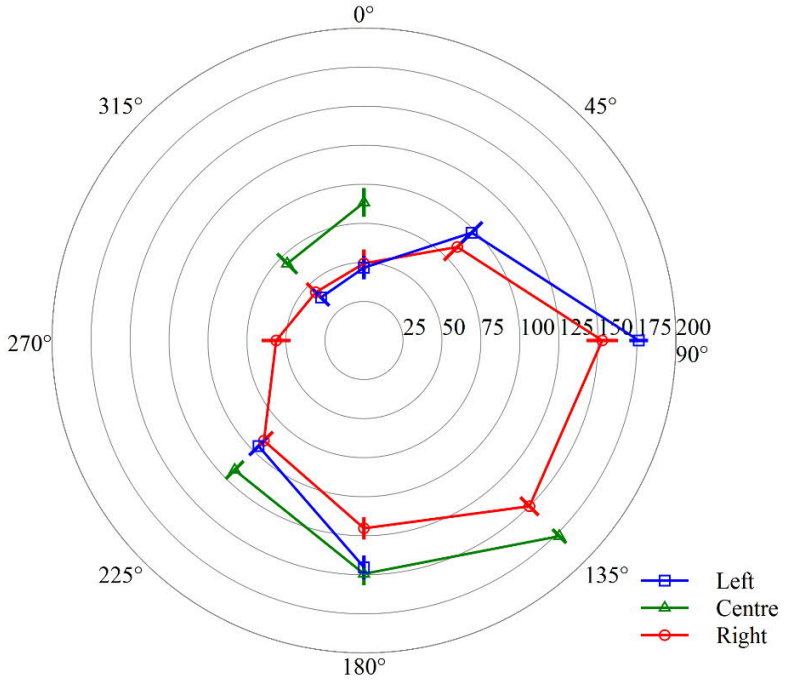

Figure A-30: Time-averaged total heat flux (kW/m^2) to calorimeter, Test 3.6 (25-29.6 min)

A.3.2 Exterior Temperatures

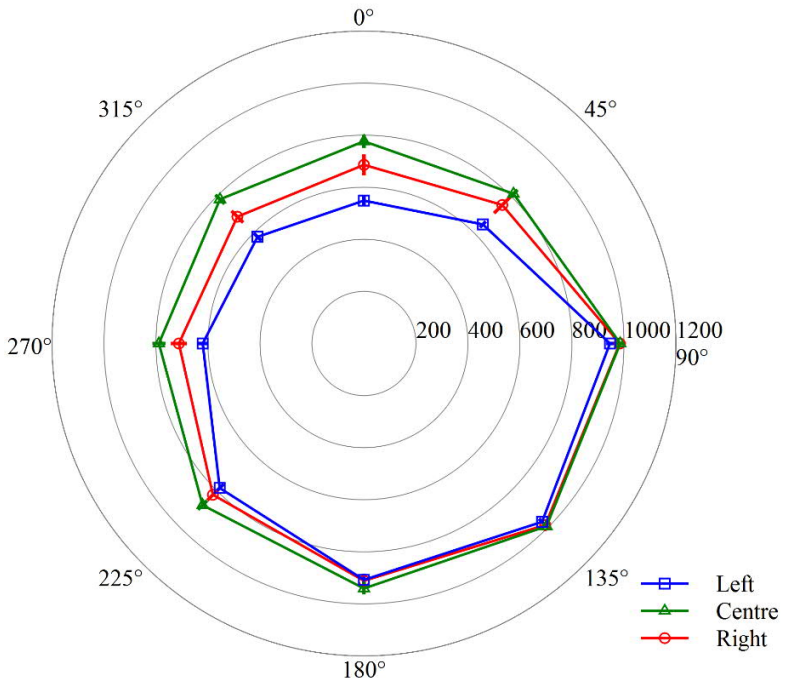

Figure A-31: Time-averaged temperatures (°C) exterior to calorimeter, Test 3.1 (3-5 min)

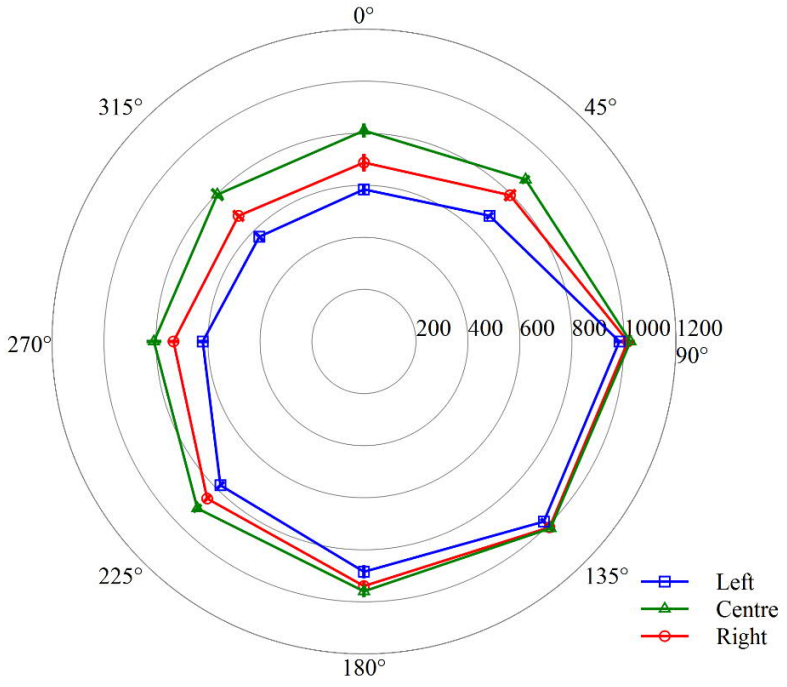

Figure A-32: Time-averaged temperatures (°C) exterior to calorimeter, Test 3.1 (8-11 min)

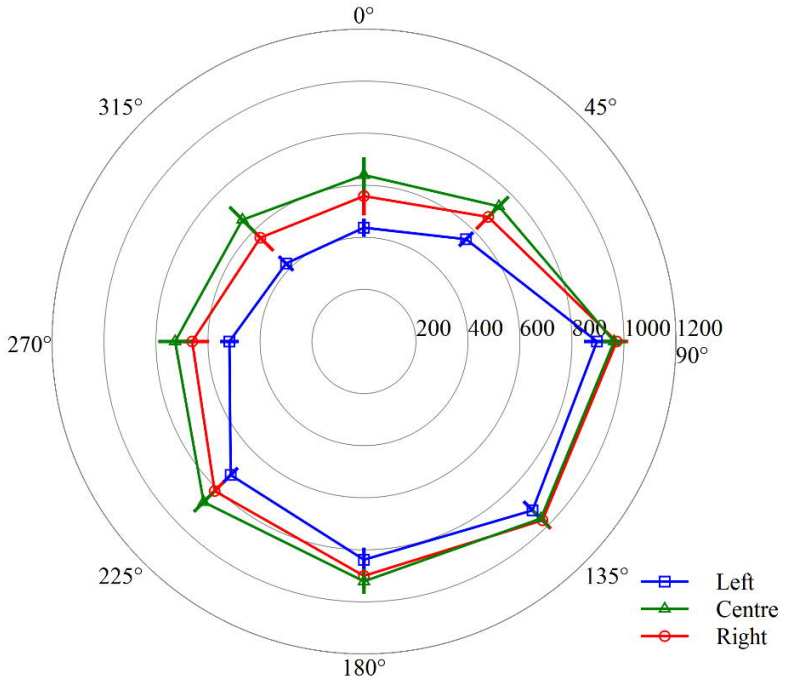

Figure A-33: Time-averaged temperatures (°C) exterior to calorimeter, Test 3.1 (16.5-18 min)

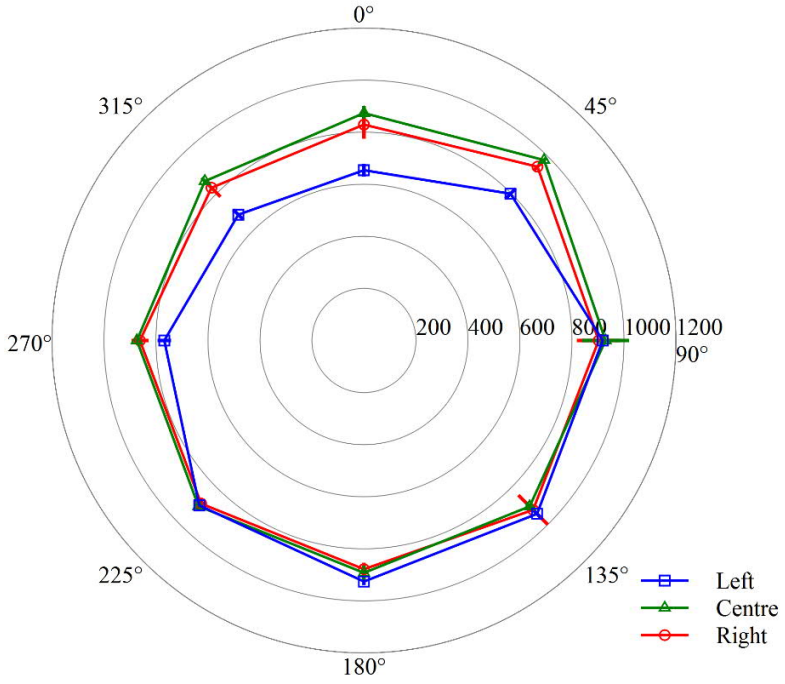

Figure A-34: Time-averaged temperatures (°C) exterior to calorimeter, Test 3.2 (11.9-12.7 min)

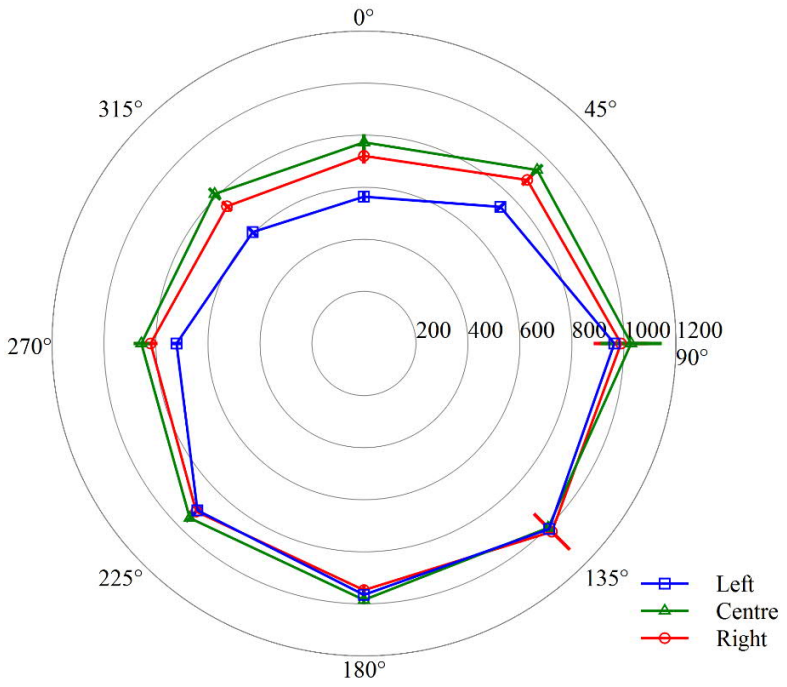

Figure A-35: Time-averaged temperatures (°C) exterior to calorimeter, Test 3.2 (15-17 min)

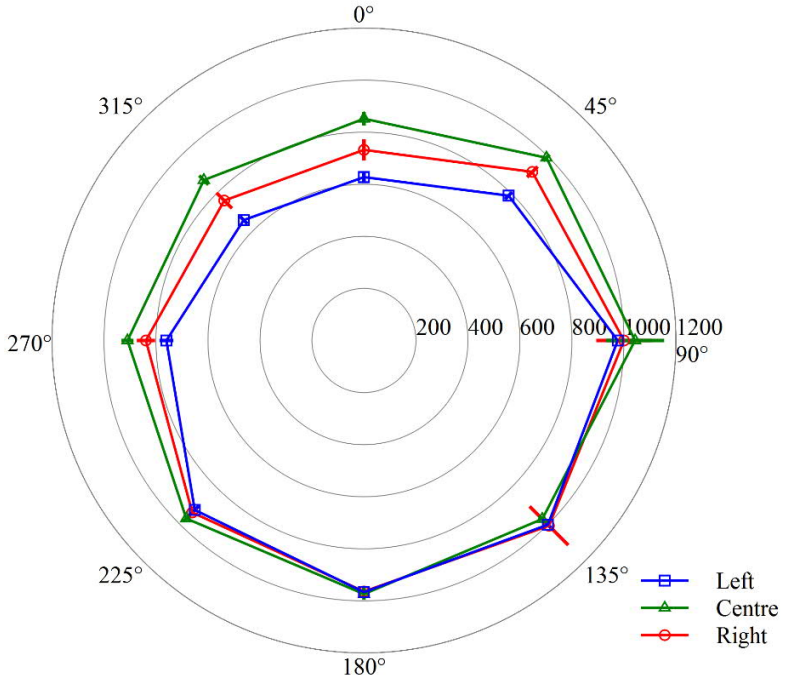

Figure A-36: Time-averaged temperatures (°C) exterior to calorimeter, Test 3.2 (18.6-23.5 min)

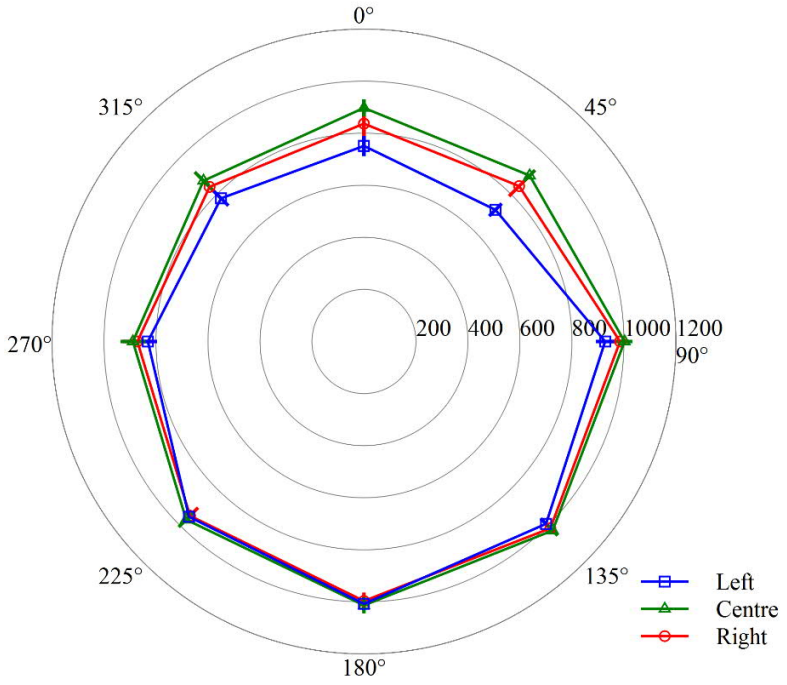

Figure A-37: Time-averaged temperatures (°C) exterior to calorimeter, Test 3.5 (3-10 min)

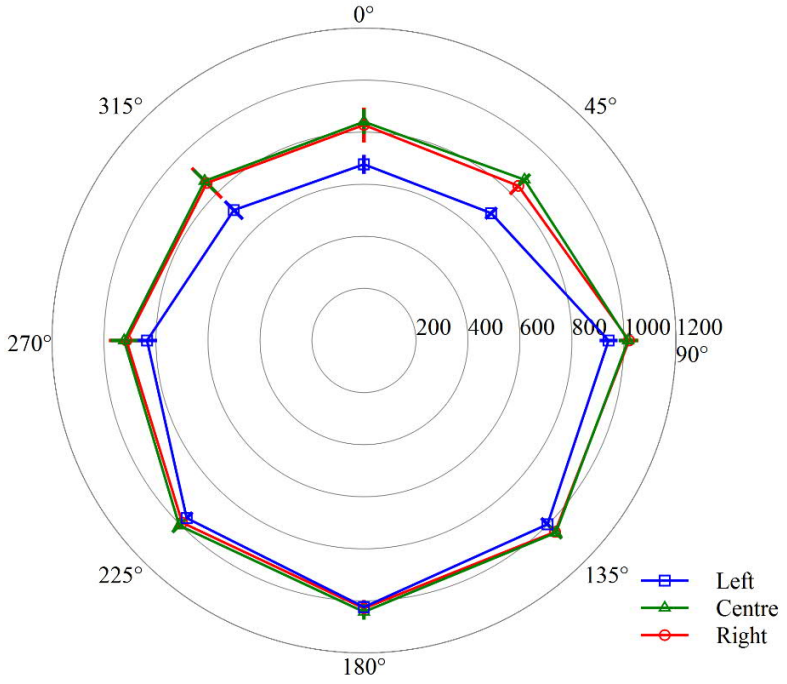

Figure A-38: Time-averaged temperatures (°C) exterior to calorimeter, Test 3.5 (16-19.5 min)

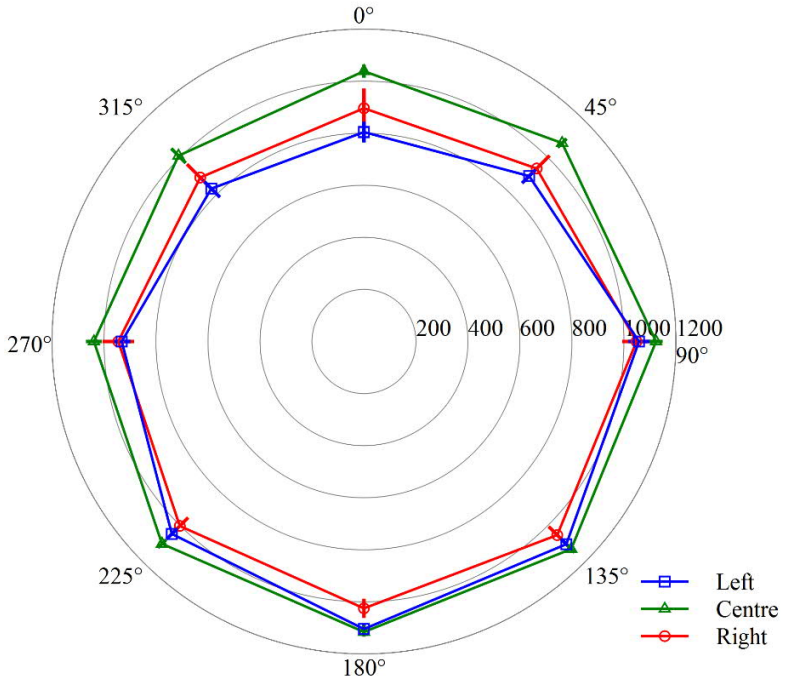

Figure A-39: Time-averaged temperatures (°C) exterior to calorimeter, Test 3.5 (27.5-30.5 min)

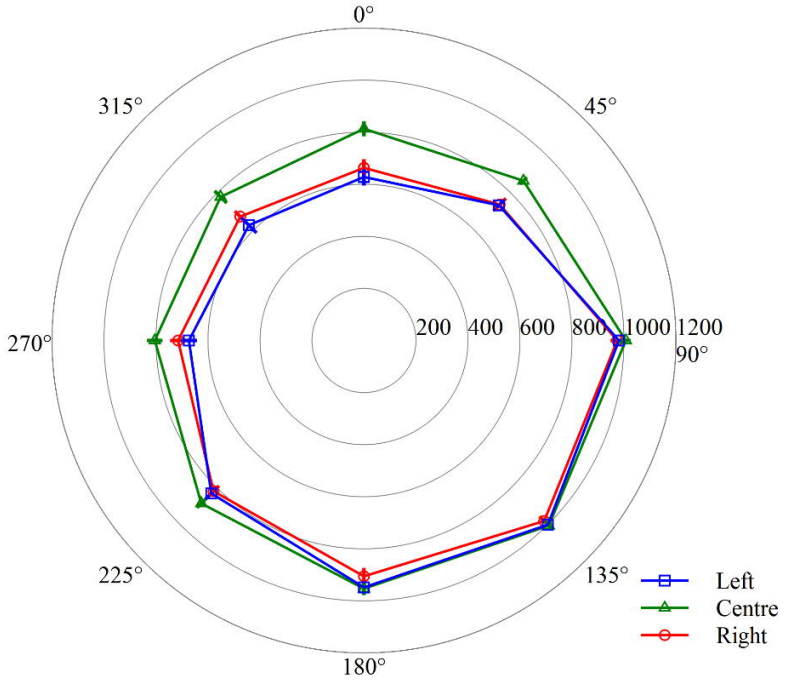

Figure A-40: Time-averaged temperatures (°C) exterior to calorimeter, Test 3.6 (4-6 min)

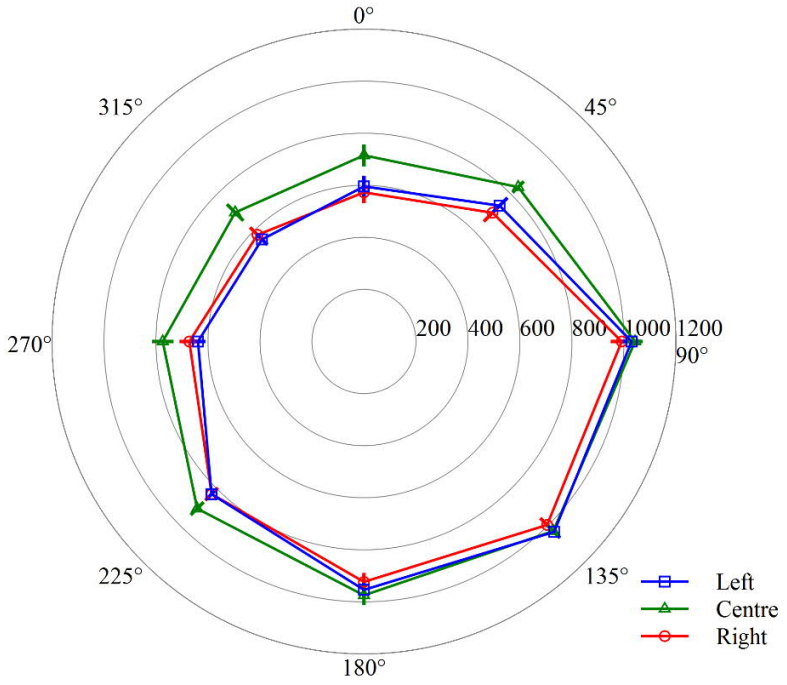

Figure A-41: Time-averaged temperatures (°C) exterior to calorimeter, Test 3.6 (14.6-20 min)

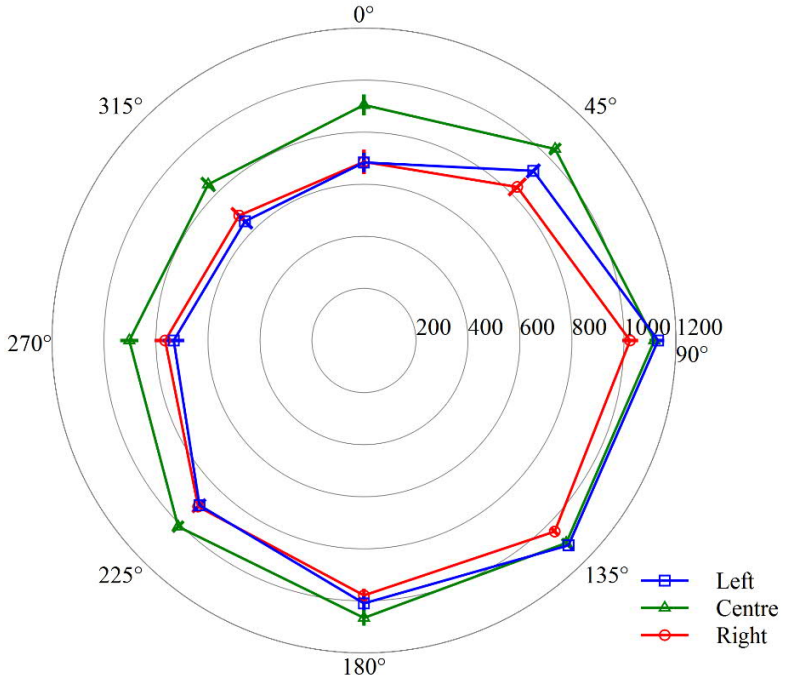

Figure A-42: Time-averaged temperatures (°C) exterior to calorimeter, Test 3.6 (25-29.6 min)

A.3.3 Outer Cylinder Temperatures

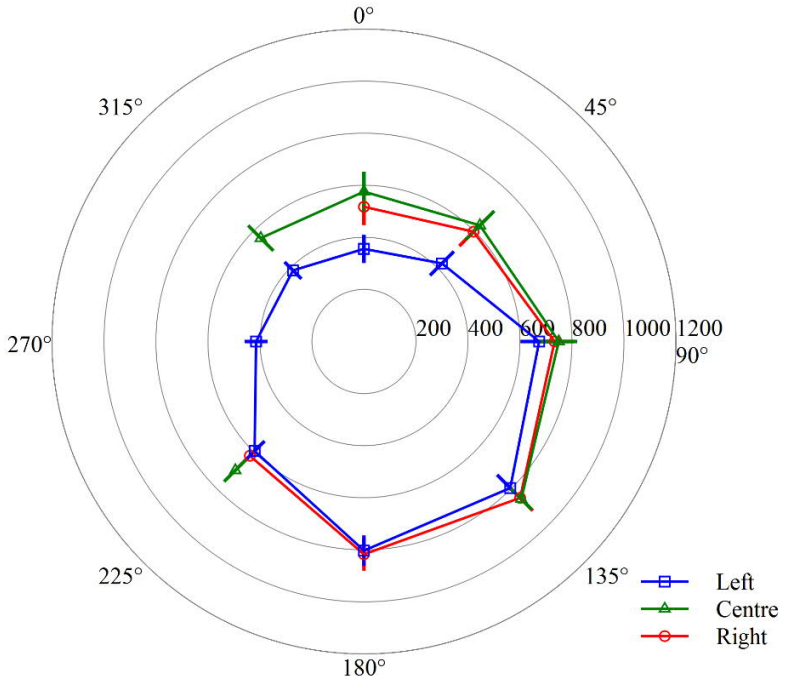

Figure A-43: Time-averaged temperatures (°C) on outer cylinder of calorimeter, Test 3.1 (3-5 min)

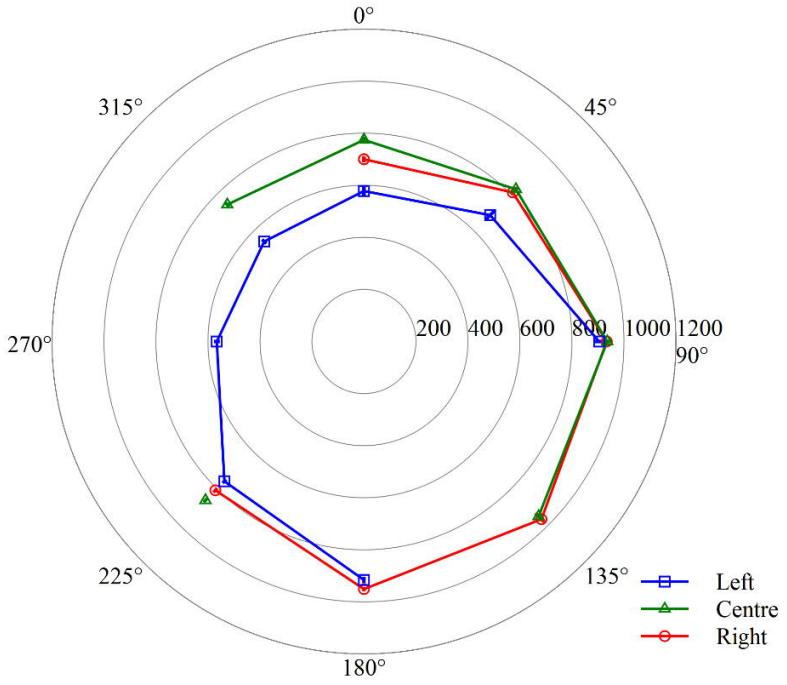

Figure A-44: Time-averaged temperatures (°C) on outer cylinder of calorimeter, Test 3.1 (8-11 min)

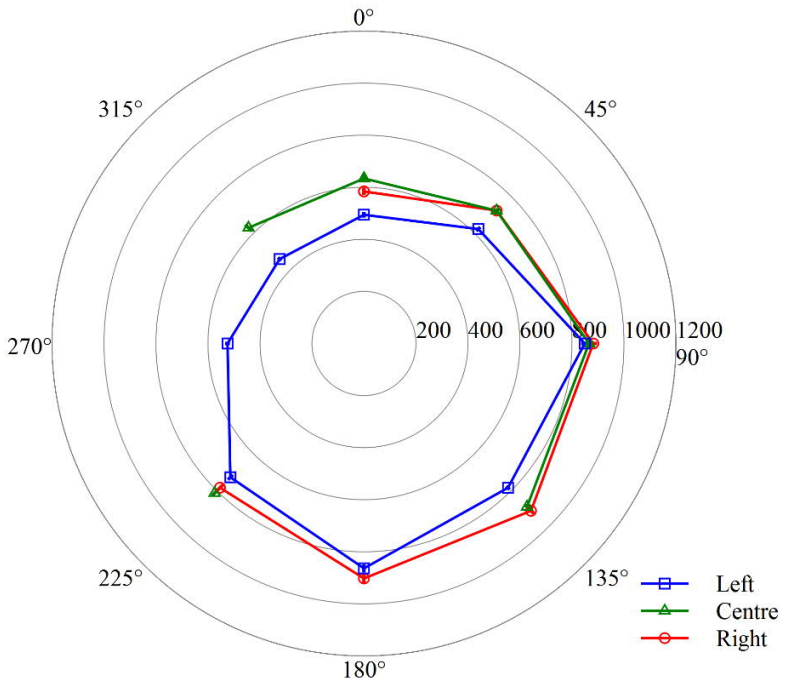

Figure A-45: Time-averaged temperatures (°C) on outer cylinder of calorimeter, Test 3.1 (16.5-18 min)

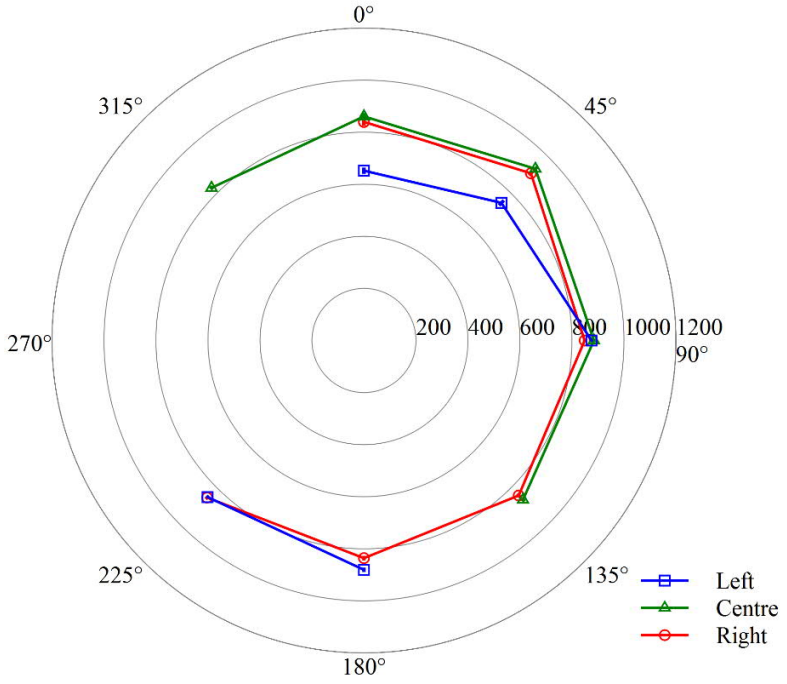

Figure A-46: Time-averaged temperatures (°C) on outer cylinder of calorimeter, Test 3.2 (11.9-12.7 min)

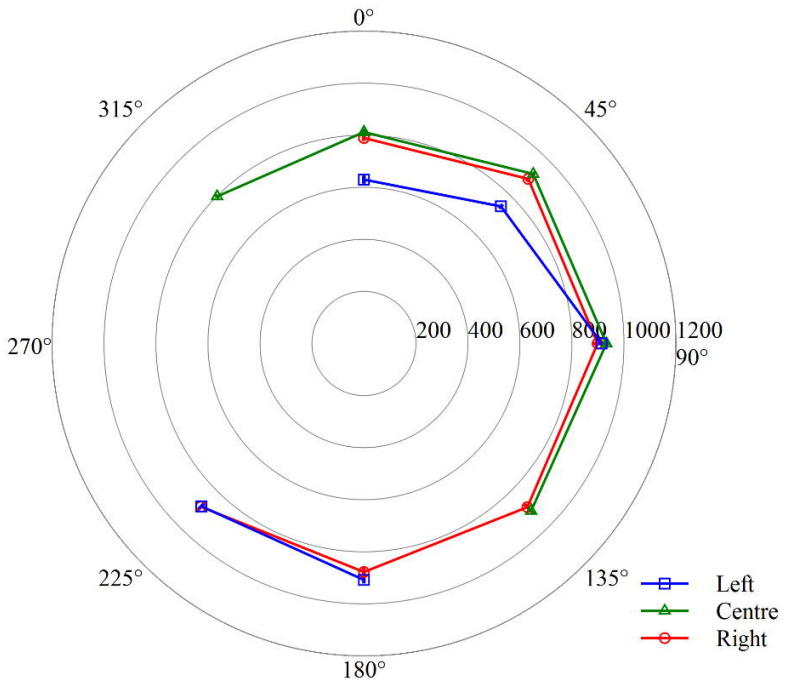

Figure A-47: Time-averaged temperatures (°C) on outer cylinder of calorimeter, Test 3.2 (15-17 min)

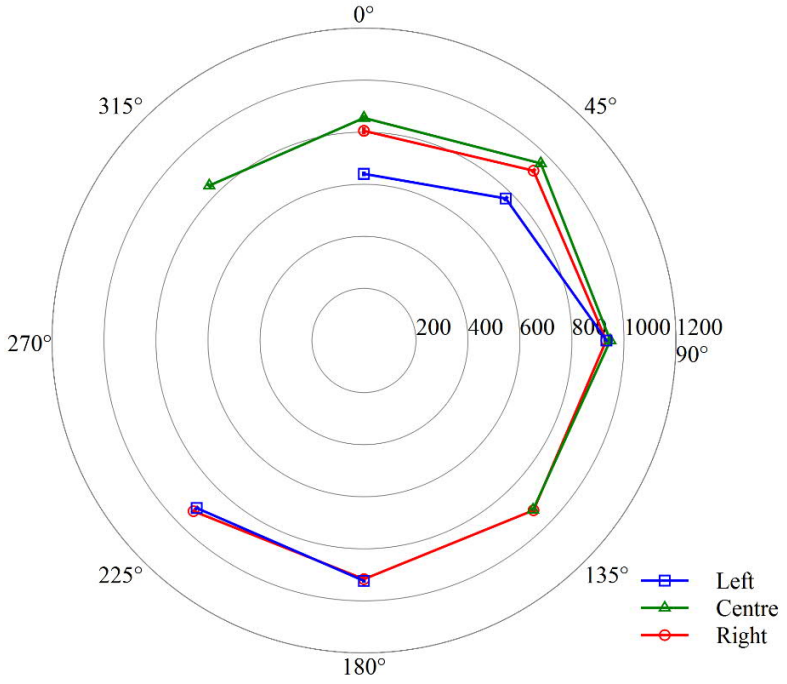

Figure A-48: Time-averaged temperatures (°C) on outer cylinder of calorimeter, Test 3.2 (18.6-23.5 min)

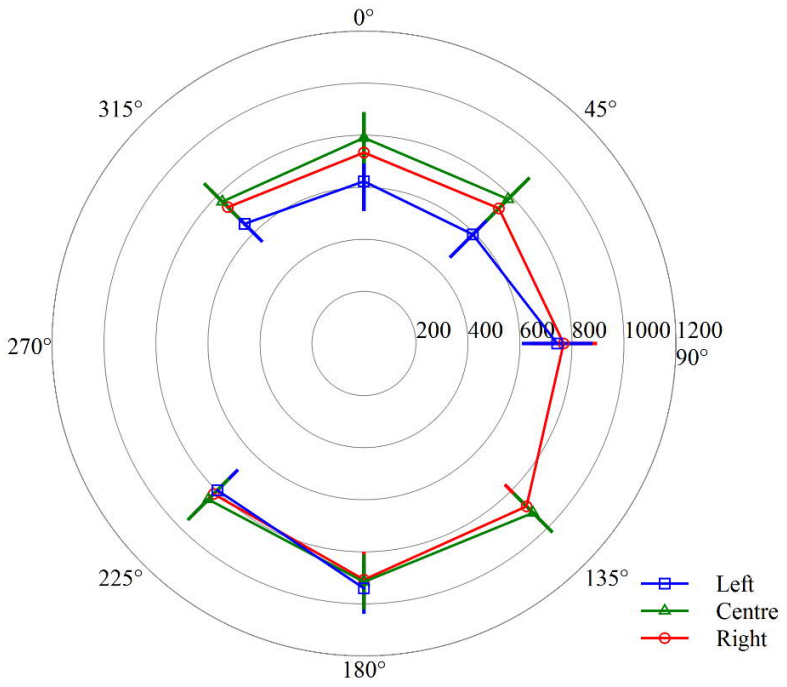

Figure A-49: Time-averaged temperatures (°C) on outer cylinder of calorimeter, Test 3.5 (3-10 min)

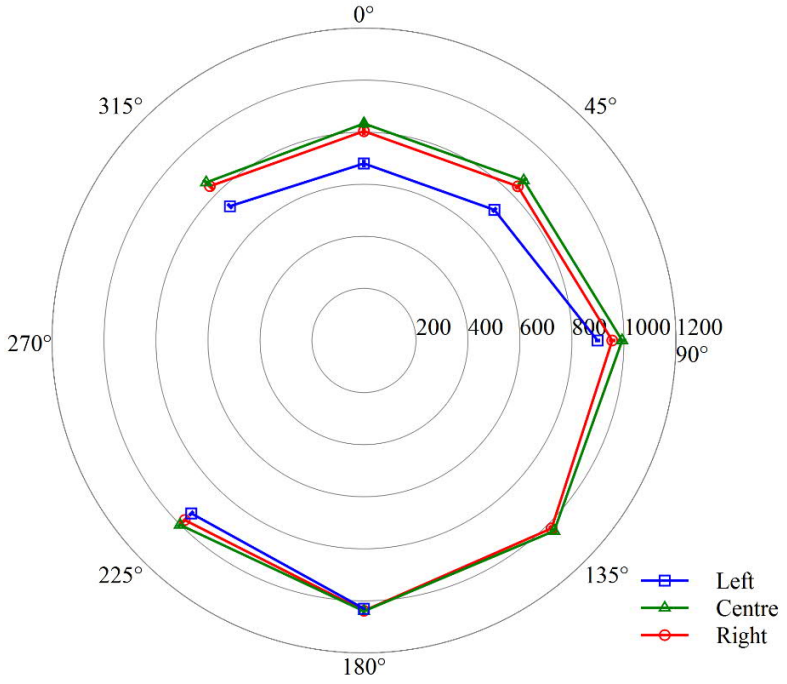

Figure A-50: Time-averaged temperatures (°C) on outer cylinder of calorimeter, Test 3.5 (16-19.5 min)

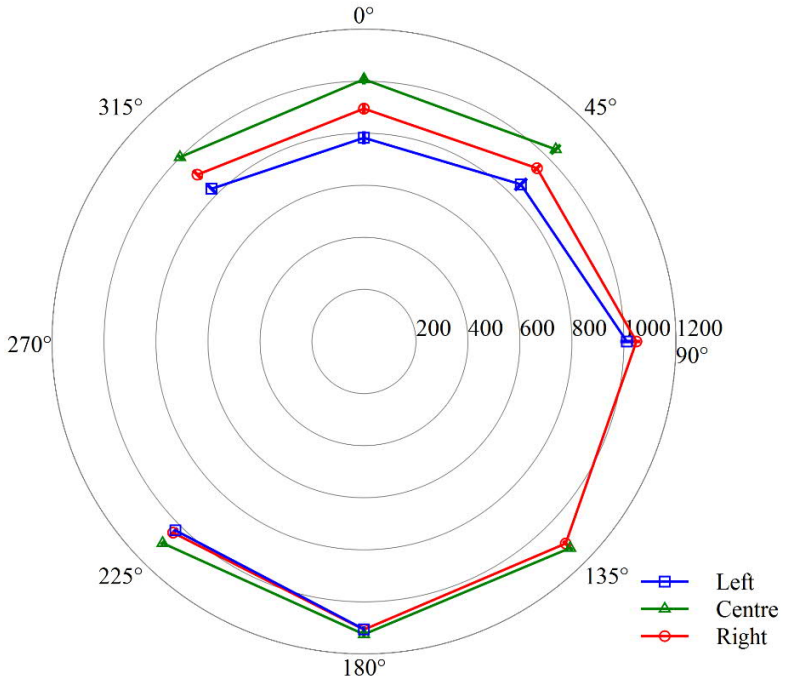

Figure A-51: Time-averaged temperatures (°C) on outer cylinder of calorimeter, Test 3.5 (27.5-30.5 min)

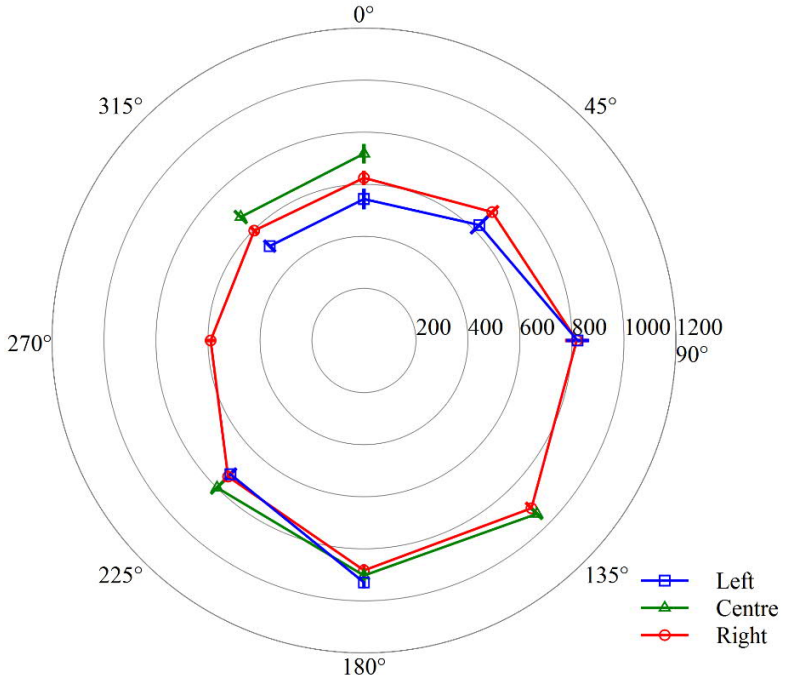

Figure A-52: Time-averaged temperatures (°C) on outer cylinder of calorimeter, Test 3.6 (4-6 min)

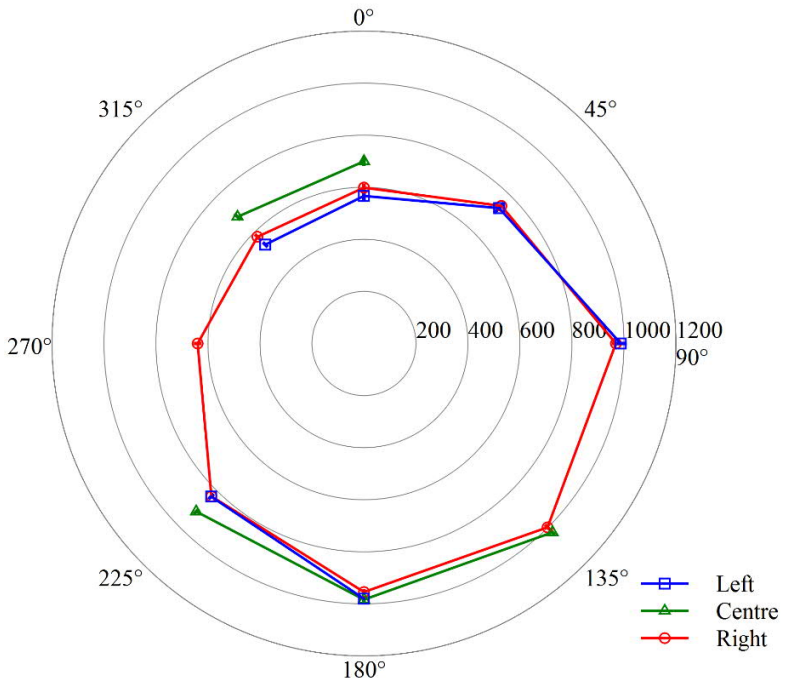

Figure A-53: Time-averaged temperatures (°C) on outer cylinder of calorimeter, Test 3.6 (14.6-20 min)

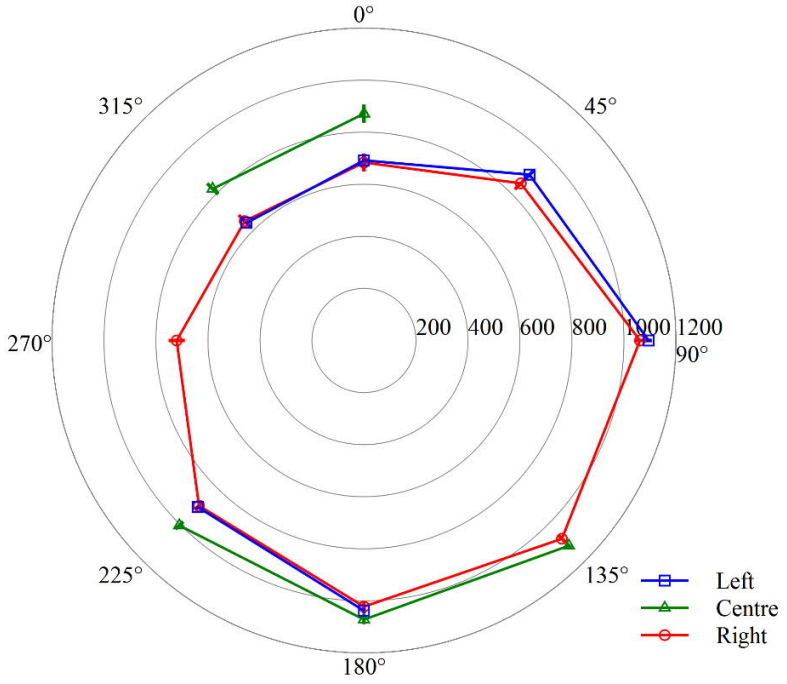

Figure A-54: Time-averaged temperatures (°C) on outer cylinder of calorimeter, Test 3.6 (25-29.6 min)

Appendix B - Comparison of Pool Fire Tests Conducted at Sandia

Appendix B_final.pdf

Sandia National Laboratories

Operated for the United States Department of Energy by National Technology and Engineering Solutions of Sandia, LLC.

Albuquerque, New Mexico 87185-0101
Livermore, California 94551-0969

date: October 28, 2020

to: Cecilia Lam, NRCC

from: Anay Luketa

subject: Comparison of pool fire tests

This memo includes comparison of data from three separate test series pertaining to pool fires. The following provides comparison of: the same crude oil as function of scale, three different crude oils at the same scale, and two crude oils to several different hydrocarbons at the same scale. Statements are provided where possible for interpretation of results, though several comparisons elicit additional research outside the work scope of these test series and is noted where pertinent.

1. Comparison of Bakken Crude oil tests as a function of scale

The following compares data on Bakken crude oil pool fires from two different studies, one sponsored by National Research Council of Canada (NRCC) and the other by the US Department of Energy (DOE), Department of Transportation (DOT), and Transport Canada (TC). The data used for the comparison in this document can be found from comprehensive reports on the two separate test series[1,2].

Pool fire experiments burning Bakken crude oil were conducted at diameters of 2 m for NRCC and 5 m for DOE/DOT/TC, allowing comparison of results at two different scales of average burn rate, flame height, heat flux to an engulfed calorimeter, and surface emissive power (SEP). Six 2-m diameter pool fire tests were performed indoors under quiescent conditions at Sandia's Thermal Test Complex (TTC) and one 5-m diameter pool fire test was performed outdoors. For the 5-m test the average wind speed, wind direction, temperature, and humidity were 3.6 m/s (8.1 mph), 204 degrees, 13.3°C, and 20%, respectively.

[1]Luketa, A., et al., "Pool Fire and Fireball Experiments in Support of the US DOE/DOT/TC Crude Oil Characterization Research Study," Sandia National Laboratories, Albuquerque, NM, SAND2019-9189, 2019.
[2] Luketa, A., et al., "Experimental Results of 2-m Heptane, Bakken Crude Oil, and Dilbit Crude Oil Pool Fire Tests Performed for the National Research Council of Canada," Sandia National Laboratories, Albuquerque, NM, SAND2020-XXXX, 2020 (to be published).

Sandia National Laboratories is a multimission laboratory managed and operated by National Technology & Engineering Solutions of Sandia, LLC, a wholly owned subsidiary of Honeywell International Inc., for the U.S. Department of Energy's National Nuclear Security Administration under contract DE-NA0003525.

Since atmospheric conditions affect the burn rate, flame height, and heat flux to the calorimeter the effect of scale on these parameters cannot be directly assessed. The direct effect of scale can be assessed for the average surface emissive power since it is not significantly affected by the wind for the range of speeds under consideration. Also, since the SEP was measured in the crosswind direction it is not biased by locally high SEP values on the downwind side of the fire that can be created from the enhanced mixing of wind-driven counter rotating vortices.

Beyond atmospheric conditions, another notable difference between the test series regards the calorimeters which were significantly different in construction and in relative size to the pool. The calorimeter for the 2-m tests was considerably more massive (~factor of 4 to 5) than the one used for the 5-m test since it was constructed with two concentric cylinders, whereas the calorimeter for the 5-m test was a single cylinder. And, the calorimeter for the 2-m tests was approximately 1.8 m in length and 0.33 m in diameter, whereas the calorimeter for the 5-m test was approximately 1 m in length and 0.27 m in diameter. Thus, the ratio of calorimeter length to pool diameter for the 2-m and 5-m tests was 1 and 0.2, respectively. The calorimeters for both test series were placed at 1 m above the pool which is a height to diameter ratio of 0.5 and 0.2 for the 2-m and 5-m tests, respectively. Thus, there isn't similarity with regards to flow patterns, heat sinks, and placement within the structure of the flame relative to the size of the pool. Also, the calorimeter for the 2-m tests had significantly more thermocouples than the calorimeter for the 5-m test to assess heat flux, namely, 48 versus 12 thermocouples.

Table 1-1 provides a comparison of time-averaged results between the two tests series. The time-averaged values for the four tests with the calorimeter placed 1 m above the pool were averaged to provide the values for the 2-m tests in Table 1-1. The following sections presents the time-averaged values for each 2-m test and discussion of the comparison between the test series.

Table 1-1: Summary of results for pool fire experiments

Oil	Average Burn rate (mm/min)	Average Flame Height (m)	Average Surface Emissive Power (kW/m^2)	Average total heat flux to calorimeter (kW/m^2)
2-m*	2.1 ± 0.05	4.4 ± 1.0	76.9 ± 10.4	102.9 ± 7.2
5-m	4.6 ± 0.1	4.5 ± 3.9	77.4 ± 12.7	70.5 ± 25.8

*averaged among all tests with calorimeter at height of 1 m

1.1 Burn rate

Table 1-2 provides time-averaged burn rates for both test series. The time-averaged burn rate for the 5-m test is about a factor of 2.2 higher than the 2-m tests. All six 2-m tests had similar time-averaged burns rates regardless of the presence of the calorimeter or its placement. In addition to differences in scale, the 5-m test was conducted outdoors under an average wind speed of 3.6 m/s. Previous pool fires tests conducted at Sandia using JP8 have indicated that wind can have a direct relationship to the burn rate, causing approximately a 60% increase in the burn rate (mm/min) for a 1 m/s increase in wind speed[3]. Thus, the difference in burn rate can be attributed

[3] J. M. Suo-Anttila and L. A. Gritzo, "Thermal Measurements from a Series of Tests with a Large Cylindrical Calorimeter on the Leeward Edge of a JP-8 Pool Fire in Cross-Flow," Sandia National Laboratories, Albuquerque, NM, SAND2001-1986, 2001.

to both scale and wind conditions. Given the limited number of outdoor tests, firm conclusions cannot be drawn as to the principal contributing factor for differences in burn rate.

Table 1-2: Average burn rate for both test series

Test	Calorimeter (height)*	Fuel supply temperature (C)	burn rate	
			mm/min (+/-)	kg/m^{2}s
	2-m pool fire			
2.1	No	21.0 ± 0.9	2.23 (+0.03/-0.02)	0.030
2.2	Yes (0.5-m)	21.7 ± 0.5	1.89 (+0.03/-0.03)	0.026
2.3	Yes (1-m)	22.2 ± 0.5	2.01 (+0.1/-0.1)	0.027
2.4	Yes (1-m)	58.2 ± 1.0	2.12 (+0.03/-0.03)	0.029
2.5	Yes (1-m)	21.3 ± 0.6	1.90 (+0.03/-0.03)	0.026
2.6	No	20.0 ± 1.7	2.21 (+0.1/-0.09)	0.030
	5-m pool fire			
	Yes (1-m)	22.0 ± 2.7	4.6 ± 0.1	0.062

*distance from fuel surface to calorimeter centerline

1.2 Flame height

Table 1-3 provides time-averaged flame heights for both tests series and indicates that both are similar, however the ratio of height to diameter (H/D) for the 2-m and 5-m tests are 2.3 and 0.9, respectively. Part of this difference in H/D can be attributed to the effect of wind. Empirically derived correlations indicate that H/D tends to decrease with increasing wind speed. The H/D ratio also decreases for increasing pool diameters due to smoke obscuration which is the principal cause of the difference. Visible comparison of the 2-m and 5-m tests indicated that the 5-m test produced significantly more smoke which shrouded the luminous portion of the flame. Thus, the reduction of the H/D ratio for increasing pool diameters is anticipated based on the behavior of pool fires as a function of scale.

Table 1-3: Average flame height for both test series

Test	Average flame height (m)
2-m pool fire	
2.1	4.5 ± 1.1
2.2	4.3 ± 1.0
2.3	4.3 ± 1.1
2.4	4.5 ± 1.0
2.5	4.5 ± 0.9
2.6	4.5 ± 1.0
5-m pool fire	
	4.5 ± 3.9

1.3 Surface emissive power

Table 1-4 provides average plume temperatures and surface emissive powers for both the 2-m and 5-m pool fires from infrared (IR) camera measurements. The comparison indicates that the average plume temperature for the 2-m tests is approximately 50-100 K higher than the 5-m test with the range of standard deviations overlapping. The average surface emissive power values are similar among the 2-m and 5-m tests. This would indicate that the 2-m diameter fire has reached the optically thick limit as anticipated by most hydrocarbon fires of this size. The maximum surface emissive power is higher for the 5-m test by about 30 kW/m^2, though the range of standard deviations overlap.

Table 1-4: Average plume temperatures and surface emissive power for Bakken crude oil tests

Test	Temperature (K)		Surface Emissive Power (kW/m^2)	
	Mean	Max.	Mean	Max.
	2-m pool fire			
2.1	904.3 ± 151.3	1265.5 ± 27.7	75.2 ± 11.7	200.8 ± 16.4
2.2	922.9 ± 158.0	1261.9 ± 31.6	74.9 ± 10.4	200.3 ± 18.4
2.3	929.8 ± 165.6	1272.2 ± 28.8	76.5 ± 10.3	203.0 ± 17.1
2.4	944.2 ± 172.6	1279.5 ± 25.1	78.7 ± 10.4	207.2 ± 15.1
2.5	942.6 ± 171.6	1279.7 ± 28.1	77.3 ± 10.3	206.1 ± 16.8
2.6	901.3 ± 147.4	1258.0 ± 29.3	73.6 ± 11.3	195.9 ± 17.0
	5-m pool fire			
	851.5 ± 116	1221.8 ± 54.9	77.4 ± 12.7	236.4 ± 38.4

1.4 Heat flux to engulfed calorimeter

Table 1-5 provides the absorbed and total heat flux to the calorimeters used for both test series. Notable is the much higher absorbed heat flux for the 5-m test than that of the 2-m tests which is reflective of the much lower thermal mass of the calorimeter for the 5-m test. Also, it was observed that the effect of wind during the 5-m test caused the calorimeter to be non-engulfed at times which results in some cooling. The much greater standard deviation of the heat flux values for the 5-m test than the 2-m tests is reflective of this.

Test 2.2, where the calorimeter was place 0.5 m above the pool, has an average total heat flux similar to the 5-m test. The ratio of placement height to pool diameter is also the most similar compared to the other 2-m tests. Despite the differences between the construction, relative placement, mass, mapping, and outdoor conditions, the range of standard deviations overlap. Further outdoor testing that approach quiescent conditions with a calorimeter that has similarity to the 2-m tests is required to provide an equitable comparison.

Table 1-5: Calorimeter average heat flux values for both test series

Test	Heat flux (kW/m^2)	
	Absorbed	Total
	2-m pool fire	
2.2	-3.4 ± 3.9	74.4 ± 4.0
2.3	-4.2 ± 9.7	94.1 ± 10.6
2.4	-4.9 ± 5.2	109.5 ± 5.8
2.5	-5.2 ± 4.8	104.9 ± 5.3
	5-m pool fire	
	-26.4 ± 33.9	70.5 ± 25.8

2 Comparison of 2-m diameter pool fires

In the following, the NRCC test series involving 2-m diameter pool fires are compared to a 2-m diameter pool fire burning Strategic Petroleum Reserve (SPR) crude oil in the SNL Thermal Test Complex funded by the DOE/DOT/TC study (see footnote 1). The fuels tested for NRCC 2-m pool fire experiments included heptane, Bakken, and dilbit crude oil. Comparison of the fuels tested in the NRCC experiments is provided in the accompanying test report (see footnote 2).

The measurements that are compared include averages of burn rate, flame height, spot SEP from narrow-view radiometers, heat flux to an engulfed calorimeter, and heat flux from directional flame thermometers (DFT). Table 2-1 provides a comparison of time-average values for these measurements for the different fuels. The values provided for the heptane, Bakken, and dilbit tests are averages among tests within a series of time-averaged values. The caveat of the comparison is that the dilbit crude oil did not display steady-state behavior, whereas the heptane and Bakken crude oil did. Due to the variable behavior of the dilbit, the average was determined by discrete integration over equivalent time periods for each dilbit test. Thus, initial transients may be included in the average which can result in higher averages and standard deviations.

Table 2-1: Comparison of average values for 2-m diameter pool fire tests

Fuel	Average Burn rate (mm/min)	Average Flame Height (m)	Average Spot Surface Emissive Power* (kW/m^2)	Average total heat flux to calorimeter (kW/m^2)	Average incident heat flux to DFT** (2-m/4-m) (kW/m^2)
heptane	3.4 ± 0.04	6.1 ± 0.9	75.8 ± 15.2	58.5 ± 3.6	39.1 ± 1.2/17.0 ± 0.5
Bakken	2.1 ± 0.05	4.4 ± 1.0	61.0 ± 18.3	102.9 ± 7.2	42.7 ± 1.6/15.9 ± 0.8
dilbit	1.4 (-0.5/+0.4)	3.5 ± 0.8	40.7 ± 16.7	71.9 ± 18.8	34.9 ± 6.4/9.1 ± 1.7
SPR	1.95 ± 0.02	2.9 ± 1.6	48.1 ±13.7	103.2 ± 5.9	36.8 ± 1.8/13.8 ± 0.6

*measurements from narrow-angle radiometers

**2-m and 4-m in parentheses are distances from center of pool

2.1 Burn rate

Table 2-2 provides the average burn rate for each 2-m diameter pool fire test. Heptane has the highest average burn rate, followed by Bakken and SPR crude oil which are similar, then the dilbit crude oil. The dilbit crude oil did not have a steady burn rate, rather it tended to be higher in the first 10 minutes of the test compared to the rest of the burn time. Evidence based on sampling and analysis indicates the variable burn rate is due to different phases of burning due to its composition, that is, a mixture of condensate and bitumen. Note that the burn rate in outdoor condition is affected by wind, pool size and configuration, and material and topography of the terrain. The burn rates among the fuels considered here is anticipated to be very different when subject to variations of these factors for larger outdoor pool fires.

Table 2-2: Average burn rate for each 2-m diameter pool fire test

Test	Calorimeter (height)*	Fuel supply temperature (C)	burn rate	
			mm/min (+/-)	kg/m^{2}s
Heptane (NRCC)				
1.1	Yes (1 m)	22.3 ± 0.2	3.21 ± 0.04	0.037
1.2	No	24.2 ± 0.3	3.51 ± 0.04	0.040
1.3	Yes (1 m)	57.7 ± 0.4	3.49 ± 0.04	0.040
Bakken crude oil (NRCC)				
2.1	No	21.0 ± 0.9	2.23 (+0.03/-0.02)	0.030
2.2	Yes (0.5-m)	21.7 ± 0.5	1.89 ± 0.03	0.026
2.3	Yes (1-m)	22.2 ± 0.5	2.01 ± 0.1	0.027
2.4	Yes (1-m)	58.2 ± 1.0	2.12 ± 0.03	0.029
2.5	Yes (1-m)	21.3 ± 0.6	1.90 ± 0.03	0.026
2.6	No	20.0 ± 1.7	2.21 (+0.1/-0.09)	0.030
dilbit crude oil (NRCC)				
3.1	Yes (1 m)	21.7 ± 0.5	3.21 (+0.03/-0.03)	0.049
			2.18 (+0.03/-0.03)	0.034
3.2	Yes (0.5 m)	22.1 ± 1.2	3.89 (+0.03/-0.03)	0.060
			1.47 (+0.03/-0.03)	0.023
3.3	No	17.6 ± 0.1	1.11 (+0.03/-0.03)	0.017
			0.94 (+0.03/-0.03)	0.014
3.4	No	22.1 ± 1.5	1.16 (+0.03/-0.03)	0.018
3.5	Yes (1 m)	24.9 ± 0.4	1.00 – 1.27 (+0.04/-0.03)	0.015 -0.019
3.6	Yes (1 m)	57.3 ± 2.1	1.20 (+0.03/-0.04)	0.018
			0.32 – 0.62 (+0.03/-0.04)	0.005-0.010
SPR (DOE/DOT/TC)				
	Yes (1 m)	59.5 ±4.5	1.95 ±0.02	0.028

2.2 Flame height

Table 2-3 provides the average flame height for all the tests. Heptane had the highest average flame height, followed by the Bakken crude oil, dilbit crude oil, and then SPR. Note that for pool fires of increasing diameter the smoke production will increase causing the effective flame heights to be similar due to obscuration. Thus, it is anticipated that the fuels would have similar flame heights at accident scale releases under equivalent environmental conditions.

Table 2-3: Average flame height for each 2-m diameter pool fire test

Test	Average flame height (m)
heptane	
1.1	5.6 ± 0.9
1.2	6.8 ± 0.9
1.3	5.8 ± 0.8
Bakken crude oil	
2.1	4.5 ± 1.1
2.2	4.3 ± 1.0
2.3	4.3 ± 1.1
2.4	4.5 ± 1.0
2.5	4.5 ± 0.9
2.6	4.5 ± 1.0
dilbit crude oil	
3.1	3.4 ± 0.9
3.2	3.6 ± 0.8
3.3	3.5 ± 0.8
3.4	3.5 ± 0.8
3.5	3.6 ± 0.8
3.6	3.5 ± 0.8
SPR	
	2.9 ±1.6

2.3 Radiometers

Since infrared cameras were not used for the SPR test to assess the average surface emissive power, comparison of narrow-view radiometer measurements is provided. These instruments view a partial region (0.8 m dia.) of the flame and not its entirety. Measurements using wide-view heat flux gauges were also taken and are compared in section 2. 4. Six narrow-view radiometers and five wide-view heat flux gauges were mounted near the test facility's wall at a distance of 28.64 ft. (8.73 m) from the center of the fire. The narrow-view radiometers are at heights of 0.5, 1, 1.5, 2, 3, and 4 m, while the wide-view heat flux gauges are at heights of 1, 1.5, 2, 3, and 4 m. The line of sight for each gauge was set to pass through the centerline of the fire at the height of the gauge. The time-averages for the spot surface emissive power provided in Table 2-1 are averaged not only among the tests within a series but also among the radiometers

at the different heights. Comparison of radiometer measurement at each location per test series is provided in the following.

2.3.1 Narrow view

Table 2-4 provides average heat flux measurements from narrow view radiometers at various heights for each fuel. The tests which had the calorimeter placed 1 m above the pool are highlighted. In comparing the SPR crude oil to other fuels its average values are most similar to the Bakken crude oil at the heights of 0.5 m and 1 m but differ at greater heights above the pool due to differences in flame height.

Table 2-4: Narrow view radiometer measurements at various heights

	height (m)					
	heptane					
	0.5	**1**	**1.5**	**2**	**3**	**4**
1.1	89.1 ± 5.8	93.1 ± 7.7	91.3 ± 13.6	77.4 ± 16.5	47.6 ± 17.3	33.8 ± 17.9
1.2	94.7 ± 12.4	84.8 ± 15.3	84.4 ± 17.0	80.9 ± 17.5	70.4 ± 20.9	61.6 ± 26.5
1.3	88.9 ± 6.5	92.1 ± 7.8	96.4 ± 13.3	85.1 ± 17.7	53.9 ± 19.0	38.8 ± 20.3
	Bakken					
2.1	120.2 ± 10.3	102.5 ± 14.4	88.7 ± 20.2	73.9 ± 24.1	39.6 ± 23.9	22.0 ± 18.2
2.2	99.6 ± 6.8	105.6 ± 13.6	86.5 ± 20.3	66.7 ± 23.5	31.0 ± 19.0	16.9 ± 14.4
2.3	58.4 ± 4.3	74.2 ± 14.3	77.0 ± 24.7	57.6 ± 25.4	24.6 ± 17.7	13.3 ± 14.3
2.4	65.1 ± 4.2	84.1 ± 13.4	89.1 ± 23.0	68.2 ± 24.3	31.3 ± 18.0	16.4 ± 13.2
2.5	65.4 ± 4.0	85.1 ± 11.8	89.9 ± 20.6	68.1 ± 22.0	29.5 ± 15.9	14.8 ± 10.7
2.6	102.1 ± 35.5	79.7 ± 33.5	62.0 ± 32.0	49.5 ± 30.4	24.2 ± 21.1	12.3 ± 14.3
	dilbit					
3.1	70.7 ± 12.9	56.1 ± 18.6	51.6 ± 25.0	36.9 ± 23.4	12.0 ± 12.0	5.5 ± 7.5
3.2	74.2 ± 14.8	72.5 ± 19.3	50.4 ± 20.2	36.0 ± 19.1	11.4 ± 8.3	4.9 ± 4.0
3.3	105.2 ± 21.8	73.4 ± 25.1	48.8 ± 26.6	35.1 ± 25.4	11.7 ± 12.3	4.6 ± 5.4
3.4	102.6 ± 22.6	74.3 ± 26.4	51.3 ± 27.9	37.2 ± 26.0	12.0 ± 11.8	4.9 ± 5.1
3.5	64.0 ± 14.3	59.6 ± 20.1	48.9 ± 24.4	33.0 ± 20.7	10.6 ± 8.7	4.6 ± 3.8
3.6	53.7 ± 8.2	53.0 ± 17.3	47.2 ± 24.9	33.2 ± 22.4	10.8 ± 10.3	4.8 ± 5.5
	SPR					
	54.7 ± 7.2	73.1 ± 7.4	43.0 ± 17.1	47.0 ± 19.9	22.6 ± 17.1	7.3 ± 7.4

2.3.2 Wide view

Table 2-5 provides average heat flux measurements from wide view radiometers at various heights for each fuel. The heptane has the highest and the SPR the lowest heat flux values. As found from the narrow-view radiometer measurements, the SPR crude oil is most similar to the Bakken crude oil tests.

Table 2-5: Wide view radiometer measurements at various heights

	height (m)				
	heptane				
	1	1.5	2	3	4
1.1	2.3 ± 0.2	2.9 ± 0.2	2.5 ± 0.2	2.5 ± 0.2	2.3 ± 0.2
1.2	2.5 ± 0.3	3.1 ± 0.2	2.7 ± 0.3	2.7 ± 0.3	2.6 ± 0.3
1.3	2.4 ± 0.2	3.0 ± 0.2	2.6 ± 0.2	2.6 ± 0.2	2.4 ± 0.3
	Bakken				
2.1	2.3 ± 0.3	2.8 ± 0.2	2.5 ± 0.3	2.5 ± 0.3	2.2 ± 0.3
2.2	2.0 ± 0.2	2.4 ± 0.2	2.1 ± 0.2	2.1 ± 0.2	1.8 ± 0.2
2.3	1.8 ± 0.4	2.2 ± 0.4	1.9 ± 0.4	1.9 ± 0.4	1.7 ± 0.4
2.4	1.9 ± 0.3	2.4 ± 0.3	2.1 ± 0.3	2.1 ± 0.3	1.9 ± 0.3
2.5	1.9 ± 0.2	2.4 ± 0.2	2.1 ± 0.2	2.1 ± 0.2	1.9 ± 0.2
2.6	1.8 ± 0.7	2.2 ± 0.8	1.9 ± 0.7	2.0 ± 0.7	1.7 ± 0.6
	dilbit				
3.1	1.1 ± 0.4	1.4 ± 0.4	1.2 ± 0.4	1.0 ± 0.4	1.0 ± 0.4
3.2	1.1 ± 0.3	1.4 ± 0.3	1.2 ± 0.3	1.1 ± 0.3	1.1 ± 0.3
3.3	1.4 ± 0.4	1.8 ± 0.4	1.6 ± 0.4	1.4 ± 0.4	1.4 ± 0.4
3.4	1.4 ± 0.4	1.7 ± 0.4	1.5 ± 0.4	1.3 ± 0.4	1.4 ± 0.4
3.5	1.1 ± 0.4	1.5 ± 0.4	1.3 ± 0.4	1.1 ± 0.3	1.1 ± 0.3
3.6	1.1 ± 0.3	1.4 ± 0.4	1.2 ± 0.4	1.1 ± 0.3	1.1 ± 0.3
	SPR				
	2.9 ± 0.3	3.0 ± 0.3	3.1 ± 0.3	3.1 ± 0.3	3.0 ± 0.3

2.3.3 Directional Flame Thermometers

Table 2-6 provides the absorbed and incident thermal radiation calculated from the directional flame thermometer measurements. Instruments were placed at 2 m and 4 m from the center of the fire. The comparison of incident heat flux indicates that the dilbit and SPR crude oils have similar values of approximately 35 kW/m^2 at the 2 m location, whereas the Bakken crude oil has some of the highest average incident heat flux values at the 2-m location reaching in the lower 50 kW/m^2 range. This is most likely due to its greater view factor due to a higher flame height compared to the other oils. It is anticipated that incident heat flux values of the fuels tested would approach similar values as pool size increases due to smoke obscuration.

Table 2-6: Directional Flame Thermometer heat flux

Test	Distance from pool center (m)	Heat flux (kW/m^2)	
	heptane		
		Absorbed	**Incident**
1.1	2	-1.5 ± 1.0	39.4 ± 1.2
	4	-0.9 ± 0.4	18.2 ± 0.5
1.2	2	-1.5 ± 0.8	35.5 ± 1.0
	4	-0.8 ± 0.3	15.1 ± 0.4
1.3	2	-1.8 ± 0.9	44.2 ± 1.1
	4	-0.9 ± 0.4	17.8 ± 0.5
	Bakken		
2.1	2	-2.1 ± 1.3	49.8 ± 1.6
	4	-0.7 ± 0.6	17.0 ± 0.7
2.2	2	-1.5 ± 0.8	35.5 ± 1.0
	4	-0.8 ± 0.3	15.1 ± 0.4
2.3	2	-2.0 ± 1.5	52.5 ± 2.0
	4	-1.1 ± 1.4	18.3 ± 1.7
2.4	2	-2.1 ± 1.4	53.8 ± 1.9
	4	-0.9 ± 0.9	18.8 ± 1.1
2.5	2	-1.8 ± 0.9	44.2 ± 1.1
	4	-0.9 ± 0.4	17.8 ± 0.5
2.6	2	-1.5 ± 1.1	32.4 ± 1.4
	4	-0.7 ± 0.4	8.3 ± 0.3
	dilbit		
3.1	2	-6.6 ± 8.6	35.5 ± 7.1
	4	-2.5 ± 2.2	8.4 ± 1.8
3.2	2	-6.9 ± 6.7	34.2 ± 5.7
	4	-2.4 ± 1.3	8.5 ± 1.5
3.3	2	-7.1 ± 9	35.6 ± 5.3
	4	-2.6 ± 2	9.7 ± 1.5
3.4	2	-7.1 ± 9	35.6 ± 5.3
	4	-2.6 ± 2	9.7 ± 1.5
3.5	2	-6.6 ± 8.2	33.2 ± 7.1
	4	-2.4 ± 1.8	8.8 ± 1.9
3.6	2	-7.1 ± 8.8	35.5 ± 7.7
	4	-2.6 ± 1.9	9.3 ± 2.2
	SPR		
	2	-3.5 ± 3.6	36.8 ± 1.8
	4	-1.9 ± 1.6	13.8 ± 0.6

2.3.4 Calorimeter temperatures and heat flux

Table 2-7 provides average heat flux values for all 2-m diameter pool fire tests. The average total heat flux values are similar among the fuels, with the exception of the Bakken crude oil which reached values up to the 100 kW/m^2 range. However, the dilbit and SPR crude oils showed significantly more variable behavior as indicated by the range of their standard deviations which indicates that some total heat flux values reached up to approximately 100 kW/m^2.

Table 2-7: Calorimeter average heat flux values for 2-m diameter pool fires

Test	Heat flux (kW/m^2)	
	Absorbed	Total
	heptane	
1.1	-3.0 ±2.5	62.5 ±2.7
1.3	-3.1 ±3.7	62.5 ±3.8
	Bakken	
2.2	-3.4 ± 3.9	74.4 ± 4.0
2.3	-4.2 ± 9.7	94.1 ± 10.6
2.4	-4.9 ± 5.2	109.5 ± 5.8
2.5	-5.2 ± 4.8	104.9 ± 5.3
	dilbit	
3.1	-13.2 ±23.6	63.9 ±15.7
3.2	-14.4 ±18.2	67.1 ±13.9
3.5	-15.9 ±24.3	83.1 ±21.3
3.6	-15.4 ±27.7	73.6 ±24.2
	SPR	
	-26.4 ± 33.9	70.5 ± 25.8

3 Comparison to other fuels (2-m diameter SNL tests)

The following compares the NRCC test series to data collected at Sandia's Thermal Test Complex from a series of 2-m diameter pool fires conducted in 2010, referred to as the SNL tests[4]. NRCC tests that did not include the calorimeter and had a constant fuel level are compared to the SNL tests. The fuels used in the SNL tests include methanol, ethanol, heptane, JP8, and blends of

[4] Blanchat, T.K., Suo-Anttila, J., "Hydrocarbon Characterization Experiments in Fully Turbulent Fires – Results and Data Analysis", Sandia National Laboratories report, Albuquerque, N.M., SAND2010-6377, 2011.

methanol/toluene and ethanol/toluene. Some of the tests included the placement of glass beads within the liquid fuel with the intent to suppress convective currents. Tests that did not include glass beads are used for the following comparison. Data obtained from the SNL tests that can be used for comparison include the burn rate, flame height, and radiometer measurements. Note that the SNL test using heptane without glass beads is not included since a period lasting only 2 minutes could be identified in which a semi-steady state occurred for which the data is reported. The test lasted about 25 minutes, but measurements were increasing up until about 15 minutes then started to decrease after this time not allowing for a sufficient steady-state duration. Also, the lip height of the pan used for the SNL tests and NRCC tests was 0.06 m and 0.27 m, respectively. This difference in lip height could affect the burn rate and ultimately the flame height, however the effect that lip height has on burn rate, that is, whether a direct or indirect relationship exists has not been resolved in the fire science community

3.1 Burn rate

Table 3-1 and Figure 3-1 provide a tabular and graphical comparison of the measured burn rates, respectively. The comparison indicates that the Bakken crude oil falls between JP8 and ethanol, whereas JP8 and heptane are similar. The methanol/toluene mixture has the highest, while the dilbit crude oil and methanol are most similar and have the lowest average burn rate among the fuels.

Table 3-1: Burn rates for 2-m diameter NRCC, DOE/DOT/TC, and SNL pool fire tests

Test	burn rate	
	mm/min (+/-)	kg/m^{2}s
heptane (NRCC)		
1.2	3.51 ± 0.04	0.040
Bakken (NRCC)		
2.1	2.23 (+0.03/-0.02)	0.030
dilbit (NRCC)		
3.3	1.11 (+0.03/-0.03)	0.017
	0.94 (+0.03/-0.03)	0.014
methanol (SNL)	1.46	0.0193
	1.52	0.02
	1.60	0.0211
	1.50	0.0198
	1.56	0.0206
JP8 (SNL)	2.65	0.0357
	2.78	0.0374
	2.84	0.0382
ethanol (SNL)	1.96	0.0258
	2.04	0.0269
72.4% methanol/ 27.6% toluene (SNL)	3.40	0.0461

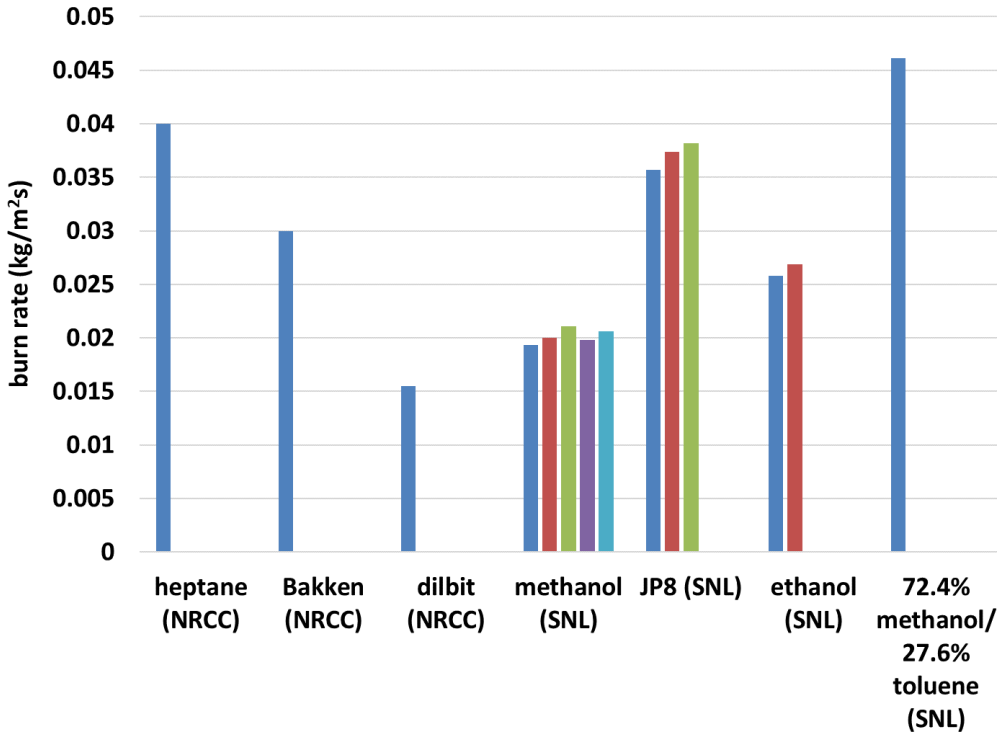

Figure 3-1: Comparison of burn rates for NRCC and SNL 2-m diameter pool fire tests.

3.2 Flame height

Table 3-2 and Figure 3-2 provide a tabular and graphical comparison among the NRCC and the SNL 2-m diameter pool fire tests. The comparison indicates that heptane, JP8, and the methanol/toluene mixture have similar average flame heights of around 6 m and are the highest among the fuels. The dilbit crude oil is most similar to ethanol with heights of around 3.5 m, while the Bakken crude oil is around 4.5 m. Methanol has the lowest average flame height of about 2 m.

Table 3-2: Average flame height for 2-m diameter NRCC, DOE/DOT/TC, and SNL pool fire tests

Test	Flame height (m)
heptane (NRCC)	
1.2	6.8
Bakken (NRCC)	
2.1	4.5
dilbit (NRCC)	
3.3	3.5
methanol (SNL)	
	2.0
	1.9
	2.0
	2.0

	2.1
JP8(SNL)	
	6.6
	6.5
	6.6
ethanol (SNL)	
	3.8
	3.8
72.4% methanol/ 27.6% toluene (SNL)	
	6.0

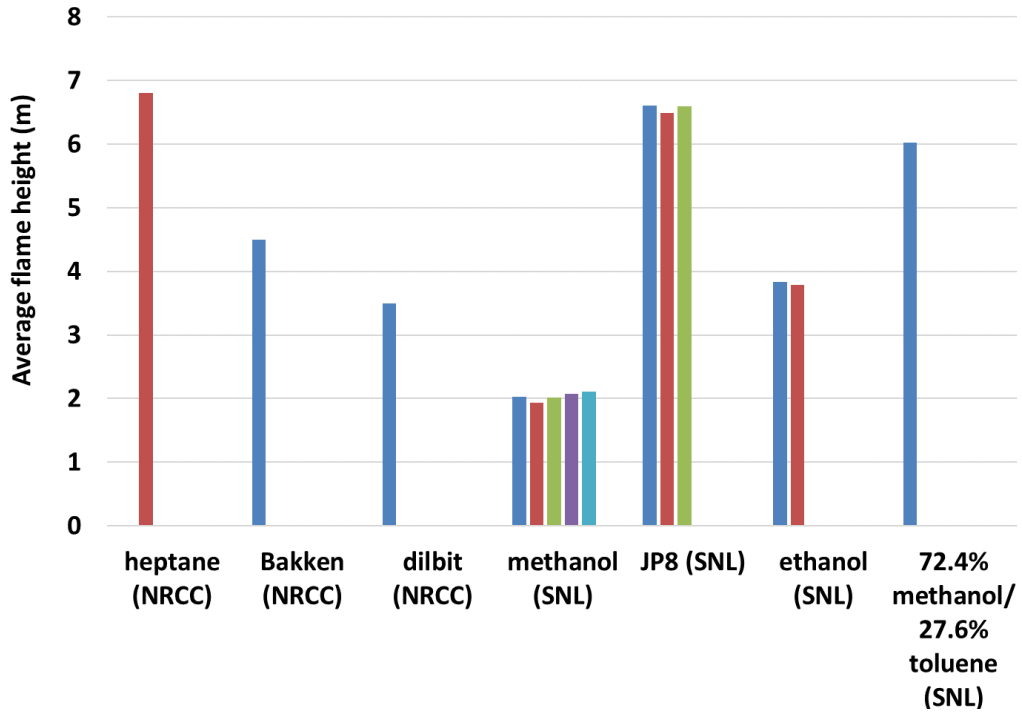

Figure 3-2: Comparison of flame heights for NRCC and SNL 2-m diameter pool fire tests.

3.3 Narrow-view radiometers

Figure 3-3 provides average heat flux measurements from narrow view radiometers at various heights for each fuel for the SNL and NRCC tests. The radiometers used in the SNL tests had a similar set-up to the NRCC tests as described in section 2.3. At the end of each dilbit test Jet-A was introduced to help flush out the system of remaining residue. The radiometer measurements during the burning of Jet-A averaged over 5 minutes is also plotted in Figure 3.3. The comparison indicates that the Bakken and dilbit crude oils have a greater decrease in heat flux with height than the other fuels tested in the SNL experiments. Though further examination of the cause of this difference is warranted as explained in the following.

Since Jet-A and JP-8 are very similar in their chemical/physical properties it is expected that their heat flux magnitudes and profiles should be similar, but the comparison indicates that heat flux levels differ by about a factor of 2 and the profiles are significantly different. To help identify weather the SNL or NRCC data has a potential error the NRCC tests did use an IR camera which facilitates this determination. The reported IR data is a temporal average of the surface emissive over the entire projected view of the flame and the vertical profile is extracted from this average. Thus, the IR measurements serve as an additional instrument to determine heat flux as a function of height and can be compared to the NRCC narrow-view radiometer measurements. However, it is not expected that the magnitude and profiles agree exactly since the IR measurements are incorporating the entire areas of the flame, whereas the NV radiometers are focused on a much smaller portion of the flame at a given height. Nonetheless, their approximate magnitudes and profiles can be compared.

Figure 3-4 shows IR measurements for the Bakken and dilbit crude oil NRCC experiments without a calorimeter. IR measurements were not taken for heptane test 1.2 and the Jet-A IR data was not reduced and thus not plotted. The IR measurements indicate a large decrease in heat flux with height similar to the radiometer data and the magnitudes agree within about 20 to 30 kW/m^2 of each other. Thus, given this agreement it is suspected that the SNL radiometer measurements potentially need correction. In going through the raw data taken for these tests it was found that the radiometer measurements were already multiplied by respective gain factors ($kW/m^2/mV$) for each radiometer in the DAQ system which were not reported in the raw data file. Thus, it is uncertain what gain factor values were used, though based on this comparison, values were potentially incorrectly entered but cannot be substantiated. The NRCC tests did not have gain factors entered into the DAQ system, rather the radiometer data was outputted in terms of millivolts and then later converted to heat flux from gain factors measured by in-house calibration. Since the experimental lead of the SNL test series has retired, it is difficult to resolve the observed differences.

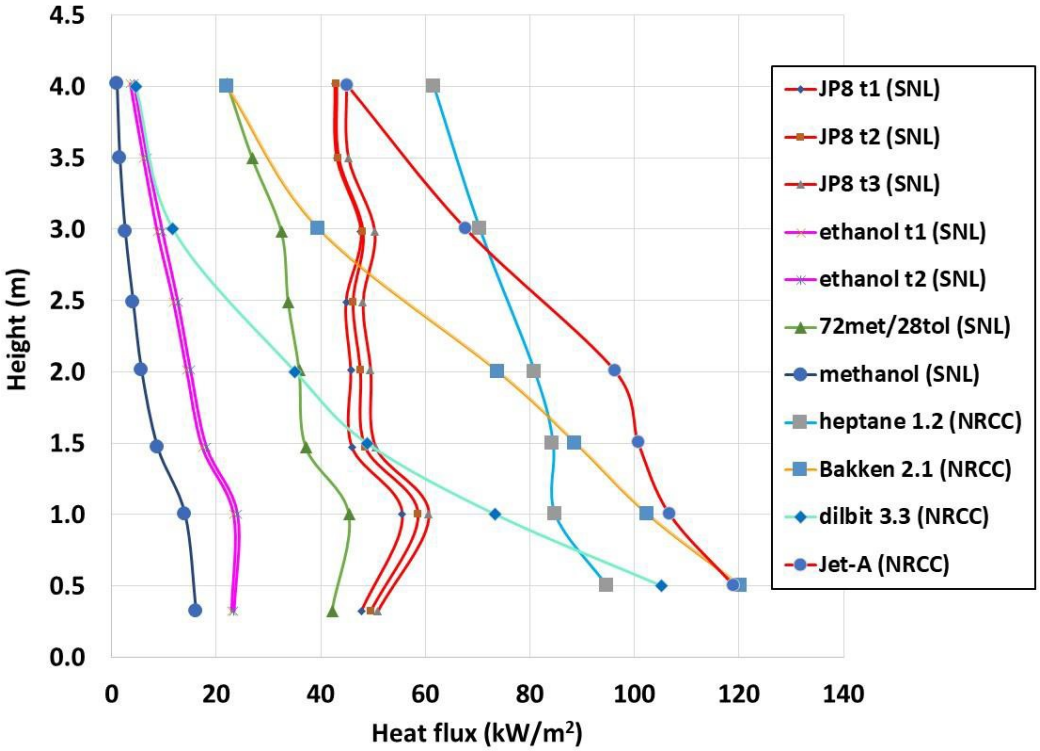

Figure 3-3: Comparison of narrow-view radiometer measurements for NRCC and SNL 2-m pool fires (no calorimeter). Jet-A introduced post-test for dilbit 3.3.

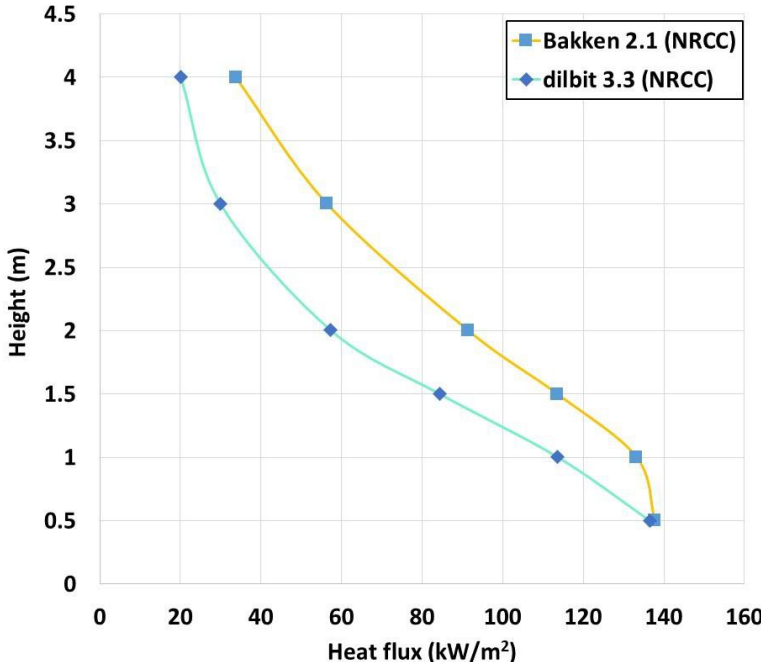

Figure 3-4: Surface emissive power measurements from IR camera.